THE EFFECT OF DIFFERING HYDROGEOLOGICAL REGIMES ON SANDSTONE DIAGENESIS: BRENT GROUP OILFIELDS, U.K. NORTH SEA.

A thesis submitted for the degree of
Doctor of Philosophy

by Mark James Osborne
B.Sc. Edinburgh University

Department of Geology and Applied Geology
University of Glasgow
October 1993

ProQuest LLC.
789 East Eisenhower Parkway
P.O. Box 1346
Ann Arbor, MI 48106 – 1346

Abstract

Deltaic sandstones of the Middle Jurassic Brent Group, northern North Sea, have a complex diagenetic history. The paragenetic sequence can be simplified to; siderite - feldspar dissolution - vermiform kaolinite - calcite - feldspar dissolution - blocky kaolinite - quartz - ankerite - illite. Petrographic and stable isotopic studies indicate that Fe-rich siderite precipitated from meteoric water which flushed through the Brent Group during the northward progradation of the delta system. Later Ca and Mg rich siderites precipitated from sea water during the subsequent marine transgression which eventually drowned the delta. Later diagenesis is related to depth of burial and hence depends upon the subsidence history of individual oilfields. In shallow buried oilfields (<1.0km) vermiform kaolinite precipitated, at temperatures of 25-47°C, while in more deeply buried oilfields blocky kaolinite precipitated (1.0-2.0km; 50-80°C). Kaolinite mainly precipitated during the late Cretaceous to early Eocene, following the dissolution of feldspar. Oxygen and hydrogen isotope studies indicate that both kaolinite types precipitated from pore-waters with $\delta^{18}O$= -6.5 to -3.5‰. These fluids are interpreted to be mixtures of meteoric water and sea water. Influx of meteoric water is inferred to have occured during the Palaeocene. Meteoric waters probably entered the Brent Group via the East Shetland Platform landmass in the west, fluid flow being driven by a hydrostatic head above sea level. These surface-derived fluids displaced and mixed with marine waters which were being expelled from compacting sediments. Oil migrating from the deeply buried source rocks into the shallower reservoirs became biodegraded as it interacted with the meteoric water flowing into the basin. In very deeply buried Brent sequences (>3.0km; >80°C), continued subsidence meant that the reservoirs were sealed-off from the influx of surface-derived meteoric fluids. Illite cement, and greater volumes of quartz cement (>5%) then precipitated in a closed geochemical system. The unusually high "palaeotemperatures" of the fluid inclusions in the quartz overgrowths are false and are a product of resetting during continued subsidence, and do not indicate that influx of hot fluids occured. Finally pore-waters evolved to present day isotopic compositions ($\delta^{18}O$= 0 to +2‰) due to water-rock interaction.

Acknowledgements

I am very grateful to Stuart and Tony, my two PhD supervisors, for educating me in petroleum geology and isotope geoscience respectively. Their enthusiasm throughout the whole project, and their attention to detail when reading the manuscript, has improved the quality of the thesis significantly. I also greatly appreciate the technical staff of both the S.U.R.R.C. in East Kilbride and the Geology department at Glasgow for their expert assistance during laboratory work. At E. K. I particularly thank Allison McDonald and Julie Gerc who instructed me in the use of the various isotope lines, and Susan Waldron for putting my samples on the mass spec. At Glasgow, Peter Ainsworth, Douglas McLean, Dougie Turner, Murdo Mcleod, John Gileece and Bill are appreciated for their thin section, XRD, SEM, geochemical and photographic expertise. My fellow post-grads have provided hours of endless entertainment, particularly when under the influence of alcohol, and I am grateful for the distraction they provided whenever the drudgery of lab. work was getting me down. Amongst these reprobates the following deserve special mention; the "Diaboredom Gang" (Orla, Fish, Robbie, Morgan, Rachel, Gordy), the "Buggerall Resources" team (Joe, Pete, Clark, Rona), the "Computer Junkies" (Chris, Dave, Campbell), the "Hard Rockers" (Gary, Richard) and the the rest (Carolyn, John, Allison, Simon, Mark W., Linda, Tim Trilobite, Gian, Derek, Bulent, Kerim, Mehmet, Hussein). 'The Jannies" (John, Eddie, Alec and Jimmy) will be fondly remembered for their many amusing and crude comments. I also could not have survived the last 3+ years without scrounging meals off several people when I was skint; Lindsey Ferguson and the Libyans (Ali, Sharif and Mohammed) are particularly thanked for their tasty contributions. The moral and financial support of my parents and sister has also been of enormous benefit to me throughout the PhD; so thanks very much folks! A special thanks also goes to Sandra for her support and companionship throughout the last 2 years.

LIST OF CONTENTS

Chapter 1 INTRODUCTION

1.1 Definition of diagenesis 9
1.2 Factors influencing diagenesis 9
1.3 Importance of diagenesis to the oil industry 11
1.4 Summary of previous work 12
1.5 Objectives 15
1.6 Approach 17
1.7 Thesis structure 18
1.8 Chapter summaries 19
1.9 Synthesis 22
1.10 Effect of diagenesis on reservoir quality 24
1.11 References 26
1.12 Figures 32

Chapter 2 ZONED SIDERITE CEMENTS DEFINE PALAEO-AQUIFERS: BRENT GROUP, UK NORTH SEA.

2.1 Abstract 34
2.2 Introduction 35
2.3 Geological setting 36
2.4 Brent Group diagenesis 37
2.5 Techniques used 37
2.6 Occurence and morphology of the cements 38
2.6.1 Zonation seen in Rannoch, Etive, Ness, and Tarbert Formations 39
2.6.2 Zonation seen in Broom Formation siderite 39
2.6.3 Siderite within degraded biotite 40
2.6.4 Concretionary siderite 41
2.6.5 Sphaerosiderites 41
2.7 Elemental analysis 41
2.7.1 Elemental chemistry of Rannoch, Etive, Ness and Tarbert Formation siderites 42
2.7.2 Elemental chemistry of Broom Formation siderite 42
2.8 Stable isotopic analysis 43
2.9 Discussion 43
2.9.1 Elemental zonation 43

2.9.2 Stable isotopic data 44
2.9.2.1 Carbon isotopes 45
2.9.2.2 Oxygen isotopes 47
2.9.2.3 Temperature constraints 47
2.9.2.4 Constraints on pore-water composition 47
2.9.2.5 Oxygen isotopic composition of concretionary siderite 48
2.9.2.6 Oxygen isotopes of siderite within biotite 48
2.9.3 Thermodynamic stability of siderite 52
2.9.4 Preferred explanation for siderite zonation 53
2.9.5 Evidence for changing hydrologies during siderite growth 55
2.9.6 Alternative hypotheses for the siderite zonation 56
2.9.6.1 Contribution of Fe and Mg ions from degrading biotites 56
2.9.6.2 Contribution of Ca and Mg ions from degrading biotites 58
2.9.7 Uses of siderite crystal zonation in diagenetic studies 59
2.10 Conclusions 60
2.11 Acknowledgements 61
2.12 References 61
2.13 Figures 66
2.14 Tables 93

Chapter 3 THE EMERALD OILFIELD, U.K. NORTH SEA: THE KEY TO SHALLOW DIAGENESIS AND PETROLEUM DEGRADATION IN THE BRENT GROUP?

3.1 Abstract 100
3.2 Introduction 101
3.3 Location and geological setting 101
3.4 Paragenetic sequence 104
3.5 Techniques used 103
3.6 Early diagenetic cements 105
3.6.1 Collophane and glauconite 105
3.6.2 Feldspar overgrowths 105
3.6.3 Pyrite and marcasite 106

3.6.4 Calcite 106
3.7 Later diagenetic cements 107
3.7.1 Kaolinite 107
3.7.2 Anatase 110
3.7.3 Ankerite 111
3.7.4 Quartz 111
3.8 Stable isotopic data 112
3.8.1 Stable isotopes of calcite 112
3.8.2 Stable isotopes of kaolinite 114
3.8.3 Stable isotopes of ankerite 114
3.9 Strontium isotopic data 115
3.9.1 Strontium isotopes of calcite 115
3.9.2 Strontium isotopes of ankerite 115
3.10 Fluid inclusion study of quartz cement 117
3.11 Biodegradation of oil 118
3.12 Discussion 120
3.12.1 Influx of meteoric water 120
3.12.2 Relationship between diagenesis, meteoric fluid flow, and biodegradation of oil. 122
3.12.3 Implications for the petroleum geologist. 125
3.13 Conclusions 127
3.14 Acknowledgements 128
3.15 References 128
3.16 Figures 134
3.17 Tables 164

Chapter 4 KAOLINITE MORPHOLOGY VARIES WITH TEMPERATURE IN ISOTOPICALLY MIXED PORE-FLUIDS, BRENT GROUP, U.K. NORTH SEA.

4.1 Abstract 171
4.2 Introduction 171
4.3 Geological setting 172
4.4 Kaolinite morphology and distribution 173
4.4.1 Petrographic data. 173
4.4.2 Interpretation of petrographic data. 175
4.5 Hydrogen and oxygen stable isotopes 179
4.5.1 Stable isotopic data 179

4.5.2 Interpretation of stable isotopic data 180
4.6 Discussion 182
4.10 Conclusions 187
4.11 Acknowledgements 188
4.12 References 188
4.13 Figures 193
4.14 Tables 208

Chapter 5 EVIDENCE FOR RESETTING OF FLUID INCLUSION TEMPERATURES FROM QUARTZ CEMENTS IN OILFIELDS.

5.1 Abstract 211
5.2 Introduction 211
5.3 Techniques used 212
5.4 Field data 212
5.5 Quartz cements and their fluid inclusions 213
5.6 Evidence for resetting from field data 214
5.7 Discussion 215
5.7.1 Resetting mechanism 217
5.7.2 Fluid inclusion salinities 219
5.7.3 Petroleum inclusions 220
5.7.4 Recognition of resetting 221
5.8 Conclusions 223
5.9 Acknowledgements 223
5.10 References 223
5.11 Figures 228
5.12 Tables 242

Appendix 1 FLUID INCLUSION TEMPERATURES IN DIAGENETIC QUARTZ RESET BY BURIAL: IMPLICATIONS FOR OILFIELD CEMENTATION. 247

LIST OF FIGURES

Figure 1.1 Porosity vs. depth. 31
Figure 1.2 Permeability vs. depth. 32
Figure 2.1 Location map. 66

Figure 2.2 Location map. 67
Figure 2.3 Burial curve. 68
Figure 2.4 Brent Group stratigraphy. 68
Figure 2.5 Paragenetic sequence. 69
Figure 2.6 Siderite within a concretion (photomicrograph). 69
Figure 2.7 Siderite rhombs within biotite (photomicrograph). 70
Figure 2.8 Siderite within micaceous horizon (photomicrograph). 70
Figure 2.9 a) Concretionary siderite compositional zonation (photomicrograph). 71
Figure 2.9 b) Compositional zonation of siderites within biotite (photomicrograph). 71
Figure 2.10 Compositional zonation of Tarbert Fm. siderite (photomicrograph). 72
Figure 2.11 Photomicrograph of concretionary siderite.
Figure 2.12 Compositional zonation of sphaerosiderite (photomicrograph). 73
Figure 2.13 Ternary plot showing elemental composition of meteoric siderite. 74
Figure 2.14 Ternary plot showing elemental composition of marine siderite. 75
Figure 2.15 Ternary plot showing elemental composition of Zone R1 siderite. 76
Figure 2.16 Ternary plot showing elemental composition of Zone R2 siderite. 77
Figure 2.17 Ternary plot showing elemental composition of Zone R3 siderite. 78
Figure 2.18 Compositional profile across a triple zoned siderite rhomb. 79
Figure 2.19 Ternary plot showing elemental composition of Broom Fm. siderite. 80
Figure 2.20 Graph showing stable isotopic composition of siderite (this study). 81
Figure 2.21 Graph showing stable isotopic composition of all Brent Group siderite. 82
Figure 2.22 Graph showing stable isotopic composition of siderite (worldwide compilation). 83
Figure 2.23 Photomicrograph showing organic matter and pyrite. 84

Figure 2.24 Compaction curve. 85
Figure 2.25 Graph of water composition vs. growth temperature for concretionary siderite. 86
Figure 2.26 Graph of water composition vs. growth temperature for siderite within biotites. 87
Figure 2.27 Stability diagrams for siderite (Eh vs. pS). 88
Figure 2.28 Stability diagram for siderite (Eh vs. pH). 89
Figure 2.29 Diagenetic model for zone R1 siderite. 90
Figure 2.30 Diagenetic model for zone R2 siderite. 91
Figure 2.31 Diagenetic model for zone R3 siderite. 92
Figure 3.1 Location map. 134
Figure 3.2 Cross section. 135
Figure 3.3 Burial curve. 136
Figure 3.4 Reservoir section. 137
Figure 3.5 Ternary plot showing sandstone composition. 138
Figure 3.6 Map of Emerald oilfield. 139
Figure 3.7 Paragenetic sequence for Emerald Sand. 140
Figure 3.8 Feldspar overgrowths (photomicrographs). 141
Figure 3.9 Pyrite (photomicrographs). 142
Figure 3.10 Calcite (photomicrographs). 143
Figure 3.11 Ternary plot showing carbonate elemental composition. 144
Figure 3.12 Vermiform kaolinite (photomicrograph). 145
Figure 3.13 Kaolinite infilling secondary porosity (photomicrograph). 145
Figure 3.14 Dissolved feldspars (photomicrographs). 146
Figure 3.15 Ankerite replacing feldspar (photomicrographs). 147
Figure 3.16 Quartz overgrowths (photomicrographs). 148
Figure 3.17 Graph showing stable isotopic composition of Emerald carbonates. 150
Figure 3.18 Pore-water vs. temperature graph for calcite. 151
Figure 3.19 Graph showing stable isotopic composition of all Brent Group calcites. 152
Figure 3.20 Pore-water vs. temperature graph for kaolinite. 153
Figure 3.21 Pore-water vs. temperature graph for ankerite. 154
Figure 3.22 Graph showing stable isotopic composition of all Brent Group ankerites. 155
Figure 3.23 Graph showing strontium isotopes of Brent Group

carbonates. 156
Figure 3.24 Graph showing strontium isotopes of Brent Group carbonates. 157
Figure 3.25 Graph showing strontium isotopes of Brent Group carbonates. 158
Figure 3.26 Histogram of fluid inclusion temperatures. 159
Figure 3.27 Histogram of carbonate carbon isotopic values. 160
Figure 3.28 Burial curve with growth temperatures superimposed. 161
Figure 3.29 Porosity and mineral abundance versus depth. 162
Figure 3.30 Model for the palaeohydrology of the Transitional shelf.163
Figure 4.1 Map of the East Shetland basin. 193
Figure 4.2 Burial curves for the oilfields studied. 194
Figure 4.3 Paragenetic sequence. 195
Figure 4.4 Vermiform kaolinite (photomicrograph). 196
Figure 4.5 Blocky kaolinite (photomicrograph). 197
Figure 4.6 Graph of relative abundance of kaolinite morphology vs. depth. 198
Figure 4.7 Graph of kaolinite content vs. depth. 199
Figure 4.8 Graph of feldspar content vs. depth. 200
Figure 4.9 Histogram of kaolinite oxygen isotopic data. 201
Figure 4.10 Histogram of kaolinite hydrogen isotopic data. 201
Figure 4.11 Hydrogen versus oxygen isotope plot for isotope exchange. 202
Figure 4.12 Water composition versus temperature plot for kaolinite. 203
Figure 4.13 Timing of kaolinite precipitation during subsidence. 204
Figure 4.14 Timing of kaolinite precipitation during subsidence. 206
Figure 4.15 Model for kaolinite precipitation. 207
Figure 5.1 Quartz cement abundance vs depth graph. 228
Figure 5.2 Quartz overgrowths (photomicrographs). 229
Figure 5.3 Quartz overgrowths (photomicrographs). 230
Figure 5.4 Quartz overgrowths (photomicrographs). 232
Figure 5.5 Fluid inclusion histogram, NW Hutton oilfield. 233
Figure 5.6 Th vs. depth. graph. 234
Figure 5.7 Graph of Th vs. inclusion size. 235
Figure 5.8 S. Brae fluid inclusions (photomicrographs). 236
Figure 5.9 Inclusion Th vs. inclusion shape. 237
Figure 5.10 Petrographic model for fluid inclusions in

quartz cement. 238
Figure 5.11 Th vs. reservoir temperature. 239
Figure 5.12 P-T diagram for inclusion resetting. 240
Figure 5.13 Graph of fluid inclusion Th vs. salinity. 241
Figure 5.14 Hypothetical plot showing effect of resetting on Th and salinity. 242

LIST OF TABLES

Table 2.1 Elemental chemistry of waters. 93
Table 2.2 Siderite stable isotopic data. 94
Table 2.3 Elemental chemistry of siderite. 95
Table 3.1 Point count data. 164
Table 3.2 Carbonate elemental data. 168
Table 3.3 Carbonate stable isotopic data. 168
Table 3.4 Kaolinite stable isotopic data. 169
Table 3.5 Carbonate strontium isotopic data. 169
Table 3.6 Quartz fluid inclusion data. 170
Table 4.1 Point count data for kaolinite morphologies. 208
Table 4.2 Stable isotopic data for kaolinite. 209
Table 4.3 Time and temperature of kaolinite growth 210
Table 5.1 Fluid inclusion data for NW Hutton. 243
Table 5.2 Th vs. depth data. 244
Table 5.3 South Brae fluid inclusion data. 245
Table 5.4 Fluid inclusion salinity data. 246

CHAPTER 1

1 INTRODUCTION AND CONCLUSIONS

1.1 Definition of diagenesis

Diagenesis can be categorised as the physical and chemical processes which affect an unconsolidated sediment and result in a solid, cemented rock. These processes include physical and chemical compaction, mineral dissolution, precipitation, and alteration. New, authigenic, minerals may form as overgrowths or as pore-filling cements. Minerals may precipitate as concretions, layers, or as disseminated cements. The net result of such cementation is to bind the grains together and eventually lithify the sediment. Compaction and cementation combined will reduce the porosity of a sediment, and generally the porosity of a sandstone decreases with depth of burial. Diagenetic reactions occur in the realm of shallow burial at relatively low temperatures and pressures (0-200°C temperature; 0.0-5.0 km burial; 1-2000 kg/cm^2 pressure). There is no clear-cut boundary between diagenesis and low grade metamorphism.

1.2 Factors influencing diagenesis

A large number of variables will directly or indirectly influence the diagenetic history of a sand.

Sediment composition.

This can be related to the source terrain of the sediment and in a wider context to plate tectonic setting. Many of the detrital minerals present in a sandstone are thermodynamically unstable at the temperatures and pressures which typify the diagenetic realm. Hence grains may undergo dissolution and replacement, though many persist metastably in a thermodynamically unsuitable environment. Generally feldspars and ferro-magnesian minerals such as pyroxene, amphibole, and biotite are the most unstable minerals in the weathering and shallow burial environment (Berner 1971; 1981). In a closed system, the type and relative abundance of detrital grains will influence which minerals precipitate following grain dissolution and alteration.

Temperature and pressure.

Both these will depend upon the burial history and temperature gradient of the basin. Generally speaking, mineral dissolution reactions will proceed faster at higher temperatures (Berner 1981). Increasing pressure will also increase the amount of chemical compaction at grain contacts. Both temperature and pressure will also exert a control on the thermodynamic stability of cements and detrital grains.

Chemical environment.

Eh (measure of reducing or oxidising potential) and *pH* measure of acidity/alkalinity) exert a strong control on the thermodynamic stability of minerals, particularly carbonates, sulphides, oxides and sulphates (Berner 1971). Type and concentration of dissolved ions in the pore-water will also directly control which minerals precipitate and which dissolve. Original pore-fluid composition is related to the depositional environment of the sediment. However with increasing depth of burial and time, depositional pore-waters can evolve chemically through water-rock interaction, or become displaced by other fluids (Sheppard 1986).

Fluid flow.

Fluid may flow through a sedimentary basin in response to various geological events (see Galloway 1987). Meteoric water, falling as rain on a landmass, can flow below sea level and penetrate sediments deep within the basin, fluid flow being driven by a hydrostatic gravitational head. Expulsion of water from compacting sediments can result in the upward migration of fluids from deeper in the basin. Fault movement and release of overpressure by fracturing can enable fluids to migrate from one pressure compartment to another. Thermal maturation of organic matter will generate liquid hydrocarbons, which may flow bouyantly to higher structural levels. Flow of aqueous fluids is important because it can potentially transport both heat and ions in solution, hence triggering dissolution/precipitation reactions in rocks through which the fluid passes (Giles 1987). The potential for diagenetic

modification is greatest where the water to rock ratio is high (i.e. when flow rates are high), because if the water to rock ratio is low the pore-fluid will quickly reach chemical equilibrium with the surrounding mineral surfaces. The ability of a fluid to flow through a sandstone will depend upon the lateral extent, connectivity, porosity, and permeability of the rock itself. All these factors can be related to depositional facies and the relative geometry of the sediment packages.

It should now be understood that the diagenetic realm is a dynamic and composite physico-chemical system, with many complex inter-relationships existing between the different component parts. Diagenetic observations made on a microscopic scale can often be related to geological events on a basin-wide scale. Hence an integrated, holistic approach must be taken if the diagenetic history of a sediment is to be correctly unravelled.

1.3 Importance of diagenesis to the oil industry

Diagenesis is of fundamental importance to the oil industry because growth of diagenetic minerals occludes pore-space and hence leaves less volume of the rock available for storage of hydrocarbons. Growth of different diagenetic minerals will affect the reservoir properties of the rock in different ways. For example, precipitation of quartz overgrowths will decrease porosities and narrow pore-throat diameters, while illite drastically decreases permeability with little effect on porosity. Migration of fine grained authigenic clay in flowing oil can cause problems during production. Laterally extensive carbonate cements can compartmentalise the reservoir, and tightly cemented sands can act as seals to hydrocarbon traps (Kantorowicz *et al.* 1987). Although cementation has a detrimental effect on reservoir properties, mineral dissolution may be beneficial if it leads to the creation of effective secondary porosity (Shanmugan 1990). If the factors controlling the growth and dissolution of minerals can be understood, then it may be possible to predict their distribution in the subsurface, and hence gain some idea of the porosity and permeability of reservoir sandstones during petroleum exploration and appraissal.

1.4 Summary of previous work

It is not the intention of this introduction to provide an in-depth summary of existing literature on the sedimentology, structural setting and other geological aspects of the Brent Group, as these have recently been dealt with by other authors (Morton *et al.* 1992). However particular aspects of the sedimentology and tectonic history of the Brent Group are discussed in detail throughout this thesis where they are directly relevant to an understanding of the diagenetic history.

The structural features of the East Shetland Basin and adjacent Viking Graben are the product of crustal extension in the early Triassic which produced tilting of basement fault blocks (Glennie 1990). These blocks were later buried under sediments accumulating in a post-rift thermal subsidence basin. This was followed by further late Jurassic faulting and block rotation. Fault related subsidence ceased in the early Cretaceous and was then replaced by temperature controlled regional subsidence.

The stratigraphy and depositional environment of the Brent Group is reviewed in Richards (1992). The Middle Jurassic Brent Group consists of deltaic and shallow marine sandstones and shales and forms one of the major oil reservoirs in the northern North Sea. The Group is approximately 300m thick in the East Shetland Basin. Researchers subdivide the Group into Broom, Rannoch, Etive, Ness and Tarbert Formations. Together the first letters of the Formations form the convenient acronym BRENT. The depositional settings of these Formations are generally well established. The Rannoch and Etive Formations have been described as regressive facies formed during northwards progradation of the clastic wedge, whilst the overlying Upper Ness and Tarbert Formations are transgressive in origin and were formed during a relative sea level rise which eventually drowned the system. The Broom Formation is regarded as a fan delta, and is not depositionally associated with the later delta system of which the Rannoch, Etive, Ness, and Tarbert Formations form a part.

For commercial reasons the diagenesis of the Brent Group has received much study. The identification of diagenetic minerals and recognition of a paragenetic sequence of mineral growth, were first elucidated in the late 1970's (Blanche & Whitaker 1978; Hancock &

Taylor 1978; Sommer 1978). The earliest cements are pyrite, calcite and siderite. These are succeded by kaolinite, ankerite and quartz cement, while illite is the last mineral to form prior to influx of oil. These basic observations have largely stood the test of time. Later studies have demonstrated that the same type and sequence of cements occurs in oilfields throughout the East Shetland Basin area, and also in laterally equivalent facies in the Norwegian North Sea (Bjorlykke *et al.* 1992; Brint 1989; Giles *et al.* 1992; Glasmann *et al.* 1989; Glasmann 1992; Hamilton *et al.* 1987; Harris 1992; Haszeldine *et al.* 1992; Hogg 1989).

Following the early petrographic studies, many later researchers concentrated on using particular techniques to further refine their understanding of Brent Group diagenesis. Fluid inclusion studies of quartz cements, for example, have been widely used by French, British and Norwegian researchers in order to constrain the temperature and origin of the fluid from which quartz overgrowths precipitated (Moge 1985; Malley *et al.* 1986; Jourdan *et al.* 1987; Konnerup-Madsen & Dypvik 1988; Brint 1989; Glasmann *et al.* 1989; Hogg 1989; Ehrenberg 1990; Walderhaug 1990). One significant observation made by these researchers was that hydrocarbon inclusions were trapped within the overgrowths. A great deal of effort has also been channeled into K-Ar dating of illite cements. As illite growth is thought to cease when oil enters the reservoir, K-Ar dating of illite cements has helped to constrain the time of filling (Ehrenberg & Nadeau 1989; Glasmann *et al.* 1989; Hamilton *et al.* 1987;1992; Hogg *et al.* 1993; Kantorowicz *et al.* 1992).

Stable isotopic studies of carbonate cements have been widely used in order to constrain growth temperature, carbon source, and pore-water origin at the time of cementation (Giles *et al.* 1992; Hamilton *et. al.* 1987; Haszeldine *et al.* 1992; Kantorowicz 1984; Lonoy *et al.* 1986). However, stable isotopic studies of illite, kaolinite and quartz cements are much rarer (Glasmann *et al.* 1989; Haszeldine *et al.* 1992).

Much of the earlier (pre-1992) literature deals with the diagenetic history of individual oilfields, or with single techniques. With time, more regional diagenetic studies have emerged, many of which adopt a multi-technique approach, integrating information from point counting, petrography, fluid inclusions, poroperm analysis, plus stable and radiogenic isotope geochemistry (Bjorlykke *et al.* 1992; Giles *et al.* 1992; Glasmann 1992; Harris 1992; Haszeldine *et al.* 1992). The availability of Brent Group core over a wide depth range (1800->4000m) has enabled

changes in diagenesis with present day depth of burial to be observed, although oilfields shallower than 1800m have not yet been studied. Such depth related studies have shown that;

a) Feldspar content decreases with depth, due to dissolution.

b) Kaolinite is the most abundant diagenetic clay at <3300m, while illite becomes the most important clay at depths >3300m.

c) Abundance of quartz cement increases steadily with depth.

d) Porosity decreases linearly with depth, while permeability declines rapidly at depths greater than 3300m.

The Brent Group is an ideal subject for diagenetic study, because its sedimentology, thermal and burial history are relatively well constrained, plus core is available over a wide area and range of depths. Hence it can be used as a case study in order to answer a variety of geological problems. Have the sandstones been flushed by cool meteoric or hot compactional fluids? Have the ions required for cementation been internally derived within the sediment via breakdown of unstable minerals? Alternatively, have the component ions liberated in this manner been exported into other rocks? Were the ions required for cementation imported into the Brent Group from an external source? It is important to establish whether cementation and dissolution occurred in a geochemically open or closed system. In a geochemically open system, ions in solution can be freely imported or exported from the rock. This has important consequences for reservoir quality; minerals may dissolve and their component ions be exported, hence improving reservoir porosities. These ions may subsequently migrate into another reservoir and precipitate as authigenic minerals, infilling porosity. Conversely, in a geochemically closed system, dissolution of minerals within the sediment will be balanced by in-situ cement precipitation, and there will be little opportunity for export of ions and improvement of reservoir porosities and permeabilities. By addressing such questions we begin to have some understanding of the palaeohydrology of sedimentary basins, and also whether reservoir properties such as porosity and permeability can be predicted.

Amongst researchers there is a general consensus that during early diagenesis (shallow burial) the Brent Group was flushed by meteoric water (i.e. water that originally fell as rain on a landmass). This argument is supported by stable isotopic studies of early carbonate cements which suggest precipitation from cool meteoric waters (Bjorlykke *et al.* 1992; Giles *et al.* 1992; Glasmann *et al.* 1989; Haszeldine *et al.* 1992). Siderite crystals show a similar chemical zonation in different oilfields and formations, while calcite cements have similar Sr isotopic compositions, implying a compositionally homogenous pore-fluid during shallow burial (Haszeldine *et al.* 1992). Pore-waters are interpreted to have been meteoric in both marine and non-marine formations, indicating much fluid flow and displacement of depositional waters in a geochemically open system. Secondary porosity after feldspar dissolution is seen in the shallow buried oilfields, and this has also been interpreted to be the result of the influx of acidic meteoric water during early diagenesis (Bjorlykke *et al.* 1992).

However opinion is still sharply divided over whether the diagenetic system was open or closed during deep burial (late diagenesis). Bjorlykke *et al.* (1992) advocate closed system diagenesis during deep burial, with no large scale fluid movement, and diffusive transport of ions in solution over short distances only. The lack of uniformity in elemental and Sr isotopic composition of late diagenetic carbonates suggests poorer fluid communication and increased compartmentalisation of the Brent Group during deep burial. However other researchers advocate large scale circulation of hot fluids through the Brent Group during late diagenesis (Jourdan *et al.* 1987; Malley *et al.* 1986). In support of this hypothesis, these authors cite the hot palaeotemperatures from fluid inclusions in quartz overgrowths, which imply either an elevated geothermal gradient at the time of cementation, or pulses of hot fluids ascending from deep in the basin via faults. However recent studies have cast doubt on the reliability of these fluid inclusion temperatures, due to the possibility of the inclusions being reset during burial (Giles *et al.* 1992; Haszeldine & Osborne 1993; Osborne & Haszeldine 1993).

1.5 Objectives

The objectives of the thesis were as follows;

1) To study in detail the diagenesis of the shallow buried Emerald oilfield (1600m), because most Brent Group sandstones examined by previous researchers have been deeply buried. This was to gain an insight into the diagenetic processes which were active during shallow burial. In addition, the Emerald oilfield lies at the very edge of the East Shetland Basin, while other Brent Group oilfields are more distant from the basin edge; hence study of the Emerald oilfield could allow us to assess how influx of meteoric waters from the East Shetland Platform would have influenced Brent Group diagenesis.

2) To study cements which precipitated during both early, intermediate and late diagenesis in order to reconstruct changes in the diagenetic environment through time, as subsidence progressed. The cements chosen were siderite (early diagenetic, shallow burial), kaolinite (early-late diagenetic, intermediate burial depths) and quartz (late diagenetic, deep burial environment).

3) Establishment of a paragenetic sequence for diagenetic minerals in the Brent Group using petrography.

4) Stable and radiogenic isotopic analysis of carbonate and silicate cements in order to determine the source and evolution of diagenetic fluids and temperatures of precipitation.

5) Assessment of the physico-chemical parameters controlling the distribution of cements and secondary porosity.

6) Modelling the movement of fluids from which the cements precipitated.

7) Collation and critical assessment of available published and unpublished stable isotopic and fluid inclusion data from the Brent Group.

8) Assessing the effect of diagenesis upon reservoir quality.

9) Establishing whether import or export of ions has occurred during cementation and dissolution episodes.

1.6 Approach

A modern, multi-technique approach was taken during this diagenetic study. A brief discussion of the various techniques used is presented below. Further information on equipment used and experimental procedures can be found within each chapter of the thesis.

a) Petrography. Point counting was used as an estimate of cement abundance. Mineral identification was achieved using a combination of thin section microscopy (transmitted and reflected light), SEM observation and EDS analysis, and X-ray diffraction. A paragenetic sequence of mineral growth was erected using textural criteria. More detailed examination of textures and variations in cement chemistry were accomplished using cathodoluminescence microscopy and on an SEM equipped with a BSE detector. Petrographic examination meant it was possible to constrain the relative timing of mineral dissolution and precipitation episodes. Rigorous petrographic interpretations were considered essential before selecting samples for further geochemical analysis.

b) Stable isotopic analysis. Petrography and mineral identification do not in themselves provide us with all the data required to fully understand the diagenetic history of a sediment. For example a mineral such as calcite may precipitate over a wide range of temperatures and in many different chemical environments, hence the mere presence of calcite in a sandstone provides us with only limited diagenetic information. However the stable isotopic $^{13}C/^{12}C$ ratio of carbonates can indicate the source of carbon during cementation (Irwin *et al.* 1977). Similarly $^{18}O/^{16}O$ and D/H analysis of carbonate and silicate minerals can help us constrain the growth temperature of the cement and the origin of the pore-water from which it precipitated (Longstaffe 1989).

c) Strontium isotopic analysis. $^{87}Sr/^{86}Sr$ ratios of carbonate cements can help pinpoint the type of fluid (e.g. meteoric or marine derived water) from which the cement precipitated, and the source of the Sr itself. In

combination with the elemental zonation exhibited by individual crystals, Sr isotopic analysis of carbonate cements can indicate whether pore-fluids were moving or stagnant at the time of precipitation (Haszeldine *et al.* 1992). It is also possible to gain some idea of reservoir connectivity.

d) Fluid inclusion microthermometry. Microthermometric analysis of fluid inclusions in cements can indicate growth temperature of the host mineral, and provide information on the salinity, composition, pressure, and presence of hydrocarbons within ancient pore-fluids (Roedder 1984).

It should be realised that each of the techniques above has limitations. Therefore if one technique is used in isolation, data will be produced that may be open to interpretation. The advantage of using several of these techniques in combination is that it becomes easier to rigidly constrain our interpretations and ensure they have a firm grounding in reality. In any diagenetic study there are many uncertainties, and the quality of the data produced must be rigorously assessed. Even petrographic observations may be open to interpretation; take for example, the argument between Burley & Kantorowicz (1986) and Hurst & Bjorkum (1986) over the recognition of supposed cement dissolution textures in sandstones.

Similarly there are uncertainties in the interpretation of stable isotopic data because fractionation factors and the isotopic composition of ancient fluids are not precisely known (Sheppard 1986). There may be further problems with non-equilibrium fractionation and post-formational isotopic exchange between minerals and water. Fluid inclusion data can also be problematic, for inclusion homogenisation temperatures can be reset during burial, resulting in apparent growth temperatures which are too high (Barker & Goldstein 1991; Osborne & Haszeldine 1993). Throughout this thesis, an attempt has hence been made to rigorously test and constrain isotopic and fluid inclusion data.

1.7 Thesis structure

The thesis comprises four papers, Chapters 2 to 5, which investigate various aspects of the diagenesis of the Brent Group of the East Shetland Basin area of the northern North Sea. All these papers

were written by the author and are entirely the product of his own research. One has recently appeared in print (Osborne & Haszeldine 1993). Appendix 1 presents a paper which was not written by the author alone, but is based upon his work.

Chapter 2 is concerned with early diagenetic siderite, its physical distribution, stable isotopic composition and crystal zonation. Chapter 3 describes the diagenesis of the Emerald oilfield, as a case study of shallow buried Brent Group sandstones. Again the diagenetic minerals are analysed using a combination of petrographic, isotopic and fluid inclusion techniques. Chapter 4 is concerned with diagenetic kaolinite, and differences in kaolinite morphology, isotopic composition and distribution are discussed. Chapter 5 is a compilation and critical evaluation of published and unpublished fluid inclusion data from quartz cements in Brent Group sandstones. Appendix 1 continues the discussion of fluid inclusion temperature data, and the implications for modelling quartz cementation in oilfields. A summary of the main conclusions of this thesis are presented below.

1.8 Chapter summaries

Chapter 2. Early diagenetic siderite in the Brent Group precipitated as concretions, sphaerosiderites and as rhombic crystals between expanded biotites. Both types of siderite show a similar intra-crystalline zonation. The earliest growth zone is of very pure Fe-rich siderite (Zone 1) which is interpreted to have precipitated from meteoric water. Zone 2 is very Mg rich and bears a strong resemblance to marine siderite. Zone 3 has a composition intermediate between that of Zones 2 and 3.

Carbon isotopes indicate the siderite precipitated using bicarbonate from a variety of origins. Sulphate/iron reduction was the most important source, but bacterial fermentation and possibly shell dissolution were also involved. Concretionary siderite has $\delta^{18}O$ values which are consistent with precipitation from meteoric or mixed meteoric-marine pore-waters at <30°C. Siderite which formed within degraded biotites shows the same three growth zones as concretionary siderite and must have precipitated at the same time. However these siderites are

more $\delta^{18}O$ depleted than the concretionary siderites. This suggests the siderite within the biotites precipitated during kinetic rather than equilibrium isotope fractionation. It is likely that siderite Zone 1 precipitated from meteoric water which flowed through the Brent Group during the advance of the delta system. Zone 2 precipitated from marine waters which entered the reservoir sands during marine transgression, when the Tarbert Formation was deposited. Zone 3 possibly precipitated from a mixed marine-meteoric water of compactional origin.

Chapter 3. The Emerald oilfield is an example of a shallow buried Brent Group oilfield (1600m). In this field, early diagenesis consisted of growth of pyrite, K-feldspar overgrowths and calcite concretions. During deeper burial, vermiform kaolinite, ankerite and quartz precipitated, accompanied by feldspar dissolution. Mass balance calculations indicate that following feldspar dissolution Al was conserved due to kaolinite precipitation, but Si partly exported, creating 5% secondary porosity. However much of this porosity was lost during later compaction, with no net improvement in reservoir porosities and permeabilities. This paragenetic sequence is remarkably similar to the early diagenetic mineral assemblages seen in the more deeply buried Brent Group fields. Stable isotopic analyses of ankerite and kaolinite cements suggest that they precipitated from meteoric or brackish pore-waters at approximately 20-50°C. This indicates that meteoric water must have flushed through the reservoir sandstones displacing depositional marine pore-waters. Influx of meteoric water resulted in the biodegradation of hydrocarbons, dissolution of feldspar, and precipitation of kaolinite, quartz and ankerite cements. Fluid flow was driven by a hydrostatic head on the landmass to the west during the Palaeocene.

Chapter 4. Two types of diagenetic kaolinite occur in the Brent Group; vermiform kaolinite and blocky kaolinite. Early diagenetic vermiform kaolinite precipitated at 25-47°C during shallow burial, and later diagenetic blocky kaolinite precipitated at 50-80°C during deeper burial (palaeotemperatures calculated from stable isotopic data). Both kaolinite types precipitated from pore-waters with $\delta^{18}O$= -6.5 to -3.5‰. These pore-waters either represent mixed meteoric-marine fluids, or alternatively meteoric waters that had evolved isotopically due to water-

rock interaction. Most kaolinite precipitated during the late Cretaceous to early Eocene. Influx of meteoric water into the Brent Group is inferred to have occured during the Palaeocene. Oil migrating into the Brent Group in the Palaeocene became biodegraded as it was flushed by meteoric water.

Vermiform kaolinite initially nucleated between the sheets of expanded muscovites, while blocky kaolinite precipitated directly into pore-space. Both kaolinite types precipitated following the dissolution of feldspar. The differences in the two morphologies is probably a product of the degree of supersaturation at the time of precipitation; at low degrees of supersaturation nucleation of kaolinite upon mica surfaces is kinetically favoured. Because kaolinite is using the mica surfaces as a template for growth a vermiform morphology is produced. At higher levels of supersaturation kaolinite can precipitate directly into pore-space, without nucleation upon mica surfaces, and so kaolinite with a characteristic blocky morphology is produced.

Chapter 5. Quartz is a major pore-occluding cement in deeply buried Brent Group reservoir sandstones. Fluid inclusions yield homogenisation temperatures (T_h) which have been thought to represent growth temperatures for the host quartz. However, early diagenetic inclusions from the detrital grain-overgrowth boundary yield excessively high palaeotemperatures which do not match the growth temperatures calculated from the depth of burial. The temperatures of these inclusions increase with present day depth of burial, and approach present day reservoir temperatures. This suggests that the inclusions have begun to reset towards present day P-T conditions. The T_h of the inclusions hence represent burial temperatures rather than growth temperatures for the quartz. Experimental studies indicate that the amount of resetting undergone by an inclusion varies depending upon its size, shape, and fluid composition. A relationship between inclusion T_h and the above variables has been observed in inclusions from deeply buried quartz cements in the North Sea.

Resetting of the inclusions is thought to be by non-elastic stretching and shape change. Experimental studies have shown that inclusion stretching occurs for lower values of internal pressure than those required to produce brittle fracture. Stretching is thought to be a time dependant process, hence when P-T conditions are suddenly

changed it will take a finite time for the inclusions to re-equilibrate. This explains why in rapidly subsiding oilfields the modal T_h of the fluid inclusions does not exactly match Formation temperature. Conversely in oilfields which have undergone a period of slow subsidence, inclusion T_h closely corresponds to reservoir temperature.

Previous researchers have regarded T_h as a valid estimate of growth temperature for the host quartz. This has led to the suggestion that quartz precipitated from fluids which were hotter than the calculated geothermal gradient, and that ascending, hot, basinal, brines must have been responsible for cementation. However if inclusion T_h has been reset to higher temperatures, then influx of hot fluids from depth is not required in order to explain the fluid inclusion data, and large scale convective transport of silica in solution is unlikely.

1.9 Synthesis

During the advance of the Brent delta system (Bajocian-Aalenian times) meteoric water flushed through the deltaic and nearshore marine sediments of the Rannoch, Etive and Ness Formations. Hence meteoric water displaced depositional marine pore-fluids in the Rannoch and Etive Formations. This acidic meteoric water dissolved feldspars and resulted in the precipitation of Fe-rich siderite (Zone 1 siderite), plus some vermiform kaolinite and anatase. During subsequent marine transgression (Bathonian times) the Tarbert Formation was deposited and the delta system was drowned by the rise in sea level. This transgression allowed sea water to enter the Rannoch, Etive, Ness and Tarbert Formations. Mg and Ca rich siderite precipitated from the marine derived pore-waters (Zone 2 siderite). During shallow burial (<30°C, Callovian-Kimmeridgian times) siderite of intermediate composition precipitated (Zone 3 siderite), from mixed marine-meteoric compactional waters.

Subsequent diagenetic modification of Brent Group sandstones was related to depth of burial, and hence is dependent upon the subsidence and temperature history of individual oilfields. In shallow buried oilfields (reservoir temperatures 25-47°C), vermiform kaolinite precipitated following the dissolution of feldspar. In more deeply buried

oilfields (reservoir temperatures 50-80°C) kaolinite with a blocky morphology precipitated. Both kaolinite types precipitated from similar pore-waters ($\delta^{18}O$= -6.5 to -3.5‰). Such fluids represent either mixed meteoric and compactional marine waters, or alternatively meteoric waters that had evolved isotopically due to water-rock interaction. In either case, the presence of a strong component of meteoric water in the pore-fluid indicates that extensive displacement and movement of fluid must have occured, because all the sediments overlying the Brent Group are marine.

Meteoric waters probably entered the Brent Group via the East Shetland Platform landmass in the west, fluid flow being driven by a hydrostatic head elevated above sea level. Regional meteoric fluid flow was most likely to have occurred during the Palaeocene, when the East Shetland Platform was sub-aerially exposed. These surface-derived fluids displaced and underwent mixing with marine waters which were being expelled from compacting sediments located above and below the Brent Group.

Significant volumes of quartz and illite cements only began to precipitate during deeper burial (reservoir temperatures >80°C). The unusually high palaeotemperatures of the fluid inclusions in the quartz overgrowths are a product of resetting during continued subsidence, and do not indicate that influx of hot fluids occurred (Jourdan *et al.* 1987; Haszeldine *et al.* 1992; Osborne & Haszeldine 1993). Hence there is no evidence for open system convective fluid movement during late diagenesis, with fluid flow transporting heat, hydrocarbons and silica into the Brent Group. Instead, it is more likely that the diagenetic system became more closed as subsidence progressed, so that the water to rock ratio decreased. Under such conditions, water-rock interaction would modify the pore-water $\delta^{18}O$ isotopic composition to the positive values seen today ($\delta^{18}O$= 0 to +2‰, Egeberg & Aagaard 1989; Haszeldine *et al.* 1992). The most likely reactions leading to pore-water modification were probably illitisation of kaolinite and recrystallisation of early calcite cements (Egeberg & Aagard 1989).

Hydrocarbons migrated bouyantly into the Brent Group reservoirs during the early Tertiary. In shallow buried oilfields this oil was biodegraded due to the influx of surface-derived meteoric water. As oil filled the reservoirs, diagenesis slowed down and was eventually halted.

1.10 Effect of diagenesis on reservoir properties

The reservoir quality of the Brent Group is partly dependent upon the grain size, sorting, and sedimentary structures present in the sandstones upon deposition. Superimposed upon these primary depositional controls on reservoir quality, are the secondary diagenetic effects of compaction, cementation and grain dissolution; processes which may either decrease or enhance reservoir porosities and permeabilities. Diagenesis has profoundly modified the primary, depositional porosities and permeabilities of these sandstones, a point which will be discussed in detail later.

The depositional controls on reservoir quality of the Brent Group are summarised in Richards (1992). The Broom Formation consists of thin, poorly sorted, sandstones of limited reservoir importance. The Rannoch Formation consists of mica-rich siltstones and sandstones, The Formation coarsens upwards, from siltstone to very fine or fine grained sandstone, with reasonable porosity and permeability characteristics. However concentrations of mica and carbonaceous material along low angle laminae may inhibit vertical flow. The Etive Formation is generally the best reservoir interval in the Brent Group, and consists of massive, well sorted, fine-coarse grained sandstones, with good porosities and very high permeabilities. Occasional mica and clay layers may reduce vertical permeability. Both the Rannoch and Etive Formations form extensive, readily correlatable sheets. The Ness is the most lithologically varied Formation of the Brent Group, consisting of interbedded sandstones, shales and some thin coals. Sandstones can have good porosity and permeability characteristics, but are often laterally and vertically discontinuous unless stacked fluvial channel sands occur. The Mid-Ness Shale forms an important non-reservoir horizon. The Tarbert Formation consists of fine grained, well sorted, micaceous, sandstones, with a coarser grained base. The Tarbert Formation is of relatively good reservoir quality, but may be absent or thin at the crest of fields due to erosion beneath the late Cimmerian unconformity.

The total porosity of Brent Group sandstones decreases systematically with depth, in all Formations and facies (Figure 1 Bjorlykke *et al.* 1992; Giles *et al.* 1992; Harris 1992). The decrease in porosity is roughly linear, and is the product of the combined effects of

compaction and cementation. Variation in sandstone permeability with depth is more complex; at depths of <3100m permeability is independent of depth of burial, and is related to grain size, sorting, and the presence of calcite, ankerite and siderite cements (Giles *et al.* 1992). However at depths >3100m permeability declines drastically in all Formations and facies (Figure 2 Bjorlykke *et al.* 1992; Giles *et al.* 1992; Harris 1992). The explanation for this decline in permeability is discussed later.

We shall now discuss the effect of volumetrically significant cements on the reservoir quality of the Brent Group. Carbonate cements (calcite with minor siderite and ankerite) are frequently found as randomly distributed concretions or laterally extensive layers in the marine Formations of the Brent Group. Carbonate cements are very common in the Rannoch Formation, common in the Tarbert Formation, and much less frequently observed in the Broom, Etive and Upper Ness Formations (Abbotts 1991; Giles *et al.* 1992). Their influence upon reservoir quality is variable depending upon the lateral extent of the cemented layers (from metres to 100's of metres), and the amount of cement present as a percentage of the total Formation thickness. The carbonate cements can completely occlude porosity, leading to a reduction in the total pore-space available to hydrocarbons; in the Dunlin and Tern oilfields carbonate cements form 12-14% of the thickness of the Rannoch Formation (Abbotts 1991). Carbonate cemented layers can also act as barriers or baffles to vertical fluid flow, directly influencing oil production (e.g. Cormorant, Heather, and Eider oilfields; Abbotts 1991). However in other oilfields, such as Thistle, Emerald and Dunlin, the lateral extent and abundance of the carbonate cemented layers are not significant enough to affect reservoir performance (Abbotts 1991).

Kaolinite precipitation converts open pore-space into inter-particle microporosity. Kaolinite cement is a by-product of feldspar dissolution. The amount of kaolinite present in the Brent Group is widely variable (0-22%), and does not seem to be controlled by the abundance of detrital feldspar. However, the Etive Formation, and massive and cross-bedded sands in the Ness Formation, have higher abundances of both kaolinite and secondary porosity than the rest of the Brent Group (Giles *et al.* 1992). These Formations and facies are the most porous and permeable horizons in the Brent Group, suggesting that accessibility of the sandstones to fluid flow may have been an important

influence governing feldspar dissolution and kaolinite precipitation. Dissolution of feldspar and the creation of secondary porosity has not greatly improved the overall porosity of the Brent Group, because later compaction has resulted in the collapse of the secondary pores (Harris 1992). This explains why the volume of secondary porosity present in the Brent Group remains fairly constant with depth (3%), despite extensive feldspar dissolution (10-20%) over the same depth range (Bjorlykke *et al.* 1992; Giles *et al.* 1992; Harris 1992). Permeability has also not been significantly improved because Al has not been exported, with kaolinite precipitating in the pore-space created.

The amount of kaolinite present in the Brent Group decreases at >3300m due to alteration to illite. Precipitation of fibrous illite cement at >3300m is largely responsible for the drastic decrease in reservoir permeabilities below this depth (Figure 2). Less than 2 volume% illite cement is usually present in the Brent Group, yet this small volume of cement can reduce permeabilities by three orders of magnitude (Giles *et al.* 1992). It is not possible to ascertain differences in illite abundance between facies and Formations due to the difficulty of accurately point counting the abundance of such small volumes of fibrous illite in thin section. However it can often be recognised that there has been preferential illite growth in the water leg compared to the oil leg; hence reservoir permeabilities are much lower beneath the oil-water contact (Giles *et al.* 1992). This may cause production problems if injection of water below the oil-water contact is used to provide aquifer support (Kantorowicz *et al.* 1992). The greater abundance of illite below the oil-water contact suggests that oil migration into the reservoir has halted illitisation.

Quartz overgrowths occlude pore space and result in a narrowing of pore-throat diameters. The abundance of quartz cement present in the Brent Group is strongly depth related, with <5% cement above 2700m, and increasing volumes (average 10%, but up to 27%) below this depth (Giles *et al.* 1992). There are no significant differences in quartz cement abundance above and below the oil-water contact, or between different facies and Formations.

1.11 REFERENCES

Abbots, I.L., 1991, United Kingdom oil and gas fields; 25 years commemorative volume, *Mem. Geol. Soc. Lond.*, **14**, 573p.

Barker, C.E., and Goldstein, R. H.,1991, A fluid inclusion technique for determining maximum temperature in calcite and its comparison to the vitrinite reflectance geothermometer: *Geology*, **18**, p.1003-1006.

Berner, R. A., 1971, Principles of chemical sedimentology, New York, McGraw Hill, 240 p..

Berner, R.A., 1981, Kinetics of weathering and diagenesis. In *Kinetics of geochemical processes*, Reviews in Mineralogy 8, Min. Soc. Am.

Bjorlykke, K., & Brendsal, A.,1986, Diagenesis of the Brent sandstone in the Statfjord field. In Gautier, D.L., (ed.), *Roles of organic matter in sedimentary diagenesis.* SEPM Special Publication No. 38. p.157-168.

Bjorlykke, K., Nedkvitne, T., Ramm, M., Saigal, G.C., 1992, Diagenetic processes in the Brent Group (Middle Jurassic) reservoirs of the North Sea ; an overview. In Morton, A. C., Haszeldine, R. S., Giles, M. R., & Brown, S., (Eds), *Geology of the Brent Group.* Geological Society of London, Bath UK. p. 263-288.

Brint, J. F., 1989, Isotope diagenesis and palaeofluid movement: Middle Jurassic Brent sandstones, North Sea *D. Phil. Thesis* University of Strathclyde, Scotland, 288 p.

Burley, S.D., Kantorowicz, J.D., 1986, Thin section and SEM textural criteria for the recognition of cement-dissolution porosity in sandstones. *Sedimentology*, **33**, p.587-604.

Egeberg, P.K., & Aagard, P., 1989, Origin and evolution of formation waters from oilfields of the Morwegian shelf. *Appl. Geochem.*, **4**, p.131-142.

Ehrenberg, S. N., 1990, Relationship between diagenesis and reservoir quality in sandstones of the Garn Formation, Haltenbanken, Mid Norwegian Continental Shelf *Am. Assoc. Petrol. Geol. Bull*, **74**, p. 1538-1558.

Ehrenberg, S.N., & Nadeau, P.H., 1989, Formation of diagenetic illite in sandstones of the Garn Formation, Haltenbank area, mid-Norwegian continental shelf. *Clay Minerals*, **24**, p.233-253.

Giles, M.R., 1987, Mass balance and problems of secondary porosity creation in deeply buried hydrocarbon reservoirs. *Marine & Petroleum Geology*, 4.p.188-204.

Giles, M.R., Stevenson, S., Martin, S. V., Cannon, S. J. C., Hamilton, P. J., Marshall, J. D., & Samways, G. M., 1992, The reservoir properties and diagenesis of the Brent Group; a regional perspective. In Morton, A. C., Haszeldine, R. S., Giles, M. R., & Brown, S., (Eds), *Geology of the Brent Group*. Geological Society of London, Bath UK. p. 289-327.

Glasmann, J.R., 1992, The fate of feldspar in the Brent Group reservoirs, North Sea: a regional synthesis of diagenesis in shallow, intermediate, and deep burial environments. In Morton, A. C., Haszeldine, R. S., Giles, M. R., & Brown, S. (Eds), *Geology of the Brent Group*. Geological Society of London, Bath U.K. p. 329-350.

Glasmann, J. R., Lundegard, P. D., Clark, R. A., Penny, B. K., Collins, I. D., 1989 a, Geochemical evidence for the history of diagenesis and fluid migration: Brent sandstone, Heather field, North Sea *Clay Minerals*, **24**, p. 255-284.

Glasmann, J. R., Clark, R. A., Larter, S., Briedis, N. A., and Lundegard, P. D.,1989 b, Diagenesis and hydrocarbon accumulation, Brent sandstone (Jurassic), Bergen High area, North Sea *Am. Assoc. Petrol. Geol. Bull.*, **73**, no. 11, p. 1341-1360.

Glennie, K. W.,1990, *Introduction to the Petroleum Geology of the North Sea* (third edition) Oxford, Blackwell Scientific Publications.

Hamilton, P.J., Fallick, A.E., Macintyre, R.M., & Elliott, S.,1987, Isotopic tracing of provenance and diagenesis of lower Brent Group sands, North Sea. In Brooks, J., & Glennie, K.W., (eds.), *Petroleum Geology of NW Europe*, Graham & Trotman, London, p.939-949.

Hancock, N.J., & Taylor, A.M., 1978, Clay mineral diagenesis and oil migration in the Middle Jurassic Brent Sand formation, *Jour. Geol. Soc. Lond.*, **135**, p.69-72.

Harris, N. B., 1992, Burial diagenesis of Brent sandstones: a study of Statfjord, Hutton and Lyell fields. In Morton, A. C., Haszeldine, R. S., Giles, M. R., & Brown, S. (Eds), *Geology of the Brent Group*. Geological Society of London, Bath U.K. p. 351-375.

Haszeldine, R. S., Brint, J. F., Fallick, A.E., Hamilton, P. J., & Brown, S., 1992, Open and restricted hydrologies in Brent Group diagenesis: North Sea. In Morton, A. C., Haszeldine, R.S.,

Giles, M. R., & Brown, S.(Eds.), *Geology of the Brent Group.* Geological Society of London, Bath UK. p. 401-419.

Haszeldine, R.S., & Osborne, M., 1993, Fluid inclusions in diagenetic quartz reset during subsidence; implications for oilfield cementation. In Horbury, A. & Robinson, A.G., (Eds.) *Diagenesis in basin development,* Am Assoc. Petrol. Geol. Spec. Publ. (in press).

Hogg A.J.C.,1989, Petrographic and isotopic constraints on the diagenesis and reservoir properties of the Brent Group sandstones, Alwyn South, Northern U.K. North Sea *D. Phil. Thesis* University of Aberdeen, Scotland, 414p.

Hogg, A.J.C., Hamilton, P.J., & Macintyre, R.M., 1993, Mapping diagenetic fluid flow within a reservoir: K-Ar dating in the Alwyn area, N.Sea. *Marine & Petroleum Geology,* **10**, p.279-295.

Hurst, A., Bjorkum, P.A., 1986, Discussion. Thin section and SEM textural criteria for the recognition of cement-dissolution porosity in sandsones, *Sedimentology,* **33**, p.605-614.

Irwin, H., Curtis, C., Coleman, M., 1977, Isotopic evidence for sources of diagenetic carbonates formed during burial of organic rich sediments. *Nature,* **269**, p.209-213.

Jourdan, A., Thomas, M., Brevart, O., Robson, P., Sommer, F., and Sullivan, M.,1987, Diagenesis as the control of Brent sandstone reservoir properties in the Greater Alwyn area (East Shetland Basin) *in Petroleum Geology of North West Europe,* Brooks, J., and Glennie, K., eds., Graham and Trotman, p. 951-961.

Kantorowicz, J.D., 1984, The origin of authigenic ankerite from the Ninian field U.K. North Sea. *Nature,* **315**, p.214-216.

Kantorowicz, J.D., Bryant, I.D., Dawans, J.M., 1987, Controls on the geometry and distribution of carbonate cements in Jurassic sandstones: Bridport, southern and Viking Group, Troll Field, Norway. *In* Marshall, J.D., (Ed.) Diagenesis of sedimentary sequences, Geological Society Special Publication No. 36, p.103-118.

Kantorowicz, J.D., Eigner, M.R.P., Livera, S.E., Van Schijndel-Goester, F.S., & Hamilton, P.J. ,1992, Integration of petroleum engineering studies of producing Brent Group fields to predict reservoir properties in the Pelican Field, U.K. North Sea. In Morton, A. C., Haszeldine, R.S., Giles, M. R., & Brown,

S.(Eds.), *Geology of the Brent Group*. Geological Society of London, Bath UK. p. 453-469.

Konnerup-Madsen, J., and Dypvik, H., 1988, Fluid inclusions and quartz cementation in Jurassic sandstones from Haltenbanken, offshore Mid-Norway *Bull. Mineral*, **111**, p. 401-411.

Longstaffe, F., 1989, Stable isotopes as tracers in clastic diagenesis, in Hutcheon, I.C., (Ed.), *Burial Diagenesis*, Miner. Assoc. of Canada, Short Course Handbook, **v.15**, p.201-277.

Lonoy, A., Akselsen, J., & Ronning, K., 1986, Diagenesis of a deeply buried sandstone reservoir:Hild field, Northern North sea. *Clay Minerals*, **21**, p.497-511.

Malley, P., Jourdan, A., Weber, F. ,1986, Etude des inclusions fluides dans les nourrissages siliceux des gres reservoirs de Mer du Nord: une nouvelle lecture possible de l'histoire diagenetique du Brent de la region D' Alwyn *Acad..Sci.Paris* **302**, p. 653-658.

Moge, M., 1985, Evolutions diagenetiques et characteristiques petrophysiques de formations greseuses a porosite secondaire *D. Phil. Thesis*, University of Nancy 125p.

Morton, A. C., Haszeldine, R.S., Giles, M. R., & Brown, S.(Eds.), 1992, *Geology of the Brent Group*. Geological Society of London, Bath UK. p. 27-43.

Osborne, M., & Haszeldine, R.S., 1993, Evidence for resetting of fluid inclusions in oilfield quartz, *Marine & Petroleum Geology*,**10**, p. 271-279.

Richards, P.C., An introduction to the Brent Group, a literature review. In Morton, A. C., Haszeldine, R.S., Giles, M. R., & Brown, S.(Eds.), *Geology of the Brent Group*. Geological Society of London, Bath UK. p. 15-26.

Roedder, E., 1984, *Fluid inclusions,in* Ribbe, P.H., ed., Reviews in Mineralogy 12, Mineralogical Society of America, p. 644.

Shanmugan, G., 1990, Porosity prediction using erosional unconformities. In *Prediction of reservoir quality using chemical modelling*, Eds. I.D. Meshri & PJ Ortoleva, AAPG memoir **49**, p.1-23.

Sheppard, S.M.F., 1986, Characterization and isotopic variations in natural waters. In Miner. Soc. Am. reviews in mineralogy, 16, p.165-183.

Sommer, F., 1978, Diagenesis of Jurassic sandstones in the Viking Graben, *Jour. Geol. Soc. Lond.*, **135**, p.63-67.

Walderhaug, O., 1990, A fluid inclusion study of quartz cemented sandstones from offshore Mid- Norway ; possible evidence for continued quartz cementation during oil emplacement *J. Sed. Pet.*, **60**, p. 203-210.

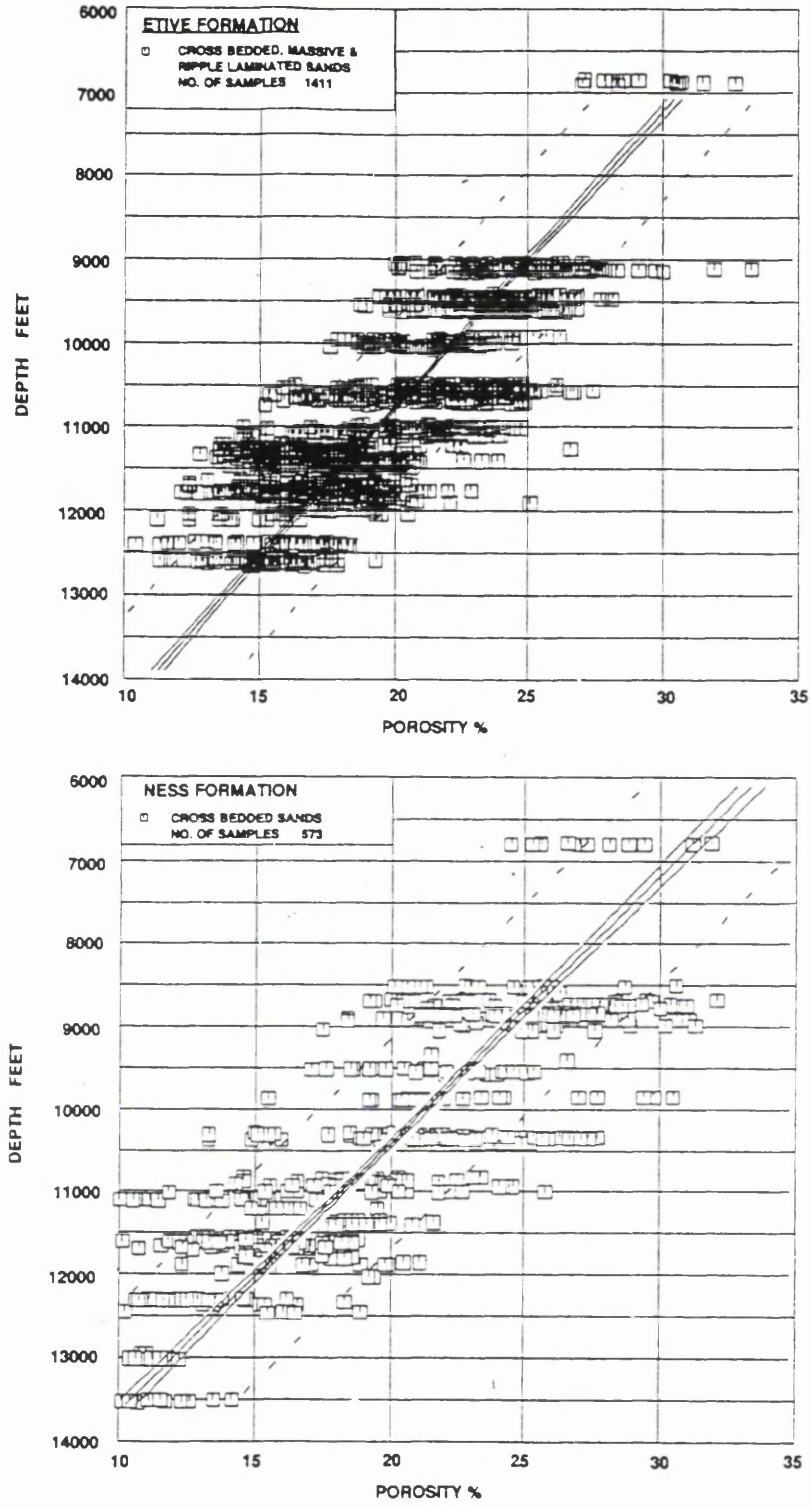

Figure 1. Core plug porosity versus present day depth for sandstones in the Etive and Ness Formations of the Brent Group. Porosity decreases steadily with depth. A similar relationship is seen in other Brent Group Formations. From Giles *et al.* (1992).

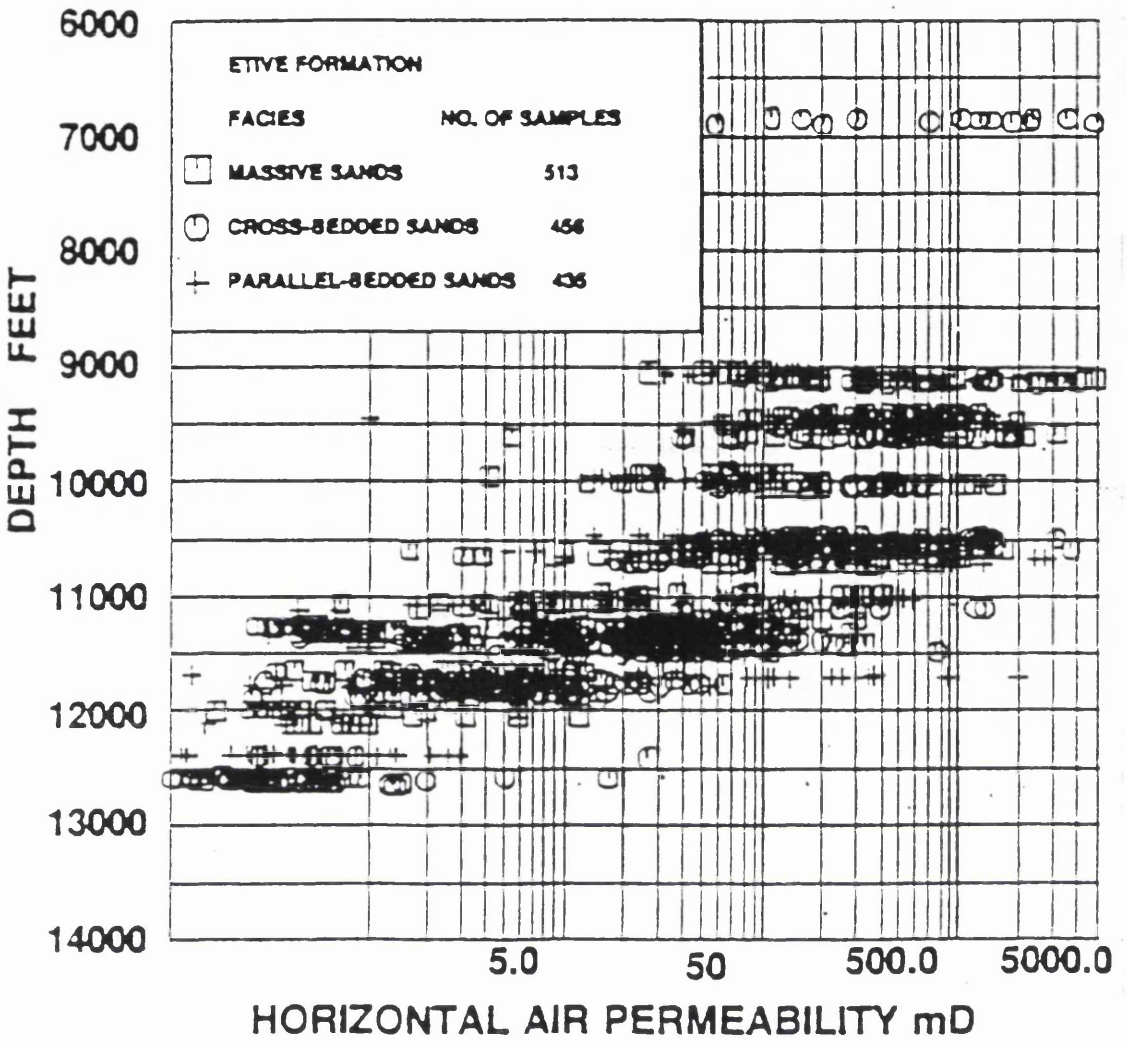

Figure 2. Horizontal air permeability versus depth for sandstones of the Etive Formation. Permeability declines rapidly below 10,000ft (3048m); a relationship seen in all Brent Group Formations. From Giles *et al.* (1992).

CHAPTER 2

ZONED SIDERITE CEMENTS DEFINE PALAEO-AQUIFERS, BRENT GROUP, UK NORTH SEA.

Mark Osborne[1], R. Stuart Haszeldine[1], Anthony E. Fallick[2]
1- Dept. of Geology & Applied Geology, Lilybank Gardens, Glasgow University, Glasgow, Scotland, U.K., G12 8QQ.
2- Isotope Geosciences Unit, Scottish Universities Research and Reactor Centre, East Kilbride, Glasgow, Scotland, U.K., G75 OQU.

2.1 ABSTRACT

Siderite cements in the reservoir sandstones of the Brent Group, UK North Sea occur in the form of concretions, sphaerosiderites, and rhombic crystals within expanded biotites. All the siderite morphologies grew during early diagenesis at less than 30°C. Siderites from the Rannoch, Etive, and Ness Formations have three concentric growth zones (R1, R2, and R3), while siderites from the Tarbert Formation usually possess only two of these zones (R2 and R3). Siderites from the Broom Formation have four concentric growth zones (B1, B2, B3, B4) which are chemically distinct from those occurring in overlying Formations. The earliest zone (Zone R1) is very Fe-rich (85.7-98.2 mole% $FeCO_3$) and is compositionally similar to siderite of meteoric origin as defined by Mozley (1989). Zone R2 is very Mg and Ca rich (60-81.4 mole% $FeCO_3$) and bears a strong resemblance to marine siderite. Zone R3 has a composition intermediate between that of Zones R2 and R3. Zones B1, B2, B3, and B4 consist of impure siderite with variable amounts of Mg and Ca substitution (68.4-81.4 mole% $FeCO_3$), and closely resemble marine siderite. Carbon isotopes indicate the siderite precipitated using bicarbonate from a variety of origins. Oxidation of organic matter accompanying sulphate reduction was the most important source, but bacterial fermentation and possibly shell dissolution were also involved. Concretionary siderite has $\delta^{18}O$ values which are consistent with precipitation from meteoric or mixed meteoric-marine pore-waters at <30°C. Siderite which formed within degraded biotites shows the same three growth zones as concretionary siderite (R1, R2 and R3) and must have precipitated at the same time. However, these siderites are more $\delta^{18}O$ depleted than concretionary siderite (by up to 9‰) which suggests the siderite within the biotites precipitated during kinetic, non-equilibrium

fractionation between siderite and water. In contrast concretionary siderite precipitated in oxygen isotopic equilibrium with the pore-water. It is likely that siderite Zone R1 precipitated from meteoric water which flowed through the Brent Group during the advance of the delta system. Zone R2 precipitated from marine waters which entered the reservoir sands during marine transgression, when the Tarbert Formation was deposited. Zone R3 possibly precipitated from a mixed marine-meteoric water of compactional origin. The Broom Formation remained an isolated aquifer, and Zones B1-4 precipitated from depositional marine waters.

2.2 INTRODUCTION

There are relationships between the trace element (Mg, Ca, Fe and Mn) composition of diagenetic carbonates such as calcite and siderite and the composition of the water from which they precipitated (Veizer 1983; Mozley 1989). This means it is possible to distinguish between carbonates precipitating from meteoric and marine pore-waters. Chemical zonation of trace elements within individual calcite crystals has often been thought to reflect variations in the bulk chemistry of diagenetic pore-fluids through time, and has been widely described and discussed in the literature (e.g. Meyers 1974; Have & Heijnen 1984).

However, the origin of similar compositional variations within individual siderite crystals has not yet been established. However this is an important point to address as siderite is a common diagenetic mineral in many different sedimentary environments, and unlike calcite, has been rarely observed to recrystallise and undergo alteration to other carbonates upon deeper burial or when pore fluid compositions are changed (Gould & Smith 1979; Matsumoto & Iijima 1981; Gautier 1982; Pearson 1985; Curtis & Coleman 1986; Mozley 1989; Mozley & Carothers 1992).

Therefore intracrystalline variations in siderite composition could successfully record changes in the composition of diagenetic palaeofluids with time. Furthermore, the composition of siderite is generally far more variable than that of calcite, due to the ability of Ca, Mg and Mn to substitute extensively for Fe in the crystal lattice, and so compositional changes can frequently be measured in terms of mole% rather than in ppm. Thus siderite is a mineral which is well suited to quantitative chemical analysis using a microprobe or SEM. This paper examines compositional variations in diagenetic siderite crystals from the

Middle Jurassic Brent Group of the North Sea and attempts to interpret their diagenetic significance.

2.3 GEOLOGICAL SETTING

The samples examined in this study came from Middle Jurassic Brent Group reservoir sandstones in the Thistle, Murchison, Dunlin, and Cormorant oilfields in the East Shetland Basin area in the UK sector of the northern North Sea (Figure 1&2). All five Formations of the Brent Group were sampled during the study (Broom, Rannoch, Etive, Ness and Tarbert Formations).

The structural features of the East Shetland Basin and adjacent Viking Graben are the product of crustal extension in the early Triassic which produced tilting of basement fault blocks. These blocks were later buried under sediments accumulating in a post-rift thermal subsidence basin. This was followed by further late Jurassic faulting and block rotation. Fault-related subsidence ceased in the early Cretaceous and was replaced by temperature-controlled regional subsidence. Schematic burial curves for the four oilfields studied are shown in (Figure 3), using sediment thicknesses incrementally decompacted from present values (Brint 1989).

The stratigraphy and depositional environment of the Brent Group is reviewed in Richards (1992). The Middle Jurassic Brent Group consists of deltaic and shallow marine sandstones and shales and forms one of the major oil reservoirs in the northern North Sea. The Group is approximately 300m thick in the East Shetland Basin. Researchers subdivide the Group into Broom, Rannoch, Etive, Ness and Tarbert Formations. Together the first letters of the Formations form the convenient acronym BRENT. The depositional environments of these Formations are generally well established and are summarised in Figure 4. The Broom, Rannoch and Etive Formations have been described as regressive facies formed during northwards progradation of the clastic wedge, whilst the overlying Upper Ness and Tarbert Formations are transgressive in origin and were formed during a relative sea level rise which eventually drowned the system.

2.4 BRENT GROUP DIAGENESIS

The diagenesis of the Brent Group has received much study, mainly because it is one of the major oil reservoirs in the northern North Sea and because growth of diagenetic minerals profoundly influences the porosity and permeability characteristics of the reservoir sandstones. A generalised paragenetic sequence for the oilfields studied is shown in Figure 5. This is based upon observations of the authors and Brint (1989).

Siderite is not one of the most volumetrically important cements in the Brent Group, though it is of widespread distribution, occurring in all the oilfields within the East Shetland Basin. Siderite is quite clearly one of the earliest diagenetic minerals to precipitate in the Brent Group, as it occurs within calcite concretions with high minus cement porosities of 35-40% (Figure 6). In addition shale laminae curve around siderite concretions indicating the cement is pre-compactional in origin. Early calcite also encloses vermiform kaolinite, pyrite and authigenic anatase, which probably precipitated co-genetically with the siderite. Anatase is found replacing detrital sphene

No siderite has been observed to have undergone alteration and replacement by any other carbonate mineral, and calcite, ankerite and siderite co-exist in contact with present day pore waters. Rare, late diagenetic siderite also occurs in the Brent Group (Giles *et al.* 1992), but has not been observed during this study.

2.5 TECHNIQUES USED

During diagenetic studies compositional zonation of calcite and dolomite crystals can been observed using cathodoluminescence (CL). However, diagenetic siderite possesses more than 15000ppm Fe^{2+}, resulting in total quenching of luminescence. This means that chemical zonation within siderite crystals can only be examined using an SEM equipped with a BSE detector. Contrast in the BSE image depends on the chemistry of the surface of the specimen; the higher the atomic number of the particles in the specimen, the brighter the BSE image becomes. Imaging of siderite was carried out on polished, perfectly flat specimens. It was found that various compositional zones could be distinguished in terms of relative brightness and image contrast.

After compositional zones were identified using BSE,

quantitative chemical analysis of the individual zones was undertaken using a Cambridge Stereoscan 360 SEM, equipped with a Link Analytical 1085 S. A ZAF4 FLS programme was used to correct the data. Accuracy of the measurements is ±0.5 mole%.

Over 130 thin sections of siderite-bearing sandstones were examined in the course of this study, and 40 polished thin sections were prepared for SEM backscattered electron imaging and quantitative analysis.

In addition a small number of siderite samples were selected for stable isotopic analysis. Rock samples were gently disaggregated using a mortar and pestle and the <100μm size fraction retained for further treatment. The samples were reacted for several days with dilute hydrogen peroxide to remove oil and other organic matter. Siderite was separated from other minerals using 1,1,2,2, tetrabromoethane adjusted to a suitable density, and then further purified using a Frantz magnetic separator. Any contaminant calcite was removed by reacting overnight with 1M tri-ammonium citrate solution. XRD was used to determine whether each stage in the purification process had been successful. Sieving was then used to subdivide the sample into size fractions. As a precaution before being reacted, the samples were plasma ashed for 2-3hrs to remove any remaining organic contamination.

Siderite was reacted with phosphoric acid overnight at 100°C in a hotblock (McCrea 1950), and the CO_2 gas purified and then analysed on a VG Isogas SIRA-10 mass spectrometer. Carbon and oxygen isotope results were corrected in the usual manner, and are presented in the conventional δ notation, as parts per thousand relative to the PDB and SMOW standards. Oxygen isotope fractionation factors derived experimentally by Rosenbaum and Sheppard (1986) were utilised to correct the raw data. The reproducability of the isotopic analyses based upon repetitive measurements and running of laboratory standards is ±0.1‰.

2.6 OCCURRENCE & MORPHOLOGY OF THE CEMENTS

Authigenic siderite occurs in all five Formations of the Brent Group, in both marine and non-marine facies. The siderite exhibits a variety of morphologies:

1. Siderite inclusions associated with degrading biotites.

2. Concretions.

3. Sphaerosiderites (i.e. siderite with spherulitic morphology).

BSE examination of polished thin sections shows that the siderite cement present in the Brent Group is chemically zoned. Four distinct cement generations are seen in siderite from the Broom Formation (Figure 12b), and three generations in the overlying Rannoch, Etive, Ness and Tarbert Formations (Figure 9). It was found that various compositional zones could be distinguished in terms of relative brightness and contrast of the BSE image. This BSE zonation is described below.

2.6.1 Zonation seen in Rannoch, Etive, Ness & Tarbert Formation Siderite

Zone R1- light grey to bright.	Earliest
Zone R2- dark, or very dark.	
Zone R3- medium grey.	Latest

Zones R1 to 3 are common to all four Formations, however Zone R1 is often absent or very rare in the Tarbert Formation (i.e. Zone R1 is present in <5% of all siderite crystals). All zones occasionally have subzones developed. Chemical analyses of these compositional zones have been undertaken, and are discussed later in this paper.

2.6.2 Zonation seen in Broom Formation Siderite

The BSE zonation seen in the Broom Formation is different from that seen in the overlying four Formations. The zones and their appearance using BSE imaging are as follows:

Zone B1- dark	Earliest
Zone B2- medium grey	
Zone B3- very dark	
Zone B4- medium grey	Latest

The morphology and occurrence of the three morphological types of siderite cement will be discussed in detail below, together with the

chemical zonation they reveal when examined using BSE imaging.

2.6.3 Siderite within degrading biotites

This type of siderite is of common occurence in micaceous sandstones. The siderite is demonstrably early diagenetic as it is enveloped by calcite cement which exhibits high minus cement porosities of 35-40% (Figure 6). Siderite often has a tendency to occur along the expanded cleavage planes of biotites which are undergoing fanning and expansion of the grain terminations (Figure 7). Some biotites are undergoing replacement by kaolinite. However both pyrite and siderite inclusions can be found outside, as well as inside, expanded biotites Biotites may exhibit fanning and expansion at the grain terminations only, or the whole biotite grain itself may be expanded. Muscovite present in the same sample also show fanning of the grain terminations and alteration to kaolinite, though in general they are much less altered than the biotites. Siderite and pyrite inclusions are never found within degrading muscovite. Where the sandstone has been cemented by early diagenetic calcite, expanded biotites are preserved in an uncompacted state, but outside of concretions they are frequently compacted. In sandstones siderite abundance is strongly related to mica content (illustrated in Figure 8). In the Etive Formation, which is mica poor, siderite is rare but in the highly micaceous Rannoch Formation siderite is more abundant.

The siderite consists of subhedral-euhedral rhombs, sometimes forming patches of cement if the biotite is fully expanded. If the biotite has only expanded slightly then the siderite may not have been able to attain a perfectly euhedral shape, because crystal growth was restricted by the lack of space available between the mica cleavage planes.

The siderite inclusions show a triple zonation in BSE mode; zone R1 is typically irregular or subrounded in shape and may show evidence of dissolution before the more rhombic and euhedral zones R2 and 3 precipitated around the early core (Figure 9). Zone R3 is generally very thin. This triple zonation is well developed in Rannoch, Etive and Ness formations. However no expanded biotites have been observed in the Broom formation, and in the Tarbert Formation zone R1 is often absent or rare, occuring in less than 5% of all siderite crystals (Figure 10).

2.6.4 Concretions

Siderite concretions in the Brent Group vary greatly from sub-spherical to irregular in shape. Sideritic layers are also found. Both in-situ and winnowed concretions occur, and the latter can be distinguished by the fact that they are typically small (<4cm), well rounded, and have no regular orientation with regard to bedding. Concretions are of two types:

1. Cryptocrystalline siderite, sometimes enclosing berthierine ooliths. Cryptocrystalline siderite concretions principally exhibit the earliest BSE zones (R1, B1); however the outer skin of the concretion may consist of euhedral siderite in which later zones are evident.

2. Euhedral siderite. Fine grained euhedral siderite forms discrete patches, perhaps replacing precursor detrital grains. In between these patches of fine grained siderite, coarser grained siderite has developed, perhaps infilling what was originally open pore-space (Figure 11). Fine grained siderite consists entirely of BSE zones R1 and 2, while the coarser grained siderite mainly exhibits zones R2 and 3, indicating it precipitated later.

2.6.5 Sphaerosiderites

Spherulitic siderite has been observed only in the Broom and Ness Formations during the present study. The earliest zones are arranged concentrically, sometimes around a pyrite core, and usually exhibit subzoning. Later zones usually form euhedral crystalline projections which nucleate on the surface of the spherule (Figure 12).

2.7 ELEMENTAL ANALYSES

Mozley (1989) has demonstrated that marine and freshwater siderites have distinctly different compositions. Siderites from fresh-water environments are relatively pure (>90 mole% $FeCO_3$), and may attain end member composition. Siderite from marine environments is always very impure, contains less Mn, and has higher Mg/Ca ratios than fresh water siderite (Figs 13&14). These compositional differences are thought to reflect the chemistry of depositional pore waters as sea water has a higher Mg/Ca

ratio and contains less Mn and Fe and more Ca and Mg than meteoric water (Table1). Mozley suggests that the composition of early diagenetic siderite is strongly influenced by the depositional pore-water chemistry.

Comparing the chemistry of Brent Group siderites with the data from marine and fresh water siderites cited by Mozley (1989) is most illuminating, revealing that siderites in the Brent Group are of both marine and meteoric origin.

2.7.1 Elemental Chemistry of Rannoch, Etive, Ness & Tarbert Formation Siderites

Zone R1 This zone is relatively pure siderite (85.7-98.2 mole% $FeCO_3$). It has lower Mg/Ca ratios than the other two zones and contains more Mn. Compositionally it is very similar to meteoric siderite (Figure 15).

Zone R2 This zone consists of very impure siderite (60-81.4 mole% $FeCO_3$). It has a higher Mg/Ca ratio than Zone R1 and contains little Mn. Compositionally it strongly resembles marine siderite (Figure 16). There is often evidence of dissolution between Zones R1 and R2 (Figure 9a).

Zone R3 Similar to Zone R2 in composition, it comprises impure siderite (68.1-88.2 mole% $FeCO_3$), with high Mg/Ca ratios and low Mn concentrations. However it is more ferroan than Zone R2. It thus has a composition intermediate between the marine and meteoric siderites cited in Mozley (1989) (Figure 17).

A compositional profile across a siderite crystal showing all three of these zones is shown in Figure 18.

2.7.2 Elemental chemistry of Broom Formation siderites

Four compositional zones can be distinguished using BSE imaging. All the zones from the Broom Formation consist of very impure siderite (68.4-81.4 mole% $FeCO_3$) showing variable amounts of Ca and Mg substitution and low Mn concentrations (Figure 19). Roughly equal amounts of Mg and Ca are present. No direct correlation can be made between the zonation seen in the Broom Formation and the zonation seen in siderite from the overlying Rannoch, Etive, Ness and Tarbert Formations. The compositions of siderite from the Broom Formation are

generally similar to those of marine siderite cited by Mozley (1989).

2.8 STABLE ISOTOPE ANALYSES

Isotope analyses are tabulated in Table 2 and presented graphically in Figure 20. The results are generally similar to those obtained from Brent Group siderite by other researchers (Brint 1989; Giles *et al.* 1992). Thus although our isotope data base is small we can assert that it is broadly representative of the Brent Group as a whole. There is a wide spread in $\delta^{13}C_{PDB}$ values evident, from -2.8 to -18.4‰. Oxygen values are also surprisingly variable considering the cements are all early diagenetic in origin (from $\delta^{18}O_{PDB}$ -3.5 to -13.0‰). Concretionary siderite, and siderite occuring within biotites, seem to have distinctive $\delta^{18}O_{PDB}$ signatures, the latter yielding more $\delta^{18}O$ depleted values (Figure 21).

2.9 DISCUSSION

2.9.1 Elemental Zonation

Trace element zonation of carbonates has been explained in the literature in two ways.

1. Chemical variation is the the result of changes in bulk pore-fluid chemistry during mineral precipitation (Meyers 1978)

2. Chemical zonation does not always reflect pore fluid chemistry. When carbonate crystals grow slowly impurities may be excluded, whereas during rapid growth more impurities may be included (Have & Heijnen 1984; Given & Wilkinson 1985).

However all of this literature refers to calcite and dolomite, not to more ferroan carbonates such as siderite, and so may not be wholly applicable to this study. Generally, the variations in trace element composition recorded in calcites are much smaller than those in siderite, and can be measured in ppm rather than mole% (Have & Heijnen 1984).

The large variations in the amounts of contaminant elements present in the Brent Group siderite make it more difficult to envisage that the incorporation of impurities was merely a product of rapid crystal growth. Intra-stage dissolution events, and sharp boundaries between siderite zones also suggest that different pore-fluids were involved in precipitation of the various cement generations (Figure 9a). It is thus more plausible that chemical zonation in Brent Group siderite predominantly reflects a varying pore fluid composition.

If the zonation seen in the Brent Group siderites is largely a reflection of fluctuating pore fluid composition, we can hypothesise that Zone R1 precipitated from a meteoric water, Zone R2 from a marine water, and Zone R3 from a water of mixed marine-meteoric composition.

Given & Wilkinson (1985) have also suggested that different morphologies of $CaCO_3$ cement may be produced by variations in the rate of precipitation. Siderite in the Brent Group shows a range of morphologies, with early formed concretionary and spheroidal siderite being overgrown by later, smaller rhombs. It is thus possible that this change in morphology may reflect fluctuation in precipitation rate with time; we might expect sphaerosiderite to be symptomatic of rapid growth rates. Euhedral siderite however, probably indicates slower precipitation rates, from solutions which are less oversaturated with respect to carbonate.

Although precipitation rate may have influenced siderite morphology it is unlikely that it controlled siderite compositional zonation, because in the samples studied there is no systematic relationship between siderite morphology and composition. Sphaerosiderites for example, can consist of either very pure or very impure siderite.

2.9.2 Stable Isotope Data

Mozley (1992) has compiled published stable isotopic data for early diagenetic siderite in both marine and non-marine facies. Marine and non-marine siderites show disinct compositional trends, although there is considerable overlap in the spread of the data. Comparison of the

Brent Group siderite $\delta^{13}C_{PDB}$ and $\delta^{18}O_{PDB}$ values with those of continental and marine siderites cited by Mozley & Wersin (1992) indicates that they have stable isotopic compositions which are not distinctive of either a marine or non-marine origin (Figure 22).

2.9.2.1 *Carbon Isotopes*

Use of carbonate $\delta^{13}C_{PDB}$ values is a well established technique in ascertaining the source of bicarbonate from which a diagenetic mineral precipitated. As organic matter is buried it under goes degradation and CO_2 is released with specific $\delta^{13}C_{PDB}$ signatures (Curtis & Coleman 1986). With increasing depth of burial these are; aerobic oxidation ($\delta^{13}C_{PDB}$ ~ -25‰); bacterial sulphate reduction ($\delta^{13}C_{PDB}$ ~ -25‰), bacterial fermentation ($\delta^{13}C_{PDB}$ ~ +15‰), and thermally-induced abiotic decarboxylation ($\delta^{13}C_{PDB}$ ~ -15‰). In addition marine carbonate from shells, sea-floor cements and calcareous microfossils can also dissolve upon burial and release bicarbonate with a $\delta^{13}C_{PDB}$ signature of approximately 0 ‰ into porewaters.

Measured siderite $\delta^{13}C_{PDB}$ compositions from this study range from -2.8 to -18.4‰ and are thus not indicative of an end member CO_2 source. Such $\delta^{13}C_{PDB}$ compositions must have been produced by mixing of bicarbonate from different origins. This is what might be expected, for as we have seen, the siderite cements are compositionally zoned, and succesive cement generations may have precipitated in different hydrologic settings. Thus stable isotope analyses of these siderite samples represent only bulk analyses of more than one cement phase.

The most depleted $\delta^{13}C_{PDB}$ values of -15.7 to -18.4‰ are close to the signature of bicarbonate produced during oxidation of organic matter accompanying/during sulphate reduction ($\delta^{13}C_{PDB}$ ~ -25‰), suggesting a very sizeable contribution of bicarbonate from this source. Pyrite is seen in association with plant fragments in some samples suggesting that sulphate reduction and oxidation of organic matter had indeed occurred (Figure 23).

If oxidation of organic matter during sulphate reduction produced some of the CO_2 for siderite growth then we might expect both siderite and pyrite to precipitate more or less co-genetically. However, within concretions and sphaerosiderites, pyrite is clearly seen to *pre-date*

siderite, although the relative timing of pyrite and siderite precipitation within degrading biotites cannot be established. Thus in some instances pyrite precipitation had ceased before siderite began to grow, presumably because pore-waters had become depleted in sulphate. It is possible that lowering of dissolved sulphate levels by flushing with sulphate-poor meteoric water may actually have helped to induce siderite development.

However other Brent Group siderites have less depleted $\delta^{13}C_{PDB}$ values ($\delta^{13}C_{PDB}$= -2.8 to -7.8‰). suggesting that the bicarbonate supply from iron/sulphate reduction must have been diluted with $\delta^{13}C_{PDB}$ of another origin in order to produce the observed $\delta^{13}C$ values. Primary marine carbonate has a $\delta^{13}C_{PDB}$ signature of ~0‰ and could have been the other end member bicarbonate source. Bioclasts would be the most likely source of primary marine carbonate. Calcite bioclasts are certainly present in most of the marine Formations of the Brent Group, and aragonitic bioclasts are also likely to have been present originally in the sediment upon deposition. Both are unstable in meteoric water, and are thus likely to have dissolved during early diagenesis when meteoric water may have flushed through the sediment. The $\delta^{13}C_{PDB}$ compositions of siderite in the shelly Tarbert Formation are similar to those in the non-marine Ness Formation, hence we have no conclusive evidence that bioclasts were an important source of bicarbonate during diagenesis.

Alternatively, CO_2 from bacterial fermentation reactions ($\delta^{13}C_{PDB}$= +15‰) could have been incorporated to produce the bulk $\delta^{13}C_{PDB}$ value analysed. During shallow burial, both bacterial fermentation and sulphate reduction processes can occur at the same time, although the latter tends to predominate until all available sulphate in the pore-water has been utilised. Hence early diagenetic carbonates could be expected to have $\delta^{13}C_{PDB}$ signatures indicating mixing of bicarbonate from these two sources.

To summarise, the carbon isotopic evidence suggests that siderite in the Brent Group precipitated from a combination of bicarbonate sources; oxidation of organic matter during sulphate reduction was certainly important, while bacterial fermentation, and perhaps shell dissolution also contributed bicarbonate to the system.

2.9.2.2 *Oxygen Isotopes*

Two types of siderite were subjected to stable isotopic analysis in this study; concretionary siderite, and siderite found within the sheets of degrading biotite. These two siderite types were found to have disinctive $\delta^{18}O$ signatures (Figure 21), the siderite forming within the biotites having the lower values.

Oxygen isotope analyses can be utilised to estimate the temperature and isotopic composition of the fluid from which a carbonate mineral precipitated. Using the isotope fractionation equation for siderite of Carothers *et al.* (1988), it is possible to construct a plot relating measured siderite $\delta^{18}O_{SMOW}$ values, precipitation temperature, and the $\delta^{18}O_{SMOW}$ value of the pore-water. However, to ascertain a fluid composition or temperature of precipitation, we must assume either of these two variables in order to calculate the other. Fortunately, we have some constraints on both the growth temperature, and the likely pore-water compositions at the time of precipitation.

2.9.2.3 *Temperature constraints*

The siderite samples analysed in this study occured within calcite cemented horizons exhibiting minus cement porosities of 35-40%. If the calcite has not re-crystallised then these minus cement porosities represent the original porosity of the sediment at the time of calcite cementation. This calcite cement *post-dates* siderite growth, therefore minus cement porosities at the time of siderite growth could have been even higher. Using the general porosity curve for the North Sea (Sclater & Christie 1982) such high primary porosities suggest that the siderite formed at roughly <750m depth, and perhaps within the first few hundred metres of burial (Figure 24). If we assume a geothermal gradient of 35°C/km existed at the time of cementation, then precipitation temperatures of <30°C are suggested. Hence we have an approximate, but useful estimate of the temperature below which siderite precipitation must have occured.

2.9.2.4 *Constraints on pore-water composition*

We also have some constraint on the composition of pore-waters during diagenesis. Because the Brent Group consists of deltaic and

shallow marine facies it is likely that two pore-water types were involved in siderite precipitation during early diagenesis; sea water and meteoric water. Jurassic sea water is held to have had an isotopic composition of $d^{18}O_{SMOW}$= -1.2‰ (Sheppard 1986), while Jurassic meteoric water in the region is thought to have had a $\delta^{18}O_{SMOW}$ composition of around -7‰ (Hudson & Andrews 1987; Hamilton *et al.* 1987).

2.9.2.5 *Oxygen isotopes of concretionary siderite*

The $\delta^{18}O$ values of concretionary siderite are isotopically distinct from those of siderite found within degraded biotites. Using Figure 25 it can be seen that if concretionary siderite precipitated from a marine pore-water it grew at 38-50°C, whereas if the siderite precipitated from a meteoric pore-water it grew at 14-20°C. We know from textural evidence, however, that the siderite is early diagenetic and probably grew at <30°C. Therefore it is unlikely that the siderite grew from purely marine pore-water, because the growth temperatures implied by precipitation from fluids of this isotopic composition are too high for an early diagenetic mineral. However, if the siderite precipitated from a mixed meteoric-marine pore-water then it could have grown at a temperature intermediate between the two end member estimates mentioned above. Hence if concretionary siderite grew at <30°C, then the $\delta^{18}O$ values of concretionary siderite are only consistent with precipitation from a fluid with a meteoric component.

2.9.2.6 *Oxygen isotopes of siderite from within biotite*

The $\delta^{18}O$ of siderite within biotites are generally lower than those of siderite forming concretions. From Figure 26 it can be seen that this type of siderite precipitated at 57-104°C if pore-waters were marine, and at 30-61°C if the pore-waters were meteoric. These temperatures are hence problematic, because the growth temperature estimated from the depth of cementation is <30°C. If these siderites precipitated at 30°C, then growth from pore-waters of $\delta^{18}O_{SMOW}$= -7 to -13‰ is required in order to explain the $\delta^{18}O$ data. If the siderite precipitated at temperatures cooler than 30°C, then even more depleted pore waters are indicated. These pore-water compositions are representative of cold climate, high latitude meteoric waters. Such pore-waters are very unlikely to have been present

during diagenesis of the Brent Group. These siderites are hence anomalously $\delta^{18}O$ depleted considering their low temperature origin and the probable composition of the pore-fluids from which they precipitated.

Normally we would interpret the difference in $\delta^{18}O$ values between the concretions and the siderite within biotites as being evidence that the siderite within the biotites grew at a higher temperature, or from a different water. However, we have good petrographic evidence that the two occurrences of siderite must have precipitated more or less simultaneously, at low temperatures, from the same pore-water.

1) The concretionary siderite has a high minus cement porosity indicating it is of early diagenetic origin. Expanded biotites within which siderite has precipitated are also often preserved within calcite cemented horizons exhibiting high minus cement porosities. This indicates that both types are early diagenetic, and cannot have precipitated at temperatures hotter than about 30°C.

2) Both concretionary siderite and siderite within biotites can show identical intracrystalline compositional zonation. This could indicate that each compositional zone precipitated from the same pore-water in each instance, and probably at roughly the same temperature.

This observation is not confined to siderites from within the Brent Group. Mozley & Wersin (1992), have compiled isotope data from the existing literature showing that many early diagenetic siderites from marine facies are anomalously $\delta^{18}O$ depleted considering they formed at low temperatures and probably from marine pore-waters.

Mozley & Carothers (1992) advance four possible explanations for these problematic $\delta^{18}O$ values.

1) Mixing between marine and meteoric water.
2) Water-sediment interaction.
3) Recrystallisation at higher temperatures.
4) Variable isotopic fractionation.

Mozley & Wersin (1992) deduce that meteoric flushing, and/or water-sediment interaction are the most likely explanations for the anomalous $\delta^{18}O$ data from siderite they have collated.

We shall examine each of these hypotheses in turn in an attempt to find a viable explanation for the depleted $\delta^{18}O$ values seen in the Brent Group siderites from within the biotites.

1) Recrystallisation. If the early diagenetic siderite underwent recrystallisation during deeper burial (i.e. at higher temperatures), then the depleted $\delta^{18}O$ values could be explained. However this is unlikely in the case of the Brent Group siderites because total recrystallisation would have destroyed the elemental zonation which is exhibited by the siderites. Atom-by-atom replacement of siderite could perhaps preserve the crystal zonation while changing $\delta^{18}O$. However it is difficult to see why concretionary siderite would have been less affected by such a replacement process than the siderite within the biotites.

2) Variable isotopic fractionation. Much of the Brent Group siderite is impure. As the siderite-water fractionation factor of Carothers *et al.* (1988) was determined experimentally using very pure siderite samples perhaps it cannot be applied to isotopic data from impure Brent Group siderite. However, as Mozley & Carothers (1992) point out, the variation in isotopic fractionation between pure and impure siderite is likely to be small, and would be in the opposite direction to that required to explain the anomalously depleted $\delta^{18}O$ values.

3) Meteoric-marine mixing. As we have seen earlier, the $\delta^{18}O$ values of the concretionary siderite are consistent with precipitation from mixed marine-meteoric waters at <30°C. However some of the $\delta^{18}O$ values from siderite within biotites are simply too depleted to be explained by mixing of meteoric and marine waters at low temperatures, therefore an alternative explanation must be sought.

4) Water-sediment interaction. Alteration of unstable detrital minerals at low temperatures can preferentially enrich alteration products in $\delta^{18}O$ while depleting reactive waters at the same time (Lohmann & Walker 1989). For example, Lawrence & Gieskes (1981), have proposed that alteration of volcaniclastics to smectite can decrease $\delta^{18}O$ of modern marine pore-waters by up to 8‰ relative to SMOW. No volcanic detritus has been reported in the Brent Group; however detrital micas are observed to have undergone alteration to kaolinite. Pore-waters within the

immediate vicinity of these degrading micas could possibly have become $\delta^{18}O$ depleted. Any siderite which precipitated between the expanded sheets of frayed micas would hence have anomalously low $\delta^{18}O$ values, even though the siderite grew at low temperatures.

Precipitation of siderite may also have lowered pore-water oxygen values. At low temperatures authigenic minerals are enriched in $\delta^{18}O$ relative to the pore-waters from which they precipitate (Lohmann & Walker 1989). If large volumes of authigenic minerals precipitate rapidly, then pore-water $\delta^{18}O$ can be lowered. Moore *et al.* (1992) have attributed depleted $\delta^{18}O$ values from carbonates in modern coastal marsh sediments to be a product of precipitation of large amounts of authigenic carbonates in a closed hydrological system. However this explanation is unlikely to apply to Brent Group siderite, because the elemental zonation seen in both the concretionary and rhombic siderite is identical, indicating that the hydrological system was an open one, with both types of siderite precipitating from the same pore-waters.

Instead we envisage a highly localised hydrological micro-environment existed between the sheets of degrading biotite micas. As biotite became expanded, H^+ ions were attracted to the freshly exposed mica cleavage surfaces. Experimental studies have shown that a pH decrease of up to 2 pH units can occur in the vicinity of these biotite surfaces, due to the attraction of the H^+ ion (Boles & Johnson 1984). This increases the pH of the pore-waters adjacent to the biotite, and hence stabilises the precipitation of carbonate (Boles & Johnson 1984). In alkaline solutions, carbonate precipitation may be rapid, and so kinetic (i.e. non-equilibrium) isotope fractionation between the carbonate and the water can occur (Macleod 1990; O'Neil & Barnes 1971). This would produce carbonates which are anomalously $\delta^{18}O$ depleted relative to the $\delta^{18}O$ of the pore-waters from which they precipitated (Macleod 1990; O'Neil & Barnes 1971).

The amount of kinetic fractionation seems to have varied greatly, judging by the wide scatter in siderite $\delta^{18}O_{PDB}$ values seen (Figure 20). Samples occuring in the same horizon, and only 40cm apart in the core, can show widely variable $\delta^{18}O_{PDB}$ values. For example, samples A30 and A31 from the Rannoch Formation of the Dunlin oilfield (Well 211/23-1), have near identical $\delta^{13}C_{PDB}$ values of -15.7 and -15.5‰ respectively, yet one has a $\delta^{18}O_{PDB}$ value of -6.7 and the other $\delta^{18}O_{PDB}$ of -13.0‰. These siderites have identical elemental composition and BSE zonation, and

both are enclosed within early diagenetic calcite cement with high minus-cement porosities. The 6‰ variation in $\delta^{18}O_{PDB}$ seen in these samples cannot reasonably be explained by growth at higher temperatures, because petrographic evidence suggests they grew at roughly the same time, from a pore-water of the same elemental composition. Therefore kinetic isotope fractionation during siderite growth is the most likely explanation for these puzzling $\delta^{18}O$ values.

In summary concretionary siderites probably provide reliable palaeotemperature information, and are consistent with growth from mixed marine-meteoric pore-waters at <30°C. Some of the siderite from within degrading biotites did not precipitate in isotopic equilibrium with the pore-water, and so their $\delta^{18}O$ signatures cannot reliably be used to determine growth temperatures.

2.9.3 Thermodynamic Stability of Siderite

According to Berner (1971) pyrite and not siderite should be the thermodynamically stable Fe^{2+} mineral in sea water (Figure 27). For siderite to form Eh must be low and pore-waters depleted in sulphate. This is unlikely in sea water which contains abundant dissolved sulphate. This apparently explains why siderite has been observed to precipitate in many deltaic, salt marsh and bog sediments at the present day (Postma 1981; Pye 1984), but has not yet been described from modern marine settings. If Berner is correct, then our observation that diagenetic siderite in the Brent Group is present in marine sediments is problematic. However siderite is definitely found in sediments of undoubted marine origin other than the Brent Group (Boles 1987; Tasse & Hesse 1984; Mozley 1988), hence the observational evidence apparently seems to contradict Berner's thermodynamic predictions.

How then can the geological evidence and the thermodynamic data be reconciled? There are at least three possible explanations.

1) It is possible for marine sediments to have their original marine pore-fluids displaced by throughflow of meteoric water. This would decrease dissolved sulphate levels and could allow precipitation of siderite. This is a feasible explanation for the occurrence of siderite within marine facies of the Brent Group, as they were deposited near to land and not far from an area of supposed meteoric recharge (Haszeldine *et al.* 1992).

2) If a marine sediment is rapidly buried then pore waters may be cut off from the overlying sea water which acts as a sulphate reservoir. If sulphate reduction utilises all the sulphate present in the pore-water then pyrite precipitation will cease and siderite growth commence, providing abundant reactive iron and organic nutrients are present in the sediment (Curtis & Coleman 1986). Hence sedimentation rate will control whether siderite or pyrite precipitates. This however, is a controversial issue, because sulphate reduction rates are observed to increase rather than decrease with high rates of sedimentation (Berner 1978).

3) Perhaps Berner's stability diagram cannot be applied to naturally occurring sediments. Maynard (1983) has demonstrated that if primary phases such as $Fe(OH)_3$ and FeS are used in place of haematite and pyrite then siderite does indeed have a small stability field under normal sea water conditions (Figure 28). These phases are the first formed iron compounds in sediments and are later transformed into stable minerals (Berner 1971 Ch10), hence their use in stability diagrams is perfectly admissable.

Taken as a whole, the available evidence suggests that siderite can indeed form in both marine and non-marine environments, although in general it is more likely to be thermodynamically stable in meteoric or brackish pore-waters, hence explaining why it is most common in non-marine sediments. However, precipitation of siderite from marine pore waters is not necessarily inconsistent with thermodynamics as Berner (1971) maintained.

2.9.4 Preferred Explanation for the Siderite Zonation

As we have seen siderite is a very early diagenetic cement in the Brent Group and the compositional zoning it displays is almost certainly a record of changes in pore fluid composition during shallow burial. The near shore and deltaic sediments of the Brent Group are likely sites of mixing between depositional marine pore-waters, and meteoric fluids flowing in from the nearby landmass. Furthermore, because sediments during shallow burial are highly porous there is great potential for flow of fluid through the aquifer, and so fluid/rock ratios will tend to be high. Fluid flow will be particularly important in the highly permeable sandy

facies which typify the Brent Group. It is thus likely that during early diagenesis pore fluid chemistry was influenced by the advance and retreat of the Brent delta system, for during progradation of the clastic wedge, meteoric fluids could flush through aquifers and displace depositional marine pore fluids, while during transgression marine pore fluids might be permitted to re-invade.

Our preferred explanation for the zonation seen in Brent Group siderite from the Rannoch, Etive, Ness and Tarbert Formations, is as follows.

Zone R1. (Figure 29) This siderite precipitated from water of meteoric composition and is present in Rannoch, Etive and Ness Formations. However, Zone R1 is very rare and frequently absent from the Tarbert Formation. This suggests that Zone R1 may have precipitated from a meteoric water which flushed the Brent Group mainly during the advance of the delta system, when the Rannoch, Etive and Ness Formations were being deposited.

Zone R2. (Figure 30) This zone compositionally appears to have formed from marine water, and is present in all four Formations. Zone R1 (meteoric) is generally absent from the Tarbert Formation, whereas Zone R2 is well developed. This suggests that Zone R2 could have precipitated during the marine transgression which drowned the Brent delta and deposited the Tarbert Formation. Relative sea level rise would allow marine pore-fluids to enter all four Formations and hence precipitate siderite with a marine composition.

Zone R3. (Figure 31). This zone is also common to all four Formations (Rannoch, Etive, Ness and Tarbert). It may have precipitated during slightly deeper burial conditions from a mixed marine and meteoric pore water of compactional origin. Another possibility is that the more ferroan nature of Zone R3 compared to Zone R2 is due to a renewed influx of meteoric water into the aquifer following marine transgression. This could have occurred during uplift and subaerial exposure of the Brent Group in the late Jurassic. Alternatively selective removal of Ca during precipitation of Zone R2 may have decreased the ratio of Ca/(Fe+Mg) in the pore fluids and promoted the precipitation of the more Fe and Mg rich Zone R3. However this latter explanation is only possible during closed system

diagenesis, and this may not be a realistic scenario during shallow burial of highly permeable sediments.

Siderite in the Broom Formation does not show the chemical zonation we observe in siderites from overlying Formations. This indicates that the Broom Formation was an isolated aquifer during siderite cementation. The impure composition of Broom Formation siderite suggests it precipitated from marine pore-waters. Thus it seems that the Broom Formation was not significantly flushed by meteoric water during early diagenesis, perhaps because it consisted of less permeable facies, and so retained its depositional marine pore-waters to a greater extent.

2.9.5 Evidence for changing hydrologies during siderite growth

We deduce that changes in pore-fluid chemistry related to the advance and retreat of the Brent delta system produced the observed siderite zonation. There is a great deal of evidence to support our hypothesis.

1. The rarity or absence of Zone R1 (meteoric) from the Tarbert Formation supports our hypothesis that Zone R2 (compositionally marine) precipitated during times of marine transgression.

2. Inter-zonal dissolution events, and sharp changes in siderite composition across zone boundaries, suggest that different pore-fluids were responsible for precipitating the various cement generations.

3. Our interpretation involving changing hydrologies is consistent with the siderite elemental analyses which suggest a change in pore-water chemistry from meteoric (Zone R1), to marine (Zone R2), to brackish water (Zone R3).

4. Oxygen isotopic data from siderite concretions are consistent with precipitation from meteoric or brackish pore-waters at low temperatures.

The simple fact that non-marine and marine facies in the Brent Group have the same siderite zonation suggests that during siderite growth these sandstones were not isolated aquifers. Instead the geochemical system was an open one, in which cross-Formational fluid

flow was occurring, at least between the Rannoch, Etive, Ness and Tarbert Formations. The Broom Formation however, remained a confined aquifer. Hence the zonation also gives an indication of the palaeo-connectivity of sand bodies at the time of siderite cementation.

2.9.6 Alternative hypotheses for the Siderite Zonation

Alternative interpretations for the siderite zonation are superficially attractive but upon closer examination are found to have several serious drawbacks.

2.9.6.1 *Contribution of Fe and Mg ions from degrading biotites*

Some siderite in the Brent Group is found within degrading biotite grains. We have interpreted the elemental zonation seen in this siderite to be representative of major fluctuations in pore-fluid composition caused by the influx of meteoric and marine pore-waters. However, it is likely that biotite has contributed at least some Fe and Mg to the adjacent siderites. It is therefore vital to assess to what extent the zonation reflects only very local changes in fluid chemistry due to the proximity of degrading biotites, rather than wholesale influx of pore-fluids with different compositions. Most of the evidence suggests that degradation of biotites was not the principal control on siderite distribution or compositional zonation.

1) $^{87}Sr/^{86}Sr$ ratios of Brent Group siderites indicate a Sr contribution from degrading detrital silicates, plus sea water or dissolved shell debris (Haszeldine *et al.* 1992). This suggests that the ions required for siderite precipitation did not come from the degradation of silicates alone.

2) An instance in which siderite geochemistry has been strongly controlled by the degradation of silicates is described by Claeys and Mount (1991). They studied carbonate inclusions within expanded biotites from the Great Valley Group, California. Biotite expansion occurred during late diagenesis when low fluid/rock ratios allowed biotite degradation to influence the chemistry of pore fluids, and thus produce the compositional variations observed within the carbonate inclusions. The inclusions are zoned and have a calcitic core and an Fe-rich sideritic rim. Siderite occurrence is

restricted exclusively to within the cleavage sheets of expanded biotites. All the above observations are in complete contrast with the features of siderite authigenesis seen in the Brent Group. This lack of similarity between Brent Group and the Great Valley Group siderite suggests that the Brent Group siderite did not form in a closed geochemical system, and that the siderite zonation and distribution was not controlled by biotite degradation.

3) Although some Fe and Mg ions released from the biotite probably became incorporated within the siderite, it is unlikely that biotite degradation controlled pore water chemistry, and hence produced the siderite zonation observed. Biotite alteration would release some Fe and Mg ions, but the significant amounts of Ca present within the siderite must be derived from another source. It is probable that during early diagenesis there were many sources of Fe available for incorporation within siderite. As well as the Fe dissolved within meteoric pore-waters, Fe would also be present within detrital hematite, goethite, amorphous hydroxides and clay vermiculites. The fact that both pyrite and siderite are found disseminated throughout the sediment proves that abundant Fe^{2+} was available during shallow burial of the Brent Group. Siderite is not confined to within biotites alone, but also occurs in the form of concretions and sphaerosiderites. Thus proximity to biotites is unlikely to be the major factor controlling siderite distribution or zonation.

4) Siderite from the Brent Group probably precipitated in degrading biotites not because they were the only source of Fe and Mg ions, but because the expanded biotites were favourable sites for carbonate nucleation. Boles and Johnson (1984) have experimentally demonstrated that H^+ cations are attracted to biotite surfaces resulting in an increase in the pH of the adjacent pore-water. This leads to the precipitation of carbonate phases upon these exposed surfaces. Also the transformation of biotite mica to kaolinite, which has also been observed in the Brent Group samples studied, is a reaction which consumes H^+ ions, increases pH and likewise stabilises carbonate minerals (Bjorlykke *et al.* 1979).

5) Evidence for inter-zonal dissolution, and sharp rather than diffuse changes in composition across the siderite growth zones suggests that chemically distinct fluids which changed rapidly were responsible for the

zonation.

To conclude this section, the Fe and Mg necessary for siderite precipitation came from a variety of sources, therefore biotite degradation alone did not produce the zonation observed. The siderite formed during early diagenesis, when fluid/rock ratios were relatively high, hence the overall control on composition was more likely to have been the chemistry of the pore fluid flowing through the sediment, rather than very localised pore scale effects.

2.9.6.2 *Contribution of Ca and Mg ions from dissolved marine carbonate*

The change in siderite composition from an Fe rich core (Zone R1) to a more Ca and Mg rich rim (Zones R2&3) could indicate that the contribution of ions from the dissolution of bioclasts increased with time. Indeed bioclasts, especially if they are aragonitic, are susceptible to dissolution in meteoric water, and are thus a feasible source of Ca and Mg for siderite precipitation. $^{87}Sr/^{86}Sr$ of Brent Group siderites also indicate a Sr contribution from degraded detrital silicates, plus dissolved shell debris or sea water (Haszeldine *et al.* 1992). Bioclasts are certainly present in some of the samples studied from the Rannoch and Tarbert Formations, however the $\delta^{13}C_{PDB}$ of siderite from these samples does not indicate that dissolution of shells was a major source of bicarbonate during siderite precipitation. Indeed the $\delta^{13}C_{PDB}$ of siderite from the marine Tarbert Formation are generally similar to the values of siderite from the non-marine Ness Formation. In addition, if the Ca and Mg rich siderite is produced by bioclast dissolution, it is difficult to see why zones R2 and R3 occur in the non-marine delta-top sediments of the Ness Formation, which contain no shell debris.

The above inconsistencies suggest that the siderite zonation observed cannot simply be explained by variations in the amount of shell material dissolving. While it is possible that bioclasts provided some of the Ca and Mg ions for siderite growth, shell dissolution does not seem to have controlled pore-water chemistry. It is also unlikely that dissolution of detrital plagioclase provided Ca for siderite growth, because most feldspar dissolution in the Brent Group occured after siderite precipitation (Giles *et*

al. 1992). It thus seems most probable that the source of Ca and Mg ions for siderite precipitation was sea water. $^{87}Sr/^{86}Sr$ of Brent Group siderites (Haszeldine *et al.* 1992), also suggest mixing between Sr derived from degrading detrital silicates, and Sr in sea water. Marine pore-waters could easily have percolated through the highly permeable sediments of the Brent Group when the delta complex was drowned during sea level rise. This influx of Ca and Mg ions triggered the precipitation of the impure Zone R2 siderite.

2.9.7 Uses of siderite crystal zonation in diagenetic studies

We have seen how siderite crystal zonation in the Brent Group has recorded fluctuations in pore-fluid composition during early diagenesis. There is no evidence that this early diagenetic siderite has undergone any dissolution or recrystallisation, even upon burial to depths of 3km or more. Furthermore the elemental composition of this siderite provides an indication of the origin of the pore-waters from which it precipitated. It thus seems likely that the technique has many potential applications in diagenetic studies, if used with care and in combination with petrographic and isotopic work. Some possible applications are discussed below.

1) The distribution of various siderite cement zones can indicate whether or not different sand bodies were connected aquifers at the time of cementation. This may be useful information when modelling oil migration pathways and fluid flow cementation in reservoir sandstones. This data holds promise for integration into sequence stratigraphic frameworks.

2) It may be possible to use siderite zonation in the correlation of facies between wells.

3) The elemental composition of siderite could assist in the interpretation of isotopic data by suggesting likely pore-fluid types during cementation. This constraint on fluid origin is particularly useful when interpreting isotopic information from carbonates, because other constraints such as

palaeotemperature and salinity information from fluid inclusions may be unreliable, due to problems with stretching and leakage of the inclusion (Barker & Goldstein 1991).

However, the use of siderite elemental composition to pinpoint pore-fluid type should be a technique used only with caution. This is because siderite composition can also be influenced by dissolution of detrital minerals and shell material in the host sediment, or by import of ions from external sources such as shales. We would expect such influences to be particularly prevalent during late diagenesis, because by the time a sediment has become deeply buried connate pore-fluids will have had their solute chemistry extensively altered by water-rock interaction.

2.10 CONCLUSIONS

1) The chemical zonation seen within early diagenetic siderite from the Rannoch, Etive, Ness and Tarbert Formations of the Brent Group reflects changes in pore-fluid chemistry during cementation from meteoric (Zone R1), to marine (Zone R2) to brackish water (Zone R3). The Broom Formation shows four growth zones which are compositionally distinct from those in the overlying Formations, indicating that this was a different aquifer.

2) Meteoric siderite (Zone R1) precipitated during the advance of the Brent delta system when meteoric water flushed through the sandstones and expelled depositional pore-waters. Marine siderite (Zone R2) grew when transgression allowed sea water to re-invade the sandstones. A mixed meteoric-marine water of compactional origin probably precipitated Zone R3.

3) Oxygen isotopic data are problematic, because within the expanded biotites, kinetic fractionation of oxygen between water and siderite has occurred, hence determination of palaeotemperatures is difficult. However in the case of concretionary siderite, equilibrium isotopic fractionation has occurred, and $\delta^{18}O$ values are consistent with precipitation from meteoric or brackish pore-waters at temperatures of <30°C. Carbon isotopes indicate mixed bicarbonate sources during siderite authigenesis, principally

oxidation of organic matter during sulphate reduction and bacterial fermentation.

4) Siderite elemental composition can pinpoint the origin of marine or meteoric pore-waters during cementation, particularly if the siderite formed during early diagenesis when pore-fluid composition was least likely to have been altered by water-rock interaction.

2.11 ACKNOWLEDGEMENTS

The staff of Isotope Geosciences Unit in the S.U.R.R.C. are thanked for their assistance during isotopic analysis, particularly Alison McDonald. At Glasgow University, Douglas Maclean, Dugie Turner, and Peter Ainsworth are thanked for their photographic, geochemical and SEM expertise respectively. Greg Samways (Badley Ashton and Associates) kindly provided some siderite samples. Mark Osborne was supported by a NERC grant, while the S.U.R.R.C. is supported by NERC and the Scottish Universities.

2.12 REFERENCES

Barker, C.E., and Goldstein, R.H., 1991, A fluid inclusion technique for determining maximum temperature in calcite and its comparison to the vitrinite reflectance geothermometer. *Geology*, **18**, p.1003-1006.

Berner, R. A., 1971, Principles of chemical sedimentology, New York, McGraw Hill, 240 p..

Berner, R.A., 1981, Kinetics of weathering and diagenesis. *In Kinetics of geochemical processes*, Reviews in Mineralogy 8, Min. Soc. Am.

Bjorlykke, K., Elverhoi, A., & Malm, O.A., 1979, Diagenesis in Mesozoic sandstones from Spitzbergen and the North sea-a comparison. *Geologische Rundschau*, **68**, p.1152-1171.

Bjorlykke, K., Nedkvitne, T., Ramm, M., Saigal, G.C., 1992, Diagenetic processes in the Brent Group (Middle Jurassic) reservoirs of the North Sea ; an overview. In Morton, A. C., Haszeldine, R. S., Giles, M. R., & Brown, S., (Eds), *Geology of the Brent Group.* Geological Society of London, Bath UK. p. 263-288.

Boles, J. R., 1987, Six million year diagenetic history, North Coles Levee,

san Joaquin Basin, Caliornia, in Marshall, J.D., ed., *Diagenesis of sedimentary sequences*: Geological society of London Special Publication, p.191-200.

Boles, J.R., Johnson, K.S., 1984, Influence of mica surfaces on pore-water pH. *Chem. Geol.*, **43**, p.303-317.

Brint, J. F., 1989, Isotope diagenesis and palaeofluid movement: Middle Jurassic Brent sandstones, North Sea D. Phil. Thesis University of Strathclyde, Scotland, 288 p.

Carothers, W.W., Landford, H.A., Rosenbaur, R.J., 1988, Experimental oxygen isotope fractionation between siderite-water and phosphoric acid liberated CO_2-siderite. *Geochimica et Cosmochim. Acta*, **52**, p.2445-2450.

Claeys, P.F., & Mount, J.F., 1991, Diagenetic origin of carbonate, sulphide, and oxide inclusions in biotites of the Great Valley Group (Cretaceous), Sacramento Valley, California. *Journ. Sed. Pet.*, **61**, p.719-732.

Curtis, C.D., & Coleman, M.L., 1986, Controls on the precipitation of early diagenetic calcite, dolomite, and siderite concretions in complex depositional systems, in Gautier, D.L., ed., *Roles of organic matter in sedimentary diagenesis*, Soc. Econ. Pal. & Miner. Spec. Publ., 38, p.23-33.

Drever, J. I., 1982, The geochemistry of natural waters, Englewood Cliffs, New Jersey, Prentice-Hall, Inc., 388p.

Garrels, R.M. & Christ, C.L., 1965, Solutions, Minerals & Equilibria, Harper & Row publishers Inc., New York.

Gautier, D.L., 1982, Siderite concretions; indicators of early diagenesis in the Gammon Shale (Cretaceous). *Jour. Sed. Pet.*, **52**, p.859-871.

Giles, M.R., Stevenson, S., Martin, S. V., Cannon, S. J. C., Hamilton, P. J., Marshall, J. D., & Samways, G. M., 1992, The reservoir properties and diagenesis of the Brent Group; a regional perspective. In Morton, A. C., Haszeldine, R. S., Giles, M. R., & Brown, S., (Eds), *Geology of the Brent Group*. Geological Society of London, Bath UK. p. 289-327.

Given, R.K., & Wilkinson, B.H., 1985, Kinetic control of morphology, composition, and mineralogy of abiotic carbonates. *Jour. Sed. Pet.* **55**, p.109-119.

Gould, K.W., & Smith, J.W., 1979, The genesis and isotopic composition of carbonates associated with some Permian Australian coals.

Chemical Geology, v.**24**, p.137-150.

Hamilton, P.J., Fallick, A.E., Macintyre, R.M., & Elliott, S.,1987, Isotopic tracing of provenance and diagenesis of lower Brent Group sands, North Sea. In Brooks, J., & Glennie, K.W., (eds.), *Petroleum Geology of NW Europe*, Graham & Trotman, London, p.939-949.

Haszeldine, R. S., Brint, J. F., Fallick, A.E., Hamilton, P. J., & Brown, S., 1992, Open and restricted hydrologies in Brent Group diagenesis: North Sea. In Morton, A. C., Haszeldine, R.S., Giles, M. R., & Brown, S.(Eds.), *Geology of the Brent Group*. Geological Society of London, Bath UK. p. 401-419.

Have, T.T., Heijnen, W., 1985, Cathodoluminescence activation and zonation in carbonate rocks; an experimental approach. *Geol. en Mijnbouw*, **64**, p.297-310.

Hudson, J.D., & Andrews, J.E., 1987, The diagenesis of the Great Estuarine Group, Middle Jurassic, Scotland. In Marshall, J.D., (ed), *Diagenesis of sedimentary sequences*. Geol. Soc. Lond. Spec. Publ., 36, p.259-276.

Lawrence, J.R., & Gieskes, J.M., 1981, Constraints on water transport and alteration in the oceanic crust from isotopic composition of pore-water. *Journ. Geophys. Res.*, **86**, p.7924-7934.

Lohmann, K.C., & Walker, J.C.G., 1989, The oxygen isotope record of Phanerozoic abiotic marine calcite cements. *Amer. Geophys. Union*, p.319-322.

Macleod, G., 1990, An isotopic and mineralogical investigation of concrete decay, (PhD thesis), Strathclyde University, Scotland, U.K.

Matsumoto, R., & Iijima, A., 1981, Origin and diagenetic evolution of Ca-Mg-Fe carbonates in some coalfields of Japan. *Sedimentology*, **28**, p.239-259.

Maynard, J.B., 1983, Geochemistry of sedimentary ore deposits, Springer Verlag, New York, Inc. 304p.

McCrea, J.M., 1950, On the isotope chemistry of carbonates and the palaeotemperature scale. *Journ. of Chem. Phys.*, **18**, p.849-857.

Meyers, W.J., 1978, Carbonate cements: their regional distribution and interpretation in Mississippian limestones of S.W. Mexico. Sedimentology, 25, p.371-400.

Moore, S.E., Ferrell, R.E., Aharon, P., 1992, Diagenetic siderite and other ferroan carbonates in a modern subsiding marsh sequence.

Journ. Sed. Pet., **62**, p.357-366.

Mozley, P.S., 1988, Petrography and diagenesis of the Sag river and Shublik Formations in the National Petroleum Reserve, Alaska, and topics in siderite geochemistry (PhD thesis), Santa Barbera, California, 252p.

Mozley, P.S.,1989, Relation between depositional environment and the elemental composition of early diagenetic siderite. *Geology*, **17**, p.704-706.

Mozley, P.S., & Carothers, W.W., 1992, Elemental and isotopic compositions of siderite in the Kuparuk Formation, Alaska, *Journ. Sed. Pet.*, **62**, p.109-129

Mozley, P.S., & Wersin, P., Isotopic composition of siderite as an indicator of depositional environment. *Geology*, **20**, p.817-820.

O'Neil, J.R., & Barnes, I., 1971, Carbon and oxygen isotope compositions of some freshwater carbonates associated with ultramafics and serpentinites, western U.S.A. *Geochimica et Cosmochimica Acta*, **35**, p.687-697.

Pearson, 1985, Some chemical aspects of diagenetic concretions from the Westphalian of Yorkshire, England. *Chem. Geol.*, **48**, p.231-241.

Postma, D., 1981, Formation of siderite and vivianite and the pore-water composition of a recent bog sediment in Denmark. *Chem. Geol.*,**31**, p.225-244.

Pye, K., 1984, SEM analysis of siderite cements in intertidal marsh sediments Norfolk, England, *Marine Geology*, **56**, p.1-12.

Richards, P.C., An introduction to the Brent Group, a literature review. In Morton, A. C., Haszeldine, R.S., Giles, M. R., & Brown, S.(Eds.), *Geology of the Brent Group*. Geological Society of London, Bath UK. p. 15-26.

Rosenbaum, J., & Sheppard, S.M.F., 1986, An isotopic study of siderites, dolomites, and ankerites at high temperatures. *Geochim. et Cosmochim. Acta*, **50**, p.1147-1150.

Sclater, J.G., & Christie, P.A.F., 1982, Continental stretching: an explanation of the post-mid-Cretaceous subsidence of the central North Sea Basin. *Journ. Geophys. Res.* **85**, p.3711-3739.

Sheppard, S.M.F., 1986, Characterisation and isotopic variations in natural waters. In Miner. Soc. Am. reviews in mineralogy, **16**, p.165-183.

Tasse, N., & Hesse, R., 1984, Origin and significance of complex diagenetic carbonates in Cretaceous black shales of the western Alps.

Journ. Sed. Pet., **54**, p.1012-1027.

Veizer, J., 1983, Chemical diagenesis of carbonates, in Arthur, M.A., (Ed.), *Stable isotopes in sedimentary geology*, Soc. Econ. Pal. Miner. Short Course 10, p.3-1-3-10

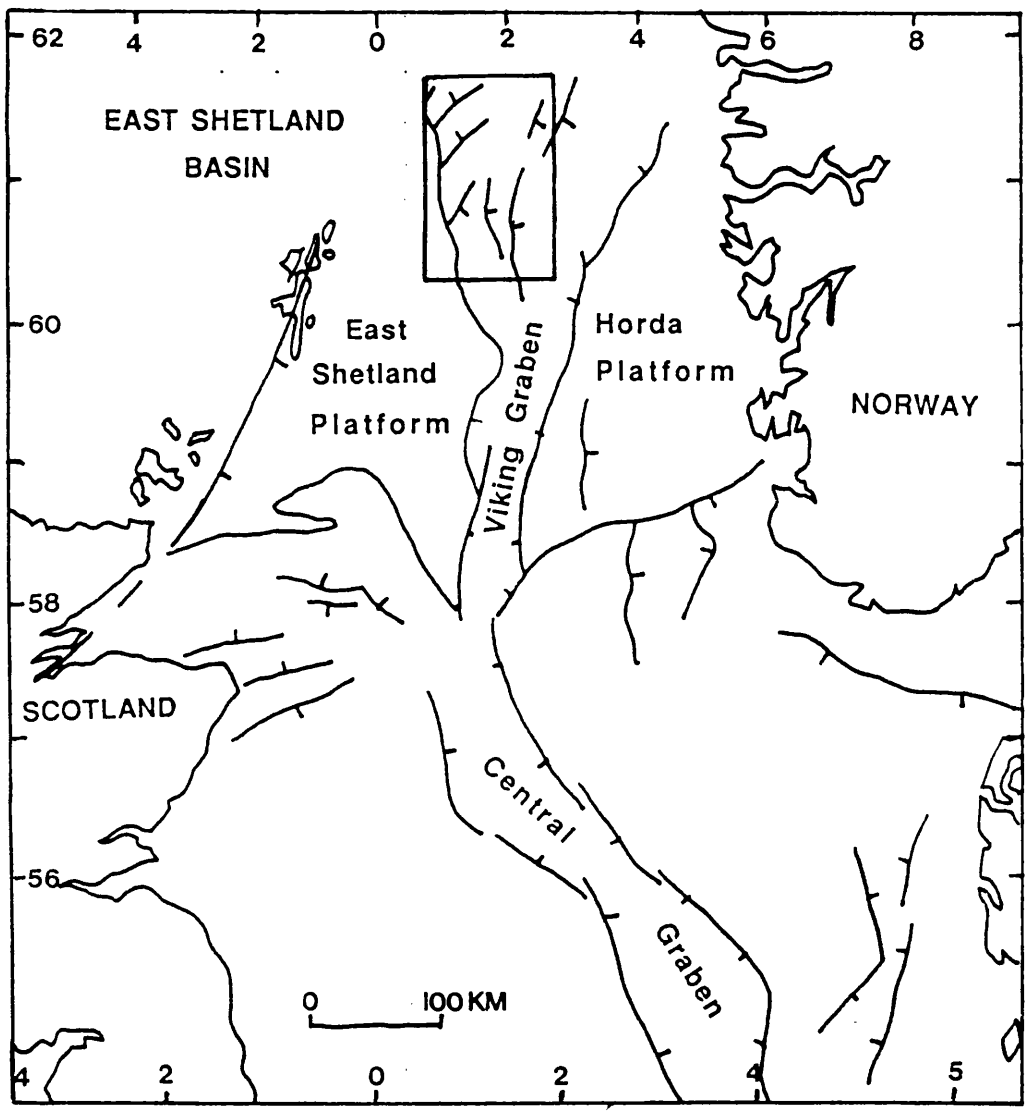

Fig 1. Map showing the location of the East Shetland Basin in the North Sea.

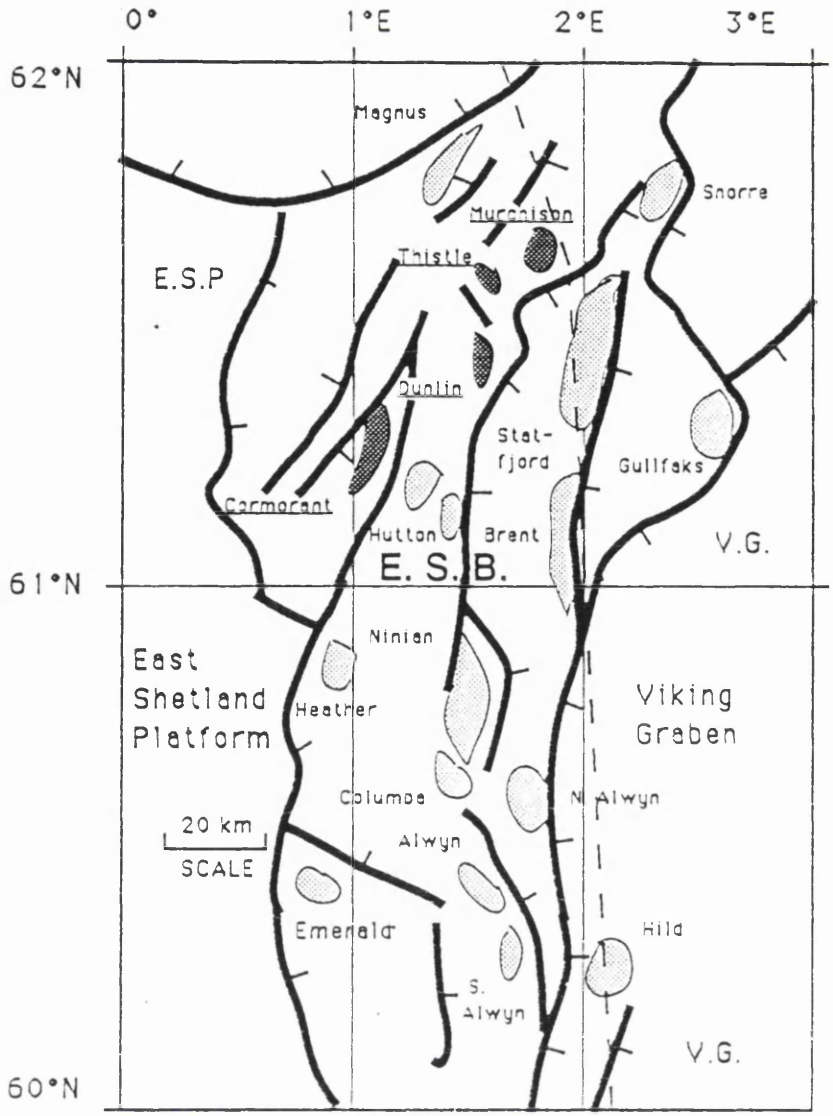

Fig 2. Location map showing the position of the Dunlin, Thistle, Murchison and Cormorant oilfields studied.

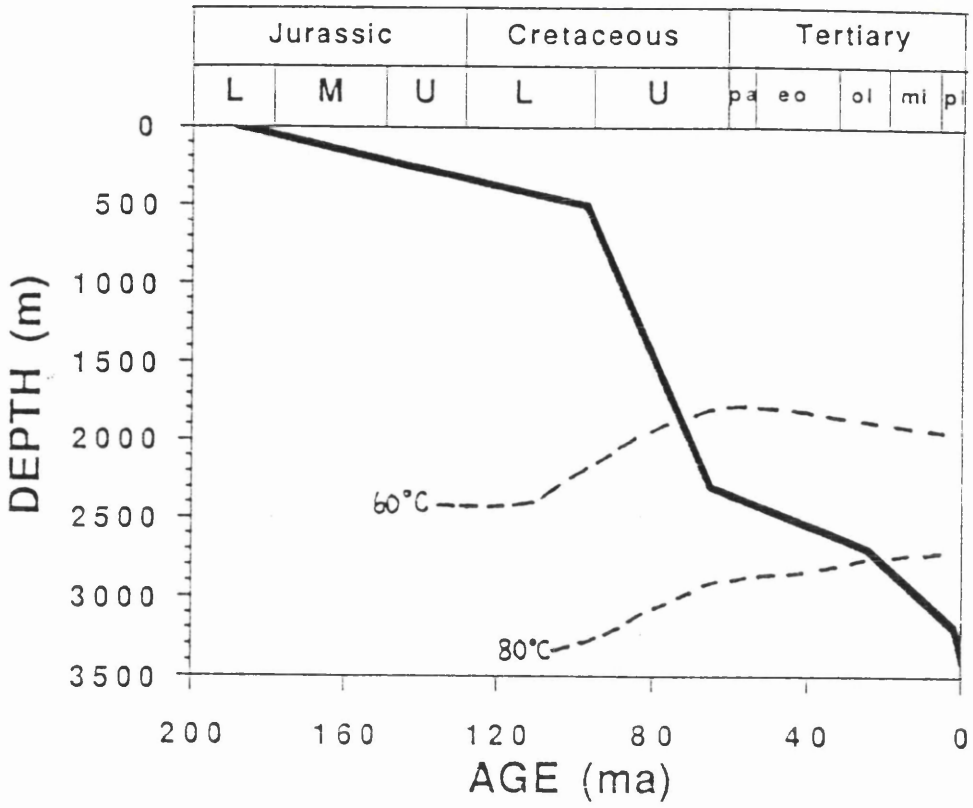

Fig 3. Schematic burial curve for the oilfields studied, redrawn from Brint (1989).

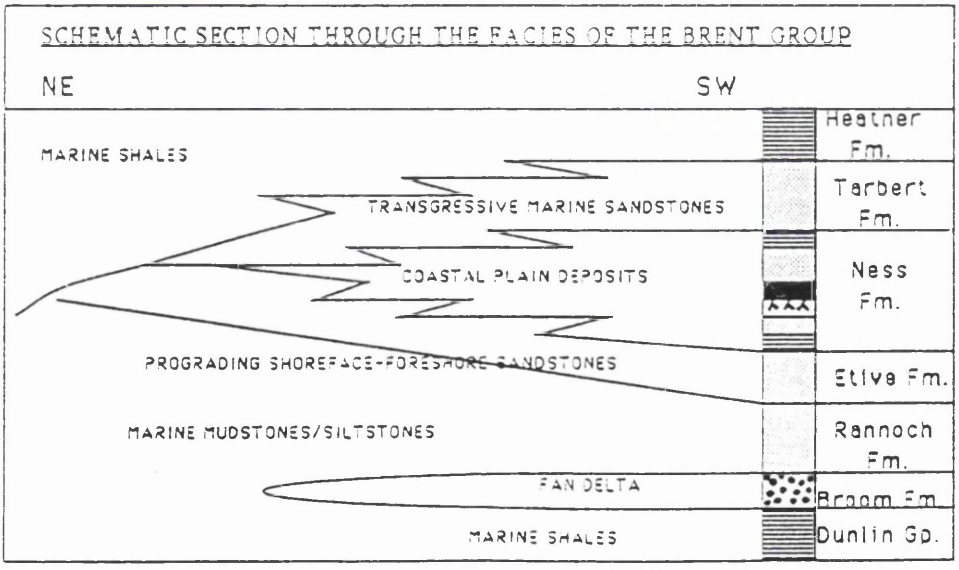

Fig 4. Schematic SW-NE section through the Brent Group showing the relative geometry of the Formations and their possible depositional environments (modified from Richards 1992).

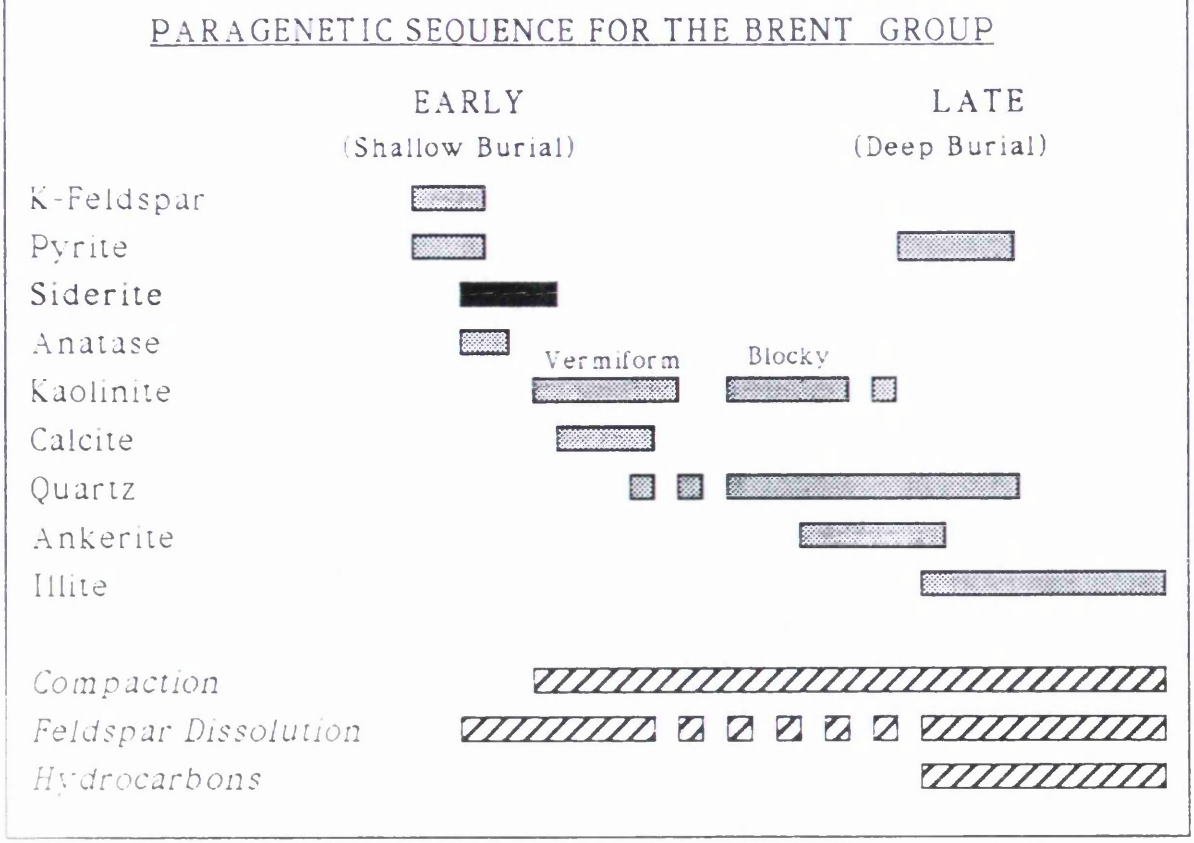

Fig 5. Generalised paragenetic sequence for the Brent Group in the Thistle, Murchison, Dunlin and Cormorant oilfields.

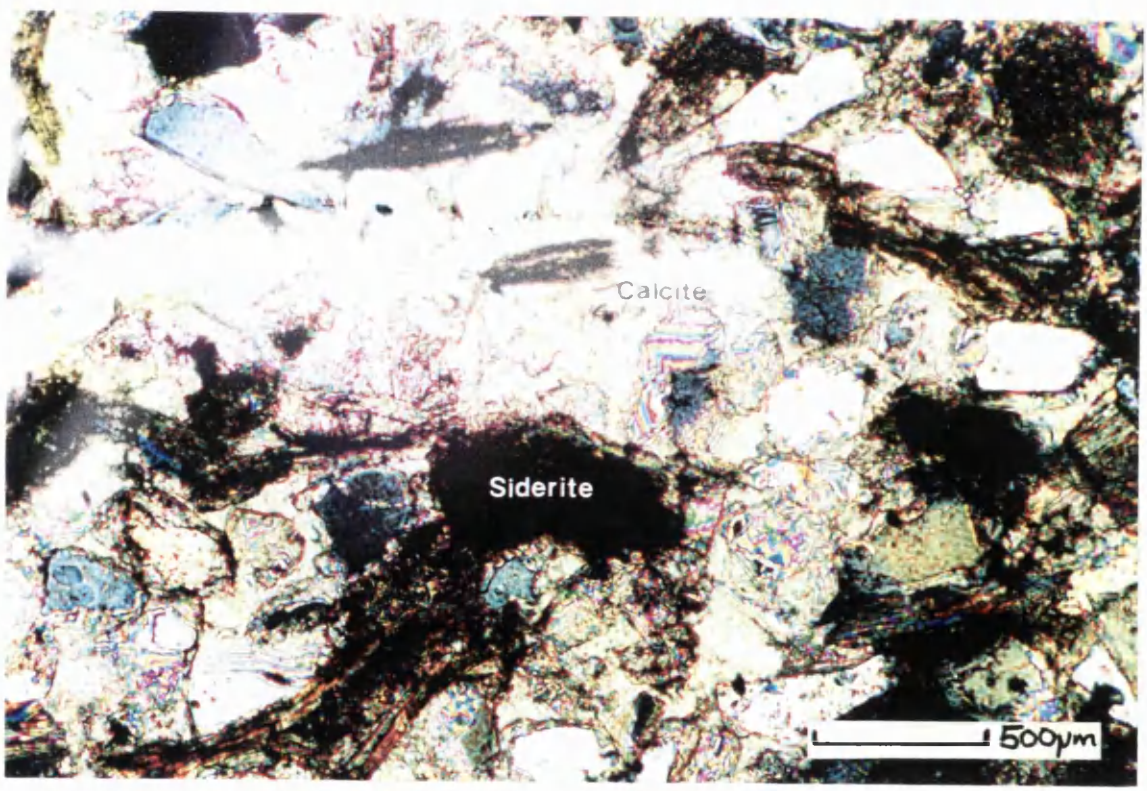

Fig 6. Siderite (dark brown) occurs within calcite cemented horizons exhibiting high minus cement porosities of 35-40%. This indicates that siderite is an early diagenetic mineral which formed during shallow burial. Transmitted light view, crossed polars. Sample A30, Dunlin oilfield, Rannoch Formation, Well 211/23-1, 9105.1 ft TVD.

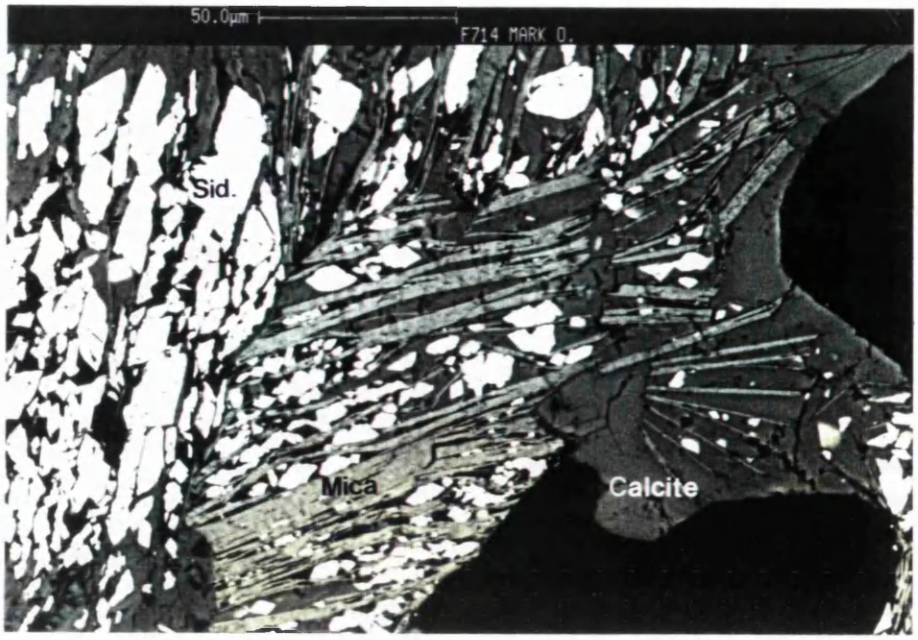

Fig 7. Siderite (bright) frequently occurs between the sheets of expanded biotite micas. BSE image, sample A30, Dunlin oilfield, Rannoch Formation, Well 211/23-1, 9105.1 ft TVD.

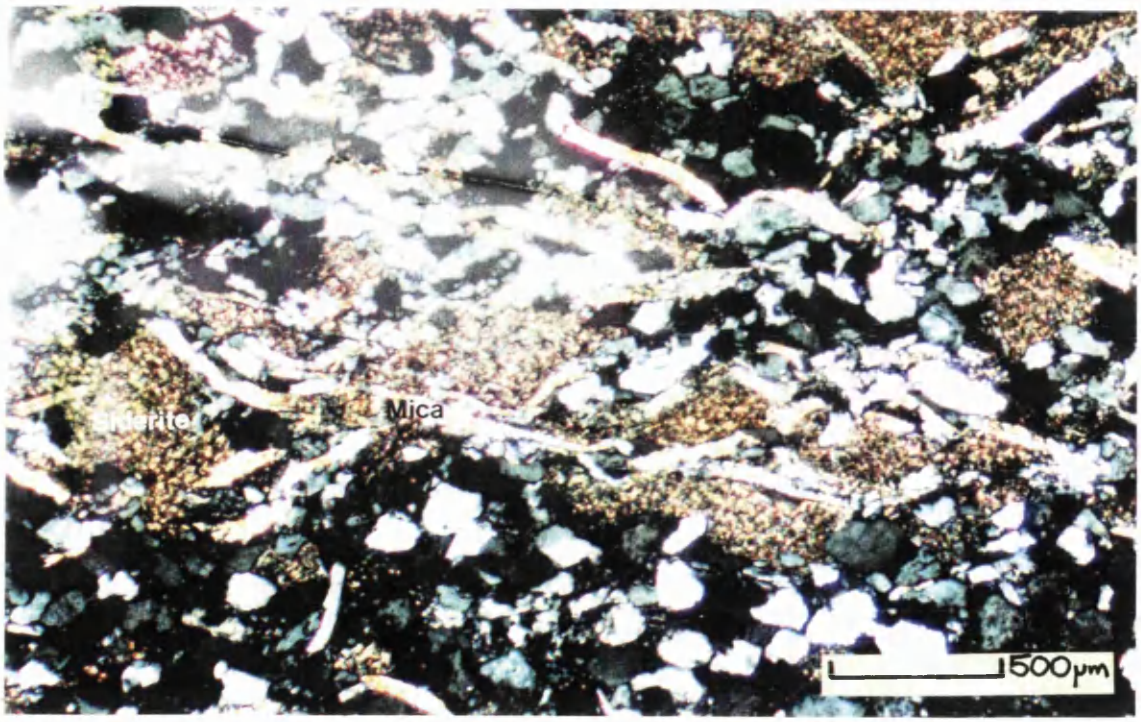

Fig 8. Siderite is particularly common within horizons which are mica-rich. Transmitted light view, crossed polars. Sample A8, Dunlin oilfield, Rannoch Formation, Well 211/23-1, 9044.6 ft TVD.

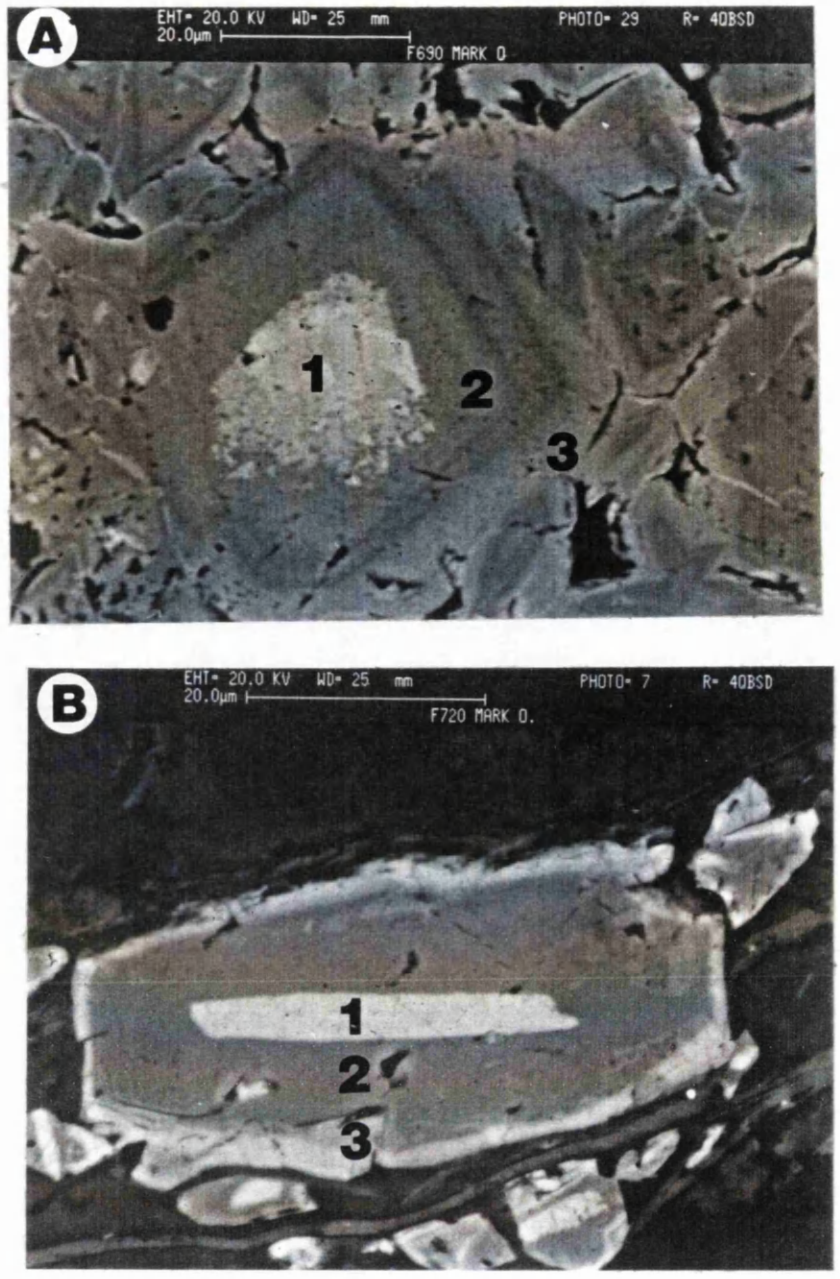

Fig 9. Siderite crystals within the Rannoch, Etive and Ness Formations show a well developed, threefold compositional zonation using BSE imaging.

a) Siderite crystal from a concretion showing three zones of cement. Zone R1 shows evidence of dissolution prior to the precipitation of the euhedral Zones R2 and R3. Sample B4, Dunlin oilfield, Ness Formation, Well 211/23-2, 9250.5 ft TVD.

b) Siderite crystal from within an expanded biotite mica showing three distinct compositional zones (R1, R2 and R3). Sample A31, Dunlin oilfield, Rannoch Formation, Well 211/23-1, 9105.5 ft TVD.

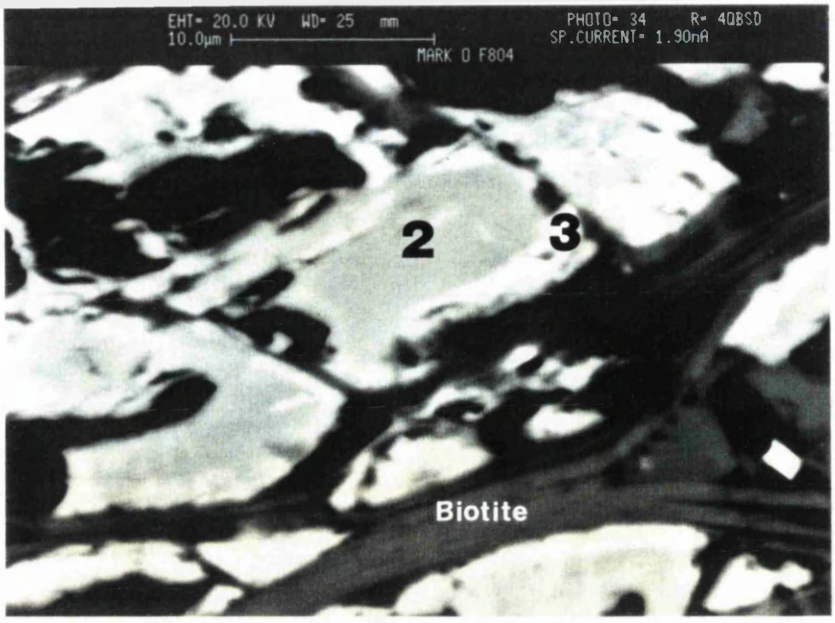

Fig 10. Siderite crystals within expanded biotites from the Tarbert Formation show BSE Zones R2 and R3 only. Zone 1 is either absent or very rare from the Tarbert Formation siderites, although it is very common within siderites from the underlying Rannoch, Etive and Ness Formations Sample B16, Dunlin oilfield, Tarbert Formation, Well 211/23-4, 9080.2 ft TVD.

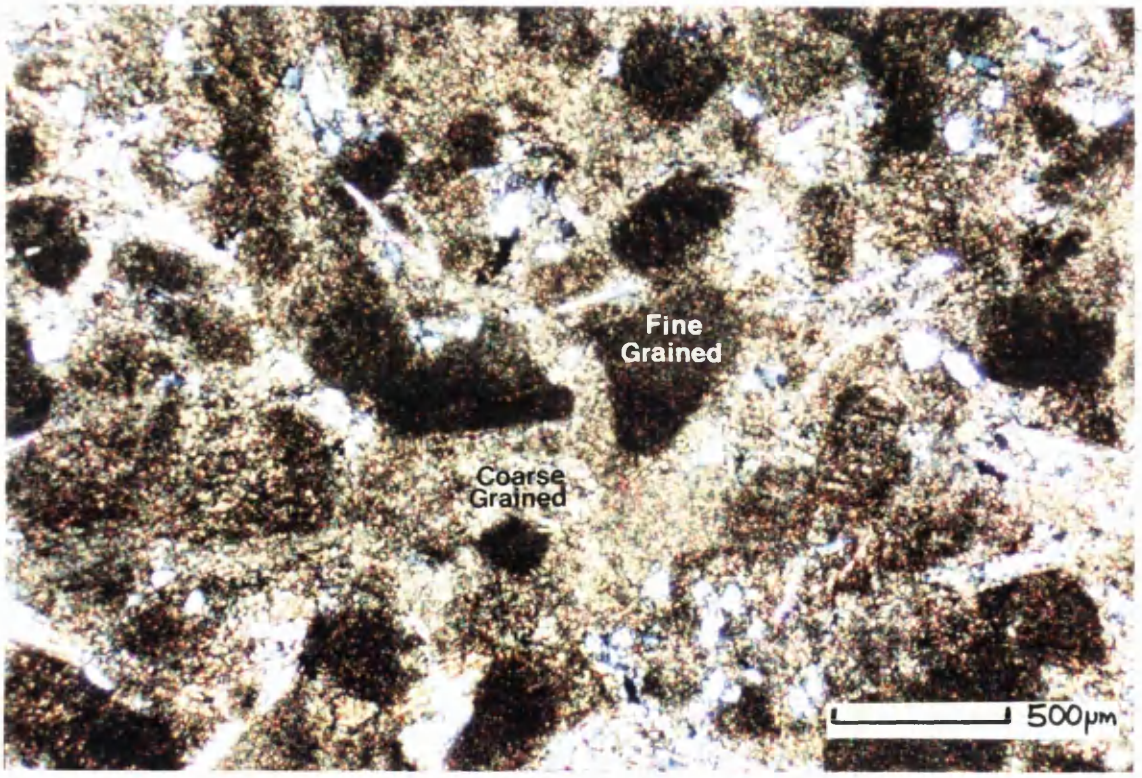

Fig 11. Concretionary siderite showing isolated fine grained patches of siderite cement within a matrix of coarser grained siderite. Detrital micas and quartz grains are also present. Transmitted light view, crossed polars. Sample B4, Dunlin oilfield, Ness Formation, Well 211/23-2, 9250.5 ft TVD.

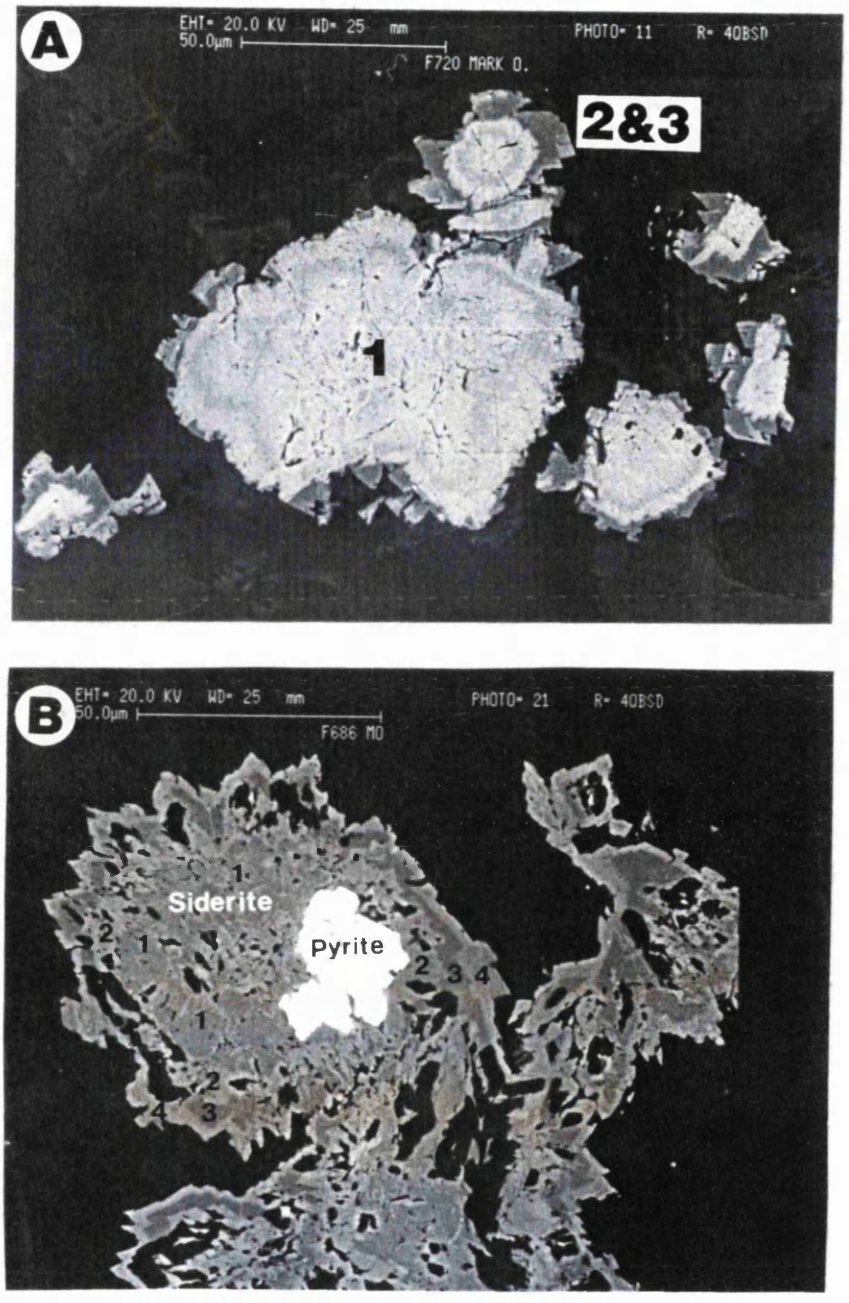

Fig 12. a) Sphaerosiderite, showing a spherulitic Zone 1 which has been overgrown by more euhedral Zones R2 and R3. BSE image, Sample A31, Dunlin oilfield, Rannoch Formation, Well 211/23-1, 9105.5 ft TVD.

b) Sphaerosiderite enveloping pyrite (bright). Siderite exhibits four distinct compositional zones (B1, B2, B3 B4). Sample M33, Cormorant oilfield, Broom Formation, Well 211/21-3a, 9026 ft TVD.

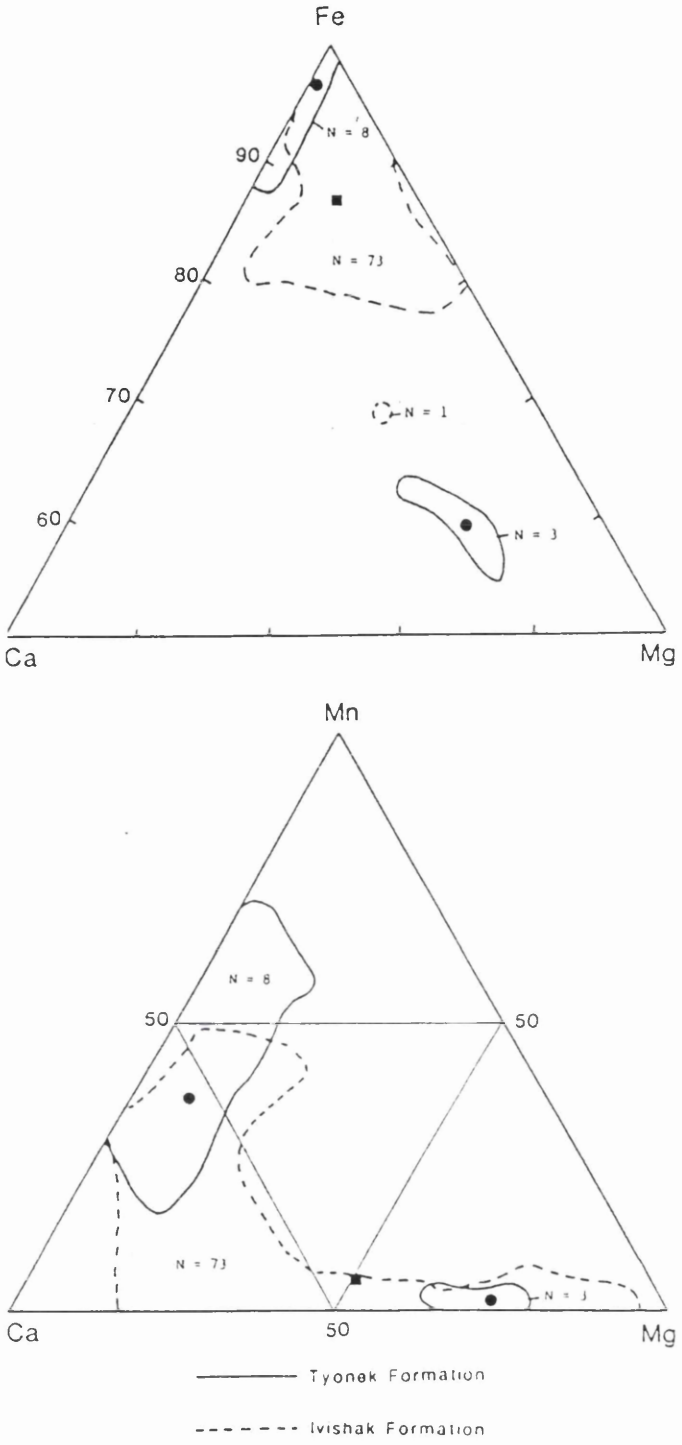

METEORIC SIDERITE

Fig 13. Ternary $CaCO_3$- $MgCO_3$ - $FeCO_3$ (top) and $CaCO_3$ - $MgCO_3$ - $MnCO_3$ (bottom) plots for meteoric siderites from the North Slope, Alaska, USA. Fresh-water siderites are relatively pure (>90 mole% $FeCO_3$) and may attain end member composition. They are Mn rich. From Mozley & Wersin (1992).

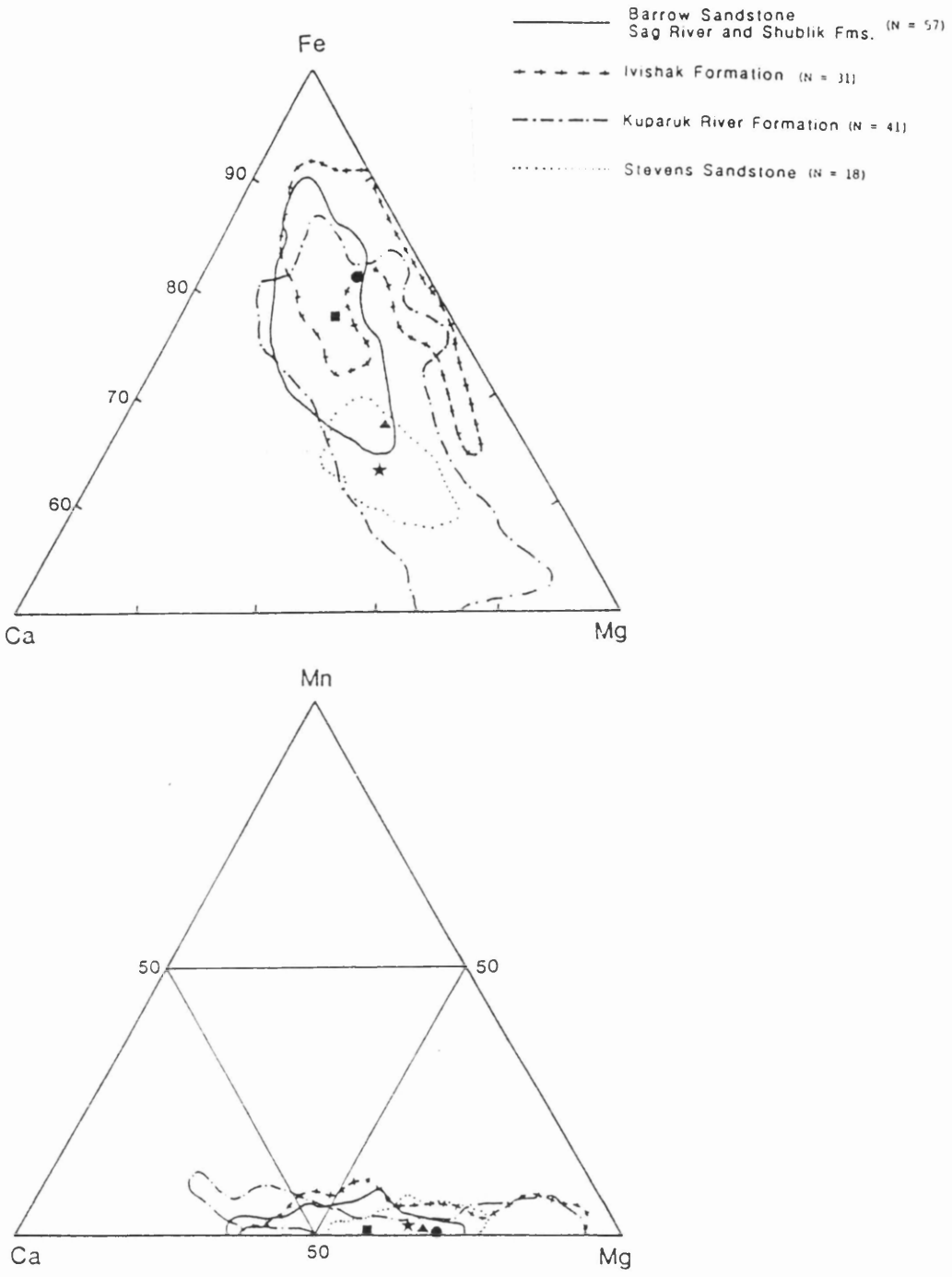

Fig 14. Ternary $CaCO_3$- $MgCO_3$ - $FeCO_3$ (top) and $CaCO_3$ - $MgCO_3$ - $MnCO_3$ (bottom) plots for marine siderites from the North Slope, Alaska, USA. Marine siderites are generally less pure and have higher Mg/Ca ratios than freshwater siderites. From Mozley & Wersin (1992).

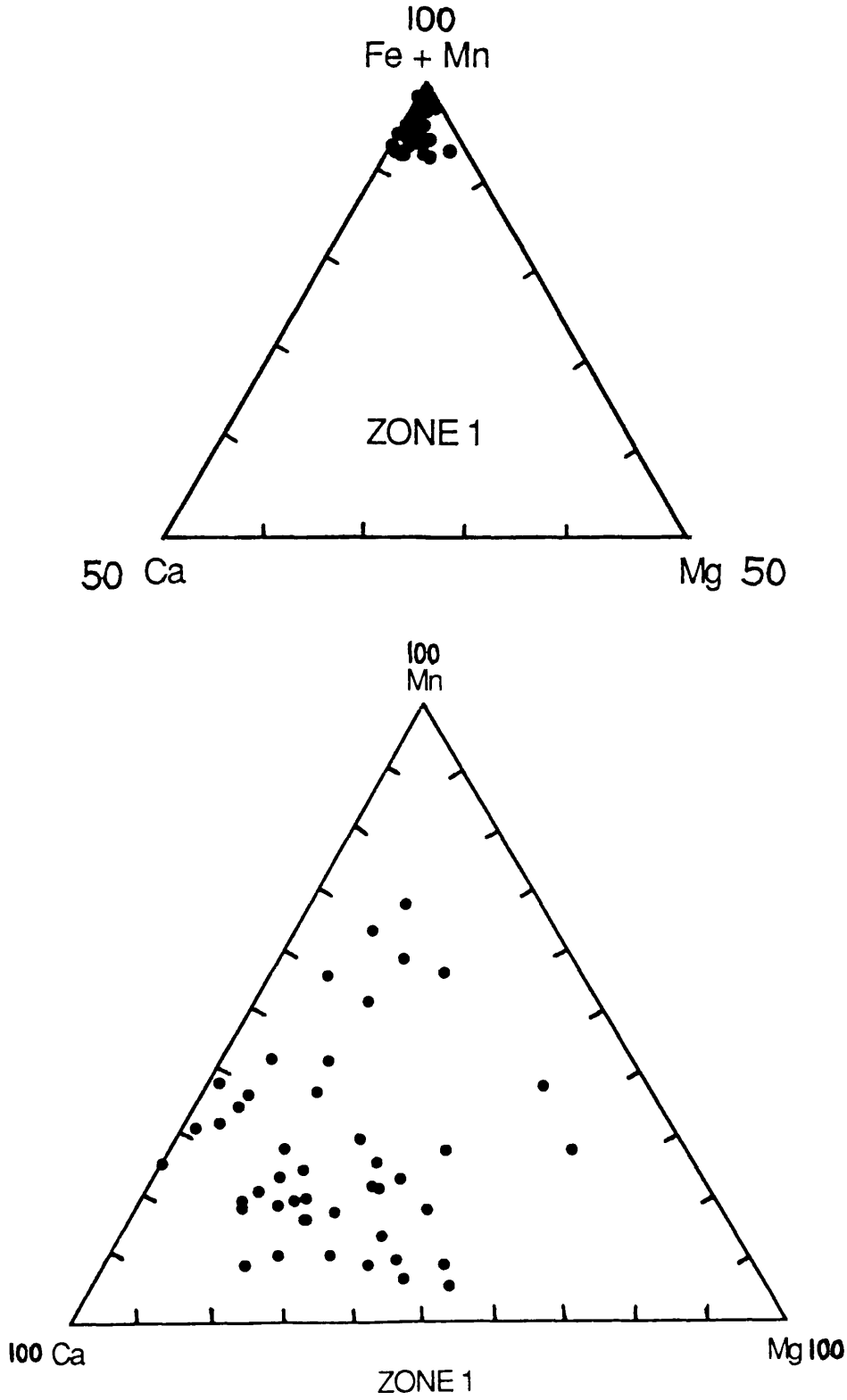

Fig 15. Ternary $CaCO_3$- $MgCO_3$ - $FeCO_3$ (top) and $CaCO_3$ - $MgCO_3$ - $MnCO_3$ (bottom) plots for Zone R1 siderites from the Brent Group, UK North Sea. These siderites are relatively pure and Mn rich with low Mg/Ca ratios. Compositionally they strongly resemble freshwater siderites.

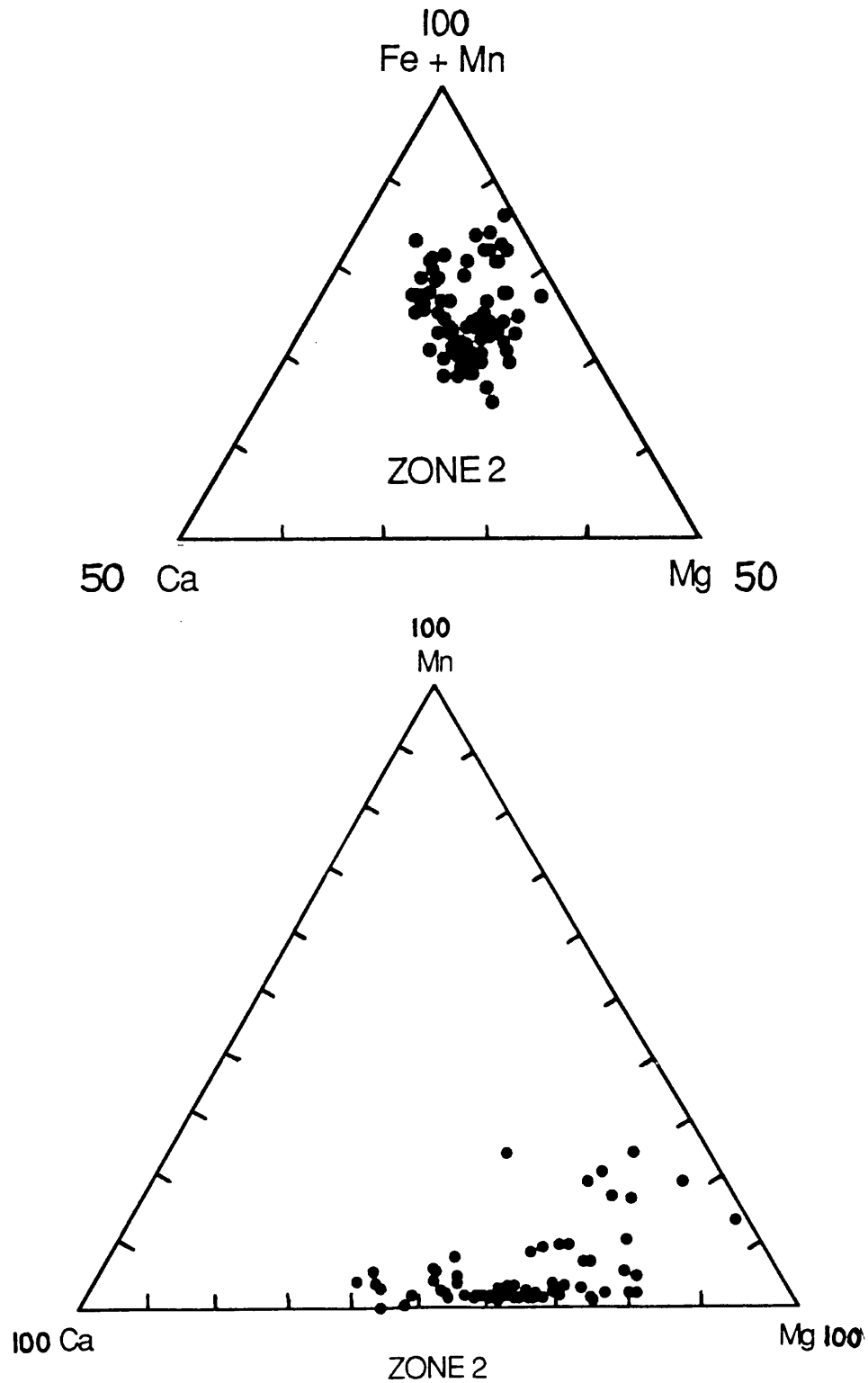

Fig 16. Ternary $CaCO_3$- $MgCO_3$ - $FeCO_3$ (top) and $CaCO_3$ - $MgCO_3$ - $MnCO_3$ (bottom) plots for Zone R2 siderites from the Brent Group, UK North Sea. These siderites are very impure with low Mn concentrations. They have relatively high Mg/Ca ratios. Compositionally they strongly resemble marine siderites.

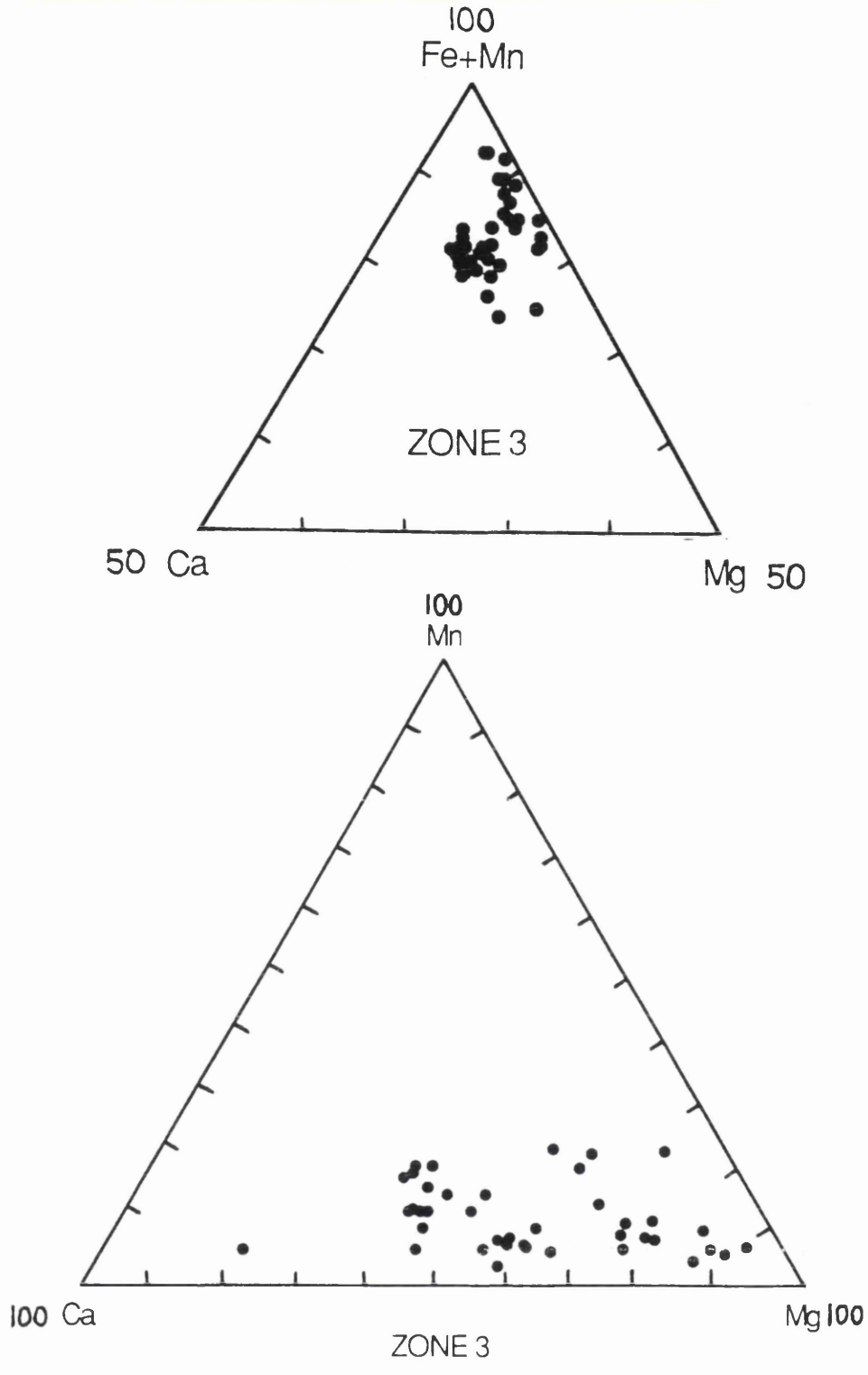

Fig 17. Ternary $CaCO_3$- $MgCO_3$ - $FeCO_3$ (top) and $CaCO_3$ - $MgCO_3$ - $MnCO_3$ (bottom) plots for Zone R3 siderites from the Brent Group, UK North Sea. These siderites have elemental compositions which are intermediate between those of Zone R2 and Zone R3 siderites.

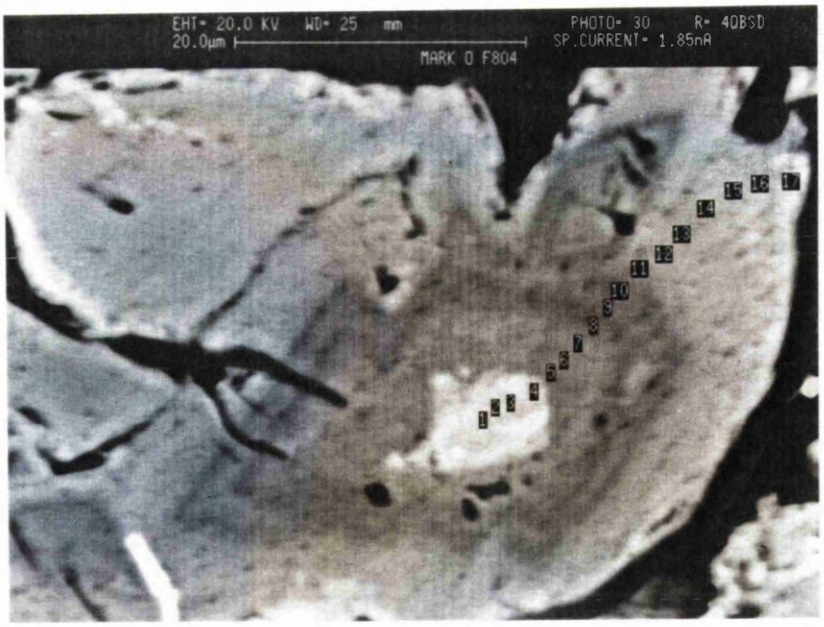

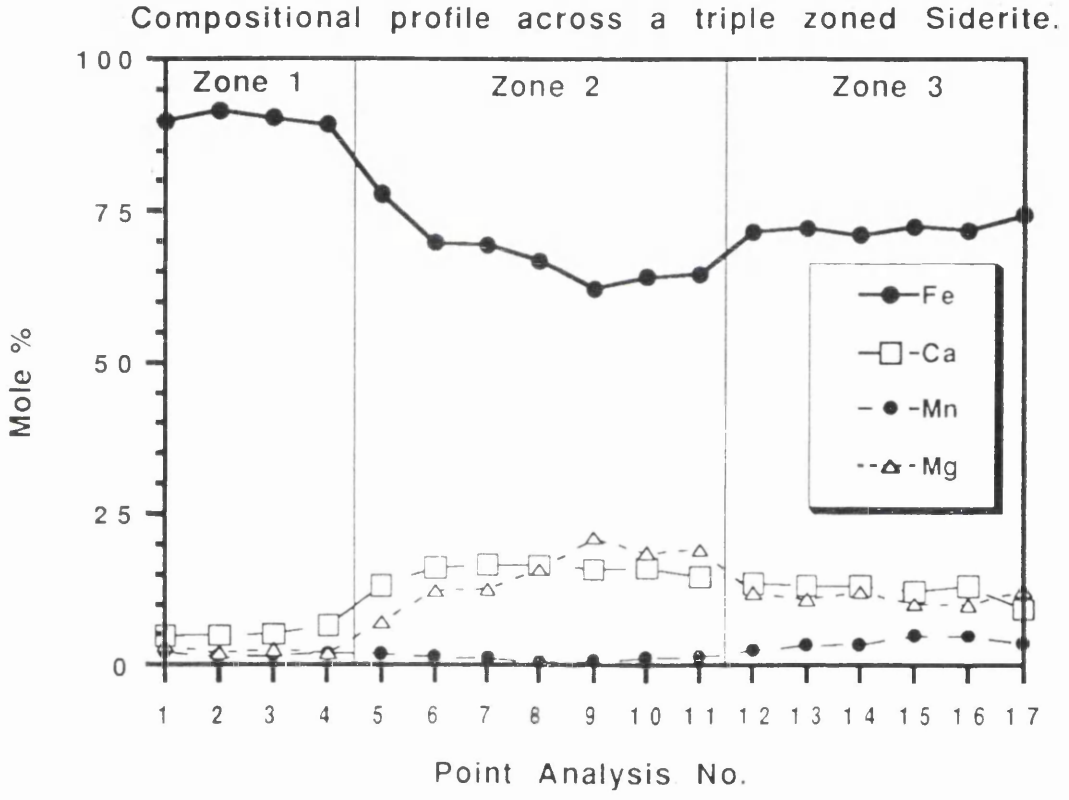

Fig 18. $CaCO_3$- $MgCO_3$ - $FeCO_3$ - $MnCO_3$ compositional profile across a triple zoned siderite crystal from a siderite concretion. Sample B4, Dunlin oilfield, Ness Formation, 211/23-2, 9250.5 ft TVD.

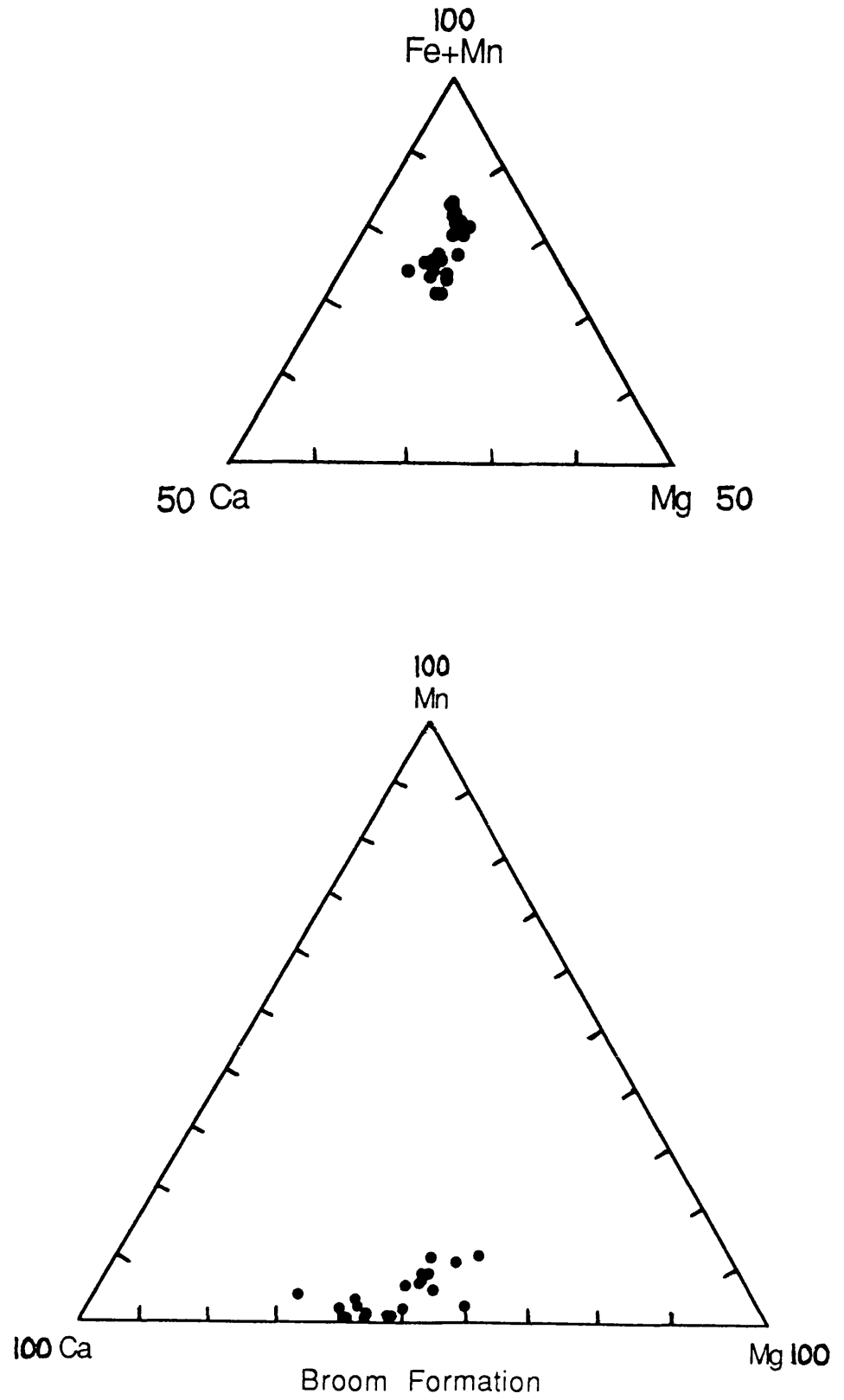

Fig 19. Ternary $CaCO_3$- $MgCO_3$ - $FeCO_3$ (top) and $CaCO_3$ - $MgCO_3$ - $MnCO_3$ (bottom) plots for Broom Formation siderites from the Brent Group, UK North Sea. These siderites are impure with low Mn concentrations and roughly equal amounts of Mg and Ca. Compositionally, they most closely resemble marine siderites.

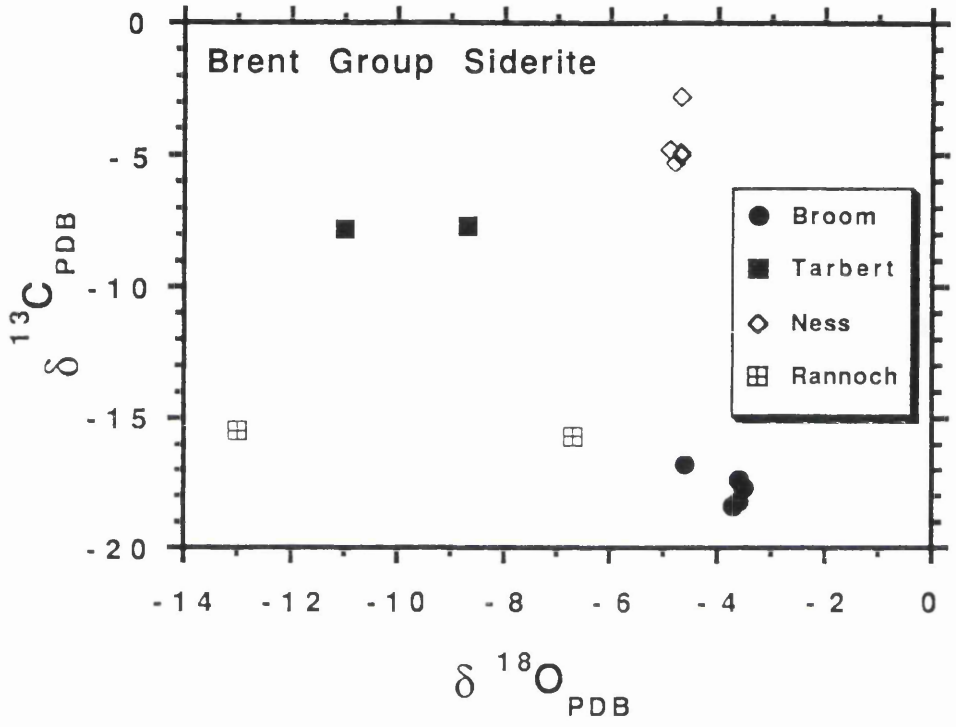

Fig 20. $\delta^{13}C_{PDB}$ and $\delta^{18}O_{PDB}$ plot for Brent Group siderites analysed during this study.

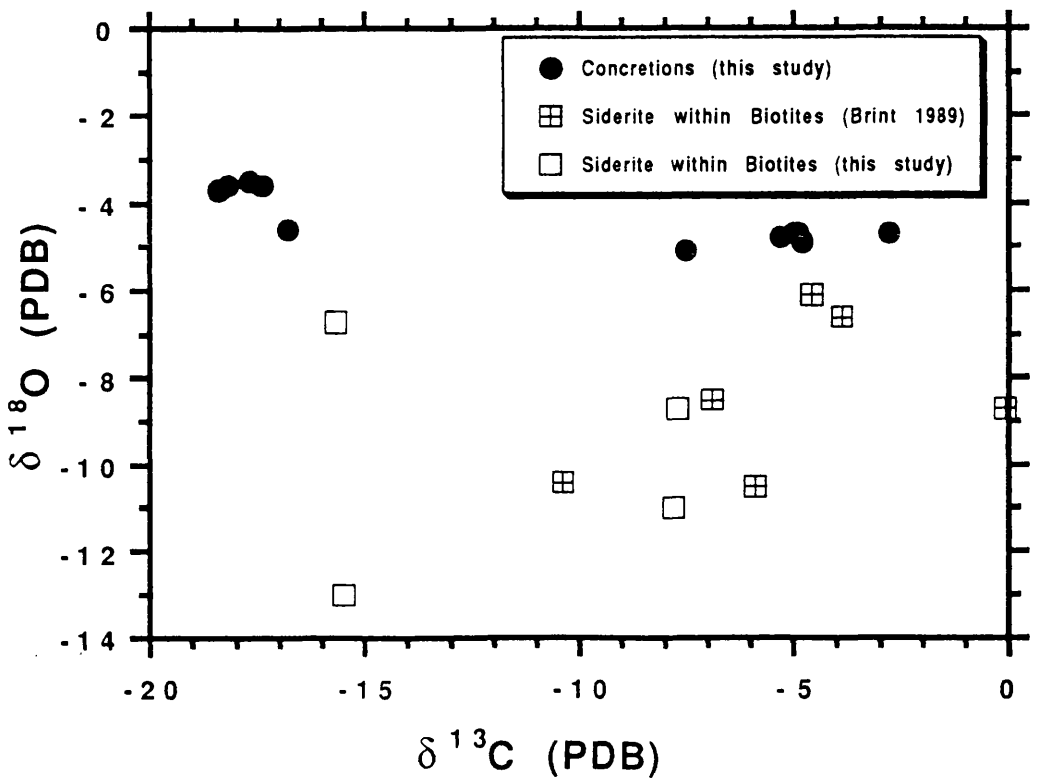

Fig 21. $\delta^{13}C_{PDB}$ and $\delta^{18}O_{PDB}$ plot for Brent Group siderites from concretions, and from within degraded biotites, which were analysed during this study. Data from Brint (1989) is also shown for comparison. Siderites from within biotites have the most depleted $\delta^{18}O_{PDB}$ values.

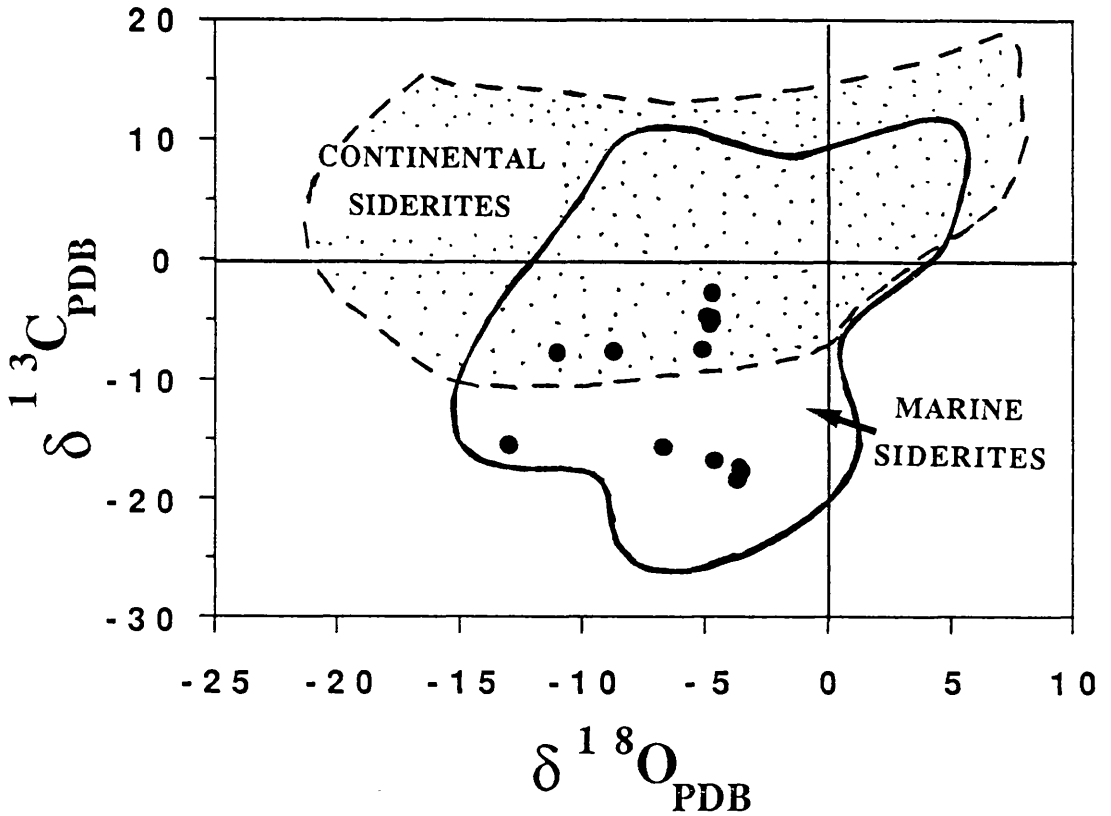

Fig 22. Plot comparing the $\delta^{13}C_{PDB}$ and $\delta^{18}O_{PDB}$ values of Brent Group siderites with those of continental and marine siderites cited by Mozley & Wersin (1992). This indicates that Brent Group siderites have isotopic compositions which are not distinctive of either a marine or a non-marine origin.

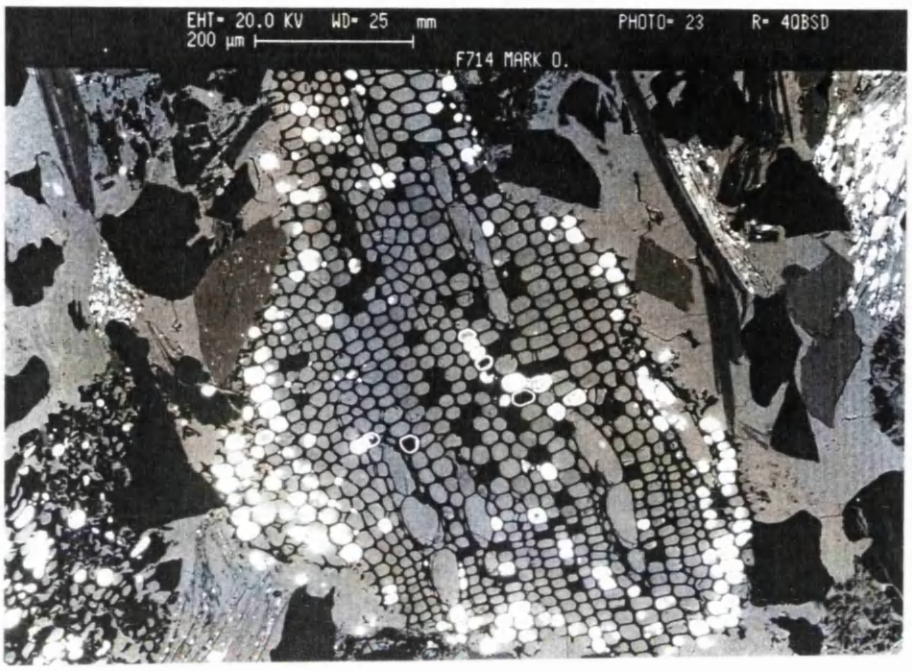

Fig 23. In siderite bearing sandstones early diagenetic pyrite is seen in association with plant fragments. This indicates that sulphate reduction of organic matter occured during shallow burial. Sample A31, Dunlin oilfield, Rannoch Formation, Well 211/23-1, 9105.5 ft TVD.

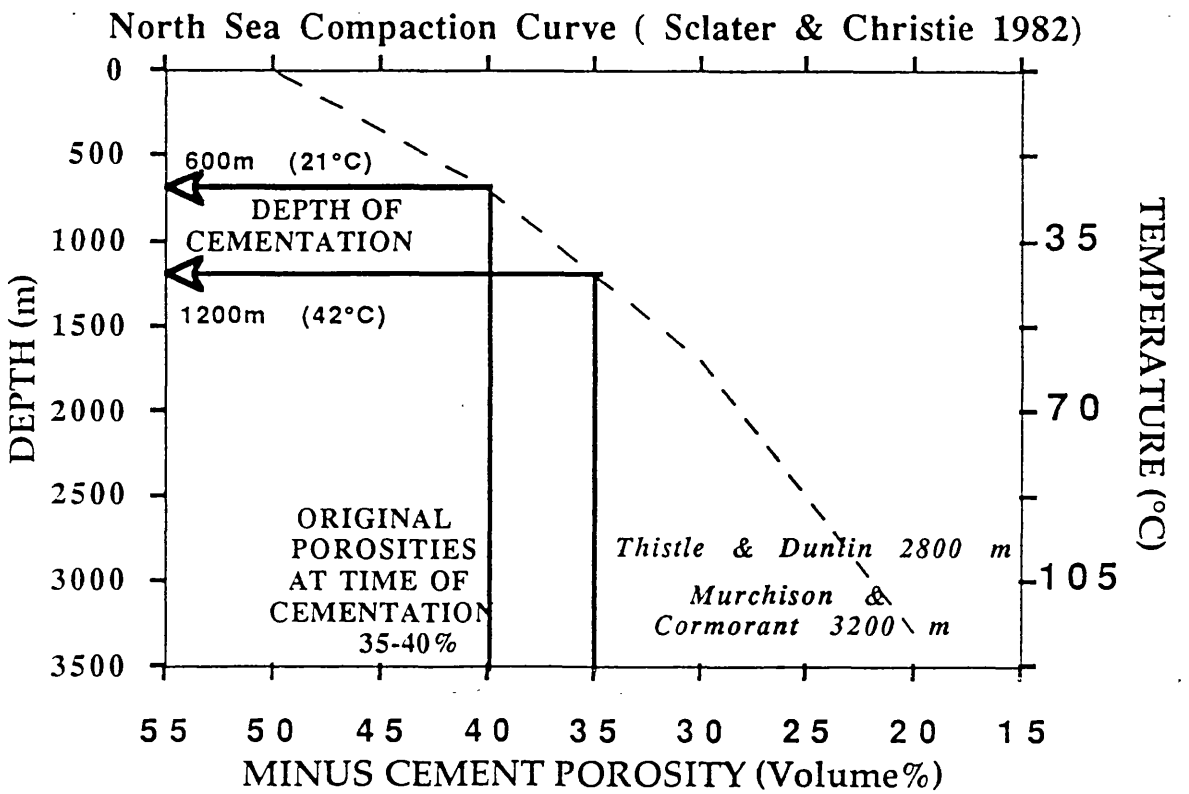

Fig 24. Siderite cement occurs within calcite cemented horizons exhibiting high minus cement porosities of 35-40%. Using the general porosity curve for the North Sea (Sclater & Christie 1982), such high primary porosities indicate that calcite cementation occured at 600-1200m, at temperatures of roughly 21-42°C. As siderite growth *pre-dates* calcite cementation, siderite growth must have occured at *even lower* temperatures than these.

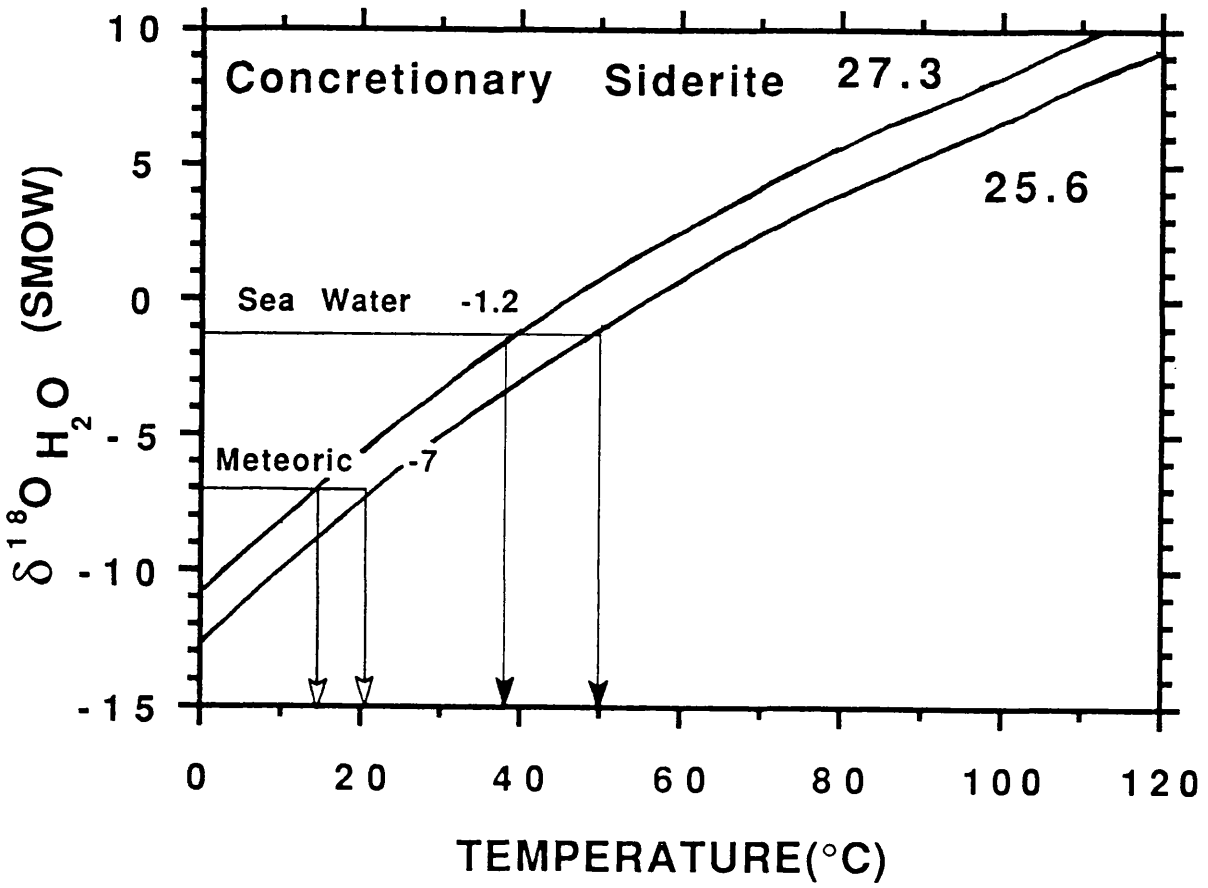

Fig 25. Maximum and minimum $\delta^{18}O_{SMOW}$ mineral curves for concretionary siderites calculated using the equation of Carothers *et al* (1988). If siderite precipitated from marine pore-waters ($\delta^{18}O_{SMOW}$= -1.2‰) it grew at 38-50°C, whereas if siderite precipitated from meteoric pore-waters ($\delta^{18}O_{SMOW}$= -7‰) it grew at 14-20°C. If siderite precipitated from mixed meteoric-marine pore-waters then it grew at temperatures intermediate between these two end member estimates. As we know from petrographic evidence that siderite grew at roughly <30°C, siderite $\delta^{18}O_{SMOW}$ mineral values are only consistent with growth from meteoric or mixed marine-meteoric pore-waters.

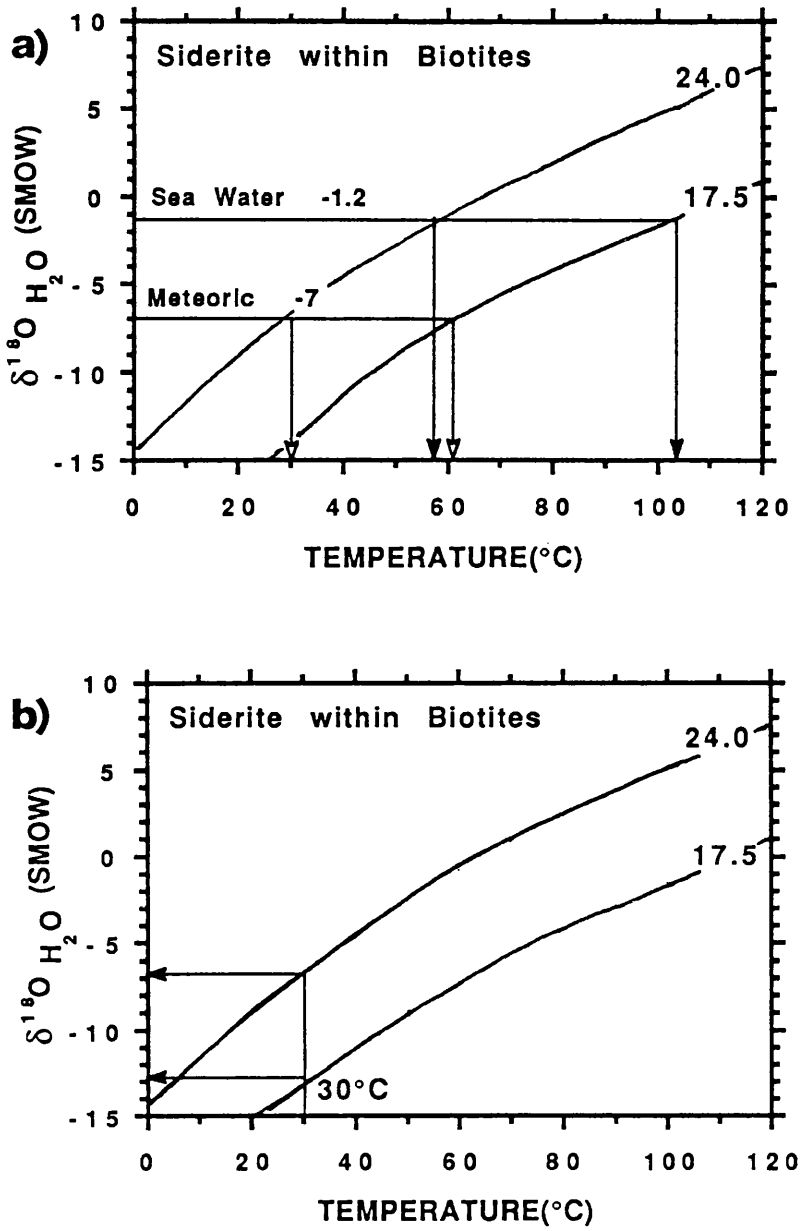

Fig. 26. Maximum and minimum $\delta^{18}O_{SMOW}$ mineral curves for siderites occuring within degraded biotites. Curves calculated using the equation of Carothers *et al* (1988).

a) If siderite precipitated from marine pore-waters ($\delta^{18}O_{SMOW}$ = -1.2‰) it grew at 57-104°C, whereas if siderite precipitated from meteoric pore-waters ($\delta^{18}O_{SMOW}$ = -7‰) it grew at 30-61°C.

b) If siderite formed at 30°C then it precipitated from a pore-water with $\delta^{18}O_{SMOW}$ = -7 to -13‰.

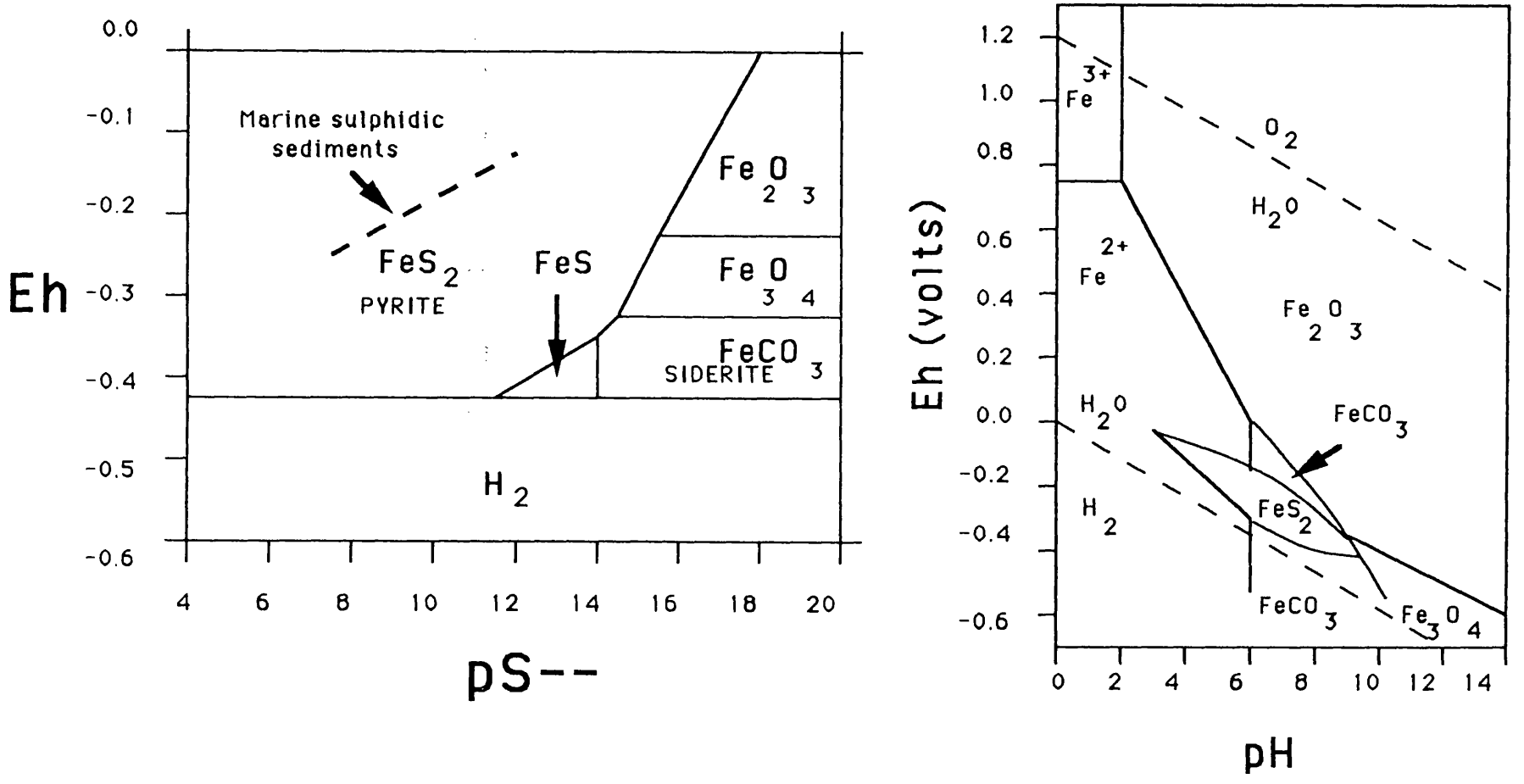

Fig 27. a) Eh-pS^{--} diagram for common Fe-bearing phases in sediments, pH=7.37, T=25°C. Measurements of natural sulphidic marine sediments fall along the dashed line. Redrawn from Berner (1971).

b) Eh-pH diagram for common Fe-bearing phas in sediments. After Garrels & Christ (1965).

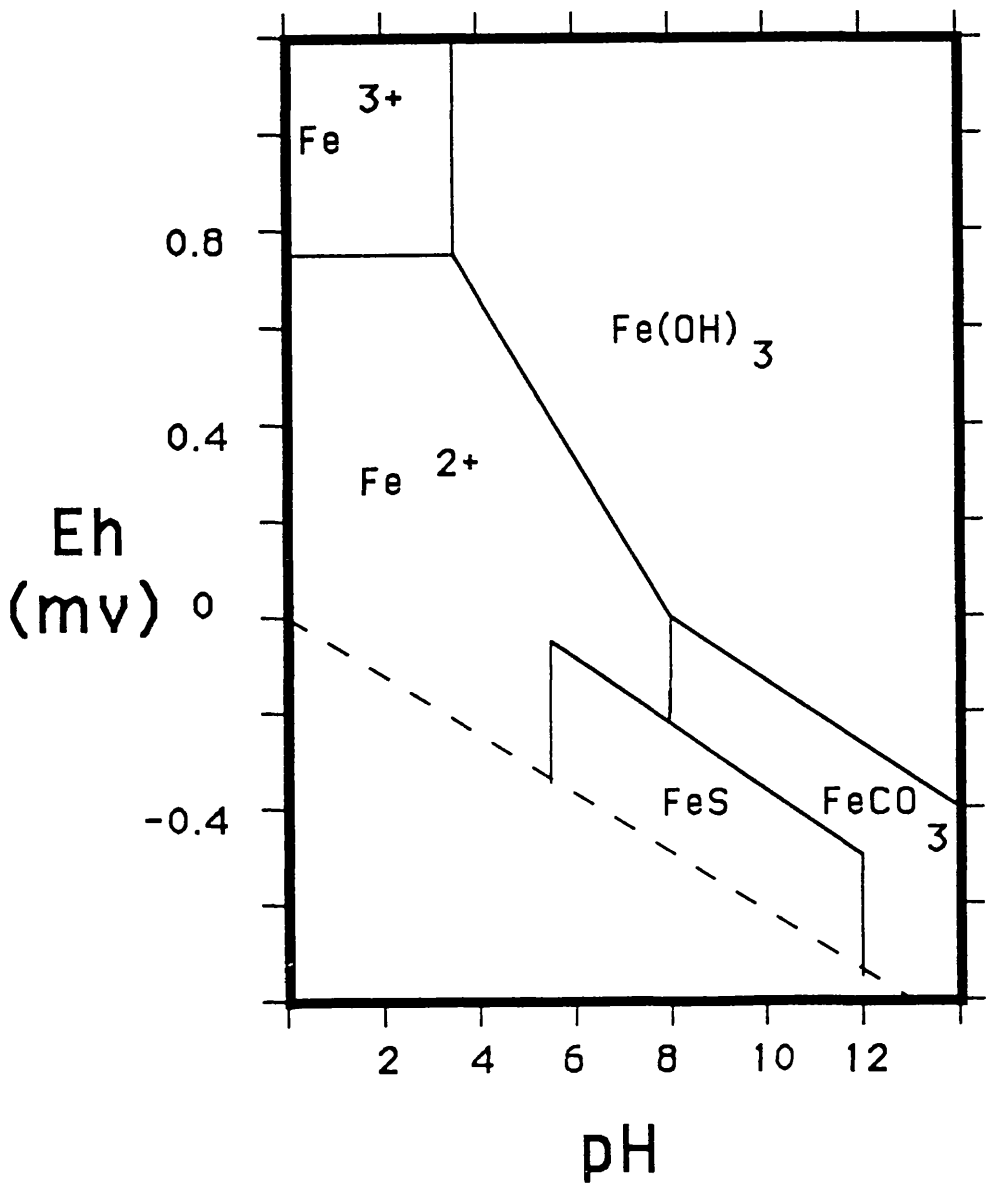

Fig 28. Eh-pH diagram for common Fe-bearing phases within sediments; siderite is a stable phase under normal sea water conditions (total $S=10^{-2.2}$) if $Fe(OH)_3$ and FeS are used instead of hematite and pyrite. Redrawn from Maynard (1983).

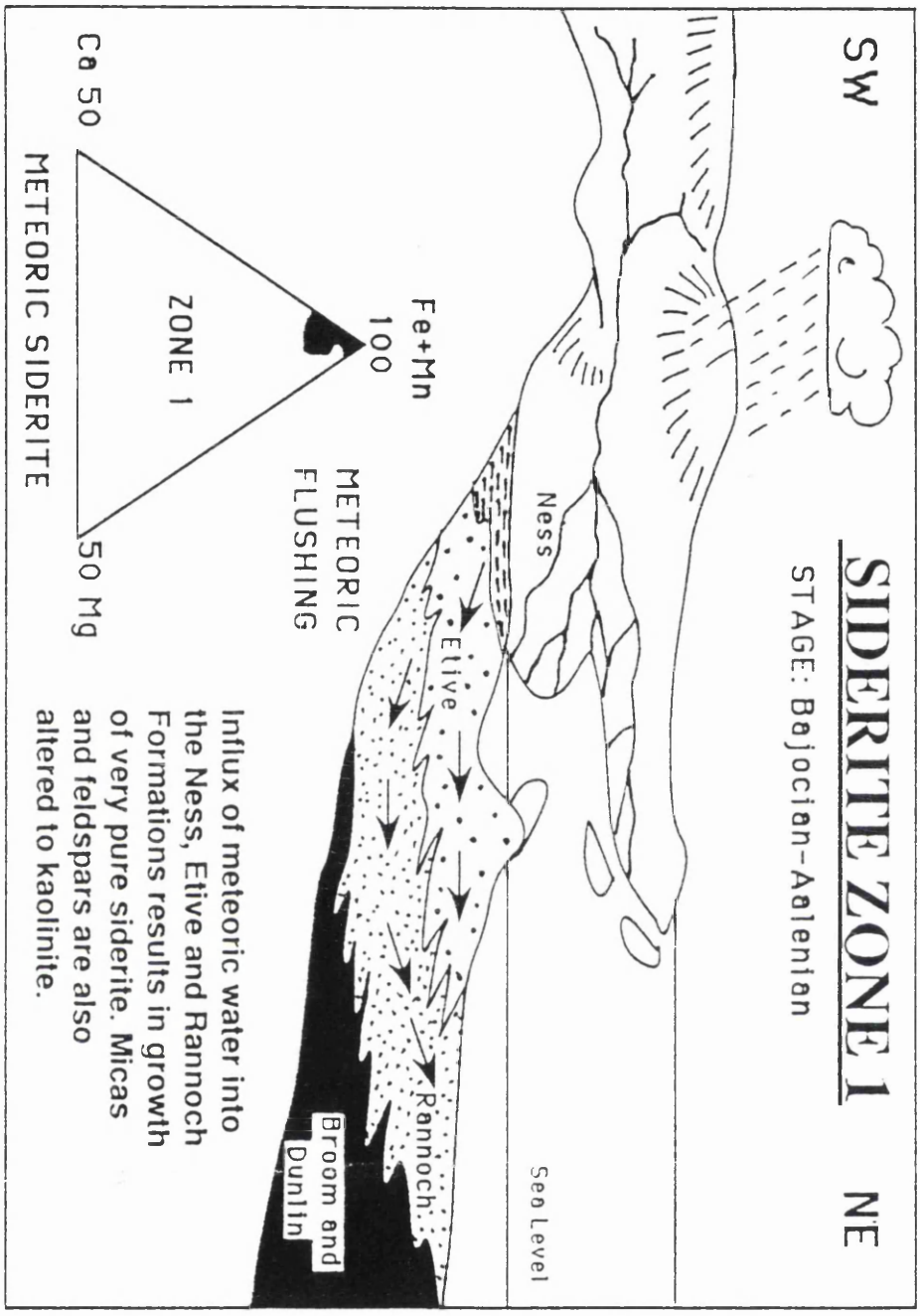

Fig 29. Schematic diagenetic model for the precipitation of Zone R1 siderite, in the Rannoch, Etive and Ness Formations.

Fig 30. Schematic diagenetic model for the precipitation of Zone R2 siderite, in the Rannoch, Etive, Ness and Tarbert Formations.

SIDERITE ZONE 3 - TWO MODELS

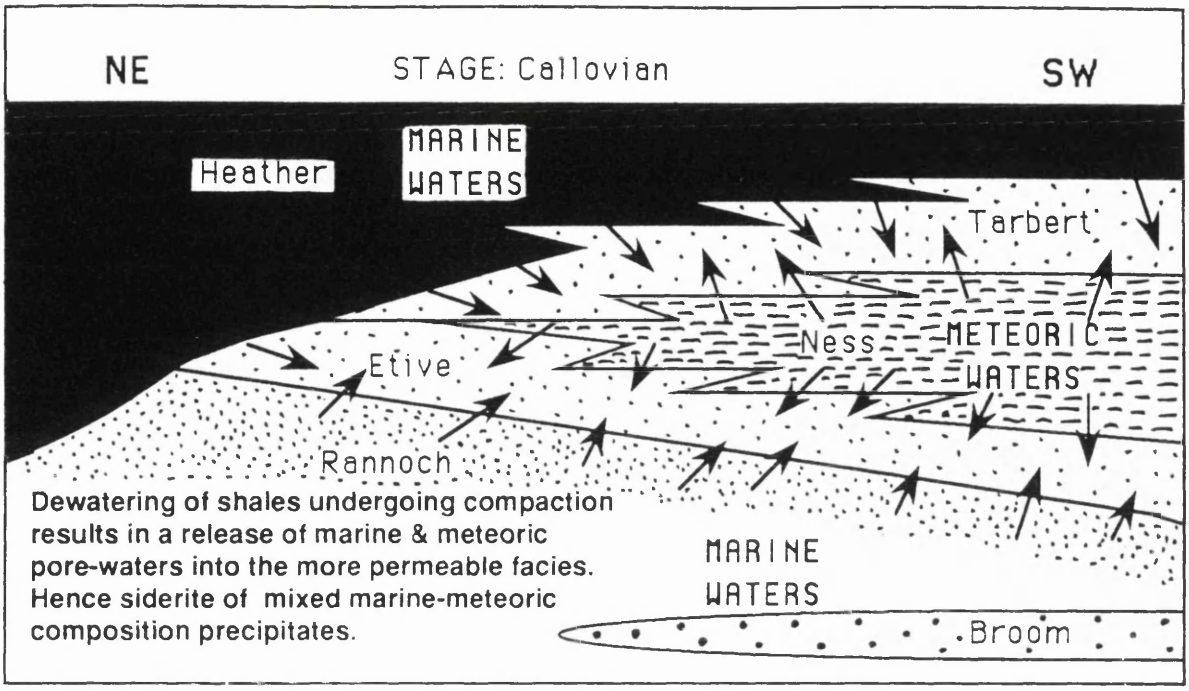

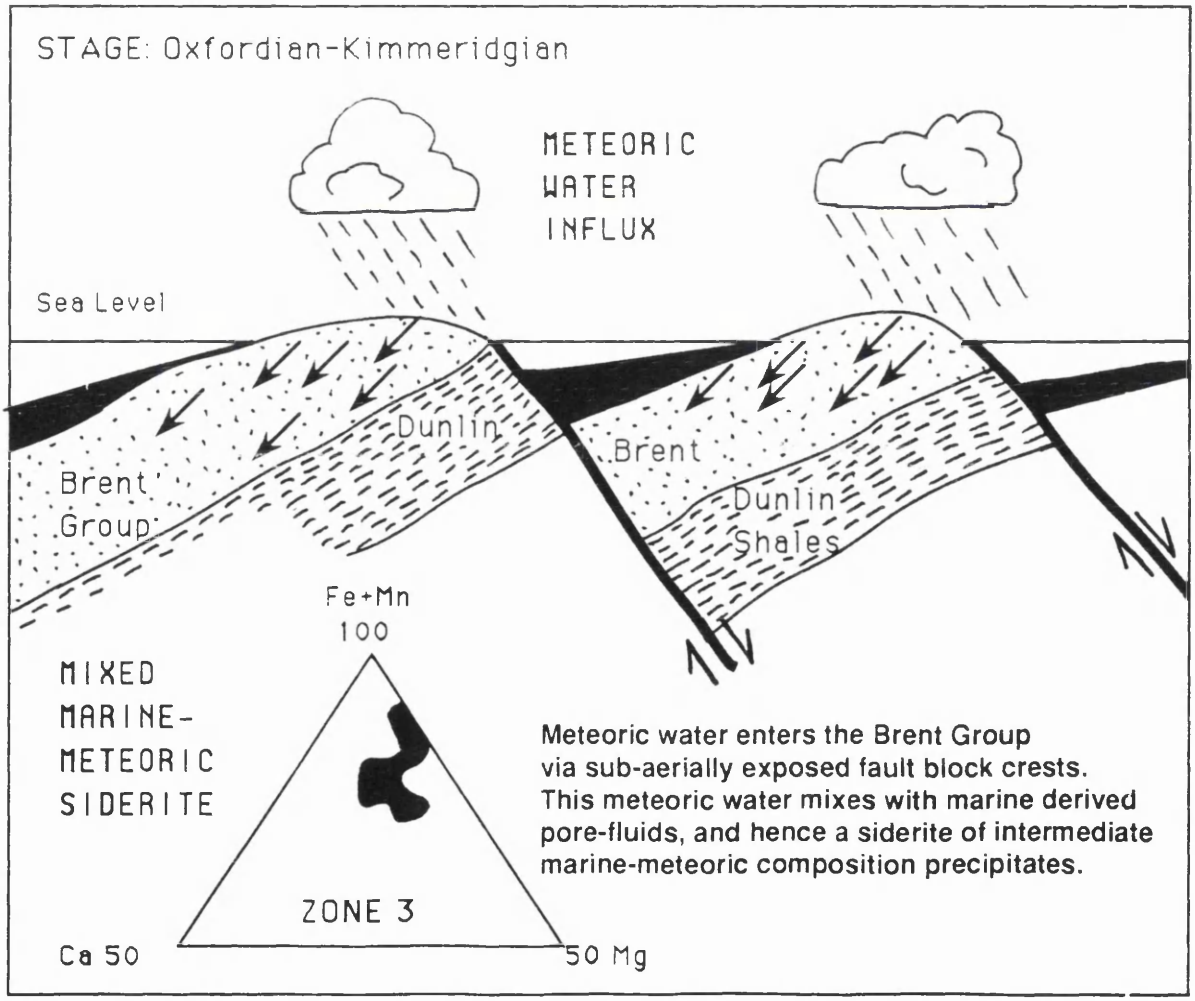

Fig 31. Two possible schematic, diagenetic models for the precipitation of Zone R3 siderite, in the Rannoch, Etive, Ness and Tarbert Formations.

Table 1. Compositional data for typical ocean and river water.

	Sulfate (ppm)	Manganese (ppb)	Magnesium (ppm)	Iron (ppb)	Calcium (ppm)
Ocean water	2710	0.2	1290	2	411
River water	8.25	8	3.35	40	13.4

Note: Data from Drever (1982).

Table 2. Stable isotopic data for Brent Group siderite.

Sample	Oilfield	Formation	Depth (TVD) and Well	$\delta^{18}O_{PDB}$	$\delta^{13}C_{PDB}$	$\delta^{18}O_{SMOW}$	Description
M33	Cormorant	Broom	211/21-3a 9026 ft				
<30μm	"	"	" "	-4.6	-16.8	26.1	Concretion
53-30μm	"	"	" "	-3.5	-17.7	27.3	"
64-53μm	"	"	" "	-3.6	-18.2	27.2	"
85-64μm	"	"	" "	-3.6	-17.4	27.2	"
>85μm	"	"	" "	-3.7	-18.4	27.1	"
B4	Dunlin	Ness	211/23-2 9250.5 ft				
<20μm	"	"	" "	-4.8	-5.3	26.0	Concretion
30-20μm	"	"	" "	-4.7	-5.0	26.1	"
53-30μm	"	"	" "	-4.7	-4.9	26.1	"
64-53μm	"	"	" "	-4.9	-4.8	25.9	"
>85μm	"	"	" "	-5.1	-7.5	26.1	"
A30	"	Rannoch	211/23-1 9105.1 ft	-6.7	-15.7	24.0	Rhombs within biotites
A31	"	Rannoch	211/23-1 9105.5 ft	-13.0	-15.5	17.5	"
B15	"	Tarbert	211/23-4 9081.6 ft	-11.0	-7.8	19.6	"
B16	"	Tarbert	211/23-4 9080.2 ft	-8.7	-7.7	21.7	"
B7	"	Ness	211/23-2 9251.7 ft	-5.1	-7.5	25.6	Concretion

Table 3- Siderite Elemental Analyses

Broom Formation

Sample M33, Cormorant, Well 211/21-3a, 9026 ft TVD

Mole %

Fe	Ca	Mg	Mn	Zone
68.4	17.0	13.0	1.6	B1
70.2	14.3	13.1	2.4	B1
69.5	14.8	13.4	2.3	B1
72.8	14.9	10.9	1.4	B1
73.0	14.1	10.6	2.3	B1
73.8	16.0	9.6	0.6	B1
73.9	15.2	10.2	0.7	B1
76.3	11.0	10.8	1.9	B2
77.2	9.9	10.4	2.5	B2
71.9	18.6	8.2	1.3	B2
77.8	9.0	11.0	2.2	B2
77.5	9.6	12.3	0.6	B2
76.5	8.6	12.3	2.6	B2
74.4	14.0	11.3	0.3	B3
72.3	16.2	11.3	0.2	B3
71.7	17.3	10.8	0.2	B3
75.6	12.6	11.2	0.6	B3
72.8	15.7	11.1	0.4	B3
69.9	16.3	13.5	0.3	B3
81.1	9.3	8.4	1.2	B4
80.0	9.1	9.7	1.1	B4
81.4	8.7	8.6	1.3	B4
80.7	9.1	8.9	1.3	B4
74.6	11.3	13.1	1.0	B4
79.2	9.4	9.7	1.7	B4

Rannoch Formation

Sample M34, Cormorant, Well 211/21-3a, 9006.9 ft TVD

Mole %

Fe	Ca	Mg	Mn	Zone
89.6	4.6	5.2	0.6	R1
90.9	4.5	3.7	0.9	R1
89.8	5.1	4.4	0.7	R1
81.4	1.3	15.7	1.6	R2
79.8	4.0	15.2	1.0	R2
74.0	9.8	15.3	0.9	R2
87.1	1.1	9.0	2.8	R3
88.2	2.8	6.4	2.6	R3

Sample A30, Dunlin, 211/23-1, 9105.1 ft TVD

Mole %

Fe	Ca	Mg	Mn	Zone
90.2	6.5	0.2	3.1	R1
89.9	5.1	0.7	4.3	R1
91.7	5.2	0.4	2.7	R1
64.4	18.7	16.2	0.7	R2
67.1	11.9	20.1	0.9	R2
72.2	5.9	21.3	0.6	R2
85.4	1.4	11.9	1.3	R3
86.2	2.2	10.2	1.4	R3
77.3	2.3	19.1	1.3	R3
80.9	0.9	17.0	1.2	R3

Sample A2, Dunlin, Well 211/23-1, 9024.1 ft TVD

Mole %

Fe	Ca	Mg	Mn	Zone
95.4	2.1	1.5	1.0	R1
95.7	1.9	1.3	1.1	R1
97.3	1.2	0.7	0.8	R1
75.4	5.2	18.0	1.4	R2
76.7	5.6	15.8	1.9	R2
78.2	5.8	13.8	2.2	R2
78.8	6.8	12.4	2.0	R3

Sample A24, Dunlin, Well 211/23-1, 9078.1 ft TVD

Mole %

Fe	Ca	Mg	Mn	Zone
85.7	8.4	0.9	5.0	R1
87.8	7.7	1.9	2.6	R1
88.6	7.6	1.7	2.1	R1
64.7	14.1	20.1	1.1	R2
60.5	19.1	19.4	1.0	R2
77.6	10.6	10.4	1.4	R2
79.0	4.5	14.8	1.7	R3
66.7	11.8	19.3	2.2	R3

Sample A31, Dunlin, Well 211/23-1, 9105.5 ft TVD

Mole %

Fe	Ca	Mg	Mn	Zone
86.1	8.3	0.2	5.4	R1
89.0	3.9	0.9	6.2	R1
90.8	5.2	0.6	3.4	R1
64.1	12.8	22.5	0.6	R2
76.0	10.5	11.6	1.9	R2
65.6	12.1	21.5	0.8	R2
78.5	1.8	18.6	1.1	R3
76.0	9.9	12.7	1.4	R3
83.0	3.1	12.6	1.3	R3

Sample A8, Dunlin, Well 211/23-1, 9044.6 ft TVD.

Mole %

Fe	Ca	Mg	Mn	Zone
94.9	3.0	1.1	1.0	R1
93.5	3.2	2.4	0.9	R1
97.3	2.0	0.0	0.7	R1
66.7	7.4	25.1	0.8	R2
64.8	13.6	20.6	1.0	R2
62.2	18.1	19.1	0.6	R2
68.1	7.1	23.0	1.8	R3
89.8	7.6	2.0	0.6	R3

Etive Formation

Sample E1, Thistle, Well 211/18-A30, 9662 ft TVD.

Mole %

Fe	Ca	Mg	Mn	Zone
98.2	0.6	0.7	0.5	R1
96.3	0.7	0.5	2.5	R1
94.5	0.8	2.6	2.1	R1
65.7	2.1	25.4	6.8	R2
69.5	8.5	14.5	7.5	R2
65.8	6.5	20.8	6.9	R2
63.0	6.3	24.2	6.5	R2
70.8	4.7	18.2	6.3	R2
71.6	2.9	18.5	7.0	R2
73.3	5.0	16.3	5.4	R2
74.7	3.6	17.3	4.4	R2
78.5	4.5	12.5	4.0	R3
84.2	3.0	9.5	3.3	R3
87.8	2.6	6.6	3.0	R3

Sample E2, Thistle, Well 211/18-A30, 9672.4 ft TVD.

Mole %

Fe	Ca	Mg	Mn	Zone
63.5	9.5	24.3	2.7	R2
66.0	11.1	20.0	2.9	R2
64.3	10.9	21.3	3.5	R2
66.4	10.9	19.7	3.0	R2
68.4	8.9	19.6	3.1	R2
71.8	11.3	13.6	3.3	R3

Ness Formation

Sample B4, Dunlin, Well 211/23-2, 9250.5 ft TVD,

Mole %

Fe	Ca	Mg	Mn	Zone
92.0	5.0	2.0	1.0	R1
89.8	4.8	3.2	2.2	R1
91.5	5.0	2.1	1.4	R1
90.4	5.2	2.7	1.7	R1
89.3	6.6	2.1	2.0	R1
89.8	6.0	1.8	2.4	R1
93.0	4.0	1.6	1.4	R1
89.3	7.6	2.1	1.0	R1
90.7	6.1	2.2	1.0	R1
92.2	4.6	1.9	1.3	R1
95.1	2.7	1.0	1.2	R1
90.8	6.1	1.3	1.8	R1
73.1	15.1	10.2	1.6	R2
71.0	17.2	10.6	1.2	R2
71.3	16.3	11.3	1.1	R2
66.7	15.4	17.2	0.7	R2
69.8	14.4	14.1	1.7	R2
70.0	13.4	15.1	1.5	R2
71.5	16.1	11.5	0.9	R2
65.2	15.3	18.9	0.6	R2
68.9	15.1	14.7	1.3	R2
67.0	14.9	16.8	1.3	R2
70.2	17.9	11.9	0.0	R2
71.1	16.8	12.1	0.0	R2
72.7	14.9	12.3	0.1	R2
77.8	13.1	7.2	1.9	R2
69.8	16.3	12.4	1.5	R2
69.4	16.7	12.7	1.2	R2
66.8	16.6	15.9	0.7	R2
62.2	15.9	21.1	0.8	R2
64.1	16.1	18.6	1.2	R2
64.6	14.7	19.2	1.5	R2

Sample B4 (CONTINUED)

Mole %

Fe	Ca	Mg	Mn	Zone
71.7	13.6	12.1	2.6	R3
72.3	13.3	11.0	3.4	R3
71.1	13.2	12.2	3.5	R3
72.5	12.3	10.2	5.0	R3
71.9	13.1	10.1	4.9	R3
74.4	9.4	12.5	3.7	R3
73.5	13.0	9.2	4.3	R3
74.7	13.0	9.2	4.3	R3
72.0	11.8	12.1	4.1	R3
74.4	12.4	10.1	3.1	R3
75.1	9.4	13.9	1.6	R3
79.1	10.6	9.1	1.2	R3

Sample B7, Dunlin, Well 211/23-2, 9251.7 ft TVD.

Mole %

Fe	Ca	Mg	Mn	Zone
94.5	1.4	0.6	3.5	R1
96.7	1.4	0.5	1.4	R1
94.4	2.6	0.9	2.1	R1
68.5	15.0	15.7	0.7	R2
65.6	15.0	18.7	0.7	R2
67.2	14.8	17.3	0.7	R2
73.1	11.2	10.5	5.2	R3
72.8	12.0	10.0	5.2	R3
75.5	10.8	9.8	3.9	R3

Sample B31, Dunlin, Well 211/23-4, 9282.8 ft TVD.

Mole %

Fe	Ca	Mg	Mn	Zone
95.7	1.8	1.5	1.0	R1
93.5	3.5	2.4	0.6	R1
91.4	3.7	4.1	0.8	R1
97.5	1.4	0.4	0.7	R1
97.5	0.8	0.4	1.3	R1
97.0	1.2	0.8	1.0	R1
95.6	1.8	1.8	0.8	R1
66.9	9.4	22.7	1.0	R2
67.8	9.9	21.2	1.1	R2
69.5	9.9	19.9	0.7	R2
68.1	8.1	23.0	0.8	R2
67.9	10.3	20.8	1.0	R2
67.3	10.7	21.1	0.9	R2
69.4	9.8	19.6	1.2	R2
74.6	8.2	15.8	1.4	R3
77.0	8.1	13.5	1.4	R3
77.0	8.1	13.5	1.4	R3
77.2	3.0	18.9	0.9	R3
83.8	3.2	11.4	1.6	R3

Tarbert Formation

Sample B16, Dunlin, 211/23-4, 9080.2 ft TVD.

Mole %

Fe	Ca	Mg	Mn	Zone
94.7	1.0	1.3	3.0	R1
87.1	2.0	7.3	7.3	R1
94.9	1.2	0.9	3.0	R1
59.6	14.6	25.4	0.4	R2
61.6	16.2	21.6	0.6	R2
61.1	15.4	22.8	0.7	R2
63.1	14.1	22.3	0.5	R2
63.4	15.9	20.0	0.7	R2
62.2	16.2	20.9	0.7	R2
61.0	17.0	21.3	0.7	R2
61.5	15.7	22.2	0.6	R2
61.8	15.6	22.1	0.5	R2
64.3	15.1	20.6	0.8	R2
62.0	16.0	21.4	0.6	R2
66.3	10.9	22.2	0.6	R2
63.8	14.0	21.7	0.5	R2
63.0	10.2	26.3	0.5	R2
79.1	4.6	13.6	2.7	R3
70.6	12.0	16.5	0.9	R3

CHAPTER 3

THE EMERALD OILFIELD, U.K. NORTH SEA:- THE KEY TO SHALLOW DIAGENESIS AND PETROLEUM DEGRADATION IN THE BRENT GROUP?

Mark Osborne[1], R. Stuart Haszeldine[1], & Anthony E. Fallick[2].

1- Department of Geology & Applied Geology, University of Glasgow, Scotland, U.K., G12 8QQ.

2- Scottish Universities Research & Reactor Centre, Isotope Geosciences Unit, East Kilbride, Glasgow, Scotland, U.K., G75 OQU

3.1 ABSTRACT

The Emerald Sand is a Callovian shallow marine sheet sandstone forming the reservoir rock to the Emerald oilfield. The oilfield is only shallow-buried (1600m) and provides an insight into the early diagenetic processes affecting the Brent Group. The Emerald Sand has a widespread distribution throughout the western-most margin of the East Shetland Basin, northern North Sea. Early diagenesis consisted of growth of pyrite, K-feldspar overgrowths and calcite concretions. During deeper burial, vermiform kaolinite, ankerite and quartz precipitated, accompanied by feldspar dissolution. Stable isotopic analyses of ankerite and kaolinite cements suggest that they precipitated from meteoric or brackish pore-waters at approximately 25-50°C. This indicates that meteoric water must have flushed through the Emerald Sand, displacing depositional marine pore-waters. Influx of meteoric water resulted in the biodegradation of hydrocarbons, dissolution of feldspar, and precipitation of kaolinite, quartz and ankerite cements. Mass balance calculations indicate that following feldspar dissolution, Al was conserved due to precipitation of kaolinite, however Si was partly exported, creating substantial secondary porosity (~5 volume%). However much of this secondary porosity was lost due to later compaction, with no net improvement in reservoir quality. Permeabilities have also not increased, due to growth of kaolinite in the secondary pores. Fluid flow was driven by a hydrostatic head on the landmass to the west during the Palaeocene. Influx of meteoric water, feldspar dissolution, and biodegradation of early migrating oil, are processes which are likely to have occurred in Brent Group oilfields during shallow burial.

3.2 INTRODUCTION

The diagenesis of Brent Group sandstones has received much study, principally because it is one of the most important oil reservoirs in the northern North Sea (Brint 1989; Hancock & Taylor 1978; Hogg 1989; Glasmann *et al.* 1989; 1992; Bjorlykke *et al.* 1992; Haszeldine *et al.* 1992; Shanmugan 1990). However most of the reservoir sandstones studied have been deeply buried. This means that it is more difficult to unravel the early diagenesis undergone by these sandstones, as eogenetic cements may have been dissolved during deep burial. It is also difficult to extract pure samples of early diagenetic clay minerals from deeply buried sandstones, since, for example, the clay separates consist of a mixture of different clay generations.

However, if we study Brent Group sandstones which have only been buried to shallow depths, we should be able to examine early cements which have not been overprinted by the effects of later diagenesis. Previous studies of the Brent Group have suggested that leaching of feldspars by meteoric water occurred during shallow burial (Bjorlykke *et al.* 1979; 1992, Blanche & Whitaker 1978; Brint 1989; Glasmann *et al.* 1989; Hancock & Taylor 1978; Shanmugan 1988). This supposedly caused grain dissolution and created secondary porosity, hence improving the reservoir quality of the sandstones (Bjorlykke *et al.* 1992; Hancock & Taylor 1978; Shanmugan 1990). Study of shallow buried Brent Group sandstones should hence enable us to study all these processes in detail. The reservoir sandstones of the Emerald oilfield have been buried to a maximum depth of only 1600m, so that they form ideal subjects for this kind of research.

3.3 LOCATION & GEOLOGICAL SETTING.

The geological setting of the Emerald oilfield has been described by Wheatley *et al.* (1987). The field lies on the Transitional Shelf, which is situated between the East Shetland Basin and the East Shetland Platform (Figure 1). A interpretation of a regional geoseismic section through the Emerald oilfield is shown in Figure 2, and a schematic burial curve in Figure 3. The reservoir unit is the Emerald Sand, of Middle Jurassic (Bajocian-Callovian age) (Figure 4). The sandstone lies unconformably upon thin Triassic and Devonian sediments, which are underlain by lower Palaeozoic - pre-Cambrian gneisses. Hence there is no large sedimentary sequence beneath the Emerald Sand.

Much of the Middle Jurassic Brent Group is absent from the Transitional Shelf area. In the Viking Graben area to the east the late Middle Jurassic (Bathonian) was a time of marine transgression, represented by the marine sandstones of the Tarbert Formation. However the marine transgression did not extend onto the Transitional Shelf until the Callovian, when the Emerald sand was deposited. Hence the depositional environment of the Emerald sandstone is similar to that of the Tarbert Formation, but the two are not exactly the same age (Wheatley *et al.* 1987).

Sedimentological studies (Wheatley *et al.* 1987) indicate that the Emerald Sand was deposited as a transgressive sheet-like sand body, in near-shore to offshore marine conditions, over the whole northern and central areas of the Transitional Shelf. The sand infills areas of low relief on the underlying basement and shows only minor variations in thickness across the whole shelf area (40-60ft). However in vicinity of well 3/11b-4 the Emerald sandstone was not deposited. This is interpreted to be an emergent palaeo-high over which the sea never transgressed. The sandstone grain size fines upwards, from medium grained sandstone to fine grained sandstone and siltstone. This is interpreted to reflect a deepening in water conditions through time. The upper part of the Emerald sandstone contains layers of shelly debris (belemnites and bivalves), which are thought to represent intermittent storm events. These layers are always cemented by calcite with minor ankerite. Bioturbation is very common throughout the Emerald Sand, and carbonised plant fragments are also present.

The sandstones are medium to fine grained and well-sorted, grains being rounded-subangular in shape. Only very small amounts of detrital clay are present in the coarser grained reservoir units. Point count data for the Emerald Sand are shown in Table 1 and in Figure 5. Petrographically they are subarkosic arenites according to the terminology of Dott (1964). The amount of feldspar relative to quartz is higher inside concretions than outside, a point which will be discussed in more detail later.

Oil is thought to have migrated into the structurally high trap in the Palaeocene (Wheatley *et al.* 1987). The oil has an API gravity of 24°, and 90-99% of the oil contains organic compounds indicative of biodegradation (Wheatley *et al.* 1987). The source kitchen was the more deeply buried Kimmeridge Clay Formation in the Graben to the east (see Figure 2, Wheatley *et al.* 1987). The cap rock to the oilfield is the overlying shales of the Heather Formation.

3.5 TECHNIQUES USED

Petrographic study of the Emerald Sand was accomplished using standard optical, SEM and cathodoluminescence mocroscopy. Elemental composition of carbonates were analysed using a Cambridge Stereoscan 360 SEM, equipped with a Link Analytical 1085 S. A ZAF4 FLS programme was used to correct the data. Precision of the measurements is +/- 0.5 mole%.

Samples were disaggregated, sieved and the 53-160μm size fraction was retained for heavy liquid (1,1,2,2, tetrabromoethane) separation of ankerite and calcite from silicate grains. Prior to isotopic analysis each sample was oxygen plasma ashed in a Polaron Bio-Rad Asher for two hours to remove labile organic matter. Calcite was reacted with phosphoric acid for 3hrs at 25°C, and the CO_2 gas produced was collected and purified using standard procedures (McCrea 1950). The oxygen isotope fractionation factor for calcite used was α=1.01025 (Longstaffe & Ayalon 1987). Ankerite was reacted overnight at 100°C and corrections were made to the isotopic analyses using a fractionation factor of α=1.01169 (Rosenbaum & Sheppard 1986). Gas produced was analysed on a VG-Isotopes SIRA-10 mass spectrometer. Oxygen and carbon isotope data are presented in the standard notation relative to the PDB and SMOW standards (Craig 1957)

Strontium and rubidium were analysed on a VG-Isomass 54E and VG Micromass MM30 respectively, after chemical separation by standard cation exchange chromatography. Concentration determination was by isotope dilution. Powdered samples (10mg) were utilised.

For clay separation, sandstones were dissaggregated using a jaw crusher and the sieved <500μm size fraction treated with hydrogen peroxide to remove organics. The samples were then treated with 0.3M Na-Citrate, 1.0M $NaHCO_3$ and sodium dithionite to remove iron oxides. NaOAc-HOAc solution buffered to pH=5 was then added to remove carbonates. Size fractions were separated using sedimentation and centrifugation (Jackson 1979).

Oxygen isotope analyses were carried out on a silicate fluorination line similar to that described by Clayton & Mayeda (1963). Samples (10mg) were loaded into a nickel reaction vessel and reacted with BrF_5 or ClF_3 to liberate oxygen. Oxygen was converted to CO_2 over a platinised carbon rod and the gas analysed on a VG-Isotopes SIRA-10 mass spectrometer. NBS 28 gives $\delta^{18}O$=9.72‰.

Samples for deuterium/hydrogen analysis were degassed overnight at 120°C to remove adsorbed water. The samples were gradually induction heated to 1200°C in a platinum crucible and the hydrogen collected. Water liberated during the heating was passed through a uranium furnace at 800°C to produce hydrogen. All hydrogen was then collected by a Toepler pump. The gas was analysed on a VG-Isotopes Micromass 602 spectrometer, with a working standard calibrated against international standards; NBS 30 gives δD=-65‰.

For fluid inclusion studies measurements were made on a Linkam TH 600 heating/freezing stage used in conjunction with a Leitz-Dialux 20-EB binocular microscope. Doubly polished wafers of sandstones 40-100μm thick were prepared using the method of Crosbie (1981). Fluid inclusions within quartz overgrowths were subjected to heating and freezing experiments. The stage was calibrated using standard compounds of a known melting point.

3.4 PARAGENETIC SEQUENCE

Sandstones from wells 2/10a-6, 2/10a-7, 2/10a-7Z, 3/11B-3, and 3/11B-5 were examined during this study (see location map Figure 6). All the sandstones came from above the oil-water contact (O.W.C. at 5580ft TVSS), as the entire cored section of the Emerald sand is oil or gas bearing.

Petrographic examination of thin sections and SEM stubs of the Emerald sand enable a paragenetic sequence to be constructed (Figure 7a). Evidence for the relative timing of these authigenic cements will be discussed later in this paper. What is remarkable about the diagenesis of the Emerald sand is how similar the sequence and mineralogy of early diagenetic cements are to those preserved within deeply buried Brent Group sandstones. The early diagenetic cements are virtually identical in both instances (Figure 7b), with the exception of siderite. Siderite is absent from the Emerald sand; probably because it is a mineral that is thermodynamically unstable in sea water, and so tends to precipitate within deltaic settings where pore-waters are meteoric (Berner 1971). In shallow marine environments, Fe reacts with sea-water sulphate to form pyrite (FeS_2) instead of siderite ($FeCO_3$).

Blocky kaolinite, illite and significant quartz cement (>3%) are not present in the Emerald sand, though these minerals are commonly reported in other Brent Group oilfields. This is what would be expected, as the latter are late diagenetic minerals in the Brent Group; they usually precipitate during deeper burial conditions. The similarity in the early diagenetic mineral

assemblage between shallow and deeply buried Brent Group sandstones suggests that study of the Emerald oilfield can be used to examine some of the diagenetic processes that were affecting the Brent Group as a whole during shallow burial.

3.6 EARLY DIAGENETIC CEMENTS

3.6.1 Collophane & Glauconite

Glauconite and collophane grains occur in trace amounts throughout the Emerald sand. Glauconite occurs as rounded pellets, greenish in colour in plane polarised light. It also coats detrital grains, and may inhibit the growth of later quartz cement on the surface of the grain. Collophane occurs as rounded, phosphatised, fish-bone and teeth fragments.

Both these very early diagenetic cements probably precipitated on the sea floor in shallow water conditions. Both cements indicate fully marine conditions and slow sedimentation rates (Berner 1971) prevailed at the time of Emerald sand deposition .

3.6.2 K-feldspar Overgrowths

K-feldspar cement occurs as euhedral overgrowths up to 50μm thick, on detrital grains of both K-feldspar (orthoclase) and Na-feldspar (albite) (Figure 8). The overgrowths are too euhedral to be reworked grains from earlier sediments, therefore they formed as authigenic cements within the Emerald sand itself. As the overgrowths occur on detrital grains within calcite concretions, they texturally must pre-date calcite cementation, and are thus very early diagenetic in origin. Under cathodoluminescence, the overgrowths luminesce dark blue in contrast to the detrital grains which appear bright blue in colour.

Outside the concretions the overgrowths often show evidence of leaching during later diagenesis, and take on a skeletal appearance. K-feldspar overgrowths are a volumetrically minor cement, forming <1.0 volume% of the rock. The ions required for K-feldspar precipitation probably came from the break down of unstable aluminosilicate grains present within the sediment itself.

3.6.3 Pyrite & Marcasite

Early diagenetic pyrite and marcasite likewise pre-date texturally early calcite cement, and are therefore also very early diagenetic in origin (Figure 9). Pyrite occurs in the form of bladed crystals, framboids, octahedra, cubes and as pore-filling cement. Marcasite also occurs as pore-filling cement, and was recognised using reflected light microscopy and X-ray diffraction. Marcasite and pyrite are polymorphic, and the specific thermodynamic conditions leading to the formation of one or the other are not known; however it is likely that marcasite is metastable with respect to pyrite (Krauskopf 1982). Pyrite/marcasite cemented horizons have high minus cement porosities indicating the pyrite is pre-compactional in origin. Pyrite and marcasite are both often associated with burrows. The abundance of pyrite varies between 0.2 and 5.8 volume%.

Both pyrite and marcasite are seen surrounding carbonised wood fragments and detrital ilmenite grains (Figure 9). This suggests that the Fe for pyrite precipitation came from the dissolution of Fe-bearing detrital grains or grain coatings. The presence of pyrite suggests that sulphate reducing bacteria were actively degrading organic matter during early diagenesis. This requires the presence of sulphate (probably from sea water), a supply of organic nutrients, and a reducing environment.

3.6.4 Calcite

Calcite cement occurs as rare horizons in core, up to 1.0m thick. It is not possible to tell from core whether these horizons are isolated concretions or more continuous layers. Often these calcite cemented horizons are rich in bioclasts, although relatively few bioclasts occur outwith the concretions, perhaps due to dissolution (Figure 10). The calcite possesses high minus cement porosities of 39-55%, indicating that calcite precipitation occured during shallow burial prior to significant compaction.

The calcite exhibits a wide variation in crystal size, from poikilotopic spar to smaller intergranular spar. The cement is pore-occluding, replaces bioclasts extensively, and may corrode detrital grains, hence explaining why minus cement porosities are higher than the theoretical maximum of 40-45% (Baldwin & Butler 1985). The cement is non-ferroan and shows no compositional zonation; under cathodoluminescence it luminesces a homogenous bright orange colour (Figure 10). Bright luminescence suggests

the presence of Mn, and the absence of significant Fe. This is supported by quantitative EDS analysis on SEM which indicates the calcite is relatively pure (average 98.2 mole% $CaCO_3$), non-ferroan, with some Mg and Mn substitution (Table 2; Figure 11). Presence of Mn in the calcite is indicative of reducing conditions at the time of precipitation, though Eh was not low enough to result in the growth of Fe-calcite. Bioclasts are also compositionally very pure (average 98.7 mole% $CaCO_3$) with only small amounts of Mg substitution.

Calcite replaces bioclasts, and pre-dates significant physical compaction. Calcite cemented horizons hence have high minus cement porosities, and relatively few of the detrital grains are observed to be touching (Figure 10). Porosity is extremely low or non-existent within calcite cemented horizons (porosity 0-1.0%). If laterally extensive these horizons could compartmentalise the reservoir or act as baffles to fluid flow. However the cemented layers are confined to well 2/10-a6, and cannot be correlated to any other wells. It seems that the calcite cement is only of localised, rather than field-wide, distribution.

These calcite cemented horizons are exclusively restricted to layers with high concentrations of bioclasts, suggesting there is a genetic link between calcite cement and bioclast abundance. Dissolution of aragonitic shell debris during shallow burial could certainly have encouraged the precipitation of calcite in the immediate vicinity of these lag deposits, and calcitic shells would act as convenient nucleation sites at low degrees of supersaturation. Early diagenetic calcite cements have been reported from the Brent Group by other researchers (Brint 1989; Giles *et al.* 1992; Hamilton *et al.* 1987). These calcites are similarly non-ferroan, and occur in the marine Formations of the Brent Group (Broom, Rannoch, Etive and Tarbert Formations), but are absent from the non-marine delta-top sediments of the Ness Formation (Giles *et al.* 1992). This is consistent with the idea that the carbonate for such concretions was partly provided by the dissolution of detrital shell debris (Brint 1989; Giles *et al.* 1992; Hamilton *et al.* 1987).

3.7 LATER DIAGENETIC CEMENTS

3.7.1 Kaolinite

The kaolinite present in the Emerald oilfield is unusual in that it is all of the vermiform variety i.e. it exhibits a snake-like morphology (Figure 12). In contrast kaolinite in the more deeply buried Brent Group fields exhibits a

blocky morphology. The delicate morphologies frequently exhibited by the kaolinite indicate it is not of detrital origin, as such structures would likely not have survived transportation. Great variation in the size of individual verms is seen; verms range from 10 to >100μm in width, and 10 to 150μm in length. Individual kaolinite plates present in the verm are typically thin, sometimes with ragged edges. Very large verms are observed to have precipitated between the sheets of fully expanded muscovite mica. Finer grained kaolinite is observed to precipitate in secondary pore-space following feldspar dissolution (Figure 13). This suggests that the kaolinite forms by the breakdown of detrital feldspar.

Evidence of feldspar dissolution is certainly common in the Emerald Sand as oversize pores were seen in every thin section looked at (42), and most feldspars have a skeletal appearance due to leaching (Figure 14). Often the K-feldspar overgrowths are less leached than the detrital grain, suggesting that the overgrowth was slightly more stable in the corroding fluid. Detrital albite has also been more extensively leached than K-feldspar, as small amounts of albite occur within early diagenetic calcite concretions, but are absent outside, due to dissolution. The greater susceptibility of Na-feldspar to dissolution is also demonstrated by the fact that the Na-rich lamellae in detrital perthites are preferentially leached in contrast to the rest of the grain (Figure 14).

Some vermiform kaolinite is enveloped by calcite cement, although greater amounts of kaolinite occur outside the concretions. This indicates that the onset of kaolinite precipitation was co-genetic with the growth of calcite concretions, although the bulk of the kaolinite post-dated calcite cementation. Point counted kaolinite abundance varies between 4.0 and 18.8 volume% (average 12.2%). However this will be an overestimate due to the high amounts of microporosity present between the clay particles (typically 40%, Nadeau & Hurst 1991). Therefore true kaolinite abundances are between 0.2 and 11.3 volume% (average 7.3%).

If we know the amount of feldspar which has dissolved in the Emerald Sand through time, then using the two feldspar decomposition reactions below (from Giles & deBoer 1990), we can calculate the volume of kaolinite and quartz which should have precipitated in a closed geochemical system.

Reaction 1

$2KAlSi_3O_8 + 2H^+_{(aq)} + H_2O \Longrightarrow 2K^+ + Al_2Si_2O_5(OH)_4 + 4SiO_2$

2moles K-Feldspar + fluid ⟹ fluid + Kaolinite + 4 moles Quartz

Reaction 2

$2NaAlSi_3O_8 + 2H^+(aq) + H_2O \Rightarrow 2Na^+ + Al_2Si_2O_5(OH)_4 + 4SiO_2$

2moles Na-feldspar +fluid ⇒fluid + Kaolinite + 4moles Quartz

The amount of feldspar dissolved will be equal to the original feldspar content of the Emerald Sand, minus the present day feldspar content. The original feldspar content of the Emerald Sand is more likely to have been preserved within early diagenetic concretions in Well 2/10-a6, because the main phase of feldspar dissolution post-dated calcite cementation (Figure 7a). Using the point count data in Table 1 it can be calculated that the percentage of feldspar grains relative to total silicate (quartz + feldspar) grains within these calcite cemented zones in Well 2/10-a6 is 30.5 %, which is much higher than that outside (16.8 %). Hence we can calculate the amount of feldspar that has dissolved since calcite cementation, as a percentage of the total silicate grains;

$$30.5 - 16.8 = \underline{13.7\%.}$$

If this volume of feldspar has dissolved, then using reactions 1 and 2 above we can calculate the amount of kaolinite and quartz cement that should be precipitated in a closed geochemical system. Note that for dissolution of both orthoclase (K-feldspar) and albite (Na-feldspar), the moles of quartz and kaolinite produced are the same, hence the relative proportions of plagioclase to orthoclase present in the samples will make little difference to our calculations. For our purposes the mass balance can be simplified to;

$$2V \text{ Feldspar} \Rightarrow V \text{ Kaolinite} + 4V \text{ Quartz}$$
$$2 \times 104.7 \Rightarrow 99.5 + 4 \times 22.7$$
$$209.4 \Rightarrow 99.5 + 90.8$$

Where V Kaolinite, V Quartz, and V Feldspar are the molar volumes of kaolinite, quartz and feldspar respectively. The molar volume of feldspar used represents a 50:50 mixture of K and Na-feldspar. If 13.7 volume% of feldspar have dissolved, then using the molar volume equation above it can be calculated that 6.5 volume% kaolinite and 5.9 volume% quartz will precipitate. In a geochemical system which is closed with respect to Al and Si,

the amount of secondary porosity created by dissolution of 13.7% feldspar will hence be; 13.7 - 6.5 - 5.9= 1.3%.

The actual average volume of kaolinite present in the Emerald Sand is 7.3 volume%. This is similar to the calculated abundance of kaolinite which should be present (6.5%), hence an approximate mass balance exists between feldspar dissolved and kaolinite precipitated in the Emerald Sand. However the volumes of quartz cement present in the Emerald Sand are <2%, while the calculated quartz abundance which should be present is 5.9%. Hence at least 3.9 volume % silica has been exported from the rock; i.e. the geochemical system was an open one at the time of feldspar dissolution. We previously calculated that the volume of secondary porosity created following dissolution of 13.7% of feldspar in a closed geochemical system would be 1.3%. However as SiO_2 has been exported, the total secondary porosity created is even greater; 3.9 + 1.3= 5.2%.

Point counted secondary porosity in the Emerald Sand is between 0.4-7.2% (average 3.0%). This is lower than the calculated average volume of secondary porosity which should be present (5.2%). However the point counted abundance of secondary porosity is likely to be an underestimate due to the collapse of secondary pores during later compaction. There is no direct correspondence between the point counted volume of secondary porosity or feldspar present in a sample and the amount of kaolinite. This indicates that following feldspar dissolution, redistribution ofthe component ions has occured, at least on a thin section scale. However the mass balance calculations above indicate that kaolinite has not been exported from the rock as a whole, hence only local redistribution of kaolinite has occurred. Conversely quartz has apparently been exported from the Emerald Sand as a whole, creating effective secondary porosity.

3.7.2 Anatase

A volumetrically minor cement, anatase occurs within the secondary porosity created by feldspar dissolution, and is frequently seen in association with kaolinite. It forms tiny (<10μm) tabular, tetragonal crystals, and is found in trace amounts only.

3.7.3 Ankerite

Ankerite occurs within calcite concretions, and is particularly abundant towards their outer edges. However it also occurs outwith calcite concretions, as disseminated patches of cement. Within concretions ankerite and kaolinite are frequently observed to replace detrital feldspars, particularly plagioclase (Figure 15). Using BSE imaging, the ankerite is seen to have two compositional zones (Figure 15). Zone 1 Ankerites are more Fe rich than the later, more Mg-rich, Zone 2 ankerites (Figure 11; Table 2). Zone 2 ankerites are rare and have only been seen within calcite concretions in Well 2/10-a6, infilling the secondary porosity created by feldspar dissolution. Outside of concretions only Zone 1 ankerites have been observed. The restriction of Zone 2 ankerites to within calcite concretions may indicate that a more closed hydrological system existed within these concretions, which have very low porosities. Because the calcite cemented sands have low porosities and permeabilities, the water to rock ratio will have been much lower inside these horizons than outside. In such a semi-closed hydrological system with a limited amount of Fe in solution, precipitation of Zone 1 ankerites could have locally lowered the content of Fe in the pore-water, so that eventually less Fe-rich Zone 2 ankerites precipitated.

All the ankerites analysed are more Ca-rich than stoichiometric ankerite. This may be because ankerite has replaced earlier formed calcite cement. Ankerite may have formed partly by replacement of existing calcite, as there is often only a diffuse boundary at the junction between calcite and ankerite cements. Brint (1989) and Kantorowicz (1985) have described Ca-rich ankerites from other Brent Group oilfields, which they also link to partial replacement of earlier calcite cement. Ankerite abundance in the Emerald Sand varies between 0.4 and 8.2 volume%.

3.7.4 Quartz

Quartz overgrowths in the Emerald Sand are generally thin (<50μm), and irregular in appearance (Figure 16). Numerous tiny subhedral-euhedral crystals of quartz are observed adhering to the surface of the detrital grain. Fluid is trapped in the numerous cavities which exist between these crystals, and so fluid inclusions are formed. Overgrowths form only 1-2% of the rock. Back-scattered SEM imaging of thin sections indicates that the quartz overgrowths are very thin and are only attached to the surface of the grain at

a few isolated points (Figure 16). This means that there are often large fluid-filled cavities located along the boundary between the detrital grain and the overgrowth. Glauconite may occasionally nucleate around quartz grains and inhibit the growth of later quartz cement, but other grain coating clays such as chlorite are absent from the Emerald Sand.

Quartz overgrowths are not found within calcite concretions; this indicates that quartz cement post-dated calcite cementation. Quartz cement also envelops vermiform kaolinite, suggesting that quartz cement either post-dated, or was co-genetic with, kaolinite precipitation (Figure 16). As discussed earlier, the volumes of quartz cement present in the Emerald sand could easily be supplied by feldspar decomposition reactions, with no need for an external source of silica.

3.8 STABLE ISOTOPE DATA

Carbon and oxygen stable isotope analyses of calcite and ankerite cements are tabulated in Table 3, and presented as a scatter plot in Figure 17.

3.8.1 Stable isotope ratios of calcite

Calcite $\delta^{13}C_{PDB}$ varies between -0.8 and -3.1‰, and $\delta^{18}O_{PDB}$ varies between -3.2 and -3.9‰. Carbon isotopic signatures are close to that of primary marine carbonate (approximately $\delta^{13}C$=0.0‰, $\delta^{18}O$=0.0‰). This suggests that the calcite was largely derived either from sea water, or from the dissolution of shell debris. Bioclasts are certainly present within the Emerald Sand itself, so that shell dissolution is a feasible source of bicarbonate.

A minor contribution from sulphate reduction of organic matter is also possible ($\delta^{13}C$= -10 to -25‰); this would explain why the signature of the cement is slightly depleted relative to marine carbonate. As pyrite is present within calcite concretions we know that sulphate reduction of organic matter has certainly occurred within these sediments during shallow burial.

A bioclast (belemnite rostrum) present in the Emerald Sand was subjected to stable isotopic analysis. $\delta^{13}C$ and $\delta^{18}O$ signatures indicate that the bioclast is depleted in both $\delta^{18}O$ and $\delta^{13}C$ relative to marine carbonate, suggesting it has been altered during diagenesis.

Using the fractionation equation of Friedman & O'Neil (1977) it is possible to construct a plot relating $\delta^{18}O$ of calcite cement, $\delta^{18}O$ of the water and growth temperature (Figure 18). From Figure 18, it can be seen that if

calcite precipitated from a pre-Miocene marine pore-water with $\delta^{18}O$= -1.2‰ (Sheppard 1986) then it grew at 26-30°C, whereas if calcite precipitated from a Jurassic meteoric pore-water with ($\delta^{18}O$= -7‰, Hamilton *et al.* 1987; Hudson & Andrews 1987; Fallick *et al.* 1993) then it grew at 1-4°C. Given that the depositional pore-water in the Emerald sand was sea water it is most likely that the calcite precipitated from a marine pore-fluid, especially as the calcite is an early diagenetic cement. This is supported by calcite $\delta^{13}C$ signatures which indicate that bicarbonate was supplied from a marine source.

Early diagenetic calcite cements have also been reported from other Brent Group oilfields, and their stable isotopic ratios have been plotted in Figure 19. All these calcite cements have a non-ferroan chemistry and exhibit high minus cement porosities, indicating they precipitated prior to significant compaction, at low temperatures (Giles *et al.* 1992; Haszeldine *et al.* 1992). Oxygen isotopic data suggests that Brent Group calcites precipitated from meteoric-derived waters at temperatures of <30°C (Giles *et al.* 1992; Haszeldine *et al.* 1992). This contrasts with calcite cement from the Emerald oilfield, which also precipitated at low temperatures (26-30°C), but from sea-water rather than meteoric water. As can be seen from Figure 19, calcite cements from the Emerald oilfield have higher $\delta^{18}O$ than all other Brent Group calcites. This can be explained if the Emerald oilfield calcites precipitated from sea-water, instead of meteoric-derived water. Temperature cannot explain the differences in $\delta^{18}O$ of the calcites, as all early diagenetic Brent Group calcite cements are thought to have grown at roughly the same temperature (<30°C) and depth of burial.

Why did calcite from the Emerald oilfield precipitate from sea-water whereas all other Brent Group calcites precipitated from meteoric water? This can be explained by differences in the depositional environment of the Emerald Sand compared to other Brent Group Formations. The Rannoch, Etive and Ness Formations of the Brent Group are deltaic or shallow marine in origin and were deposited during delta progradation. Hence influx of meteoric water through the delta top sediments of the Ness Formation could have resulted in the displacement of depositional marine pore-waters from the Rannoch and Etive Formations. By contrast the Emerald Sand is a transgressive marine sand-body; hence depositional pore-waters would be marine, and there would be less opportunity for the incursion of meteoric waters during relative sea level rise than during delta progradation.

3.8.2 Stable isotope ratios of kaolinite

Isotopic data for kaolinite are tabulated in Table 4. Using the fractionation equations of Savin & Lee (1988) and Lambert & Epstein (1980), we can construct a δD_{SMOW} versus $\delta^{18}O_{SMOW}$ cross-plot, relating kaolinite mineral isotopic compositions to the temperature and stable isotopic composition of the pore-water from which the kaolinite originally precipitated (Figure 20). This approach assumes that no post-formational hydrogen isotopic exchange has occurred between the kaolinite and organic compounds, or later pore-waters. From the combined δD_{SMOW} versus $\delta^{18}O_{SMOW}$ plot in Figure 20 we can see that the stable isotopic composition of the kaolinite indicates that it precipitated at 25-50°C from pore-waters with $\delta^{18}O$= -6.5 to -4‰. As pre-Miocene sea water is thought to have had $\delta^{18}O$= -1‰ (Sheppard 1986) it is unlikely the kaolinite precipitated from a marine water. Instead the calculated low $\delta^{18}O$ values suggest that there was a large component of meteoric water in the pore-fluid. Jurassic meteoric water is thought to have had $\delta^{18}O$= -6 to -7‰ (Hamilton *et al.* 1987; Hudson & Andrews 1987; Fallick *et al.* 1993) and Tertiary meteoric water $\delta^{18}O$= -10‰ (Fallick *et al.* 1993). The calculated pore-water values for the kaolinite ($\delta^{18}O$= -6.5 to -4‰) could hence represent a mixture of meteoric water and depositional marine pore-water, or alternatively a meteoric water that had evolved isotopically due to water-rock interaction (Sheppard 1986). Hence meteoric water must have flushed through the Emerald Sand and partially expelled depositional marine pore-fluids at the time of kaolinite precipitation.

3.8.3 Stable isotope ratios of ankerite

Using Figure 17 it can be seen that ankerite is isotopically distinct from the diagenetically earlier calcite cement. Ankerite $\delta^{13}C$ values are enriched in the heavy isotope, indicating that ankerite bicarbonate was produced by microbial fermentation reactions (Irwin *et al.* 1977). The CO_2 produced during microbial methanogenesis has $\delta^{13}C$ of approximately +15‰, which is close to the maximum observed in this study. However most other ankerites are less enriched in ^{13}C, this may be due to the incorporation of relatively ^{13}C depleted carbonate following the replacement of calcite cement and dissolution of bioclasts. Alternatively the variation in $\delta^{13}C$ values could simply reflect the isotopic composition of the CO_2 released at a particular stage in organic maturation.

Using the fractionation equation for ankerite of Fisher & Land (1986), it can be seen that if ankerite precipitated from meteoric pore-waters with $\delta^{18}O$= -7.0‰ then it grew at 35-50°C (Figure 21). Conversely, if we assume that ankerite precipitated from sea water ($\delta^{18}O$= -1.2‰), then it grew at 67-90°C (Figure 21). These latter growth temperatures are far higher than the reservoir temperature of the Emerald oilfield today (60°C Wheatley *et al.* 1987); hence it is very unlikely that ankerite precipitated from sea water. It is thus more probable that ankerite precipitated from meteoric or brackish pore-waters, with similar $\delta^{18}O$ and temperature to those from which kaolinite precipitated.

Ankerite cement has also been found in more deeply buried Brent Group oilfields, where it is a relatively late diagenetic phase coinciding with oil migration (Brint 1989; Giles *et al.* 1992; Kantorowicz 1985). Stable isotopic compositions of these ankerites are shown in Figure 22. In the Emerald oilfield, $\delta^{13}C$ values clearly indicate that ankerite bicarbonate was supplied by bacterial fermentation reactions. However, ankerite from deeply buried Brent Group oilfields have more negative $\delta^{13}C$ ($\delta^{13}C$= -4.1 to -13.6‰), suggesting that CO_2 produced during abiotic degradation of organic matter ($\delta^{13}C$= -10 to -25‰; Irwin *et al.* 1977) was more important as a source of carbonate. This would certainly be expected if these ankerites formed at greater depths of burial (higher temperatures) than the ankerites from the Emerald oilfield. Oxygen isotopic data also suggests that ankerites from deeply buried oilfields precipitated at much higher temperatures from pore-waters with a different isotopic composition. Kantorowicz (1985) has argued that ankerite in the Ninian oilfield precipitated at 98-144°C, from an isotopically evolved or mixed water with $\delta^{18}O$ approximately -1‰.

3.9 STRONTIUM ISOTOPE DATA

Sr isotope data for ankerite and calcite from the Emerald oilfieldare shown in Table 5, and presented graphically in Figure 23. None of the calcites and ankerites have high Rb concentrations, therefore recalculation for Rb-Sr decay changes $^{87}Sr/^{86}Sr$ insignificantly.

3.9.1 Calcite $^{87}Sr/^{86}Sr$

As can be seen from Figure 23 the $^{87}Sr/^{86}Sr$ ratios of calcite cement in the Emerald Sand are above that of Jurassic sea water (Burke *et. al.* 1982). This

indicates that the Sr present in the calcite was not derived from sea water or from the dissolution of shell material alone. The $^{87}Sr/^{86}Sr$ values of other Brent Group siderites, calcites and ankerites have been interpreted to be a product of mixing between two sources of Sr; Jurassic shell debris or sea water (Sr=7000-9400ppm; $^{87}Sr/^{86}Sr$= 0.707) and degrading detrital feldspars and micas (Sr= 33-1238ppm; $^{87}Sr/^{86}Sr$=0.70635-0.709752) (Brint 1989; Haszeldine *et al.* 1992). Dating of detrital muscovites from the Rannoch Formation by Hamilton *et al.* (1987) yielded an age of 440 Ma, which suggests that they were derived from the Scottish Caledonides. As can be seen from Figure 24 calcites, ankerites and some siderites from the Brent Group have Sr concentrations and $^{87}Sr/^{86}Sr$ which could reflect two component mixing between Jurassic sea water (or shell material) and detrital K-feldspar sourced from the Scottish Caledonides. It is hence possible that Sr in calcite cement from the Emerald Sand is a mixture of Sr from sea water or shells, plus Sr derived by the leaching of aluminosilicates. As calcite is seen replacing both detrital feldspars and bioclasts in the Emerald Sand, this hypothesis is certainly feasible.

From Figure 24 it can also be seen that a few Brent Group siderites have relatively low Sr concentrations and high radiogenic $^{87}Sr/^{86}Sr$ ratios which cannot be explained by mixing of Sr derived from shell debris and K-feldspar. However it is likely that these siderites derived some of their Sr from the degradation of detrital micas, as their Sr concentrations and $^{87}Sr/^{86}Sr$ ratios are roughly intermediate between those of Jurassic sea water (shell debris) and detrital micas (Figure 25). Authigenic siderite in the Brent Group is commonly observed to precipitate between the expanded cleavage planes of frayed biotites (Haszeldine *et al.* 1992), hence a Sr contribution from mica is very likely.

3.9.2 Ankerite $^{87}Sr/^{86}Sr$

As can be seen from Figure 23 ankerite from the Emerald oilfield has slightly more radiogenic values ($^{87}Sr/^{86}Sr$=0.70974) than the texturally earlier calcite cement ($^{87}Sr/^{86}Sr$=0.70857-0.709896). Ankerite is also more Sr rich (679ppm) than calcite (454-525ppm) (Table 5). The more radiogenic Sr in the ankerite suggests an increased component of Sr derived via the leaching of detrital feldspars. Indeed ankerite is commonly observed to replace detrital feldspars within calcite concretions. This suggests that dissolving shell debris was less important as a source of Sr, Ca, and Mg ions and bicarbonate for

ankerite precipitation. However ankerite Sr values still suggest an input of marine derived strontium. As ankerite is observed to replace calcite, marine Sr could be inherited from the dissolution of calcite.

3.10 FLUID INCLUSION STUDY OF QUARTZ CEMENT

Quartz overgrowths are very thin in the Emerald Sand, which makes it difficult to find any intact primary fluid inclusions trapped within the cement. Nevertheless, a number of inclusions were located and subjected to microthermometric analysis. Fluid inclusion homogenisation temperatures (T_h) range from 51-89°C, with a clear mode at 60-70°C (N=60) (Figure 26, data from Table 5). No pressure correction has been applied to the inclusion T_h data because the contents are assumed to be saturated in methane (Hanor 1980), therefore inclusion T_h should approximate to the true trapping temperature of the inclusion fluids.

These fluid inclusion temperatures are problematic as they are equal to, or hotter (51-89°C) than the present day reservoir temperatures (60°C). If the fluid inclusion temperatures are correct, then quartz cement must have precipitated during the late Tertiary when the reservoir was approaching maximum depth of burial. This is very difficult to envisage because oil migration into the Emerald oilfield would have been complete by the late Palaeocene-early Eocene (Wheatley *et al.* 1987) when the reservoir was only buried to a depth of 1400m and at a temperature of approximately 49°C assuming the geothermal gradient was similar to today's (35°C/km^{-1}). As the migration of oil into the reservoir would eventually have halted diagenesis, continued quartz growth during the late Tertiary is hence infeasible. There are two possible explanations for these apparently spuriously hot fluid inclusion temperatures.

1) Perhaps the ambient geothermal gradient at the time of quartz cementation was much higher than today; fluid inclusion temperatures would indicate that it could have been as much as 85°C/km^{-1}. Alternatively hot fluids could have entered the reservoir via faults from the basin in the east. Note however, that we have no corroborative evidence that hot reservoir temperatures were attained during the early Tertiary. Oxygen isotope analyses of ankerite and kaolinite cements are consistent with precipitation from meteoric water at low temperatures. Furthermore the oil in the Emerald oilfield is biodegraded (Wheatley *et al.* 1987). This could not have occurred if reservoir temperatures

were as high as the fluid inclusions suggest, as biodegradation is possible only at low temperatures (Dimitrakopoulos & Meuhlenbachs 1987; Hunt 1979). Hence we have no strong evidence that the fluid inclusions are correct.

2) The fluid inclusion temperatures could have been reset during burial so that they are no longer representative of the growth temperatures of the quartz (Osborne & Haszeldine 1993). We would certainly expect the fluid inclusions in the Emerald oilfield to be reset because the overgrowths are very thin and the inclusions are only trapped by a slender layer of quartz, sometimes only a few microns thick. This renders the inclusions liable to decrepitation. Leakage or stretching of the inclusion will also tend to increase the homogenisation temperature of the inclusions so that they become representative of maximum burial temperatures (Barker & Goldstein 1991). It is interesting to note that the modal T_h of the inclusions is 60-70°C, similar to today's reservoir temperatures (60°C). This suggests that the inclusions have been reset and record no useful information on the growth temperature of the host quartz.

3.11 BIODEGRADATION OF OIL

In the Emerald field 90-99% of the oil contains organic compounds which are indicative of biodegradation (Wheatley *et al.* 1987). Bacterial degradation of hydrocarbons has resulted in the development of low API (24°), relatively heavy oils, which are typical of those found on the Transitional Shelf today (Wheatley *et al.* 1987). Aerobic degradation of hydrocarbons in this manner requires the following conditions (Hunt 1979);

1. Low temperatures (20-50°C) to permit growth of bacteria.
2. Influx of oxygenated waters ($8mg/l^{-1}$ dissolved O_2) to support bacteria.
3. Absence of H_2S, which poisons aerobic bacteria.

Influx of oxygenated meteoric water into the Emerald Sand during shallow burial (low temperatures) would fulfil all the above criteria. This is supported by oxygen isotope ratios of both ankerite and kaolinite cements, which indicate that meteoric water was present in the pore-fluid at the time these cements precipitated. In addition, the unusually enriched $d^{13}C$ signatures of the ankerite cements which are associated with dissolved feldspars indicate that anaerobic fermentation of organic compounds was the source of CO_2 for carbonate precipitation. Dimitrakopoulos & Muehlenbachs (1987) have recorded similar values from carbonates from the Lower

Cretaceous heavy oil deposits of the Alberta basin ($\delta^{13}C$ as high as +14.3‰). They believe such carbonates are produced by the in-situ degradation of petroleum via a two stage process. In the first stage meteoric water with dissolved O_2 interacts with the petroleum and aerobic bacteria degrade the hydrocarbons, releasing large volumes of acids, alcohols and ketones. CO_2 with a very depleted $\delta^{13}C$ signature is produced. This can result in the precipitation of $\delta^{13}C$ depleted carbonates (Figure 27). However in other instances the organic acids produced during biodegradation will actually inhibit the precipitation of carbonates and result in feldspar dissolution (Curtis 1983; Surdam *et al.* 1984). The second stage in the biodegradation process occurs once the oxidising potential of the meteoric water has been exhausted, either because meteoric flow has ceased or because the volume of oil is so great that all O_2 available is utilised. Under such circumstances bacterial degradation of the organic acids occurs in anoxic conditions. This will raise the pH and result in the precipitation of carbonates. Because hydrocarbons have been biodegraded by anaerobic fermentation reactions the CO_2 produced is enriched in $\delta^{13}C$. Hence carbonates with enriched $\delta^{13}C$ signatures are precipitated (Figure 27).

We can hypothesise that such bacterial fermentation of hydrocarbons has occured in the Emerald oilfield because a high percentage of hydrocarbons are biodegraded (Wheatley *et al.* 1987), and because carbonates have very enriched $\delta^{13}C$ signatures. Integration of mineral growth temperatures with a model of subsidence history (Figure 28) indicates that kaolinite and ankerite cementation, and feldspar dissolution, were roughly synchronous with the migration of oil into the reservoir. Hydrocarbons underwent biodegradation in the low salinity pore-waters. With deeper burial the Emerald Sand was perhaps cut-off from meteoric water ingress, allowing the migration of a small amount of unbiodegraded oil (Wheatley *et al.* 1987). Alternatively this small component of non-biodegraded oil may indicate that the oxidising potential of the meteoric water was exhausted through interaction with the large volume of hydrocarbons entering the reservoir. Once oil completely filled the reservoir, further diagenesis was halted.

Biodegradation of petroleum has also occured in other Brent Group oilfields; in the Gullfaks field oil became degraded as it migrated into the shallow reservoir (<2000m) in the late Cretaceous-Palaeocene (Larter & Horstad 1992). Similarly, Miles (1990) found that oil in the Ninian field contained a small biodegraded component. This was produced during the late Cretaceous, when early-migrating hydrocarbons were degraded through

interaction with meteoric waters as they entered the shallow buried reservoir (<1500m). However, in the Ninian oilfield, the effect of this early biodegradation has been masked by the later Tertiary migration of non-biodegraded oils. The presence of a component of biodegraded oil in these reservoirs suggests that influx of meteoric water into the Brent Group was a common process during shallow burial. Hence meteoric flushing may have have influenced the early diagenesis of the reservoir sandstones. This supports the idea that study of the Emerald oilfield could provide an insight into the early diagenetic history of the Brent Group as a whole.

3.12 DISCUSSION

3.12.1 Influx of meteoric water

As has been discussed previously, early cements such as pyrite and K-feldspar and calcite probably precipitated from depositional marine pore-waters. Kaolinite and ankerite cements post-date the development of calcite concretions. On stable isotopic grounds both kaolinite and ankerite are inferred to have precipitated from meteoric or brackish water at low temperatures (25-50°C). If the hot fluid inclusion temperatures from quartz overgrowths are rejected as being unreliable, then it is likely that quartz cement precipitated at the same time and temperature as kaolinite, following the dissolution of feldspar.

Hence the diagenetic minerals present in the Emerald Sand record a change in the chemistry of the pore-fluid through time, with depositional marine pore-waters being replaced by meteoric waters. There are at least two possible scenarios whereby meteoric water could have entered the Emerald Sand.

1) During the lower Cretaceous the Transitional Shelf tilted to the west and the fault block crest may have become subaerially exposed in the vicinity of the present day Emerald oilfield. Hence it is possible that meteoric waters could have penetrated the Emerald Sand via the fault block crest. Other Brent Group oilfields have been interpreted to have been flushed by meteoric water in this manner (Bjorlykke *et al.* 1992; Haszeldine *et al.* 1992; Shanmugan 1990).

However this is an unlikely scenario in the case of the Emerald oilfield, because boreholes show that the Emerald Sand itself was not subaerially

exposed, but remained capped by at least 75m of Jurassic claystones and siltstones. These overlying sediments would have low permeabilities, and because they were relatively unconsolidated at the time of exposure they would probably be rapidly eroded to wave-base. Hence fault block topography was probably not elevated to any great extent above sea level. This means it is unlikely that large volumes of meteoric water could have entered the Emerald Sand via the fault block crest.

In support of this conclusion we note that there is no systematic variation in the amount of total porosity, feldspar, secondary porosity, kaolinite and stable isotopic signature of the cement, from the top to the bottom of the reservoir unit (Figure 29). If corrosive meteoric water was percolating down into the Emerald Sand from above we would expect the top of the sandstone to exhibit greater amounts of leaching. Such weathering profiles have been seen in the Magnus oilfield where the reservoir sandsone was sub-aerially exposed at the fault crest in the Cimmerian (Emery *et al.* 1990; Macaulay *et al.* 1993). Cements beneath this Magnus unconformity also exhibit systematic changes in stable isotopic composition with increasing depth (Macaulay *et al.* 1993). However this type of leaching profile is absent from the Emerald Sand (Figure 28).

2) As an alternative to the model discussed in 1 above, it is possible that meteoric water entered the Emerald Sand via the landmass in the west. Meteoric water falling as rain on a landmass may flow below the sea floor far into marine sedimentary basins (Bethke 1989). For example freshwater aquifers occur 120km off the Florida coast in Tertiary carbonate aquifers (Mannheim, 1967). The depth of penetration of meteoric water is also considerable; in the Great Artesian Basin of Australia the meteoric aquifer lies at depths of up to 2000m (Habermehl, 1980). Hence it is perfectly possible that the Emerald Sand was flushed by meteoric water during relatively shallow burial. The flux of meteoric water into the Emerald Sand would be encouraged by the widespread sheet distribution of the sandbody; the presence of underlying fractured, permeable, basement; and the close proximity of the elevated landmass (3-15km distant, Wheatley *et al.* 1987) during late-Jurassic to early Cretaceous and Palaeocene times.

Meteoric water flowing into the basin through permeable aquifers must continue up to the surface. In the case of the Emerald Sand, this would mean that flow must continue up through the overlying claystones and siltstones, which we would expect to have a lower permeability. However recently

deposited and poorly compacted clays have considerable vertical permeability and are not good aquitards. At a burial depth of a few hundred metres muddy sediments may have horizontal permeabilities up to 1mD, with vertical permeabilities less than this (Riecke & Chillingarian 1974), therefore meteoric flow could have been allowed to continue to the surface.

During the Palaeocene there was rapid regional uplift of the East Shetland Platform and the Scottish landmass, and vast amounts of clastics were shed over the whole Transitional Shelf area (Wheatley *et al.* 1987). Uplift of adjacent landmasses could have created a large hydrostatic head of meteoric water which would have been capable of penetrating deep into the subsurface and flushing through the marine sediments to the east, displacing the depositional marine pore-fluids (Figure 30).

Hence it appears that the most likely mechanism for allowing meteoric water to enter the Emerald Sand is a regional meteoric flow model, with the fluid being derived from the landmass to the west during the Paleocene.

3.12.2 Relationship between diagenesis, meteoric fluid flow, and biodegradation of oil

Within calcite concretions in the Emerald oilfield, detrital feldspars have been dissolved and both ankerite and kaolinite cements have precipitated in the secondary porosity created. This opens the possibility that there may be some kind of genetic link between the dissolution of feldspars and the growth of ankerite and kaolinite cements. Oxygen isotope studies of these two cements suggests that they precipitated from meteoric or brackish waters at similar temperatures (approximately 25-50°C). Textural evidence further suggests that the two have precipitated at roughly the same time.

There are several possible mechanisms that could generate corrosive fluids, and hence result in the dissolution of feldspar.

1. Acidic fluids produced during the thermal maturation of organic matter (Surdam *et al.* 1984).
2. Acidic fluids generated by clay mineral reactions (Bjorlykke, 1983).
3. Meteoric water penetration (Giles & Marshall 1986).
4. Acidic fluids released by aerobic degradation of petroleum (Dimitrakopoulos & Meuhlenbachs 1987).

We shall now critically examine each of these possible mechanisms in turn, in order to constrain what processes were responsible for feldspar dissolution in the Emerald Sand.

1. Acidic fluids from organic matter maturation. CO_2 and carboxylic acids can be released from organic compounds as they undergo thermal maturation. Solution of these compounds into water could result in feldspar dissolution, and the subsequent precipitation of kaolinite as a by-product of the dissolution reaction. However the mass balance calculations of Giles & Marshall (1986) indicate that most of the CO_2 and organic acids produced would interact with carbonates and silicates present within the organic rich source rocks themselves, and hence be unavailable for the leaching of reservoir sandstones. In addition most carboxylic acids are released at temperatures of 80-120°C; temperatures far hotter than those found in the Emerald oilfield, hence production of large volumes of acids from the overlying Heather Formation shales is unlikely. The source rock for the oil in the Emerald field is thought to be the deeply buried Kimmeridge Clay in the basin to the east (Wheatley *et al.* 1987). However, acidic fluids released from the Kimmeridge Clay would be neutralised by interaction with minerals before entering the Emerald Sand, and hence are unlikely to have produced the feldspar dissolution observed.

2. Acidic fluids released by clay mineral reactions. Bjorlykke (1981) has proposed that conversion of smectite to illite, and the illitisation of kaolinite can both release H^+, which would result in acidic fluids capable of leaching feldspars. Neither of these reactions is a feasible source of aggresive fluids in the case of the Emerald Sand, as no illite and only trace amounts of other detrital clays have been observed within the reservoir itself. Again any acids produced from the Kimmeridge Clay or Heather formation shales would probably be buffered at source by reaction with enclosing mineral surfaces (Giles & Marshall 1986).

3. Meteoric water is a potential feldspar leaching agent because it is slightly acidic due to the presence of dissolved CO_2 in rainwater, and organic acids derived from soil profiles. Rate of feldspar dissolution is not directly proportional to the flux, but a minimum flux is required to remove K^+ and keep the pore-water in the stability field of kaolinite (Bjorlykke & Aagaard 1992). Because meteoric water leaching occurs at low temperatures when

mineral dissolution rates are slow, the pore-water may remain in the stability field of kaolinite for a long time. This allows leaching to take place over a flow pathway of great length. For a meteoric fluid to remain corrosive, a rapid flow of fluid through overlying strata into the aquifer is required, otherwise the acidity of the fluid will be neutralised by reaction with minerals in the overlying rocks. However it is possible that meteoric water could remain acidic for a greater length of time if it passed through shallow buried sediments which were generating CO_2 during the decomposition of organic matter (Bjorlykke & Aagaard 1992). As meteoric water flows through the rock its pH and content of alkali ions will gradually increase. The pH necessary to saturate the pore-water with respect to Na-feldspar is higher than that required for saturation with respect to K-feldspar (Bjorlykke & Aagaard 1992); this explains why Na-feldspar is more leached than K-feldspar in the Emerald Sand.

In the case of the Emerald Sand, there is strong circumstancial evidence that meteoric water was the leaching agent because;

a) Oxygen isotopic evidence indicates that kaolinite and ankerite precipitated from meteoric water-influenced fluid. Both these minerals are texturally associated with dissolved feldspars.
b) The Emerald oilfield lies close to the East Shetland Platform, a palaeolandmass and hence a source of meteoric fluid.
c) The Emerald field is only shallow buried, hence acidic meteoric fluid might have been able to enter the reservoir relatively quickly, before its leaching capacity was reduced by reaction with minerals in overlying rocks. Incorporation of CO_2 generated from overlying shallow buried sediments may also have allowed the meteoric water to retain its acidity.
d) The oil in the Emerald oilfield is biodegraded, probably as a result of the interaction of oxygen-bearing meteoric water with hydrocarbons.

4. Acidic fluids released by the aerobic degradation of petroleum.

Where hydrocarbons are subject to microbiological attack vast amounts organic acids will be produced, which will result in feldspar dissolution (Dimitrakopoulos & Muehlenbachs 1987). Biodegradation of oil in this manner is likely to occur at shallow depths (low temperatures) in the presence of sulphate-poor, oxygenated water (i.e. meteoric fluid). We know such processes have been active in the Emerald oilfield because;
a) The oil is biodegraded (API gravity 24.5°).

b) Oxygen isotopes indicate that kaolinite and ankerite cements precipitated from meteoric water, hence meteoric fluids must have flushed through the reservoir displacing depositional marine pore-waters.
c) Ankerite cements have unusually enriched $\delta^{13}C$ signatures ($\delta^{13}C$= +6.7 to +15.8‰). According to Dimitrakopoulos & Meuhlenbachs (1987) anaerobic fermentation of petroleum in meteoric waters can generate $\delta^{13}C$ enriched CO_2, which can subsequently precipitate as $\delta^{13}C$ rich carbonate cement ($\delta^{13}C$ as high as +14.3‰).

Hence it appears that there are two possible mechanisms capable of producing the feldspar dissolution observed in the Emerald Sand; meteoric flushing, and in-situ biodegradation of petroleum. Both these processes can be linked, as petroleum biodegradation requires that sulphate-poor oxygenated meteoric water interacts with the hydrocarbons. In the Emerald Sand, precipitation of kaolinite and partial export of silica has occured following feldspar dissolution. This selective removal of silica can also be explained by influx of meteoric water through the aquifer. Kaolinite is extremely insoluble, hence following feldspar dissolution, the aluminium concentration of pore-waters does not have to build up very far before saturation with respect to kaolinite will be acheived (Giles & deBoer 1990). However, at low temperatures, the silica saturation required for quartz precipitation is much higher than that for kaolinite. In addition, silica precipitation rates at low temperatures are slow, hence even if silica saturation with respect to quartz has been reached, quartz may not immediately precipitate (Giles & deBoer 1990). If large volumes of meteoric water flushed through the Emerald Sand at the same time as feldspar was dissolving, then the silica concentration may have been kept sufficiently low to avoid quartz precipitation, while still allowing kaolinite growth. This would have resulted in the export of Si ions from the Emerald Sand, creating effective secondary porosity.

3.12.3 Implications for the petroleum geologist

1. Dissolution of feldspar in the Emerald Sand and export of Si ions would have resulted in the production of at least 7% effective secondary porosity, potentially improving the reservoir quality of the sandstone. However, in order to prove that secondary porosity really has improved reservoir quality, it is necessary to show that sandstone porosities in the Emerald Sand are significantly higher than those occurring in similar rocks buried to the same

depth (Giles & deBoer 1990). Unfortunately the helium porosities of the Emerald Sand (averaging 30-27%, Wheatley *et al.* 1987) are not significantly higher than those of other Brent Group sandstones buried to similar depths (averaging 30% at 6700ft, Giles *et al.* 1992). This implies that the extra porosity created by feldspar dissolution in the Emerald Sand has been lost during later compaction. This observation is consistent with those of other Brent Group researchers, who find that the feldspar content of the Brent Group decreases with increasing depth of burial, yet the amount of secondary porosity present remains roughly constant (averaging 3%; Bjorlykke *et al.* 1992; Harris 1992). The amount of secondary porosity present is thought to be limited by the mechanical strength of the sandstone, with most of the large secondary pores produced by feldspar dissolution being crushed during compaction (Harris 1992). Hence despite extensive feldspar dissolution, reservoir porosities have not been greatly improved.

Mass balance calculations suggest that Al has been conserved following feldspar dissolution, due to kaolinite precipitation. Hence permeabilities have not been significantly increased, due to growth of kaolinite in the secondary pores. This is supported by permeability data which indicates that the Emerald Sand has similar, or lower permeabilities than other shallow buried Brent Group sandstones. Emerald Sand permeabilities average 933-159mD, (Wheatley *et al.* 1987), while Brent Group sandstones have horizontal air permeabilities averaging 1000mD at 6700ft burial (Giles *et al.* 1992). Hence despite significant dissolution of feldspar during shallow burial, there has been no net improvement in either the porosity or permeability of the Emerald Sand due to secondary porosity creation.

2. As ankerite cements were produced following the biodegradation of migrating hydrocarbons, carbonates with unusually high $\delta^{13}C$ could be used to pinpoint oil-bearing Formations throughout the Transitional Shelf area.

3. Oil should become more biodegraded (lower API gravity) towards the westerly part of the Transitional Shelf area, as this was the point of entry for meteoric water. The amount of secondary porosity in the Emerald Sand may also increase towards the west, again because this was closer to the point of entry for acidic meteoric fluid.

4. Extensive calcite cemented horizons in the Emerald Sand are likely to occur wherever laterally-extensive storm deposits with a high concentration of

bioclasts are found. Such horizons, which have <1% porosity, could compartmentalise the reservoir if they were laterally continuous. In the Emerald oilfield these carbonate cemented zones are restricted to well 2/10a-6, and cannot be correlated across the field. However in other areas of the Transitional Shelf they may be important permeability barriers. As ankerite cement is produced following the biodegradation of petroleum, there is also the possibility of enhanced ankerite precipitation at the oil-water contact. This could impair the connection between the oil leg and the water leg, directly influencing oil production. However as no well has been drilled through the oil-water contact in the Emerald oilfield this hypothesis cannot be tested at present.

5. As influx of meteoric water into the Emerald Sand is thought to have occurred during the Palaeocene, any oil migrating into a shallow buried reservoir (<1400m; <50°C) at this time is likely to have undergone biodegradation. It is likely that overlying Tertiary sands also contain biodegraded oils. Non-biodegraded oils will occur in more deeply buried reservoirs on the Transitional Shelf, or in reservoirs which were filled in post-Palaeocene times.

6. The diagenetic processes which have affected the Emerald Sand are broadly similar to those which occured in the Brent Group as a whole during early diagenesis (shallow burial). In both instances influx of meteoric water is inferred to have occured; this resulted in feldspar dissolution, and created effective secondary porosity. This secondary porosity was subsequently lost during compaction. Early migration of hydrocarbons into the shallow buried reservoirs during Cretaceous-Palaeocene resulted in the biodegradation of oil, though in more deeply buried Brent Group reservoirs later Tertiary migration of hydrocarbons masked the effect of early biodegradation.

3.13 CONCLUSIONS

1) The diagenesis undergone by the Emerald Sand reflects a change in the chemistry of the pore-fluid through geologic time. Early diagenetic cements (pyrite, K-feldspar, and calcite) precipitated from sea water trapped in the sediment upon deposition. Later cements (ankerite, kaolinite, and quartz) precipitated from a meteoric derived pore-fluid.

2) The hydrocarbons in the Emerald oilfield have been biodegraded due to the influx of oxidising, low salinity meteoric water. Degradation of petroleum may have produced organic acids hence leading to feldspar dissolution, the formation of secondary porosity, and the precipitation of kaolinite within secondary pores. Mass balance calculations indicate that following feldspar dissolution Al was conserved, but Si partly exported, creating secondary porosity (5 volume%). However much of this porosity was lost during later compaction, with no net gain in reservoir quality. Anaerobic bacterial fermentation of the degraded petroleum produced ankerite cements with unusually enriched $\delta^{13}C$ signatures.

3) Meteoric water entered the Emerald oilfield from the East Shetland Platform during the Palaeocene, when the Scottish landmass was being uplifted and a large hydrostatic head was available to drive fluids deep into the subsurface.

3.14 ACKNOWLEDGEMENTS

The technical staff of the isotope geology unit at the S.U.R.R.C. are thanked for their unstinting aid, especially Alison McDonald, and Julie Gerc. Douglas Maclean, Murdo Mcleod, Dougie Turner, John Gileece and Peter Ainsworth from the Glasgow Geology Department also assisted during mineral separation and analysis. Sovereign Oil and Gas p.l.c. provided samples of Emerald core. Lomond Associates kindly loaned some thin sections of the Emerald sand. Mark Osborne acknowledges the receipt of a N.E.R.C. postgraduate studentship grant. The S.U.R.R.C. is supported by N.E.R.C. and the Scottish Universities.

3.15 REFERENCES

Baldwin, B. & Butler, C.O., 1985, Compaction curves. Bull. Am. Assoc. Petrol. Geol., **69**, p.622-626.

Barker, C.E., & Goldstein, R.H., 1991, A fluid inclusion technique for determining maximum temperature in calcite and its comparison to the vitrinite reflectance geothermometer, Geology, **18**, p.1003-1006.

Bjorlykke, K., 1983, Diagenetic reactions in sandstones. In: Parker, A., & Sellwood, B.W., eds., Sediment Diagenesis, NATO, ASI Series, Reidel Publishing Company, p.169-213.

Bjorlykke, K., & Aagaard, P., 1992, Clay minerals in North Sea sandstones. In: Origin, Diagenesis and Petrophysics of Clay Minerals in Sandstones, SEPM Spec. Publ. **47**, p.65-80.

Bjorlykke, K., Nedkvitne, T., Ramm, M., Saigal, G.C., 1992, Diagenetic processes in the Brent Group (Middle Jurassic) reservoirs of the North Sea ; an overview. In Morton, A. C., Haszeldine, R. S., Giles, M. R., & Brown, S., (Eds), *Geology of the Brent Group*. Geological Society of London, Bath UK. p. 263-288.

Borthwick, J., & Harmon R. S., 1982, A note regarding ClF_3 as an alternative to BrF_5 for oxygen isotope analysis. Geochim. Cosmochim. Acta, **46**, p. 1665-1668.

Brint, J. F.,1989, Isotope diagenesis and palaeofluid movement: Middle Jurassic Brent sandstones, North Sea *D. Phil. Thesis* University of Strathclyde, Scotland, 288 p.

Berner, R. A., 1971, Principles of chemical sedimentology, New York, McGraw Hill, 240 p.

Bethke, C.M., 1989, Modelling subsurface flow in sedimentary basins. Geologische Rundschau, **78**, p.129-154.

Burke, W.H., Denison, R.E., Hetherington, E.A., Koepnick, R.B., Nelson H.F., & Otto, J.B., 1982, Variation of sea water $^{87}Sr/^{86}Sr$ throughout Phanerozoic time. Geology, **10**, p.516-519.

Clayton, R.N., & Mayeda, T.K., 1963, The use of bromine pentafluoride in the extraction of oxides and silicates for isotopic analysis. Geochim. Cosmochim. Acta., **27**, p. 43-52.

Craig, H., 1957, Isotopic standards and isotopic correction factors for mass spectrometric analysis of carbon dioxide. Geochim. et Cosmo. Acta., **12**, p.133-149.

Craig, H., 1961, Isotopic variations in meteoric waters. Sci., **133**, p.1702-1703.

Crosbie, T., 1981, Polished wafer preparation for fluid inclusion and other studies: Transactions of the Institute of Mining and Matallurgy, **90**, p.82-83.

Curtis, C.D., 1983, Link between aluminium mobility and the destruction of secondary porosity. Bull. Am. Assoc. Petrol. Geol., **67**, p. 380-393.

Dimitrakopoulos, R., & Muehlenbachs, K., 1987, Biodegradation of petroleum as a source of ^{13}C enriched carbon dioxide in the formation of carbonate cement. Chemical Geology, **65**, p.283-291.

Donovan, T.J., 1974, Petroleum microseepage at Cement, Oklahoma: Evidence and mechanism. Amer. Assoc. Petrol. Bull., **58**, p.429-446.

Emery, D., Myers, K.J., & Young, R., 1990, Ancient subaerial exposure and freshwater leaching in sandstones. Geology, **18**, p.1178-1181.

Fallick, A.E., Macaulay, C.I., & Haszeldine, R.S., 1993, Implications of linearly correlated oxygen and hydrogen isotopic compositions for kaolinite and illite in the Magnus sandstone, North Sea. Clay Minerals (in press).

Fisher, R.S., & Land, L.S., 1986, Diagenetic history of Eocene Wilcox sandstones, South-Central Texas. Geochim. et Cosmochim. Acta, **50**, p.551-661.

Giles, M.R., 1987, Mass balance and problems of secondary porosity creation in deeply buried hydrocarbon reservoirs. Marine & Petroleum geology, **4**.p.188-204.

Giles, M.R., & Boer, R.B., 1990, Origin & significance of redistributional secondary porosity. Marine & Petroleum geology, 7.p.378-397.

Giles, M.R., Stevenson, S., Martin, S. V., Cannon, S. J. C., Hamilton, P. J., Marshall, J. D., & Samways, G. M., 1992, The reservoir properties and diagenesis of the Brent Group; a regional perspective. In Morton, A. C., Haszeldine, R. S., Giles, M. R., & Brown, S., (Eds), *Geology of the Brent Group*. Geological Society of London, Bath UK. p. 289-327.

Glasmann, J.R., 1992, The fate of feldspar in the Brent Group reservoirs, North Sea: a regional synthesis of diagenesis in shallow, intermediate, and deep burial environments. In Morton, A. C., Haszeldine, R. S., Giles, M. R., & Brown, S. (Eds), *Geology of the Brent Group*. Geological Society of London, Bath U.K. p. 329-350.

Glasmann, J. R., Lundegard, P. D., Clark, R. A., Penny, B. K., Collins, I. D., 1989 a, Geochemical evidence for the history of diagenesis and fluid migration: Brent sandstone, Heather field, North Sea *Clay Minerals*, **24**, p. 255-284.

Glennie, K. W.,1990, *Introduction to the Petroleum Geology of the North Sea* (third edition) Oxford, Blackwell Scientific Publications.

Gould, K.W., & Smith, J.W., 1978, Isotopic evidence for microbiologic role in genesis of crude oil from Barrow Island, Western Australia. Amer. Assoc. Petrol. Geol Bull., **62**, p.455-462.

Habermehl, M.A., 1980, The Great Artesian Basin, Australia, BMR. J. Australian Geol. Geophys., **5**, p. 9-38.

Halliday, A.N., Aftalion, M., Van Breemen, O., & Jocelyn, J., 1979, Petrogenetic significance of Rb-Sr and U-Pb isotopic systems in the 400Ma old British Isles granitoids and their hosts. In; Harris, A.L., Holland, C.H.,

& Leake, B.E., (Eds.) *The Caledonides of the British Isles- reviewed.* Geol. Soc. Lond. Spec. Publ., 8, p.653-662.

Hamilton, P.J., Fallick, A.E., Macintyre, R.M., & Elliott, S.,1987, Isotopic tracing of provenance and diagenesis of lower Brent Group sands, North Sea. In Brooks, J., & Glennie, K.W., (eds.), *Petroleum Geology of NW Europe,* Graham & Trotman, London, p.939-949.

Hancock, N.J., & Taylor, A.M., 1978, Clay mineral diagenesis and oil migration in the Middle Jurassic Brent Sand formation, Jour. Geol. Soc. Lond., **135**, p.69-72.

Hanor, J.S., 1980, Dissolved methane in sedimentary brines; potential effect on the PVT properties of inclusion fluids. Econ. Geol. **75**, p.603-617.

Harris, N. B., 1992, Burial diagenesis of Brent sandstones: a study of Statfjord, Hutton and Lyell fields. In Morton, A. C., Haszeldine, R. S., Giles, M. R., & Brown, S. (Eds), *Geology of the Brent Group.* Geological Society of London, Bath U.K. p. 351-375.

Haszeldine, R. S., Brint, J. F., Fallick, A.E., Hamilton, P. J., & Brown, S., 1992, Open and restricted hydrologies in Brent Group diagenesis: North Sea. In Morton, A. C., Haszeldine, R.S., Giles, M. R., & Brown, S.(Eds.), *Geology of the Brent Group.* Geological Society of London, Bath UK. p. 401-419.

Haszeldine, R.S., & Osborne, M., 1993, Fluid inclusion temperatures in diagenetic quartz reset by burial: implications for oilfield cementation. In: Diagenesis and Basin Development (Eds. A. Horbury & A. Robinson), Amer. Assoc. Petrol. Geol. Mem. (in press).

Haughton, P.D.W., Rogers, G., & Halliday, A.N., 1991, Provenance of Lower Old Red Sandstone conglomerates in S.E. Kincardineshire; evidence for the relative timing of Caledonian terrane accretion in Central Scotland. Journ. Geol. Soc. Lond., **147**, p.105-120.

Hogg A.J.C.,1989, Petrographic and isotopic constraints on the diagenesis and reservoir properties of the Brent Group sandstones, Alwyn South, Northern U.K. North Sea *D. Phil. Thesis* University of Aberdeen, Scotland, 414p.

Hudson, J.D., & Andrews, J.E., 1987, The diagenesis of the Great Estuarine Group, Middle Jurassic, Scotland. In Marshall, J.D., (ed), Diagenesis of sedimentary sequences. Geol. Soc. Lond. Spec. Publ., **36**, p.259-276.

Hunt, J.M., 1979, Petroleum geochemistry and geology, W.H. Freeman, San Francisco, California. 617p.

Irwin, H., Curtis, C.D., & Coleman, M., 1977, Isotopic evidence for source of diagenetic carbonates formed during burial of organic rich sediments. Nature, **269**, p.209-213.

Jackson, M.L., 1956, Soil chemical analyses-advanced course. Published by the author, Madison, Wisconsin.

Jackson, M.L., 1979, Soil chemical analyses-advanced course 2nd edition. Published by the author, Madison, Wisconsin.

Kantorowicz, J.D., 1985, The origin of authigenic ankerite from the Ninian field, UK North Sea. Nature, **315**, p.214-216.

Krauskopf, K.B., 1982, Introduction to Geochemistry, McGraw Hill Book Company, Second Edition, 617p.

Lambert S.J., & Epstein, S., 1980, Stable isotope investigations of an active geothermal system in Valles Caldera, Jemez Mountains, New Mexico. J. Volcan. Geotherm. Res., **8**, p.111-129.

Larter, S. & Horstad, I.,1992, Migration of petroleum into Brent Group reservoirs: some observations from the Gullfaks field, Tampen Spur area, North sea: North Sea. In Morton, A. C., Haszeldine, R.S., Giles, M. R., & Brown, S.(Eds.), *Geology of the Brent Group*. Geological Society of London, Bath UK. p.441-452.

Longstaffe, F.J., & Ayalon, A., 1987, Oxygen isotope studies of clastic diagenesis in the Lower Cretaceous Viking Formation, Alberta. In: Marshall J.D., ed., Diagenesis of Sedimentary Sequences, Geol. Soc. Lond. Spec Publ. **36**, p.277-296.

Macaulay, C.I., & Haszeldine, R.S., 1993, Distribution, chemistry, isotopic composition and origin of diagenetic carbonates: Magnus Sandstone, North Sea. Journ. Sed. Petrol., **63**, p. 134-140.

Manheim, F.T., 1967, Evidence for submarine discharge of water on the Atlantic continental slope of the southern United States. Trans. New York Acad. Sci., **11**, p.839-835.

McCrea, J.M., 1950, On the isotope chemistry of carbonates and a palaeotemperature scale scale. Journ. Chem Phys., **18**, p.849-857.

Miles, J.A., 1990, Secondary migration routes in the Brent sandstones of the Viking Graben and East Shetland Basin, Amer. Assoc. Petrol. Geol. Bull., **74**, p.1718-1735.

Nadeau, P.H, & Hurst, A., 1991, Applications of back scattered electron microscopy to the quantification of clay mineral microporosity, Journal of Sedimentary Petrology, 61, p.921-925.

Osborne, M. & Haszeldine, S., 1993, Evidence for resetting of fluid inclusion temperatures from quartz cements in oilfields. Marine and Petroleum Geology, (in press).

Riecke, H.H., & Chillingarian, G.V., 1974, Compaction of argillaceous sediments. In: Developments in Sedimentology, 16, Elsevier, 424p.

Rosenbaum, J. & Sheppard, S.M.F., 1986, An isotopic study of siderites, dolomites and ankerites at high temperatures. Geochim. et Cosmochim. Acta, **50**, p.1147-1150.

Sadd, J.L., 1990, Tectonic influences on carbonate deposition and diagenesis, Buckhorn asphalt, Deese Group, Arbuckle Mountains, Oklahoma. Journ. Sed. Petrol., **61**, p.28-42.

Savin, S.M., & Epstein, S., 1970, The oxygen and hydrogen isotope geochemistry of clay minerals. Geochim. Cosmochim. Acta, **34**, p.43-63.

Savin, S.M., & Lee, M., 1988, Isotopic studies of phyllosilicates. In Miner. Soc. Am. reviews in mineralogy, 16, p.188-223.

Shanmugan, G., 1990, Porosity prediction using erosional unconformities. In: Prediction of reservoir quality using chemical modelling, Eds. I.D. Meshri & PJ Ortoleva, AAPG memoir **49**, p.1-23.

Sheppard, S.M.F., 1986, Characterization and isotopic variations in natural waters. In Miner. Soc. Am. Reviews in Mineralogy, 16, p.165-183.

Sheppard, S.M.F., Nielsen, R.L., & Taylor, H.P., 1969, Oxygen and hydrogen isotope ratios of clay minerals from porphyry copper deposits, Econ. Geol., **64**, p.755-777.

Sommer, F., 1978, Diagenesis of Jurassic sandstones in the Viking Graben, Jour. Geol. Soc. Lond., **135**, p.63-67.

Surdam, R.C., Boese, S.W., Crossey, L.J., 1984, The chemistry of secondary porosity, In *Clastic Diagenesis*, McDonald, D, Surdam, R., (Eds.), American Association of Petroleum Geologists Memoir, 37, p.127-151.

Wheatley, T.J., Biggins, J., Buckingham, & Holloway, N.H.,1987, The geology and exploration of the Transitional Shelf, an area to the west of the Viking Graben. In Brooks, J., & Glennie, K.W., (eds.), *Petroleum Geology of NW Europe*, Graham & Trotman, London, p. 979-989.

Yielding, G., Badley, M.E., & Roberts, A.M., 1992, The structural evolution of the Brent Province. In Morton, A. C., Haszeldine, R.S., Giles, M. R., & Brown, S.(Eds.), *Geology of the Brent Group*. Geological Society of London, Bath UK. p. 27-43.

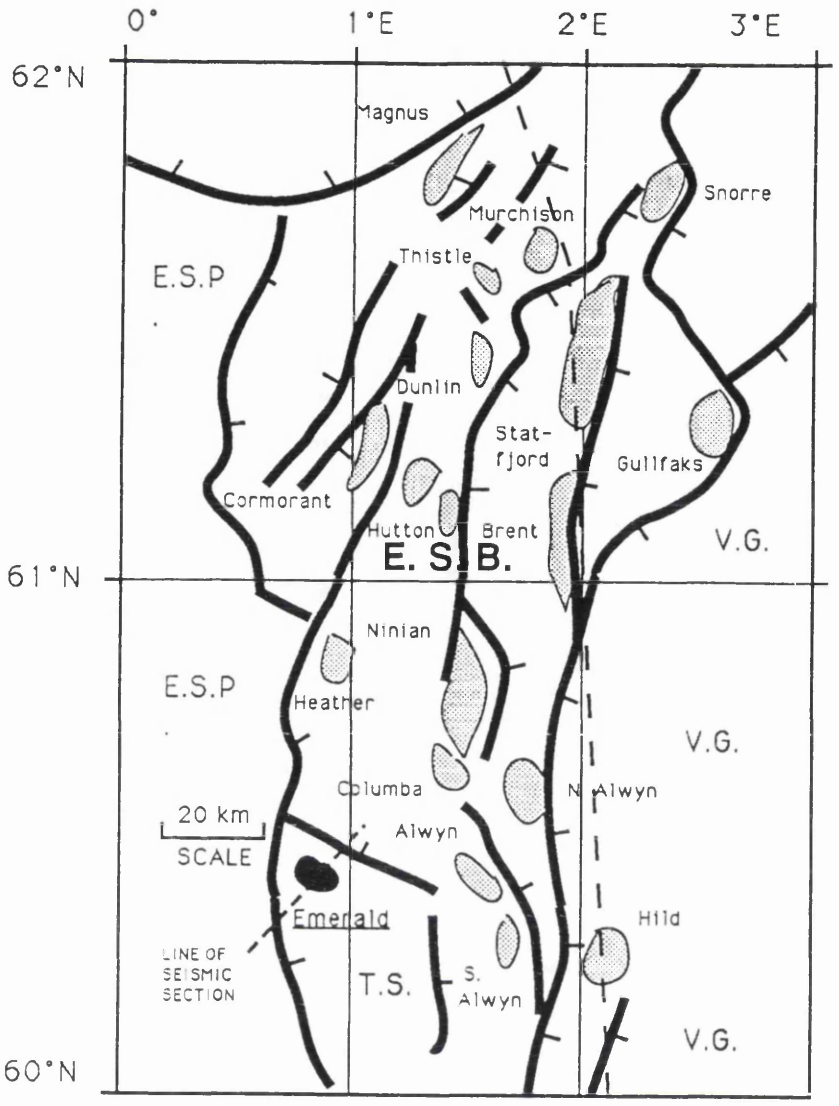

Figure 1. Map of the East Shetland Basin area of the northern North Sea showing the location of the Emerald oilfield. ESP- East Shetland Platform; ESB- East Shetland Basin; TS Transitional Shelf; VG= Viking Graben. Location of seismic section in Figure 2 is shown.

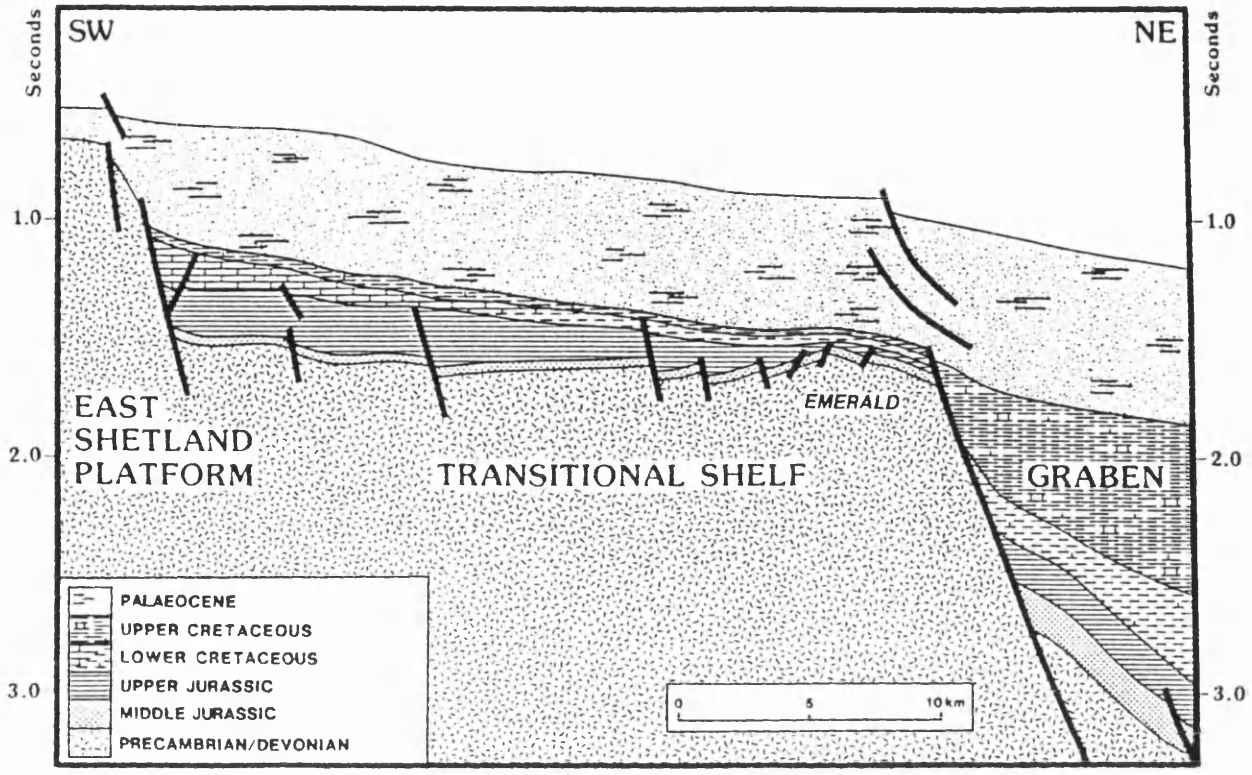

Fig. 2. Regional geoseismic section.

Figure 2. Interpreted seismic section through the Transitional Shelf showing the location of the Emerald oilfield (From Wheatley *et al.* 1987).

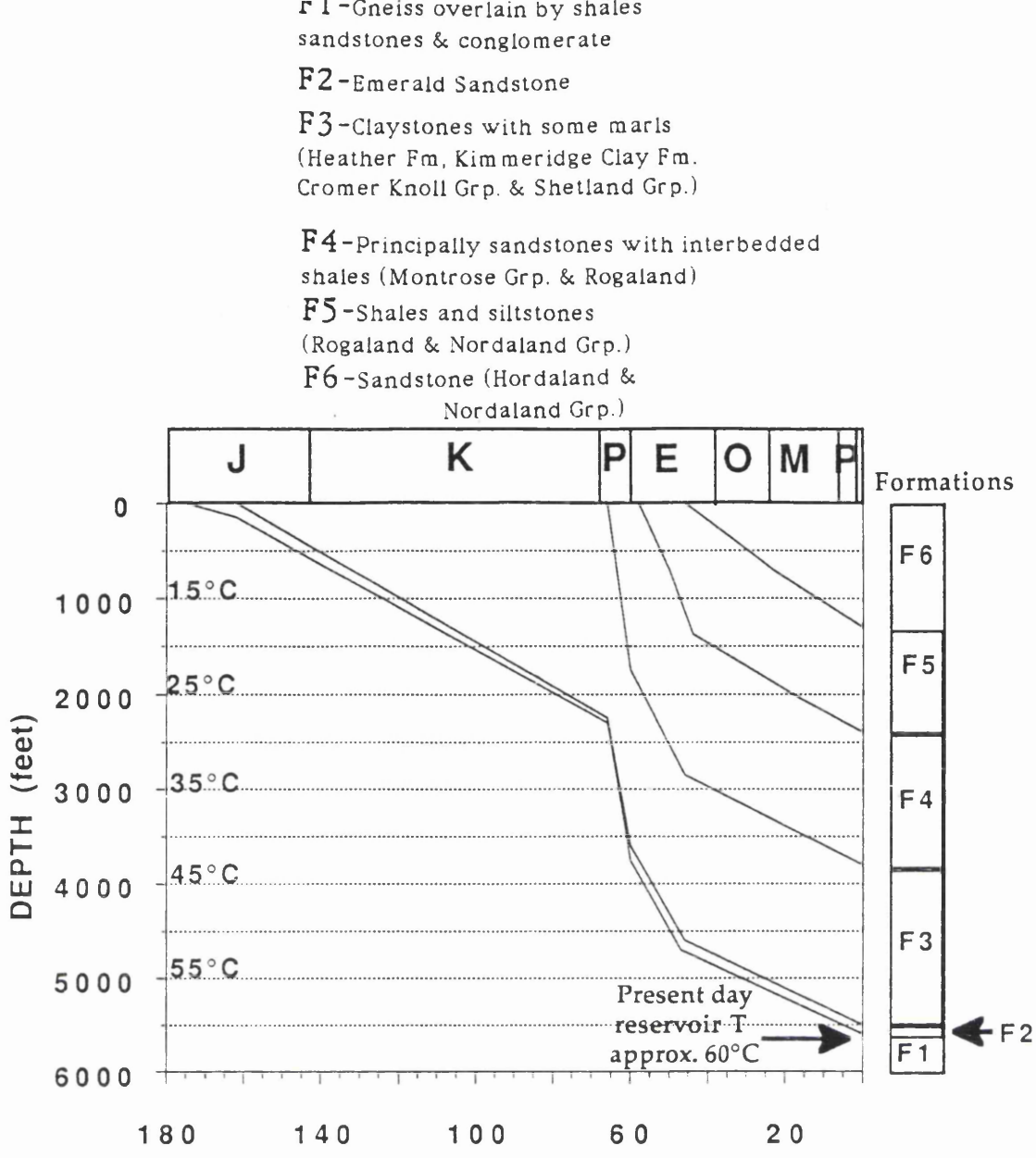

Figure 3. Decompacted burial curve for the Emerald Sand, constructed utilising information in Wheatley *et al.* 1987.

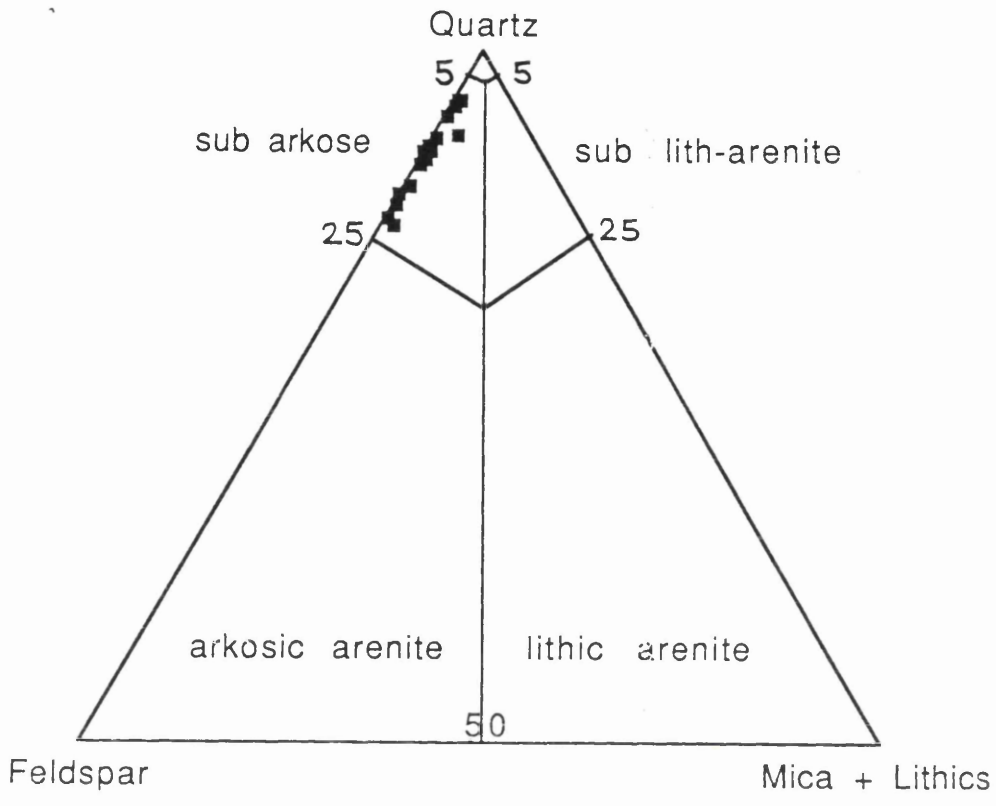

Figure 5. Quartz-feldspar-mica + lithics plot (Dott 1964) for the Emerald Sand (N=24, Wells 2/10-a7, 2/10-a6, 2/10-a7z, 3/11b-3 and 3/11b-5). Data from Table 1.

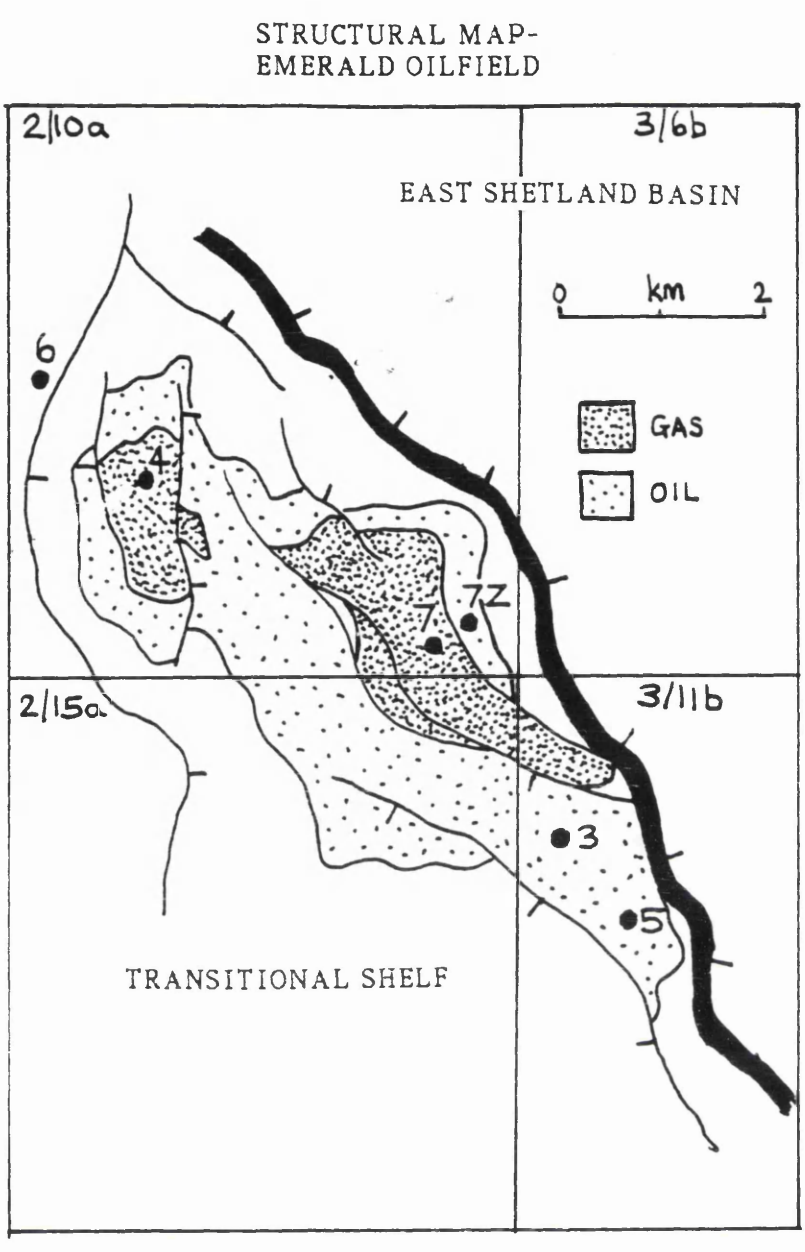

Figure 6. Structural map of the Emerald oilfield showing location of wells, from Wheatley *et al.* (1987).

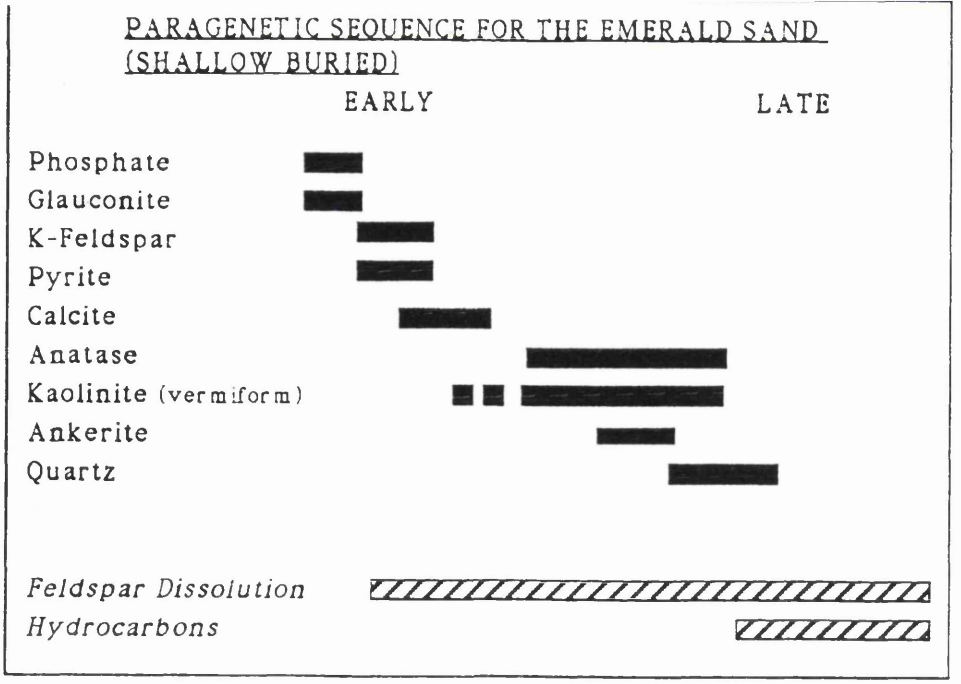

Figure 7a). Paragenetic sequence for the Emerald Sand.

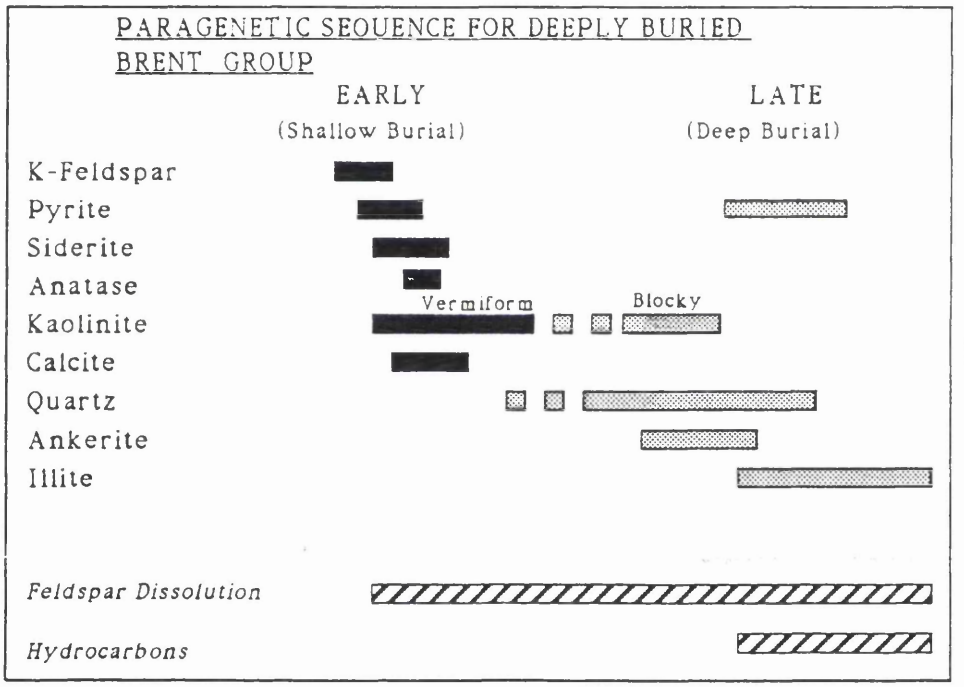

Figure 7b). Paragenetic sequence for deeply buried Brent Group sandstones. The early diagenetic cements (shown in black) are similar to those in the shallow buried Emerald oilfield. Modified from Brint (1989).

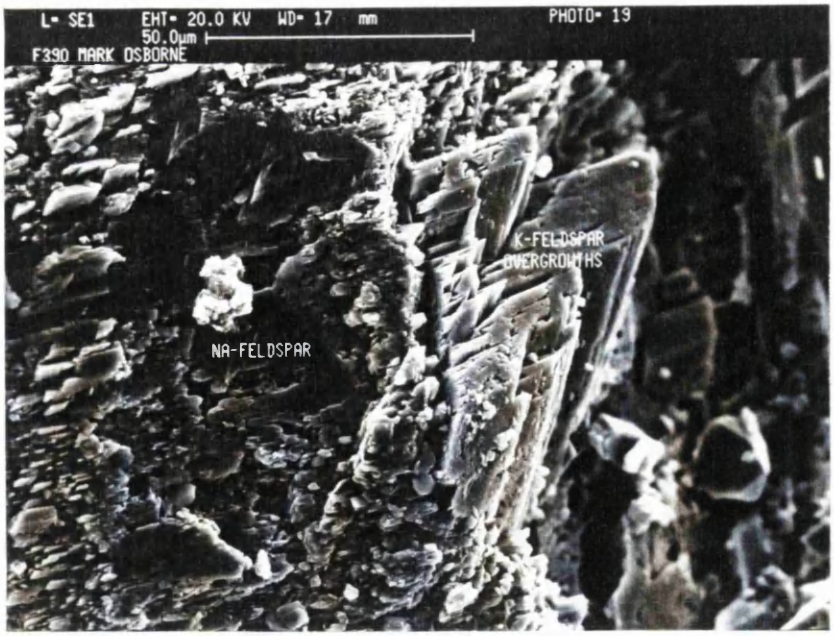

Figure 8a) Small euhedral K-feldspar overgrowths which have precipitated upon the surface of a detrital Na-feldspar grain. Well 2/10-a7, 1635.7m TVD.

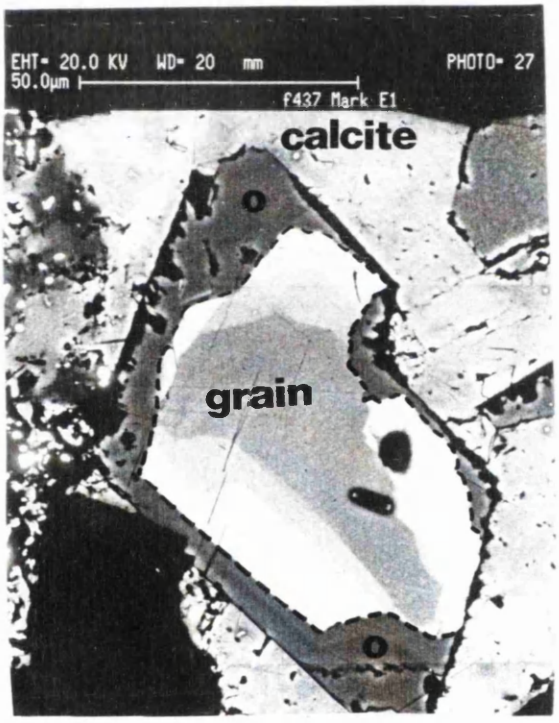

Figure 8b) Back-scattered electron image of a chemically zoned detrital K-feldspar grain containing small amounts of Ti and Ba. The grain is enveloped by pure K-feldspar overgrowth (O). The overgrowth is enveloped by calcite cement; this indicates that the K-feldspar overgrowth precipitated prior to calcite cementation. Well 2/10-a6, 1674.4m TVD.

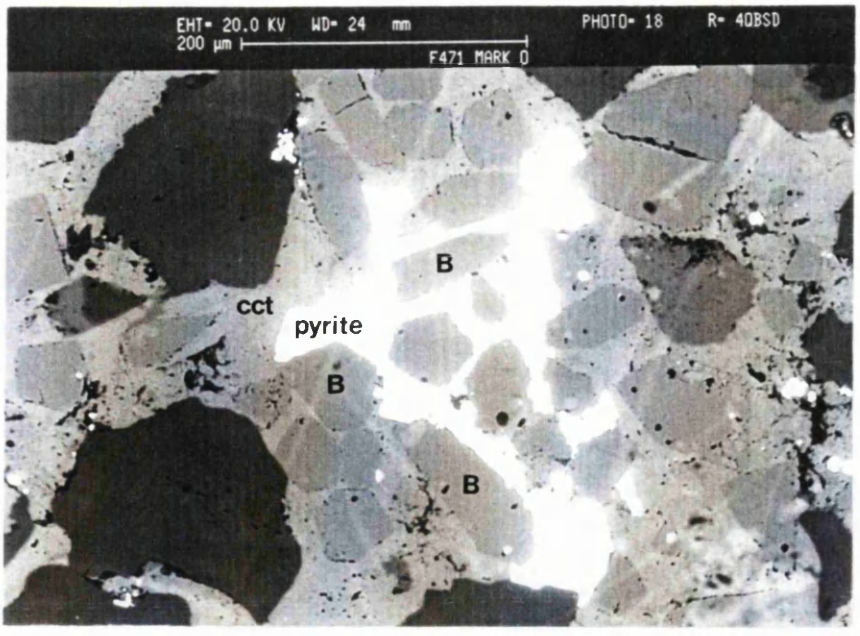

Figure 9a) Pore-filling pyrite cement corrodes detrital bioclasts (B) and is enclosed within calcite cement (CCT). Well 2/10-a6, 1674.4m TVD. BSE image.

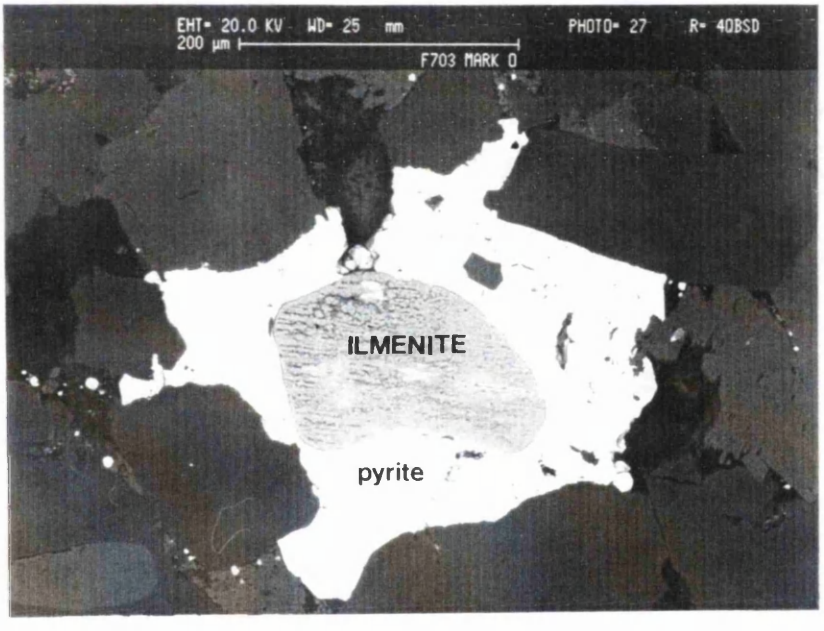

Figure 9b) Pyrite is seen surrounding and replacing detrital ilmenite grains. Well 2/10-a7, 1635.7m TVD.

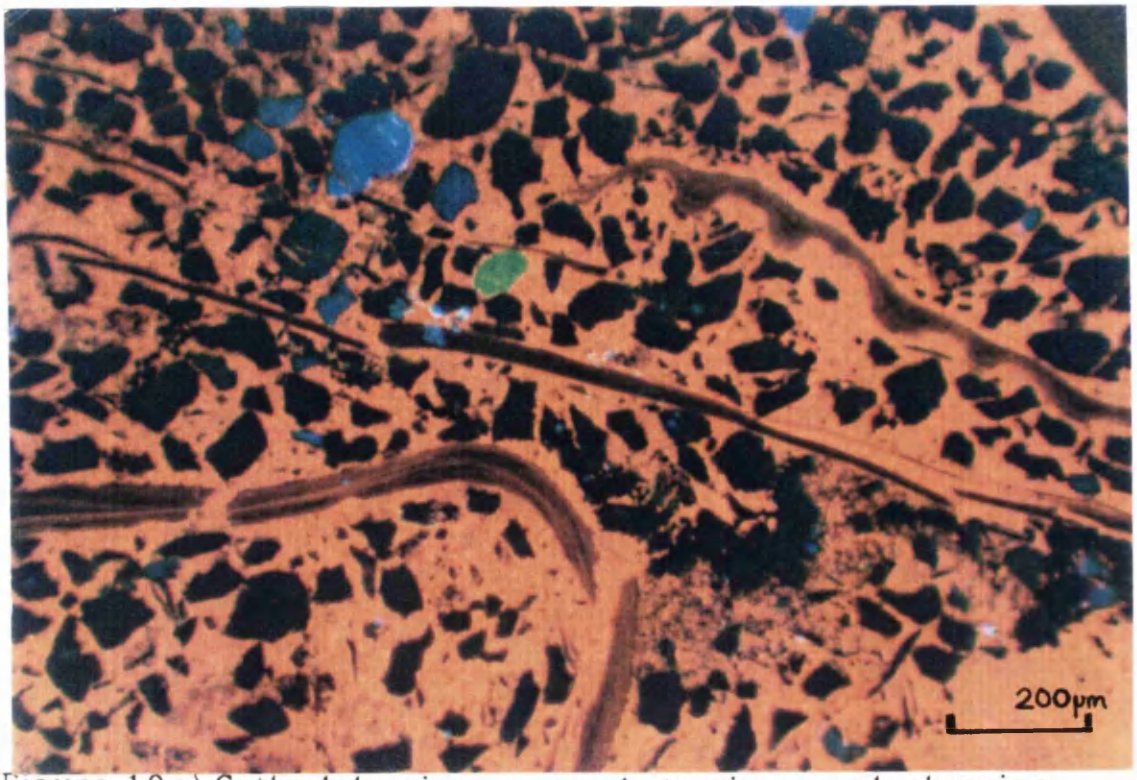

Figure 10a) Cathodoluminescence photomicrograph showing homogenous, bright orange luminescing calcite cement enveloping dully luminescent bivalve bioclasts and bright blue feldspars. Well 2/10-a6, 1674.4m TVD.

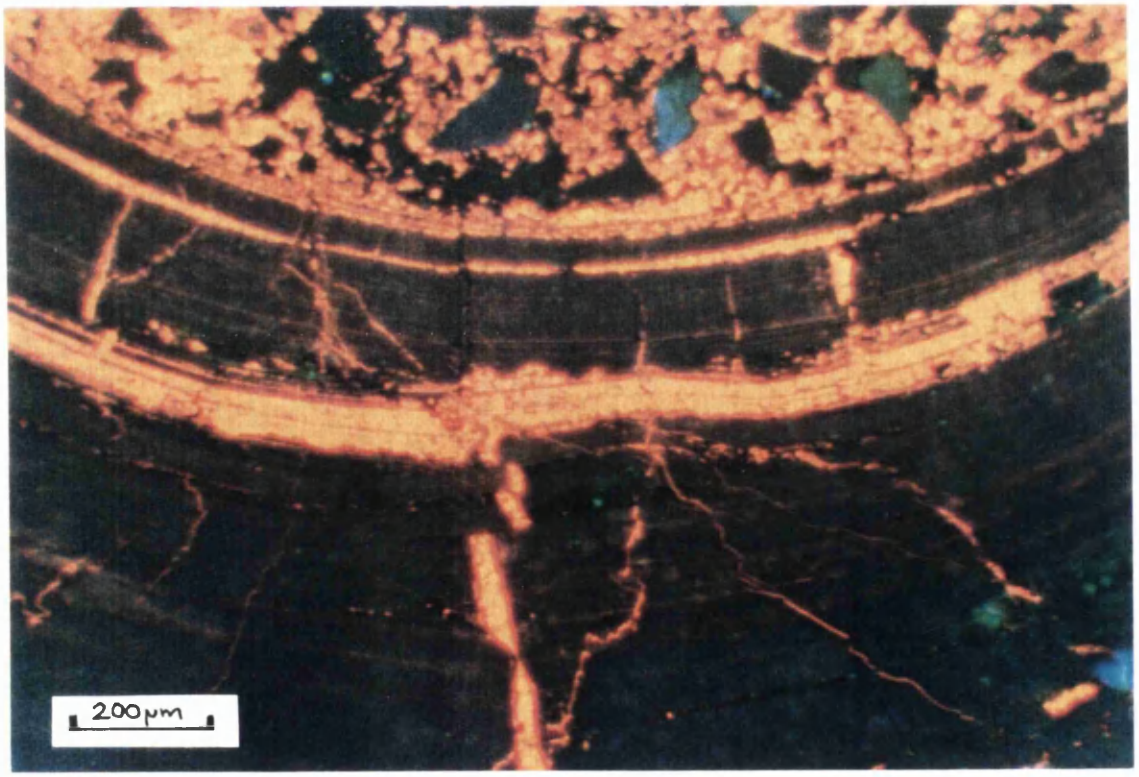

Figure 10b) Cathodoluminescence photomicrograph showing brightly luminescing calcite replacing a dully luminescent belemnite rostrum. Calcite clearly predates final physical compaction as calcite-filled layers in the shell have been offset during compaction. Same sample as in 9a).

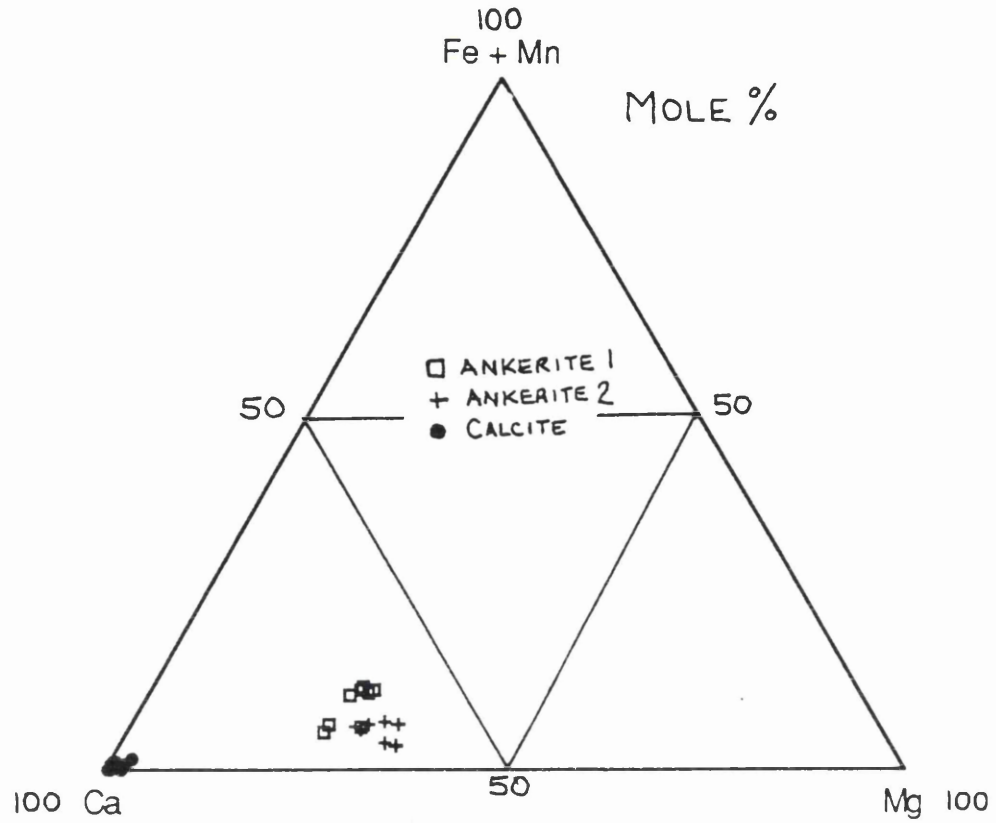

Figure 11. Triangular plot showing the elemental composition of authigenic carbonates in the Emerald Sand, data from Table 2 (N=33).

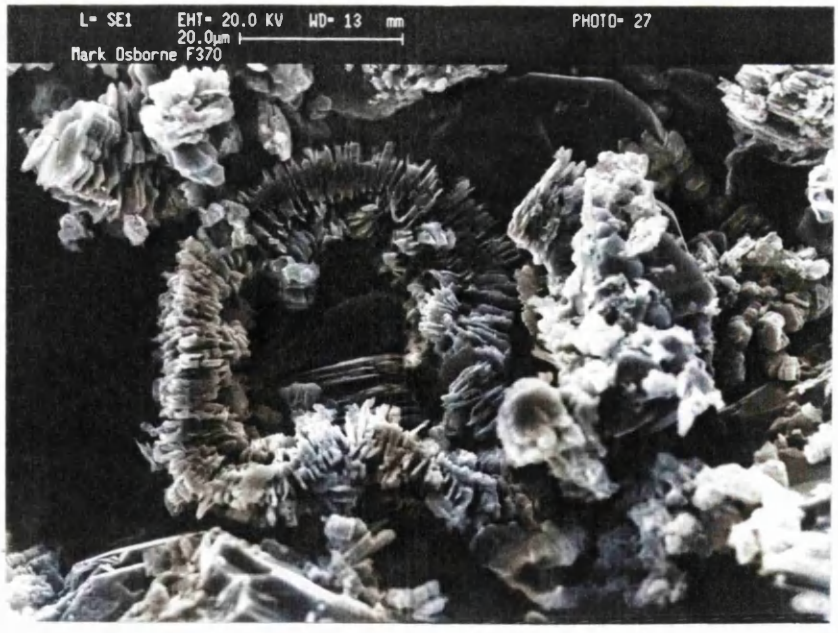

Figure 12 Typical vermiform kaolinite. Well 3/11b-3, 1675.3m TVD.

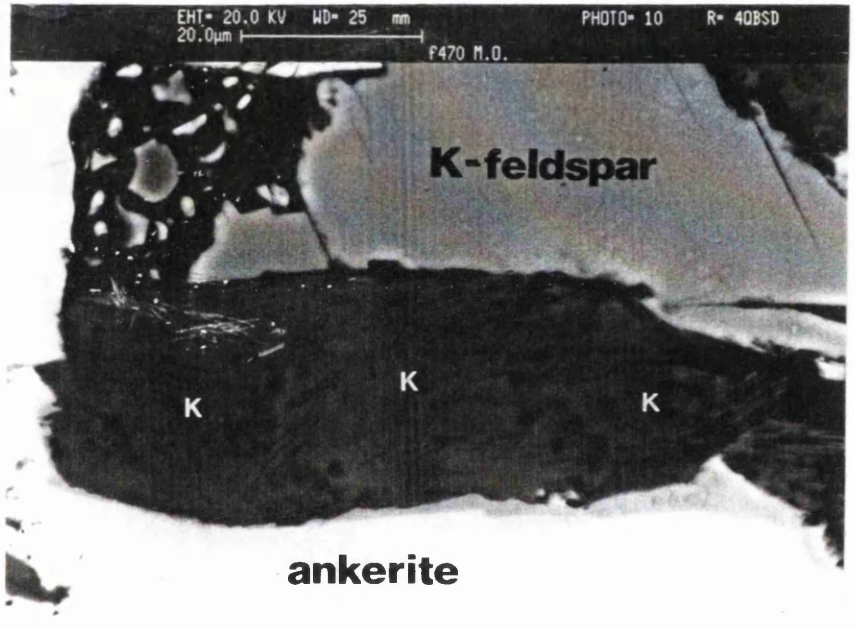

Figure 13 Kaolinite (K) is seen infilling the secondary porosity created by the dissolution of K-feldspar within a calcite concretion. Well 2/10-a6, 1674.4m TVD.

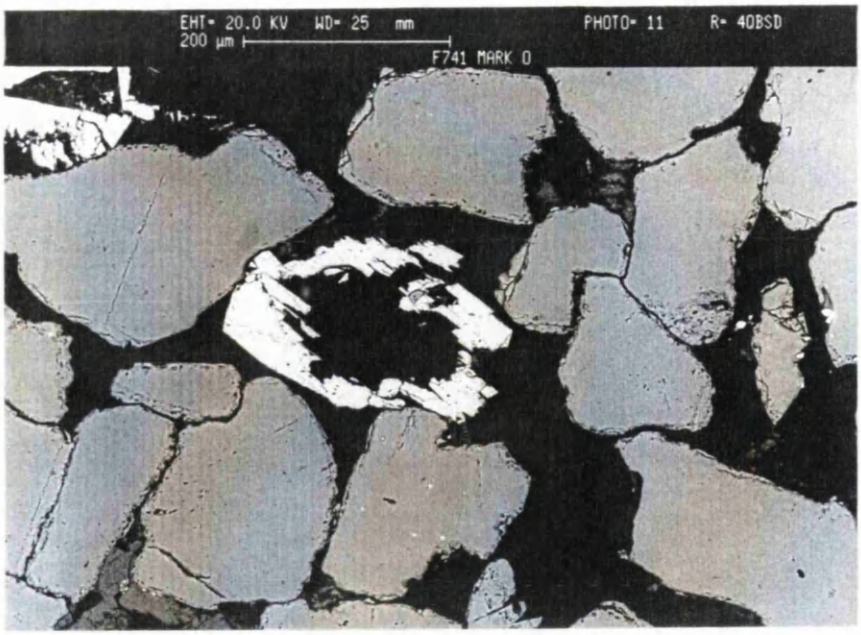

Figure 14a) BSE image of a thin section showing a dissolved, skeletal K-feldspar. Well 3/11b-3, 1696.9m TVD.

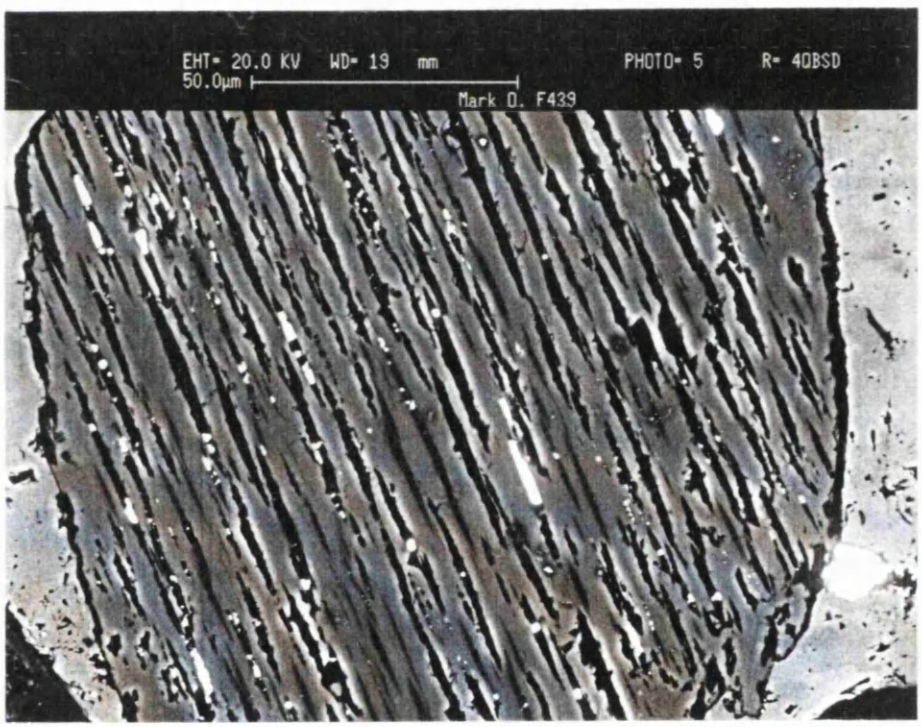

Figure 14b) Na-rich lammelae of a perthitic K-feldspars are preferentially leached in contrast to the rest of the grain. BSE image, Well 2/10-a7Z 1809.6m TVD.

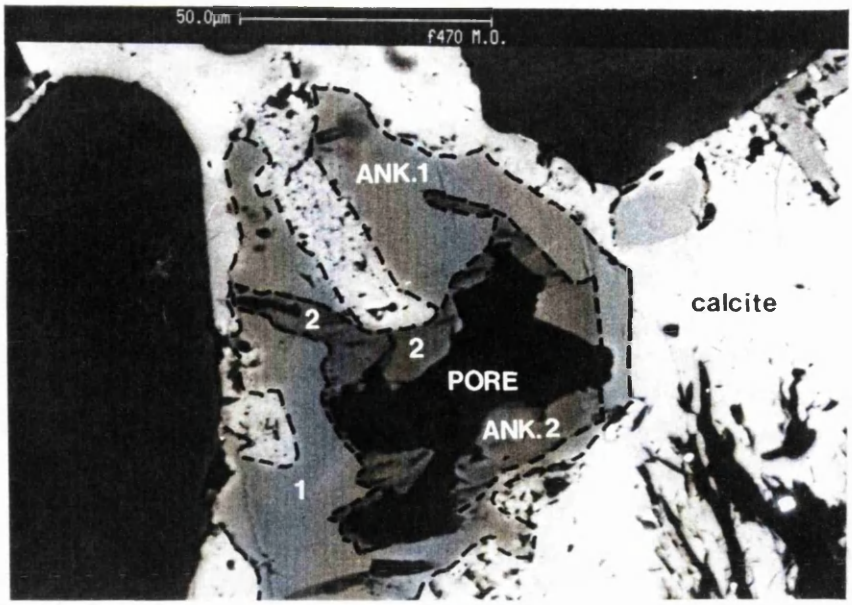

Figure 15a) Two chemically distinct ankerites (1&2) can be seen infilling secondary porosity created by feldspar dissolution. BSE image, calcite concretion, Well 2/10-a6, 1674.4m TVD.

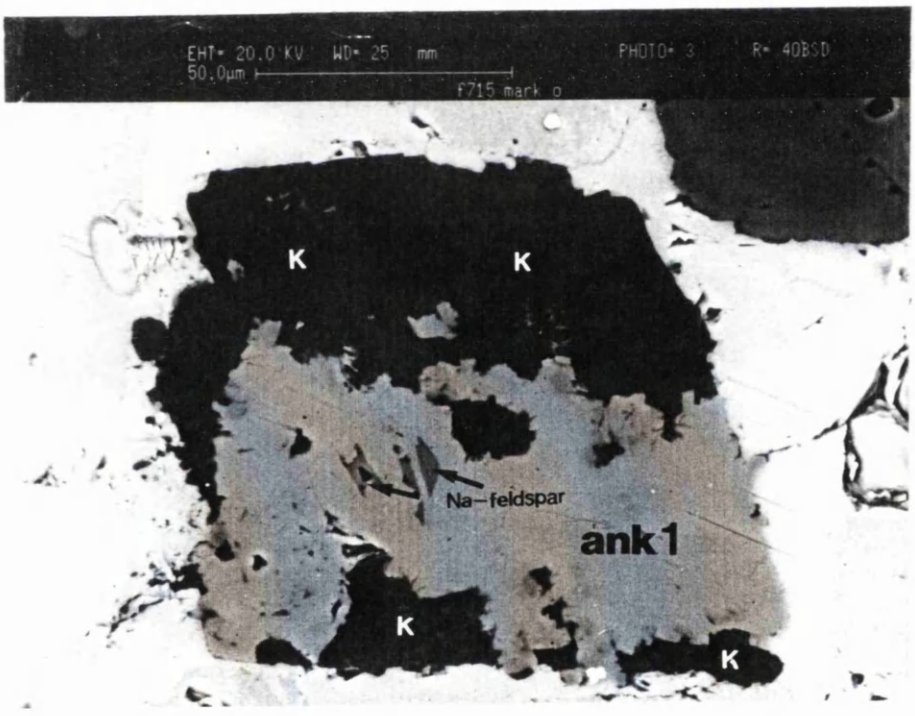

b). Ankerite (ANK) and kaolinite (K) are frequently observed to infill the secondary porosity created by feldspar dissolution. Relict fragments of detrital Na-feldspar are arrowed. BSE image, calcite concretion, Well 2/10-a6, 1674.4m TVD.

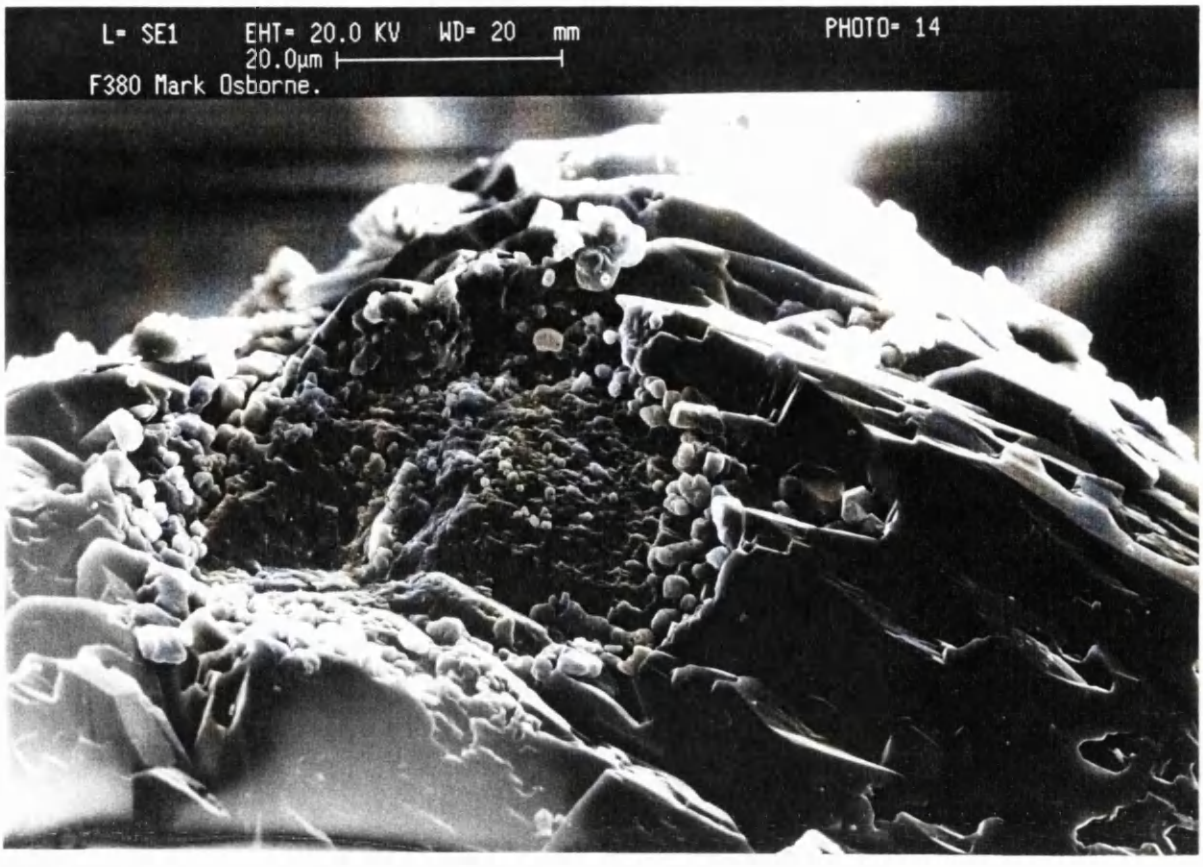

Figure 16a) SEM photomicrograph of a typical quartz overgrowth from the Emerald oilfield. Overgrowths are irregular in appearance and consist of numerous crystallites. Well 2/10-a7, 1674.4m TVD.

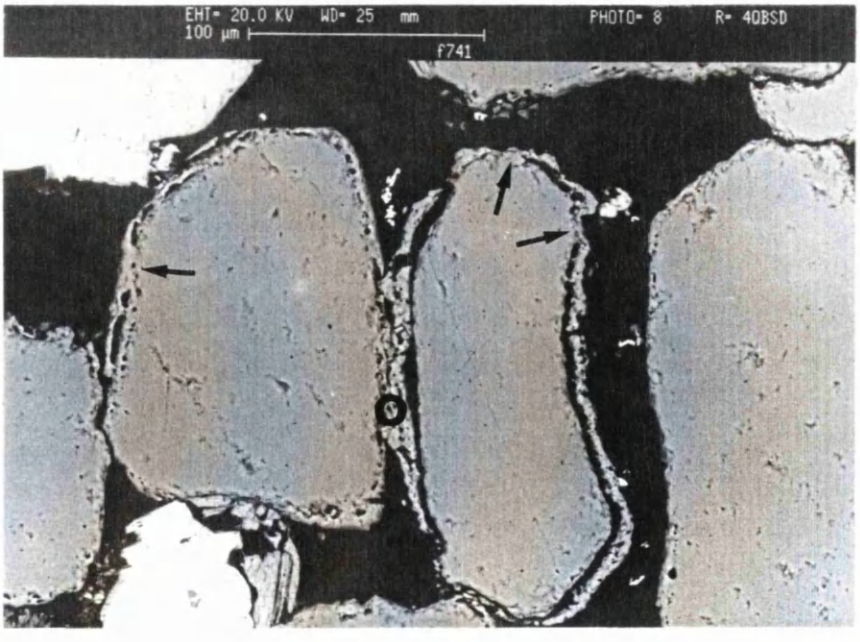

Figure 16b) BSE image of a thin section showing quartz grains with very thin overgrowths (O), which are only attached to the grains at a few isolated points (arrowed). Well 3/11b-3 1696.9m TVD.

Figure 16c) Vermiform kaolinite enveloped by quartz overgrowths (arrowed). This indicates that quartz cement either post-dated or was co-genetic with, kaolinite precipitation. Well 3/11b-3, 1675.3m TVD.

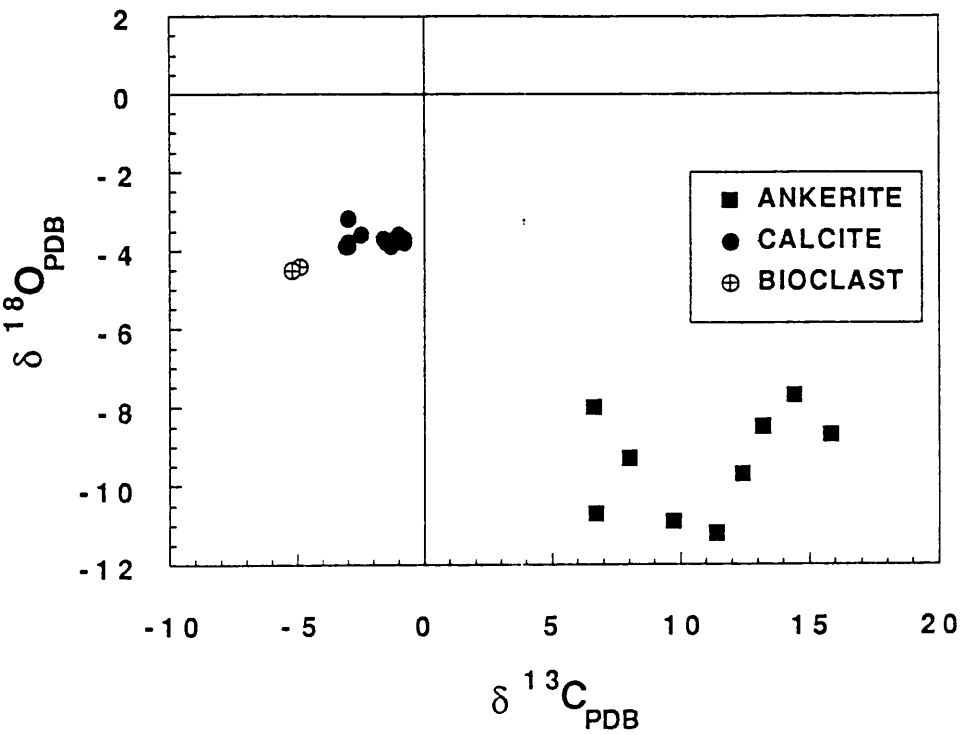

Figure 17. Combined $\delta^{13}C_{PDB}$ and $\delta^{18}O_{PDB}$ plot showing the stable isotopic composition of diagenetic carbonates from the Emerald oilfield. Data from Table 2.

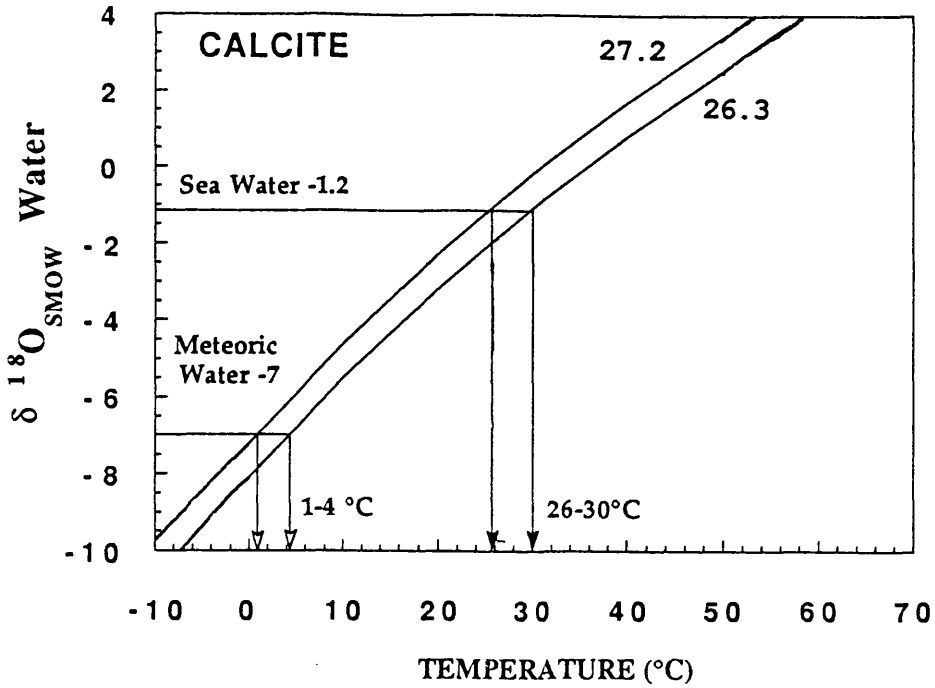

Figure 18. Pore-water $\delta^{18}O_{SMOW}$ versus temperature plot for calcite cement. Curves calculated using the fractionation equation of Friedman & O'Neil (1977). If calcite precipitated from Jurassic sea water it grew at 26-30°C. If calcite precipitated from meteoric water it grew at 1-4°C.

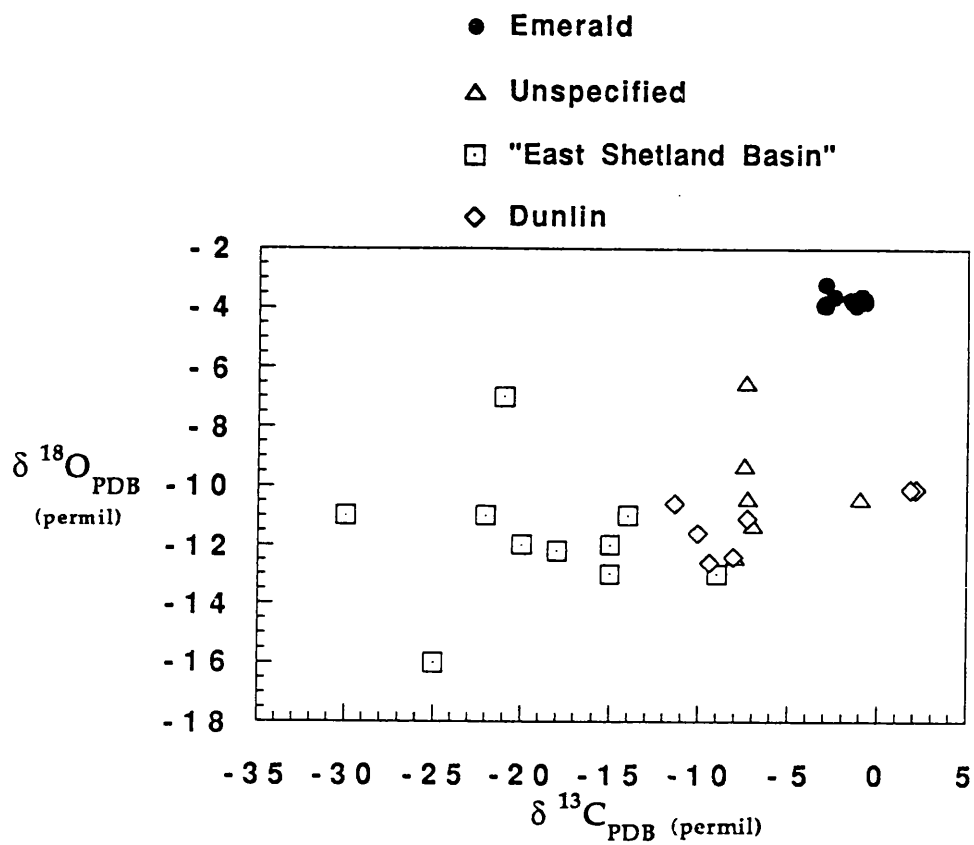

Figure 19. Combined $\delta^{13}C_{PDB}$ and $\delta^{18}O_{PDB}$ plot showing the stable isotopic compositions of all non-ferroan, early diagenetic calcite cements from the Brent Group. Calcite cements from the Emerald oilfield have higher $\delta^{18}O$ than all other Brent Group calcites. All these calcites grew at roughly similar temperatures (<30°C); however the differences in $\delta^{18}O$ probably indicate that calcite cement from the Emerald oilfield precipitated from sea-water, whereas other Brent Group calcites precipitated from meteoric-derived pore-waters. For further discussion see text. Data from Brint (1989)-Dunlin oilfield; Hamilton *et al.* (1987)- unspecified Brent Group location; Giles *et al.* (1992)- regional study of the Brent Group of the East Shetland Basin. Emerald oilfield data from this study.

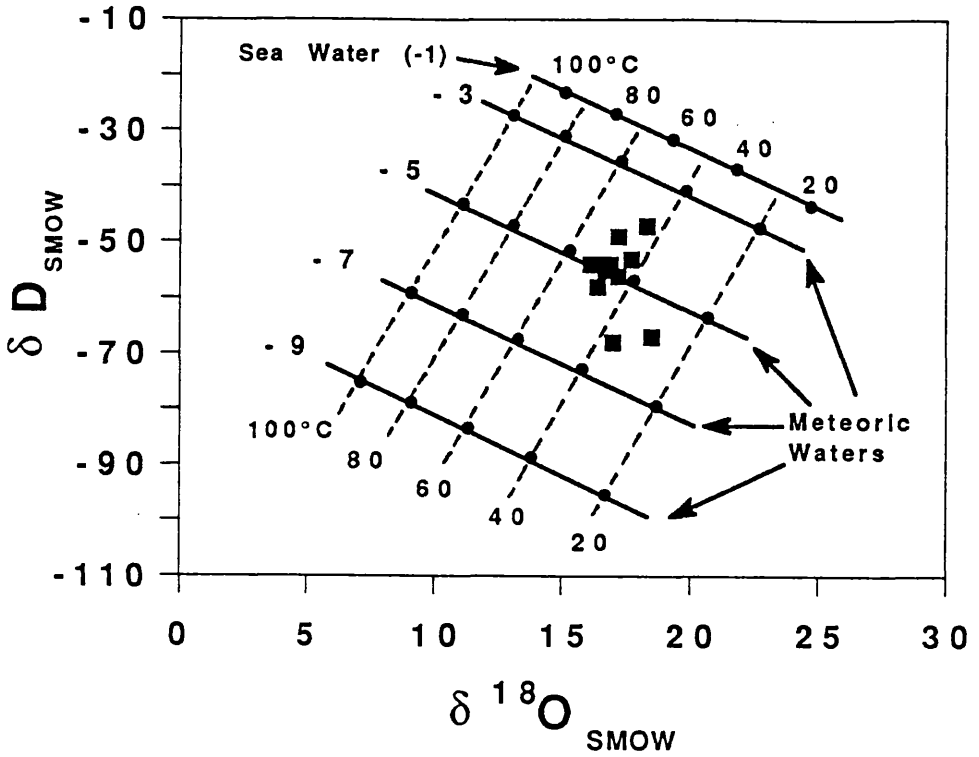

Figure 20. $\delta^{18}O_{SMOW}$ versus δD_{SMOW} plot showing the stable isotopic composition of authigenic kaolinite from the Emerald oilfield (solid squares). Solid black lines represent the stable isotopic composition of kaolinite that would have precipitated from a meteoric water with a specific $\delta^{18}O$ composition ($\delta^{18}O$= -3, -5, -7 or -9‰). The composition of kaolinite precipitating from pre-Miocene sea water ($\delta^{18}O$= -1; δD= -10‰, Sheppard 1986) is also shown. Broken black lines represent constant temperature. The kaolinite apparently precipitated at 25-47°C from pore-waters with $\delta^{18}O$= -6.5 to -4‰. Fractionation equations used were those of Savin & Lee (1988) for oxygen and Lambert & Epstein (1980) for hydrogen. $\delta^{18}O$ and δD compositions of ancient meteoric waters were calculated from the relationship $\delta D = \delta^{18}O + 8$‰. The latter equation would represent the meteoric water line in an ice-free world, where sea water $\delta^{18}O$= -1, and δD= -10‰ (Craig 1961; Sheppard 1986).

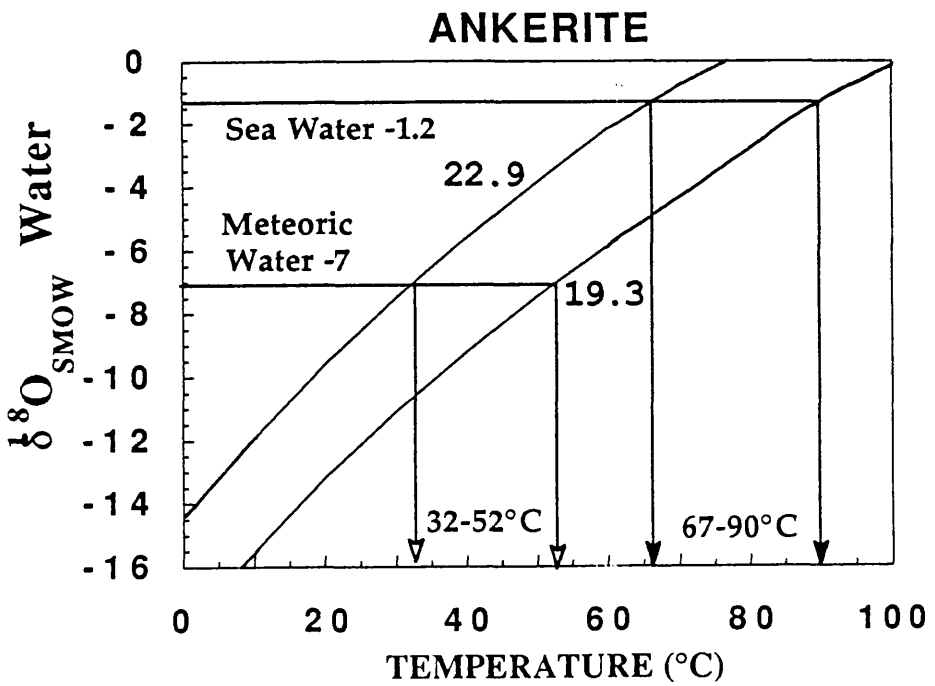

Figure 21. Pore-water $\delta^{18}O_{SMOW}$ versus temperature plot for ankerite cement. Curves calculated using the fractionation equation of Fisher & Land (1986). If ankerite precipitated from sea water it grew at 67-90°C, whereas if it precipitated from Jurassic meteoric water it grew at 35-50°C.

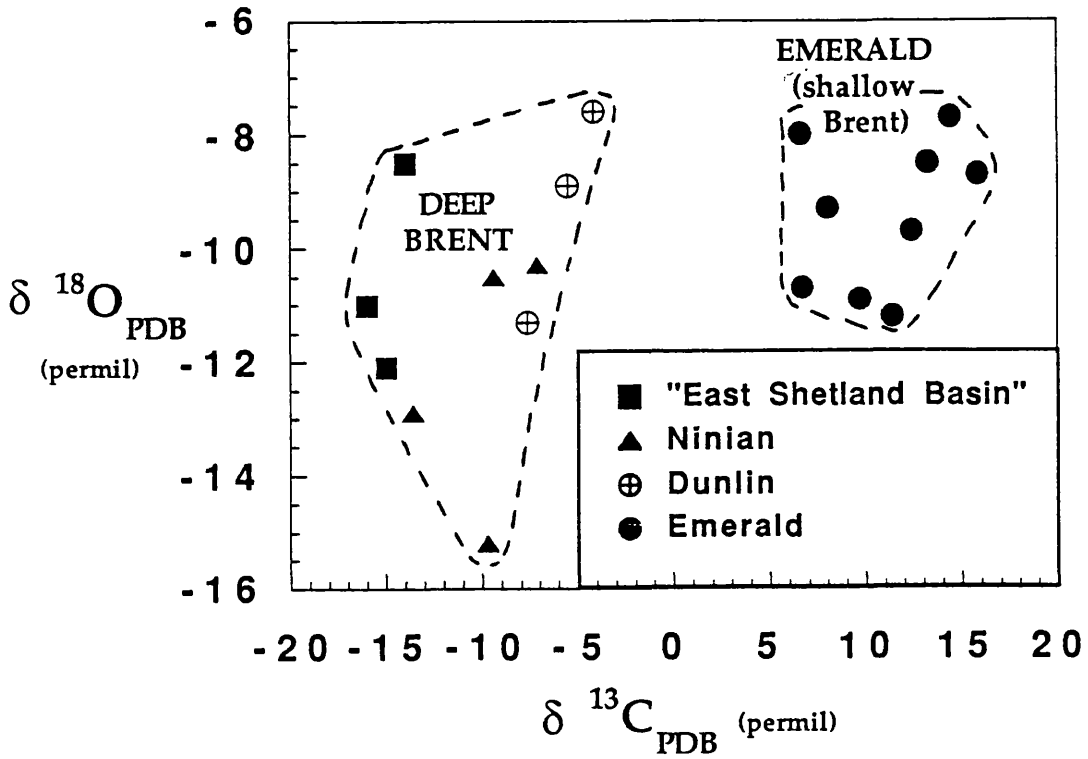

Figure 22. Combined $\delta^{13}C_{PDB}$ and $\delta^{18}O_{PDB}$ plot showing the stable isotopic compositions of all Brent Group ankerite cements. Ankerite cements from the Emerald oilfield have higher $\delta^{13}C$ than ankerites from more deeply buried Brent Group oilfields. These high $\delta^{13}C$ values indicate that carbon was derived via fermentation of organic matter. For further discussion see text. Data from Brint (1989)-Dunlin oilfield; Kantorowicz (1985)- Ninian oilfield; Giles *et al.* (1992)- regional study of the Brent Group of the East Shetland Basin. Emerald oilfield data from this study (Table 2).

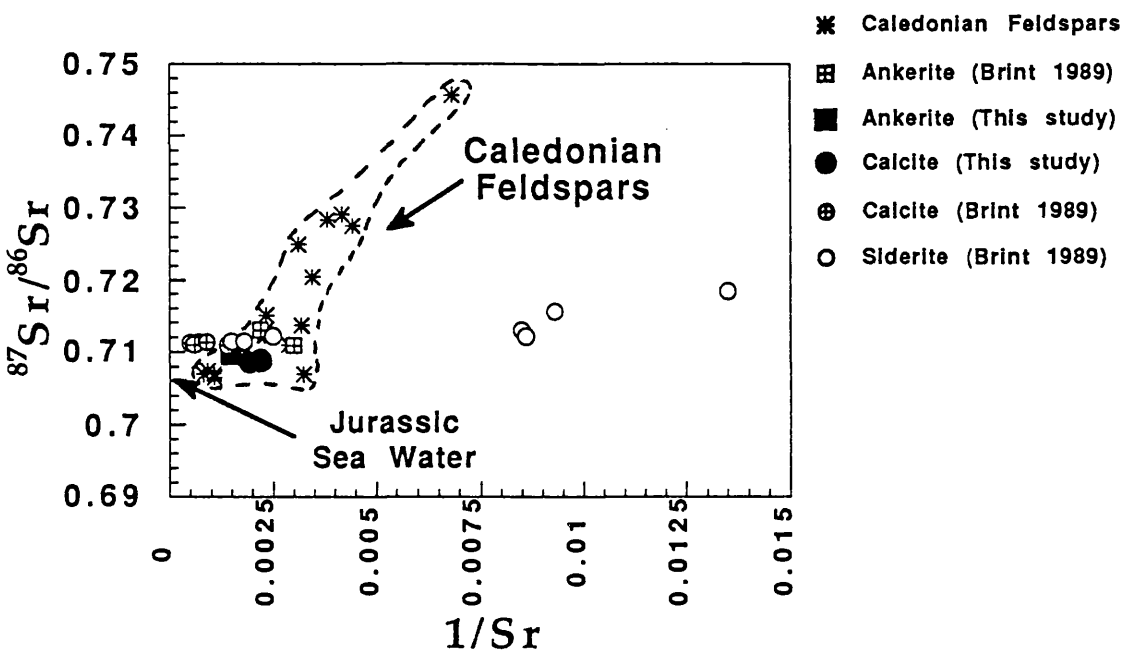

Figure 24. $^{87}Sr/^{86}Sr$ versus1/Sr plot for authigenic carbonates in the Emerald Sand. Data for carbonates from the Dunlin oilfield are shown for comparison (Brint 1989). Many Brent Group carbonate cements (calcites, ankerites, and some siderites) have strontium isotopic compositions and concentrations which suggest that their Sr was derived from mixing of two sources; Jurassic sea water or shell debris, and detrital feldspars. Feldspar data from Halliday *et al.* (1979) and Haughton *et al.* (1991). For further discussion see text.

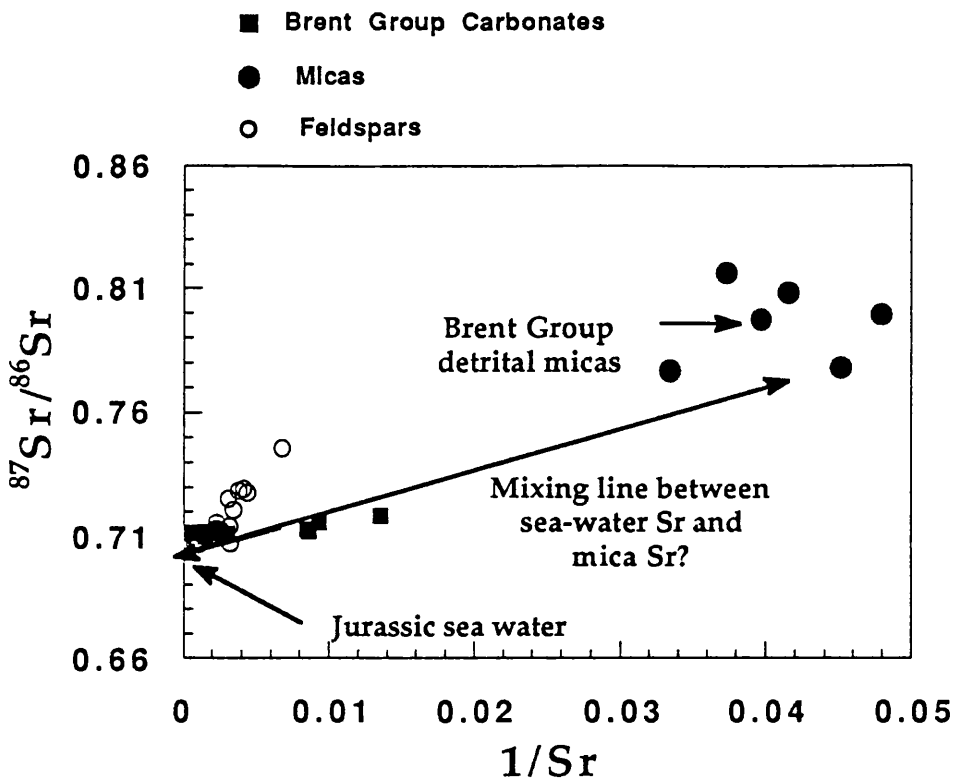

Figure 25. $^{87}Sr/^{86}Sr$ versus1/Sr plot for authigenic carbonates in the Emerald Sand. Data for carbonates from the Dunlin oilfield are shown for comparison (Brint 1989). Some Brent Group siderites have have strontium isotopic compositions and concentrations which indicate that their Sr was derived from a mixture of sea-water (or dissolving shell debris) and degrading detrital mica. For further discussion see text. Mica data from Hamilton *et al.* (1987).

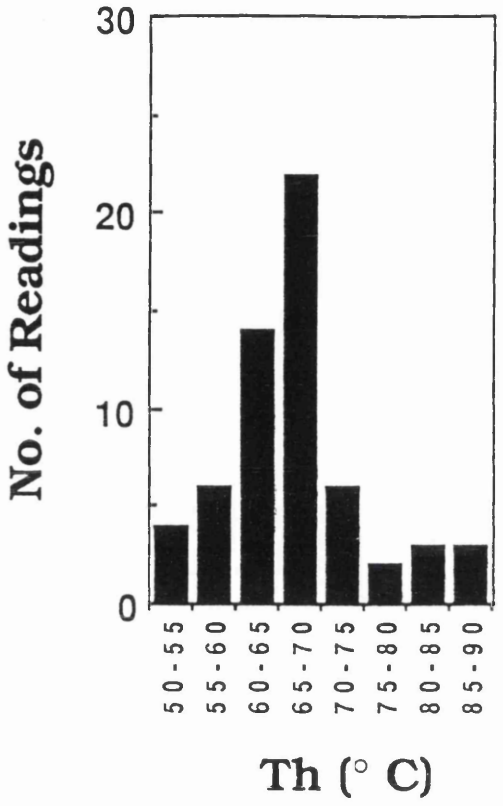

Figure 26. Histogram of homogenisation temperatures for fluid inclusions in authigenic quartz (N-60). Well 2/10-a7, 1649.4m TVD. Data from Table 5.

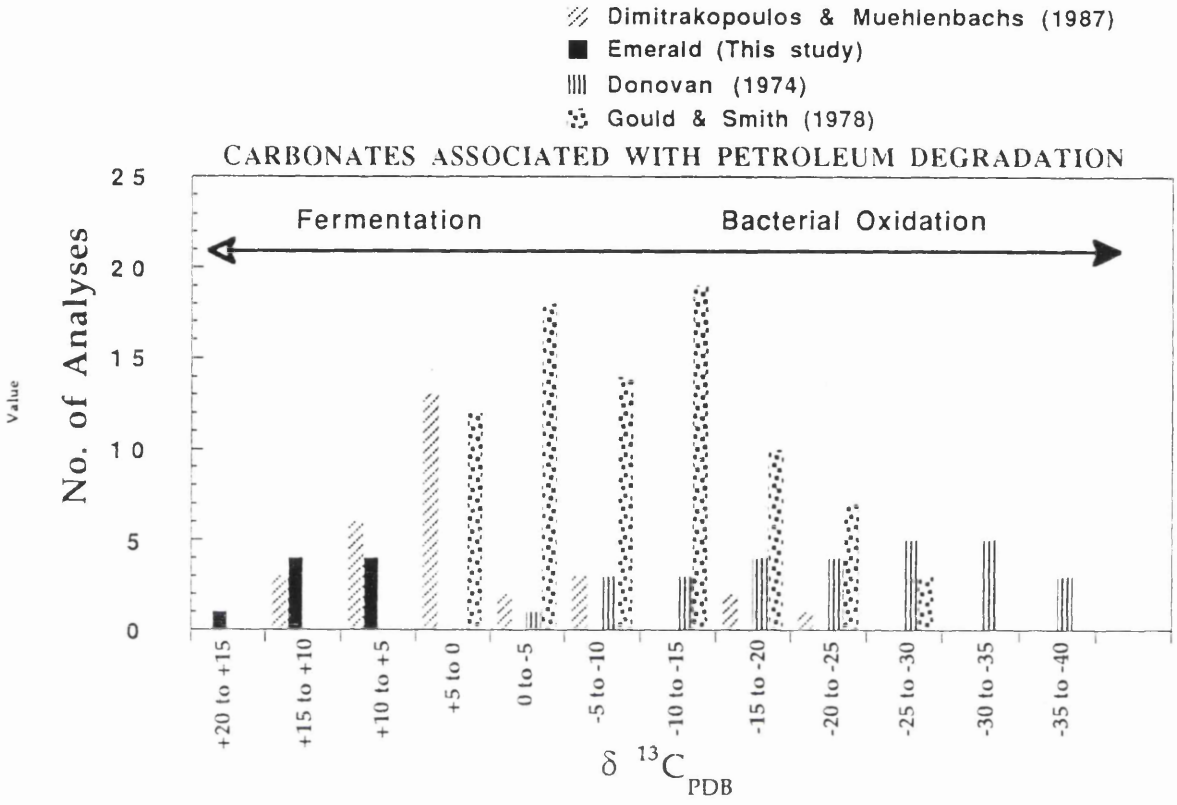

Figure 27. Histogram showing the $\delta^{13}C$ stable isotopic compositions of diagenetic carbonates associated with biodegradation of crude oil. A wide range in $\delta^{13}C$ is evident; very high $\delta^{13}C$ indicates biodegradation by anoxic fermentation reactions, very low $\delta^{13}C$ indicates biodegradation by aerobic oxidation. Data from Dimitrakopoulos & Muehlenbachs (1987); Donovan (1974) and Gould & Smith (1978). Data for the Emerald oilfield from this study (Table 2).

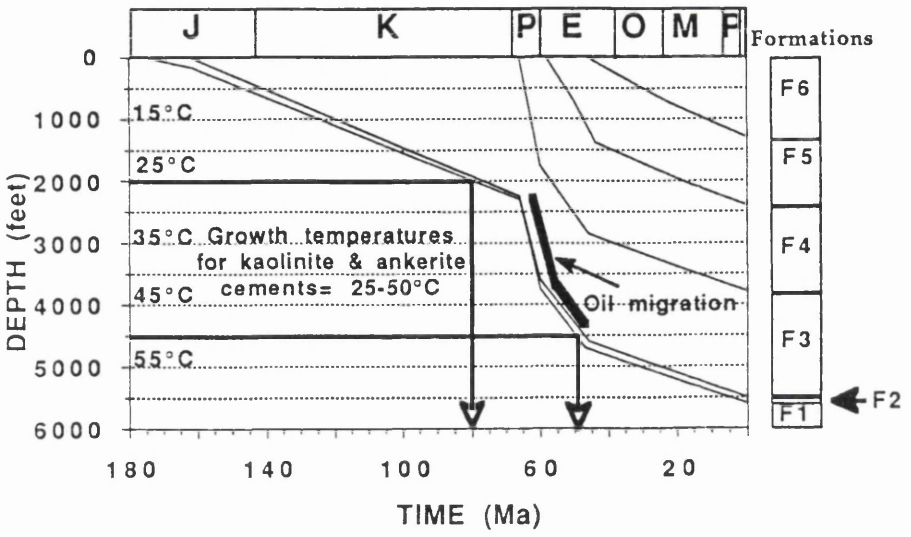

Figure 28. Burial curve for the Emerald oilfield. Mineral growth temperatures indicate that precipitation of ankerite and kaolinite cements partly overlapped with migration of oil into the Emerald Sand during the Palaeocene.

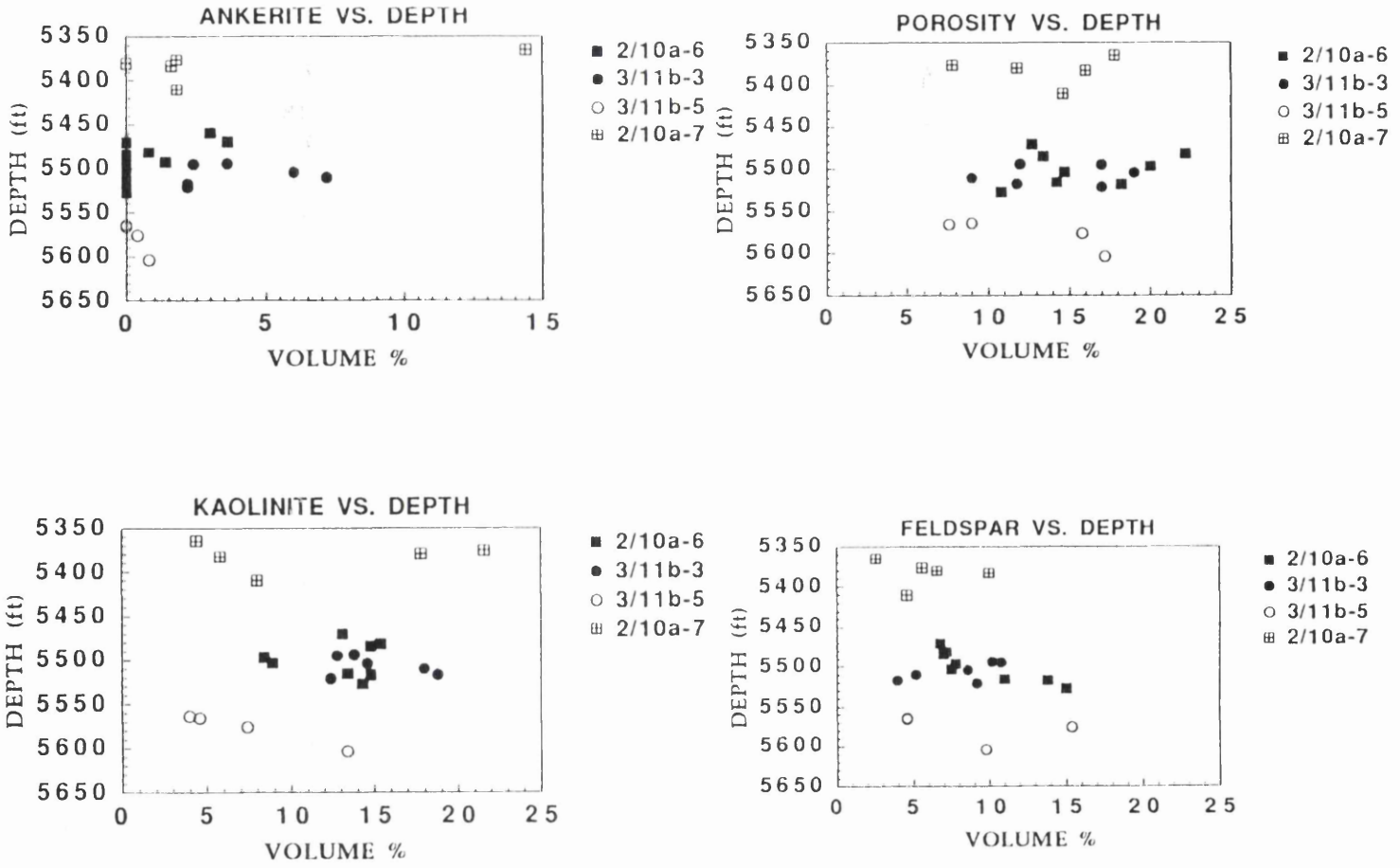

Figure 29. The abundance of minerals and porosity in the Emerald Sand shows no systematic variation with increasing depth of burial. Point count data from Table 1 (N=19).

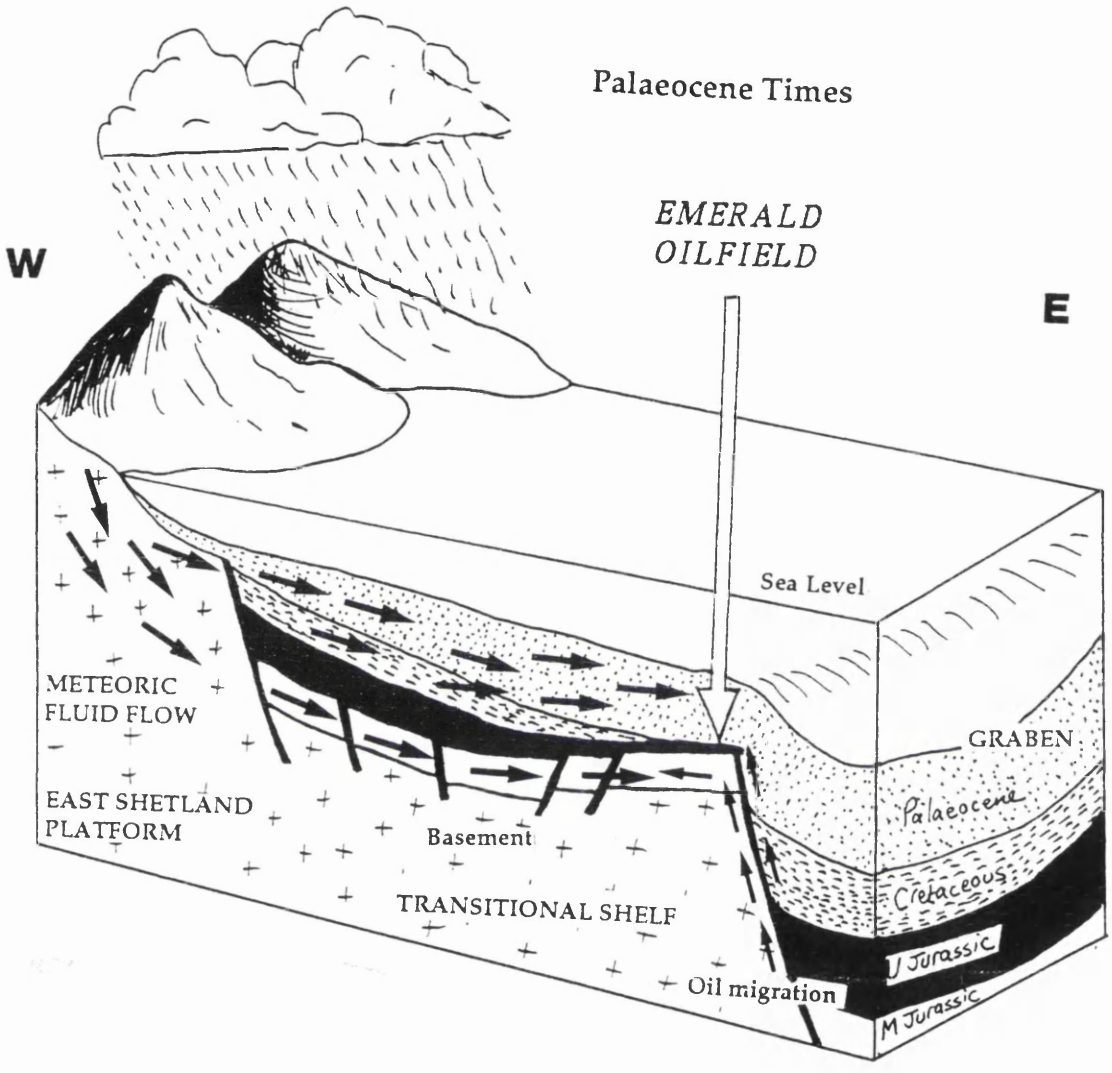

Figure 30. Schematic palaeohydrological model for the Transitional Shelf during the Palaeocene.

Table 1. Point count data (500 points per thin section)

Well 3/11-b3

	Depth					
	5504' (1683.9m)	5521' (1682.7m)	5495' (1675.3m)	5494' (1674.6m)	5510' (1679.5m)	5517' (1681.6m)
Quartz	48.2	58.2	60.8	59.6	59.8	63.0
K-feldspar	8.6	9.2	10.8	10.2	5.2	4.0
Detrital Clay	Trace	Trace	---	---	---	---
Muscovite	0.4	0.2	0.2	0.4	0.6	---
Pyrite	1.0	0.6	0.8	0.4	0.8	0.2
Ankerite	8.2	2.4	6.0	3.6	7.2	2.2
Kaolinite	14.6	12.4	12.8	13.8	18.0	18.8
Primary porosity	15.4	12.0	5.6	12.0	7.0	6.5
Secondary porosity	3.6	5.0	3.0	---	2.0	5.3

	Well 3/11-b5				Well 2/10-a7Z	
	Depth					
	5604' (1708.5m)	5576' (1700m)	5564' (1696.3m)	5566' (1696.9m)	5902' (1798.9m)	5904' (1799.6m)
Quartz	58.0	54.0	70.4	65.8	57.8	78.3
K-feldspar	9.8	15.4	4.6	4.6	5.8	8.7
Detrital clay	---	1.8	9.2	11.4	---	---
Muscovite	---	0.2	0.8	0.4	0.4	---
Pyrite	0.8	5.0	2.0	5.6	5.4	0.1
Ankerite	0.8	0.4	---	---	---	1.3
Kaolinite	13.4	7.4	4.0	4.6	12.8	1.7
Primary porosity	13.4	12.6	7.2	7.2	14.8	8.7
Secondary porosity	3.8	3.2	1.8	0.4	3.0	1.0

Well 2/10a-6

	Depth						
	5515 (1680.9m)	5469 (1667.3m)	5492 (1674.4m)	5459 (1664.2m)	5517 (1671m)	5481 (1675.6m)	5496 (1675.9m)
Quartz	58.6	27.0	32.8	33.4	52.4	52.8	48.0
K-feldspar	11.0	8.6	10.2	9.6	13.8	7.2	7.8
Detrital clay	---	---	---	---	---	---	---
Muscovite	0.4	0.6	0.2	1.8	---	0.4	0.4
Pyrite	0.6	5.8	3.2	0.2	0.8	1.2	1.6
Ankerite	---	3.6	1.4	3.0	---	0.8	---
Calcite	---	37.3	50.6	35.8	---	---	---
Bioclasts	---	10.3	---	15.2	---	---	
Kaolinite	13.4	Trace	Trace	Trace	14.8	15.4	8.4
Primary porosity	7.0	---	---	0.2	14.2	19.6	18.0
Secondary porosity	7.2	---	---	0.8	4.0	2.6	2.0

Well 2/10a-6

	Depth (ft)			
	5484' (1671.5m)	5470' (1667.3m)	5503' (1683.0m)	5527' (1684.6m)
Quartz	62.8	60.6	66.7	51.2
K-feldspar	7.0	6.8	7.5	15.0
Muscovite	1.1	0.9	---	1.2
Pyrite	0.9	4.7	0.6	7.5
Kaolinite	14.8	13.1	8.9	14.3
Porosity	13.4	12.7	14.7	10.8

Well 2/10a-7

	Depth (ft)				
	5365 (1635.7m)	5376 (1638.6m)	5380 (1639.8m)	5383 (1640.8m)	5410 (1648.9m)
Quartz	56.8	60.6	60.8	62.2	71.0
K-feldspar	2.6	5.6	6.6	10.0	4.6
Muscovite	1.2	1.0	0.4	1.4	---
Pyrite	2.8	1.6	2.6	3.0	---
Ankerite	14.4	1.8	---	1.6	1.8
Kaolinite	4.4	21.6	17.8	5.8	8.0
Porosity	17.8	7.8	11.8	16.0	14.6

Table 2 Elemental analyses of carbonates

All analyses from Well 2/10-a6, 1674.4m TVD.

Mole % Sample	Ca	Fe	Mn	Mg	Sample		Ca	Fe	Mn	Mg
Bioclast	99.4	0.2	0.0	0.4	Ankerite	1	65.9	4.9	0.2	23.4
Bioclast	98.6	0.0	0.0	0.4	Ankerite	1	61.5	10.8	0.4	27.4
Bioclast	97.9	0.0	0.0	2.1	Ankerite	1	59.5	10.8	0.4	27.4
Bioclast	99.6	0.0	0.0	0.4	Ankerite	1	60.3	5.3	0.6	27.1
Bioclast	99.3	0.0	0.0	0.7	Ankerite	1	61.6	11.0	0.5	26.4
					Ankerite	1	61.1	11.0	0.5	26.4
Calcite	99.0	0.2	0.4	0.4	Ankerite	1	61.7	11.6	0.4	26.3
Calcite	98.8	0.0	0.8	1.4	Ankerite	1	64.1	10.2	0.4	25.3
Calcite	97.3	0.0	0.6	2.1	Ankerite	1	62.1	11.2	0.5	26.2
Calcite	98.6	0.2	0.8	0.4	Ankerite	1	65.0	5.8	0.3	23.3
Calcite	98.5	0.0	0.8	0.7	Ankerite	2	63.0	3.6	0.2	33.2
Calcite	95.9	0.0	1.7	2.4	Ankerite	2	61.8	3.2	0.3	34.7
Calcite	98.8	0.0	0.8	0.4	Ankerite	2	63.8	5.8	0.2	30.2
Calcite	99.4	0.1	0.9	0.6	Ankerite	2	63.6	6.4	0.2	29.8
Calcite	96.9	0.1	1.3	1.7	Ankerite	2	66.7	6.4	0.2	26.7
Calcite	99.0	0.0	0.7	0.3	Ankerite	2	61.6	6.4	0.4	31.6
					Ankerite	2	65.1	5.6	0.2	29.1
					Ankerite	2	65.4	6.0	0.2	28.4

Table 3. Stable isotopic data for authigenic carbonates

Well	Depth (ft)	Mineralogy	Size Fraction (μm)	δO_{PDB}	δC_{PDB}	δO_{SMOW}
2/10-a6	5492'-94	Calcite	<50	-3.2	-2.9	27.6
2/10-a6	5492'-94	Calcite	<50	-3.9	-3.1	26.9
2/10-a6	5492'-94	Calcite	<50	-3.8	-3.0	27.0
2/10-a6	5492'-94	Calcite	<50	-3.9	-3.0	26.9
2/10-a6	5492'-94	Calcite	53-64	-3.6	-2.5	27.2
2/10-a6	5492'-94	Calcite	64-90	-3.8	-1.5	27.0
2/10-a6	5492'-94	Calcite	64-90	-3.7	-1.6	27.1
2/10-a6	5492'-94	Calcite	90-100	-3.9	-1.3	26.9
2/10-a6	5492'-94	Calcite	100-125	-3.7	-0.8	27.1
2/10-a6	5492'-94	Calcite	100-125	-3.7	-1.1	27.0
2/10-a6	5492'-94	Calcite	100-125	-3.8	-0.8	27.0
2/10-a6	5492'-94	Calcite	>250	-3.6	-1.0	27.2
2/10-a6	5492'-94	Calcite (bioclast)	N/A	-4.4	-4.9	26.4
2/10-a6	5492'-94	Calcite (bioclast)	N/A	-4.5	-5.3	26.3
2/10-a6	5492'-94	Ankerite	<100	-8.7	+15.8	21.9
2/10-a6	5528'	Ankerite	<100	-9.3	+8.0	21.3
2/10-a6	5528'	Ankerite	<100	-8.1	+6.7	22.6
2/10-a6	5523'	Ankerite	<100	-10.7	+6.7	19.9
2/10-a7	5409'	Ankerite	<100	-7.7	+14.4	22.9
2/10-a7	5407'	Ankerite	<100	-8.5	+13.2	22.2
3/11-b3	5517'	Ankerite	<100	-11.2	+11.4	19.3
3/11-b3	5521'	Ankerite	<100	-9.7	+12.4	20.9
3/11-b3	5494'	Ankerite	<100	-10.9	+9.7	19.7

Table 4. Stable isotopic data for Emerald oilfield kaolinite

DEPTH (m)	WELL	FIELD	SIZE (μm)	$\delta^{18}O$	δD	SOURCE
1672.8	2/10-a6	Emerald	<0.5	18.2		This study
1672.3	2/10-a6	Emerald	0.5-2	16.7	-55	This study
1672.3	2/10-a6	Emerald	2-10	17.7	-53	This study
1672.8	2/10-a6	Emerald	53-64	17.8		This study
1672.3	2/10-a6	Emerald	53-64	18.3	-47	This study
1672.8	2/10-a6	Emerald	53-64	17.9		This study
1672.8	2/10-a6	Emerald	2-10	18.1		This study
1648.7	2/10-a7	Emerald	2-10	17.0	-68	This study
1638.6	2/10-a7	Emerald	<53	16.5		This study
1638.6	2/10-a7	Emerald	0.5-2	17.0		This study
1679.5	2/10-a7	Emerald	0.5-2	16.5		This study
1638.6	2/10-a7	Emerald	<0.5	17.0		This study
1638.6	2/10-a7	Emerald	2-10	17.2		This study
1679.5	2/10-a7	Emerald	<0.5	16.1	-54	This study
1638.6	2/10-a7	Emerald	2-10	16.9	-54	This study
1638.6	2/10-a7	Emerald	0.5-2	17.7		This study
1679.5	2/10-a7	Emerald	<0.5	16.3	-54	This study
1681.6	3/11-b3	Emerald	0.5-2	16.4	-58	This study
1681.6	3/11-b3	Emerald	2-10	17.2	-56	This study
1679.5	3/11-b3	Emerald	2-10	16.8		This study
1682.8	3/11-b3	Emerald	2-10	17.2	-49	This study
1681.6	3/11-b3	Emerald	64-85	18.5	-67	This study

Table 5. Strontium isotopic data for authigenic carbonates

Well 2/10-a6, 5492'-5494 ft TVD.

Mineral	Size Fraction (μm)	Rb	Sr	$^{87}Rb/^{86}Sr$	$^{87}Sr/^{86}Sr$	2σ	$(^{87}Sr/^{86}Sr)_{150M}$
Calcite	<53	0.902	456.5	0.0057	0.70896	9	0.70895
Calcite	53-64	0.624	463.0	0.0039	0.70872	3	0.70871
Calcite	64-90	0.317	524.6	0.0018	0.70857	3	0.70857
Calcite	>250	0.617	454.5	0.0039	0.70877	4	0.70876
Ankerite	<100	4.080	679.0	0.0174	0.70974	5	0.70970

Table 6. Fluid inclusion data, Well 2/10-a7, 1649.4m TVD.

Inclusion No.	T_h(°C)	Inclusion No.	T_h(°C)
1	64	45	60
2	64	46	65
3	55	47	75
4	65	48	68
5	68	49	68
6	69	50	57
7	68	51	51
8	68	52	52
9	68	53	68
10	62	54	73
11	76	55	67
12	62	56	60
13	63	57	64
14	58	58	66
15	60	59	68
16	58	60	70
17	65		
18	68		
19	64		
20	68		
21	58		
22	64		
23	60		
24	64		
25	70		
26	65		
27	69		
28	69		
29	83		
30	81		
31	81		
32	83		
33	88		
34	65		
35	65		
36	73		
37	87		
38	52		
39	71		
40	71		
41	57		
42	67		
43	87		
44	86		

CHAPTER 4

KAOLINITE MORPHOLOGY VARIES WITH GROWTH TEMPERATURE IN ISOTOPICALLY MIXED PORE-FLUIDS, BRENT GROUP, U. K. NORTH SEA.

Mark Osborne[1], R. Stuart Haszeldine[1], & Anthony E. Fallick[2]
1- Dept. of Geology & Applied Geology, Glasgow Univ., Glasgow G12 8QQ.
2-Isotope Geosciences Unit, S.U.R.R.C., East Kilbride, Glasgow, G75 0QU.

4.1 ABSTRACT

Diagenetic kaolinite in reservoir sandstones of the Brent Group precipitated following the dissolution of detrital feldspar. Two distinct morphologies of kaolinite occur; early diagenetic vermiform kaolinite which is often associated with expanded detrital micas, and later diagenetic "blocky" kaolinite. Combined hydrogen and oxygen isotopic studies suggest that vermiform kaolinite precipitated at 25-50°C, and blocky kaolinite at 50-80°C, from pore-waters of a similar isotopic composition ($\delta^{18}O$= -6.5 to -3.5‰). These pore-waters are interpreted to be either a mixture of meteoric and compactional waters, or alternatively a meteoric water that had evolved isotopically due to water-rock interaction. Kaolinite precipitation occured predominantly during the late Cretaceous to early Eocene. Influx of meteoric water into the Brent Group likely occurred during the Palaeocene. Fluid flow across the entire basin was driven by a hydrostatic head on the East Shetland Platform palaeo-landmass to the west. The development of the two kaolinite morphologies is possibly related to the degree of supersaturation at the time of precipitation. At low degrees of supersaturation vermiform kaolinite precipitated slowly upon detrital mica surfaces. Blocky kaolinite precipitated more rapidly into open pore-space at higher degrees of supersaturation. Precipitation of blocky kaolinite was perhaps triggered by the decay of oxalate.

4.2 INTRODUCTION

Diagenetic kaolinite and illite have a detrimental effect on the permeabilities of Brent Group sandstones, and can block pore-throats during oil production. Recent studies have shown that diagenetic

kaolinite and illite occur in oilfields throughout the whole of the East Shetland Basin, but in detail the volumes and morphologies of the clays differ with present day depth of burial (Giles *et al.* 1992; Glasmann *et al.* 1992; Haszeldine *et al.* 1992).

In this paper we present a compilation of some of the published and unpublished stable isotopic data ($\delta^{18}O$, δD) available to us from authigenic kaolinite in the Brent Group. These isotopic data have been used to constrain the growth temperature of the kaolinite and the origin of the pore-water from which it precipitated. These data come from 6 different oilfields in the East Shetland Basin area of the Northern North Sea, and cover a wide depth range of 1600-4400m. Present depth of burial, in all instances, is thought to have been the maximum depth attained. The objective of this study is to improve our understanding of the origins of the kaolinite, and to generate a better predictive model for its distribution in the subsurface.

4.3 GEOLOGICAL SETTING

The samples examined in this study came from reservoir sandstones in the Thistle, Murchison, Dunlin, Emerald, Heather, and South Alwyn oilfields in the East Shetland Basin area in the U.K. sector of the northern North Sea (Figure 1).

The stratigraphy, facies and depositional environment of the Brent Group is reviewed in Richards (1992). The Middle Jurassic Brent Group, consisting of deltaic and shallow marine sandstones, is approximately 300m thick, and is subdivided into five Formations. The Broom Formation is a separate fan delta and is not depositionally related to the overlying Rannoch Formation. The Rannoch and Etive Formations have been described as regressive facies formed during northwards progradation of the clastic wedge, whilst the overlying Tarbert Formations are transgressive in origin and were formed during a relative sea level rise which eventually drowned the system.

The Broom Formation consists of thin, poorly sorted, sandstones of limited reservoir importance. The Rannoch Formation is thought to have been deposited within a storm wave influenced shoreface setting, the sediments coarsen upwards, from siltstone to very fine or fine grained sandstone. Concentrations of mica and carbonaceous material along low angle laminae may inhibit vertical flow. The Etive Formation

is generally the best reservoir interval in the Brent Group, and consists of massive, well sorted, fine-coarse grained beach-barrier sandstones. Occasional mica and clay layers may reduce vertical permeability. Both the Rannoch and Etive Formations form extensive, readily correlatable sheets. The deltaic and coastal plain sediments of the Ness Formation are the most lithologically varied succesion in the Brent Group, consisting of interbedded sandstones, shales and some thin coals. Sandstones are often laterally and vertically discontinuous unless stacked fluvial channel sands occur. The Mid-Ness Shale forms an important non-reservoir horizon. The Tarbert Formation consists of fine grained, well sorted, micaceous, sandstones, with a coarser grained base which is interpreted to be a transgressive lag deposit. The Tarbert Formation was deposited in a shoreface setting during overall marine transgression. The Formation may be absent or thin at the crest of fields due to erosion beneath the late Cimmerian unconformity.

Schematic burial curves for the oilfields discussed are shown in Figure 2.

4.4 KAOLINITE MORPHOLOGY & DISTRIBUTION

4.4.1 Petrographic data

A generalised paragenetic sequence for the Brent Group sandstones studied is shown in Figure 3. Three morphological types of diagenetic kaolinite have been recognised within the Brent Group; kaolinite seen in association with detrital micas, vermiform kaolinite, and blocky kaolinite (Giles *et al.* 1992; Glasmann *et al.* 1989; Harris 1992).

Vermiform kaolinite and kaolinite associated with detrital micas are observed to occur within early diagenetic calcite concretions. It is likely that the vermiform kaolinite and the kaolinite within micas have a common origin, as they possess a similar morphology. Both kaolinites consist of large platy crystals, often with irregular edges. The plates are stacked on top of one another, roughly parallel to the 001 face. This results in large composite crystals (up to 200μm wide and 300μm in length) which are usually curvilinear in shape. Very thin sheets of muscovite occur within the vermiform kaolinite crystal (Figure 4).

Blocky kaolinite is typically fine grained (<30μm) and consists of very euhedral, pseudo-hexagonal, blocky crystals (Figure 5). Blocky kaolinite

is found in both primary porosity and secondary porosity created by the dissolution of feldspars. It is rarely seen in association with detrital micas. Blocky kaolinite has not been observed within early diagenetic calcite concretions occurring in the Emerald, Cormorant, Dunlin, Thistle, Alwyn South and Murchison oilfields. In contrast vermiform kaolinite and kaolinite associated with detrital micas are frequently found within these concretions.

Point count data on the distribution of the three kaolinite morphologies with depth indicates that vermiform and kaolinite cemented micas predominate within early diagenetic calcite concretions at any depth (Figure 6). Vermiform kaolinite and kaolinite associated with detrital micas also predominate in shallow buried Brent Group sandstones (<6000ft, 1800m). With increasing depth of burial the relative amount of blocky kaolinite present in the samples becomes increasingly volumetrically important (Figure 6).

Collation of published and unpublished point count data (Brint 1989; Giles *et al.* 1992; Harris 1992; Hogg 1989) shows that the volume of kaolinite present in the Brent group is highly variable, from 0-22 volume%, averaging 6.5% (Figure 7). Outside early diagenetic calcite concretions, kaolinite abundances are 2-3 times higher than inside concretions (Figure 7). In a study of the Statfjord, Hutton and Lyell fields, Harris (1992) found that more kaolinite was present in micaceous sandstones of the Rannoch and Ness Formations. Similarly, Bjorlykke & Brendsall (1986) found that there was a good relationship between mica content and kaolinite abundance in the Statfjord field. However detrital mica content is not the only facies related variable apparently linked to kaolinite distribution. In a regional study Giles *et al.* (1992) found that more kaolinite was present in the Etive than in any other Formation, and also that massive and cross-bedded sands in the Ness Formation were more kaolinite rich.

Ehrenberg (1991) has described unusually kaolinite rich sandstones which occur adjacent to organic rich shales at the top and bottom of the Middle Jurassic Garn Formation in the Norwegian North Sea, which is laterally equivalent to the Brent Group of the U.K. sector. These sandstones contain greater volumes of kaolinite but less feldspar than the rest of the Garn Formation. Ehrenberg noted however, that the leached zones are thin (always <9m) and are not present in all the wells

studied. Such leached zones have not been reported from the U.K. sector.

It has also been suggested that kaolinite abundance is greater immediately beneath the late Jurassic unconformity which occurs at the fault block crests of many Brent Group oilfields (Shanmugan 1990). Harris (1992) however, in a study of the Statfjord and Hutton fields, found that there was no increase in feldspar dissolution or kaolinite abundance below the unconformity. Bjorkum *et al.* (1990) also found that most of the kaolinite beneath the unconformity in the Gullfaks field was detrital in origin, and not a product of in-situ weathering, whilst Giles *et al.* (1992), in an extensive regional study of the Brent Group, found that only a very few wells had enhanced porosities beneath the unconformity, and that there was no marked increase in kaolinite abundance.

There is a general decline in kaolinite abundance below ~3300m, when illite replaces kaolinite as the predominant diagenetic clay. This decline in kaolinite abundance is seen in all facies and formations of the Brent Group (Giles *et al.* 1992).

To summarise this section, kaolinite abundance in the Brent Group is highly variable, with most kaolinite occurring in micaceous sandstones of the Rannoch and Ness Formations, and in massive and cross bedded sandstones in the Etive and Ness Formations. Enhanced abundances of kaolinite are rarely seen beneath late Jurassic unconformity surfaces or in sandstones adjacent to organic rich mudrocks.

4.4.2 Interpretation of petrographic data

More kaolinite is found outside early diagenetic calcite concretions than inside (Figure 7). This indicates that an extra volume of kaolinite have grown over time as subsidence progressed. Both vermiform kaolinite and kaolinite associated with detrital micas are found inside early diagenetic concretions. This suggests these kaolinite morphologies precipitated during shallow burial. Blocky kaolinite only occurs outside early concretions and is thus a diagenetically later precipitate that formed during deeper burial. This is supported by the fact that the volume of blocky kaolinite present in the Brent Group increases with present day depth of burial (Figure 7).

Kaolinite probably precipitated within muscovites because the mica surfaces may have facilitated kaolinite precipitation by reducing the interfacial free-energy barrier to nucleation. Hence kaolinite could have precipitated upon mica surfaces for lower levels of supersaturation than those required for homogeneous nucleation (Crowley 1991). The mica exhibits fanning and expansion of the grain terminations and kaolinite has precipitated between the cleavage planes without replacement of the mica itself (Crowley 1991). Although vermiform kaolinite often precipitated within the expanded sheets of detrital micas, blocky kaolinite is rarely seen in association with micas. This suggests that blocky kaolinite did not require the presence of mica surfaces in order to nucleate.

Textural evidence indicates that dissolution of detrital feldspar is the most likely source of Al and Si ions for kaolinite precipitation, because in thin section corroded feldspar edges interfinger with diagenetic kaolinite (Figure 4), suggesting that feldspar dissolution and kaolinite precipitation are genetically linked. Feldspar is the only volumetrically significant mineral present in the Brent Group which could dissolve to produce diagenetic kaolinite, and many feldspar grains have a skeletal appearance due to leaching (Giles *et al.* 1992; Harris 1992). Feldspar abundance declines with depth in all Brent Group facies and formations, suggesting that increasing volumes of feldspar have dissolved through time as subsidence progressed (Figure 8). Bulk geochemical analyses of Brent Group sandstones from a wide range of depths suggest that Al and Si ions have not been exported from the rock following feldspar dissolution (Harris 1992). The most likely sink for these Al and Si ions would have been kaolinite precipitation. Mass balance calculations can ascertain the amount of feldspar dissolution needed to produce the kaolinite. The average kaolinite abundance in the Brent Group is 6.5 volume %, but this will be an overestimate due to the high amount of microporosity present between the clay particles (40%, Nadeau & Hurst 1992), hence the true average kaolinite abundance is 3.3 volume%. Using the feldspar decomposition reactions of Giles & deBoer (1990), and knowing the molar volumes of the minerals involved, it can be calculated that 3.3% kaolinite would be produced by the dissolution of 6.9% feldspar. Inspection of the feldspar abundance versus depth trend in Figure 8 suggests that dissolution of 6.9% feldspar during burial is feasible. Hence import of Al and Si ions into the Brent Group is

apparently not required in order to explain the observed kaolinite abundances.

There are a number of possible reasons for the high variability in kaolinite abundance seen in the Brent Group.

1. Kaolinite microporosity. Clay minerals contain high amounts of microporosity, so that their point-counted abundance will be overestimates. Diagenetic kaolinite has microporosities varying from 25-50% (Nadeau & Hurst 1991), hence some of the variability in kaolinite abundance can easily be explained by differences in clay microporosity.

2. Variation in facies may also be an important factor influencing kaolinite distribution. For example, Giles *et al.* (1992) found that more kaolinite was present in the Etive than in any other Formation, and also that massive and cross-bedded sands in the Ness Formation were more kaolinite rich. These same facies also contain less feldspar than the rest of the Brent Group (Bjorlykke *et al.* 1992). The higher kaolinite abundance in these facies may be a reflection of the more porous and permeable nature of these sandstones compared to the rest of the Brent Group. If the Brent Group was flushed by feldspar-dissolving fluids then we would expect the more permeable and laterally extensive Formations to act as preferential conduits for fluid flow. Hence more feldspar dissolution would occur in these units and greater amounts of kaolinite precipitate. If kaolinite precipitated from a moving pore-fluid which was flowing through the sandstones, then some of the variability in kaolinite abundance at any single depth could also be explained by local redistribution of ions in solution.

3. Replacement of kaolinite by illite. There is a general decline in kaolinite abundance below ~3300m, and an increase in illite abundance (Giles *et al.* 1992). Using the SEM it can be seen that kaolinite plates are overgrown by fibrous illite, and EDS x-ray analyses indicates that the kaolinite contains significant potassium. This suggests that kaolinite is altering to illite, though high resolution TEM studies are needed in order discover details of the exact replacement process. The development of illite in the Brent Group is also apparently influenced by the presence of detrital K-feldspar in the sediment. Where K-feldspar is absent, kaolinite may persist to much greater depths than usual

(Ehrenberg 1991). This suggests that local feldspar dissolution is the source of K^+ ions for illite growth, and is consistent with thermodynamic and kinetic considerations which suggest that with increasing temperature, illite can form through reaction of silica in solution with detrital feldspar and authigenic kaolinite (Giles & deBoer 1990).

4. Acidic fluids released from shales. During the thermal maturation of organic matter in source rocks, organic acids and CO_2 can be released. These acidic fluids could enter nearby reservoir sandstones and result in feldspar dissolution and subsequent kaolinite precipitation (Curtis 1983; Surdam *et al.* 1984). However feldspar leached zones containing abundant kaolinite have rarely been observed adjacent to shales in the Brent Group (Ehrenberg 1991). This suggests that the potential for organic acids to cause widespread feldspar dissolution has been limited.

5. Shanmugan (1990) has argued that subaerial weathering of fault block crests during the late Jurassic resulted in extensive feldspar dissolution and secondary porosity creation. Enhanced feldspar dissolution could also have produced increased abundances of diagenetic kaolinite. However, the potential for leaching by weathering beneath the unconformity surface is thought to be limited, as fault block uplift in the late Jurassic was probably accompanied by rapid erosion (Bjorkum *et al.* 1990; Yielding *et al.* 1992). This has resulted in reworked sandstones downflank of the crest in some fields. Hence only insignificant topographic relief was likely to have been developed on most fault blocks. Observed leaching profiles are very thin; in the Upper Jurassic Magnus oilfield Emery *et al.* (1990) found that porosities and kaolinite contents were enhanced for a distance of only <10m beneath the unconformity. In an extensive regional study of the Brent Group Giles *et al.* (1992) found that enhanced porosities only occurred in a very few wells, where thick uniform sands were present beneath the unconformity. Hence sand-body connectivity and effective large scale permeability may have influenced the penetration of acidic, meteoric water. Giles *et al.* (1992) also found that there was no extra volume of kaolinite present in these wells, suggesting that the enhanced porosities may have been the result of dissolution of early carbonate cements, rather than detrital feldspar. Thus weathering zones beneath the

unconformity are very rare, and where they do occur they are very thin. Hence we can conclude that influx of meteoric water at the fault block crest has had only a minor effect on kaolinite distribution during subaerial weathering in the Brent Group.

To summarise this section, diagenetic kaolinite in the Brent Group was a by-product of feldspar dissolution. Variations in kaolinite abundance can be partly explained by differences in kaolinite microporosity, and by replacement of kaolinite by illite at depths >3300m. Facies also has a very important effect on kaolinite distribution, as the more porous and permeable facies have higher kaolinite abundances than the rest of the Brent Group. Despite all these factors influencing local kaolinite abundance, the total amount of kaolinite present in the Brent Group has increased through time. Early diagenetic vermiform kaolinite precipitated during shallow burial, and extra volumes of blocky kaolinite precipitated later, during deeper burial.

4.5 HYDROGEN AND OXYGEN STABLE ISOTOPES

4.5.1 Stable isotopic data

During the present study vermiform kaolinite from the Emerald oilfield has been subjected to stable isotopic analysis. Glasmann *et al.* (1989) have published stable isotope data from blocky kaolinite in the Heather field, while Brint (1989) managed to obtain analyses of kaolinite from the Thistle, Murchison, and Dunlin oilfields, although his samples consisted of a mixture of the blocky and vermiform types.

As can be seen from Figure 9 vermiform kaolinite is typified by relatively high values ($\delta^{18}O$), while blocky kaolinite possesses lower values ($\delta^{18}O$). In the mixed samples studied by Brint (1989), the highest values were associated with separates rich in vermiform kaolinite. Conversely, the lowest values came from samples containing a greater preponderance of blocky kaolinite. Brint (1989) does not provide quantitative data on the relative abundance of vermiform and blocky kaolinite in his mixed samples, and so we are unable to calculate the isotopic compositions of the end-members by mass balance methods. However, the consistent relationship between kaolinite morphology and $\delta^{18}O$ does suggest that the data of Glasmann *et al.* (1989) and our

own data can be used to isotopically constrain the conditions under which the blocky and vermiform end-members precipitated. In contrast to the strong relationship between kaolinite morphology and $\delta^{18}O$ compositions, there are no marked differences in δD between the different morphologies (Figure 10).

4.5.2 Interpretation of stable isotopic data

After crystallisation it is possible that structural hydrogen and oxygen in the clay mineral will be exchanged with hydrogen and oxygen present in the pore-water. It is therefore important to assess whether isotopic exchange between existing kaolinite and pore-waters has occurred during burial.

Experimental evidence suggests that the amount of oxygen isotope exchange for kaolinite is insignificant below 350°C (O'Neil & Kharaka 1976). Bird & Chivas (1988) have argued that marked hydrogen exchange has occurred at <80°C in Permian kaolinites they have studied. However they note that oxygen isotopes have not been exchanged, probably because change of structural H^+ and not $(OH)^-$ was involved. Longstaffe & Ayalon (1990) have similarly demonstrated that hydrogen isotopes in kaolinite have exchanged with present day formation waters at temperatures as low as 40°C, though oxygen isotopes remain unaffected.

It is possible to test whether significant stable isotope exchange has occurred if we know the isotopic composition of both the kaolinite and the Formation water. In the Thistle oilfield, the isotopic composition of the present day water has been directly measured ($\delta^{18}O$= +2, δD= -24 to -27‰ Brint 1989). Using the clay data of Brint (1989) from the Thistle oilfield we can calculate the composition of the pore-waters that would be in isotopic equilibrium with kaolinite at 112°C, the present day reservoir temperature in Thistle, using the isotopic fractionation equations of Savin & Lee (1988) for oxygen and Lambert & Epstein (1980) for hydrogen (Figure 11). If complete oxygen and hydrogen isotopic exchange had occurred then the calculated pore-water values for the kaolinite should be the same as present day Formation waters. However neither kaolinite $\delta^{18}O$ nor δD is in isotopic equilibrium with the formation water at present day burial temperature. Hence there is no evidence that kaolinite has undergone complete stable isotopic exchange with present day pore-waters. We will therefore assume there has been

no post-precipitation stable isotope exchange and combine the $\delta^{18}O$ and δD data to constrain the temperature and isotopic composition of the pore-water from which the kaolinite precipitated. By solving simultaneously the isotopic fractionation equations of Savin & Lee (1988) for oxygen and Lambert & Epstein (1980) for hydrogen, it can be seen (Figure 12) that both vermiform and blocky kaolinite precipitated from pore-waters with an overlapping isotopic composition ($\delta^{18}O$= -6.5 to -3.5‰). It is also clear that differences in $\delta^{18}O$ of the kaolinite partly reflect growth at different temperatures, with late diagenetic blocky kaolinite precipitating at higher temperatures (50-80°C) than the early diagenetic vermiform variety (25-50°C). If we assume a burial temperature gradient of 35°Ckm^{-1} and a surface temperature of 5°C existed at the time of kaolinite precipitation, then vermiform kaolinite precipitated at depths of 571-1286m and blocky kaolinite at 1286-2143m. The assumed burial temperature gradient is similar to that measured in North Sea boreholes today, and is considered to be a reasonable estimate for the conductive geothermal gradient during the Cretaceous and Tertiary (Glennie 1990, Ch. 11)

The calculated water $\delta^{18}O$ are lower than pre-Miocene sea water ($\delta^{18}O$= -1.0‰; Sheppard 1986); therefore the kaolinites are unlikely to have precipitated from depositional marine pore-waters. Jurassic meteoric water is thought to have had $\delta^{18}O$= -6 to -7‰ (Fallick *et al.* 1993; Hamilton *et al.* 1987), while Tertiary meteoric waters are estimated to have had $\delta^{18}O$= -10‰ (e.g. Fallick *et al.* 1993). These values represent the range of possible meteoric waters which could have had access to the Brent Group since deposition. However the pore-waters from which the kaolinite precipitated had $\delta^{18}O$ values which are generally higher than any possible meteoric water. Therefore the kaolinite must have precipitated from a mixed meteoric-marine water, or from a meteoric pore-fluid that had evolved isotopically during water-rock interaction to become more enriched in ^{18}O (Sheppard 1986). As many of these kaolinite samples came from open marine Formations, this suggests that meteoric water must have flushed through the Brent Group, partly displacing depositional marine pore-fluids.

It is possible to estimate the timing of kaolinite precipitation by combining the growth temperatures calculated from the stable isotopic data, with subsidence curves for the individual oilfields (Figure 13, data from Table 3). It can be seen (Figure 14) that kaolinite precipitated at

similar times in different oilfields, during the late Cretaceous to early Eocene. It should be remembered however, that Brint (1989) analysed mixtures of vermiform and blocky kaolinite, hence his stable isotopic data represent bulk values for a mixture of different kaolinite generations. Thus we cannot rule out the possibility that some kaolinite precipitated earlier or later than the times calculated. Nevertheless, it is still probable that the greatest volume of kaolinite grew during the late Cretaceous to early Eocene.

4.6 DISCUSSION

As outlined earlier, vermiform kaolinite and blocky kaolinite precipitated from waters with a similar isotopic composition ($\delta^{18}O$= -6.5 to -3.5‰), which suggests that there was a component of meteoric water in the pore-fluid. Integration of kaolinite growth temperatures with subsidence histories for the individual oilfields suggests that most kaolinite precipitated during the late Cretaceous to early Eocene (Figures 13 & 14).

Why did extensive kaolinite precipitation (and by inference, feldspar dissolution) occur at this time? Any diagenetic model advanced to explain this cementation event must also consider the stable isotopic data, which suggest that pore-waters in the Brent Group were meteoric or brackish in composition at the time of kaolinite precipitation.

We suggest that the most likely mechanism allowing meteoric water to enter the Brent Group during the late Cretaceous to early Eocene is regional meteoric fluid flow. This meteoric flow would be driven by a gravitational hydrostatic head on the East Shetland Platform to the west, which was a landmass during the Palaeocene (Glennie 1990). This meteoric water could have undergone mixing with compactional, marine-derived pore-fluids, which were probably being expelled from rapidly subsiding marine sediments at this time. Mixing of meteoric waters and compactional marine waters, would explain the brackish pore-water compositions suggested by the stable isotopic data.

The amount of uplift during the Palaeocene is not well constrained, but the Tertiary volcanic province on the west coast of Scotland is thought to have attained a height of at least 3km (White & McKenzie 1989). Meteoric water precipitating as rain on a landmass may certainly flow below the sea floor far into sedimentary basins. For example

freshwater aquifers occur 120km off the Florida coast in Tertiary carbonate aquifers (Mannheim 1967). The depth of penetration of meteoric water is also considerable; in the Great Artesian Basin of Australia the aquifer lies at depths of up to 2000m (Hebermehl 1980). In this East Shetland Basin study area, Mullis & Haszeldine (1994) have quantitatively modelled the ancient hydrogeology of the Brent Group fault blocks. They conclude that large scale meteoric flow was feasible with rates of 2-6cm/yr $^{-1}$ resulting from a hydraulic head of only 100m.

In support of regional fluid flow we note that oil columns in the Emerald, and Gullfaks fields are biodegraded due to the influx of oxygen bearing meteoric water (Wheatley *et al.* 1987; Larter & Horsted 1992). (Larter & Horstad 1992) have suggested that meteoric water entered the Gullfaks field from the west in the late Cretaceous when the reservoir was shallow buried (<2000m). However, Mullis & Haszeldine (1994) suggest that biodegradation in the Gullfaks field occurred in the early Tertiary. Wheatley *et al.* (1987) similarly believe that meteoric water flushed through the Emerald oilfield from the west in the Palaeocene, resulting in biodegradation (1000m burial). Miles (1990) also found that oil in the Ninian field contained a small biodegraded component. In the Ninian oilfield, biodegradation of early migrating oil is thought to have occurred in the late Cretaceous at <2100m burial. However the effect of this early biodegradation has been masked by the influx of greater volumes of non-biodegraded oil during the early Tertiary, when the oilfield was buried to depths of 2100-3000m (Miles 1990). Hence the amount of biodegraded oil present in Brent Group oilfields is apparently related both to oilfield subsidence history, and to the timing of hydrocarbon charging. If oil entered shallow buried reservoirs during the late Cretaceous to Palaeocene, then hydrocarbons were biodegraded due to flushing by meteoric waters. However by the Eocene, most Brent Group oilfields were deeply buried, and reservoir temperatures were too high for biodegradation to proceed. Hence hydrocarbons migrating at this time were not biodegraded.

If meteoric water entered the Brent Group, then it may be directly responsible for feldspar dissolution, because dissolution is faster in acidic pore-water and meteoric water is often slightly acidic due to dissolved CO_2 and organic acids produced in soil profiles (Giles & deBoer 1990). This may explain why the most permeable facies in the Brent Group possess greater volumes of authigenic kaolinite; such facies would be

would be preferential conduits for aggressive meteoric waters leading to intense feldspar dissolution and subsequently greater kaolinite precipitation. Oxidative biodegradation of migrating oil by meteoric waters can also lead to the production of large volumes of organic acids, which would further enhance feldspar dissolution rates, particularly in the most permeable carrier-bed sandstones (Dimitrakopoulos & Meuhlenbachs 1987). Note however, that acidic pore-waters would not necessarily be required for feldspar dissolution to proceed. Feldspar dissolution is faster in acidic pore-waters, but still occurs in waters with a neutral pH (Giles & deBoer 1990).

Because dissolution rates at low temperatures are slow, a large flux of acidic meteoric water through the Brent Group would probably not have been needed to dissolve the detrital feldspars. However a minimum flux must have been available to keep K^+/H^+ low and ensure that the pore-waters remained in the stability field of kaolinite (Bjorlykke & Aagaard 1992). Oxidative biodegradation of oil also requires a moving pore-water, because dissolved O_2 must be continually supplied to the bacteria which are degrading the oil.

We suggest that kaolinite morphologies are related to depth of burial; at shallow depths (571-1286m, 25-47°C) vermiform kaolinite precipitated, while at greater depths (1286-2143m, 50-80°C) blocky kaolinite precipitated. This interpretation is supported by the paragenetic sequence, petrographic observations, and by palaeotemperature information calculated using stable isotope data.

Hurst & Irwin (1982) have suggested that influx of meteoric water results in rapid feldspar dissolution and consequently rapid kaolinite precipitation. In their model, rapid kaolinite growth results in the precipitation of vermiform kaolinite. However if there is no flow of meteoric pore-water then kaolinite precipitation proceeds more slowly, leading to finer grained, blocky kaolinite. Hence in this model the growth of different kaolinite morphologies is a transport controlled process, with growth being fastest in a flowing fluid which is continually transporting additional ions to the crystal surface.

Our own tentative model for kaolinite growth is shown in Figure 15. This differs from the transport-controlled growth model of Hurst & Irwin (1982) in several respects. XRD studies of vermiform and blocky kaolinite show that both are well-crystalline, indicating they precipitated from fluids with a low degree of supersaturation (Berner 1981); hence

vermiform kaolinite could not have precipitated rapidly from a highly supersaturated fluid as suggested by Hurst and Irwin. Transport-controlled kaolinite growth also does not explain why vermiform kaolinite precipitates preferentially within expanded micas. Instead the association with micas strongly suggests that growth of vermiform kaolinite was from solutions with a very low degree of supersaturation, so that mica surfaces were the only kinetically favourable sites upon which kaolinite could nucleate (Crowley 1991). In such a situation, the rate of kaolinite growth would be at least partly controlled by reactions at the mica surface. In surface-controlled growth nutrient ion supply is so slow that ions can easily be supplied by molecular diffusion, so that the growth rate will not be affected by the rate of fluid flow (Berner 1981).

Instead it is likely that the difference in the kaolinite morphologies is related to the degree of supersaturation at the time of precipitation. At low temperatures (shallow burial) feldspar dissolution rates will be low, hence we would expect only low levels of supersaturation with respect to kaolinite (Giles & deBoer 1990). Similarly, kinetic constraints mean that mineral precipitation rates are very slow at low temperatures (Berner 1981). Under such conditions, kaolinite precipitation upon mica surfaces could have been kinetically favoured, as this would have reduced the interfacial free-energy barrier to nucleation (Crowley 1991). Expanded mica also possesses many minute cracks and interstices, and Berner (1971) has theoretically shown that mineral nucleation may proceed in cracks even from undersaturated solutions. Once the kaolinite had initially nucleated upon the mica surface, more kaolinite could have precipitated upon the pre-existing kaolinite crystals. Succesive plates could then precipitate face to face, producing the characteristic vermiform morphology (Crowley 1991).

At higher temperatures (deeper burial), the rate of feldspar dissolution is greater, increasing 29,220 times, as temperature rises from 25 to 200°C (Helgeson & Murphy 1983). The rate of feldspar dissolution at depth will be further be enhanced if acidic fluids are being expelled from adjacent organic-rich mudrocks over the temperature range 70-110°C (Surdam *et al.* 1984). Oxidative biodegradation of migrating oil by meteoric waters could also have lead to in-situ production of large volumes of organic acids (Dimitrakopoulos & Muehlenbachs 1987). Such acidic fluids contain oxalate (carboxylic acid anions), which act as an Al-complexing agents, greatly enhancing the solubility of aluminium (Surdam *et al.*

1984). This could have allowed the Al concentration of the pore-water to increase following feldspar dissolution. However, as this oxalate decomposed, the Al in solution would have precipitated in the form of diagenetic clay (Curtis 1983). It has been experimentally demonstrated that kaolinite precipitation is very rapid under such conditions, and is dependent only upon the rate of oxalate decay (Small 1993). Hence during deeper burial, the combined effects of increased rates of feldspar dissolution and complexing of some Al in solution could have led to higher states of supersaturation being achieved. It is thus possible that blocky kaolinite precipitated from solutions which were supersaturated to a higher degree.

The smaller size of the blocky kaolinite crystals compared to the vermiform variety is consistent with precipitation at higher degrees of supersaturation, because high supersaturation encourages rapid nucleation of greater numbers of smaller crystals in preference to slower growth of a few large crystals (Berner, 1971). If supersaturation was high, mica surfaces would not be required in order to nucleate kaolinite, and blocky kaolinite could have rapidly precipitated directly into open pore-space. This explains why blocky kaolinite is rarely seen in association with muscovite in the Brent Group. Because the kaolinite was not using mica surfaces as a template for growth, it was possible for the kaolinite to develop its characteristic pseudo-hexagonal, platy, morphology.

The available experimental data is consistent with this hypothesis. In the laboratory, Small (1993) managed to precipitate blocky kaolinite from solution following the decay of oxalate (carboxylic acid anions). Initially a metastable Al-oxyhydroxide gel is thought to have precipitated, which subsequently transformed into the blocky kaolinite by the incorporation of silica (Small 1993). Rapid precipitation of a precursor gel indicates high levels of supersaturation (Berner 1981). By contrast, Small *et al.* (1992) managed to precipitate vermiform kaolinite following HCl dissolution of feldspar, without any oxalate being present, and with no precipitation of a precursor gel. Small (1993) suggests that the different vermiform and blocky morphologies are the result of precipitation via different mechanisms.

We suggest that in the Brent Group, early diagenetic vermiform kaolinite precipitated on mica surfaces at low temperatures. Vermiform kaolinite precipitated slowly, under conditions of low supersaturation. During deeper burial (higher temperatures) increased rates of feldspar

dissolution resulted in higher degrees of supersaturation, and blocky kaolinite precipitated rapidly into open pore-space. Precipitation of blocky kaolinite was perhaps triggered by the decay of oxalate. This oxalate had been generated during the biodegradation of crude oil. This hypothetical model is consistent with the available petrographic, isotopic and experimental data.

4.7 CONCLUSIONS

1) The distribution of kaolinite morphologies in the Brent Group is related to depth of burial. At shallow depths (<1800m) and within early diagenetic calcite concretions, vermiform kaolinite and kaolinite associated with detrital micas predominate. At greater depths blocky kaolinite predominates. The most permeable and laterally continuous facies of the Brent Group contain the greatest volumes of kaolinite.

2) Stable isotopic data suggest that vermiform kaolinite precipitated at 25-50°C and blocky kaolinite at 50-80°C from pore-waters with a similar composition ($\delta^{18}O$= -6.5 to -3.5‰). These pore-waters are interpreted to be a mixture of meteoric fluid and compactional marine pore-waters. Most kaolinite precipitated during late Cretaceous to early Eocene times.

3) Kaolinite precipitation may be linked to the influx of meteoric water into the Brent Group during the Palaeocene. Fluid flow across the entire basin was driven by a hydrostatic head on the East Shetland Platform palaeo-landmass to the west. This acidic meteoric water flushed preferentially through the most permeable formations, resulting in enhanced feldspar dissolution and kaolinite precipitation in these facies. Oil migrating into shallow buried reservoirs at this time was flushed by meteoric waters and became biodegraded.

4) The development of the vermiform and blocky morphologies is possibly dependent upon the degree of supersaturation at the time of precipitation. For low degrees of supersaturation vermiform kaolinite precipitated slowly upon mica surfaces. At higher degrees of supersaturation blocky kaolinite rapidly precipitated directly into pore-space. Blocky kaolinite precipitation may have been triggered by the decay of oxalate.

4.8 ACKNOWLEDGEMENTS

The technical staff of the stable isotope lab at SURRC are thanked for their inestimable help, particularly Allison McDonald and Julie Gerc. Peter Ainsworth and Douglas Maclean are thanked for their SEM and photographic expertise respectively. Incisive comments by two anonymous reviewers improved the quality of the paper. Mark Osborne acknowledges the receipt of a NERC grant. The SURRC is supported by NERC and the Scottish Universities.

4.9 REFERENCES

Baldwin, B., & Butler, C.O., 1985, Compaction curves, *Am. Assoc. Petrol. Bull.*, **69**, p. 622-626.

Berner, R. A., 1971, *Principles of Chemical Sedimentology*, New York, McGraw Hill, 240 p..

Berner, R.A., 1981, Kinetics of weathering and diagenesis. In *Kinetics of geochemical processes*, Reviews in Mineralogy 8, Min. Soc. Am.

Bird, M.I., & Chivas, A.R., 1988, Stable isotope evidence for low temperature kaolinitic weathering and post-formational hydrogen isotope exchange in Permian kaolinites. Chem. Geol., **72**, p. 249-265.

Bjorkum, P.A., Mjos, R., Walderhaug, O., & Hurst, A., 1990, The role of the late Cimmerian unconformity for the distribution of kaolinite in the Gullfaks field, northern North sea. Sedimentology, **37**, 395-406.

Bjorlykke, K., & Aagaard, P., 1992, Clay minerals in North Sea sandstones. In *Origin, diagenesis and petrophysics of clay minerals in sandstones*, SEPM Spec. Publ. 47, p.65-80.

Bjorlykke, K., & Brendsal, A.,1986, Diagenesis of the Brent sandstone in the Statfjord field. In Gautier, D.L., (ed.), *Roles of organic matter in sedimentary diagenesis*. SEPM Special Publication No. 38. p.157-168.

Bjorlykke, K., Nedkvitne, T., Ramm, M., Saigal, G.C., 1992, Diagenetic processes in the Brent Group (Middle Jurassic) reservoirs of

the North Sea ; an overview. In Morton, A. C., Haszeldine, R. S., Giles, M. R., & Brown, S., (Eds), *Geology of the Brent Group*. Geological Society of London, Bath UK. p. 263-288.

Brint, J. F., 1989, Isotope diagenesis and palaeofluid movement: Middle Jurassic Brent sandstones, North Sea *D. Phil. Thesis* University of Strathclyde, Scotland, 288 p.

Craig, H., 1961, Isotopic variations in meteoric waters. Sci., **133**, p.1702-1703.

Crowley, S.F., 1991, Diagenetic modification of detrital muscovite: an example from the great limestone cyclothem (Carboniferous) of Co. Durham, U.K. Clay Minerals, **26**, p.91-103.

Curtis, C.D., 1983, Link between aluminium mobility and the destruction of secondary porosity. Bull. Am. Assoc. Petrol. Geol., **67**, p. 380-393.

Dimitrakopoulos, R., & Muehlenbachs, K., 1987, Biodegradation of petroleum as a source of ^{13}C enriched carbon dioxide in the formation of carbonate cement. Chemical Geology, **65**, p.283-291.

Ehrenberg, S.N., 1991, Kaolinized, potassium-leached zones at the contacts of the Garn Formation, Haltenbanken, mid-Norwegian continental shelf. Marine and Petroleum Geology, **8**, p. 250-269.

Emery, D., Myers, K.J., & Young, R., 1990, Ancient subaerial exposure and freshwater leaching in sandstones. Geology, **18**, p.1178-1181.

Fallick, A.E., Macauley, C.I., & Haszeldine, R.S., 1993, Implications of linearly correlated loxygen and hydrogen isotopic compositions for kaolinite and illite in the Magnus sandstone, North Sea. Clay Minerals (in press).

Giles, M.R., & deBoer, R.B., 1990, Origin & significance of redistributional secondary porosity. Marine & Petroleum Geology, **7**, .p.378-397.

Giles, M.R., Stevenson, S., Martin, S. V., Cannon, S. J. C., Hamilton, P. J., Marshall, J. D., & Samways, G. M., 1992, The reservoir properties and diagenesis of the Brent Group; a regional perspective. In Morton, A. C., Haszeldine, R. S., Giles, M. R., & Brown, S., (Eds), *Geology of the Brent Group*. Geological Society of London, Bath UK. p. 289-327.

Glasmann, J.R., 1992, The fate of feldspar in the Brent Group reservoirs, North Sea: a regional synthesis of diagenesis in shallow, intermediate, and deep burial environments. In Morton, A. C., Haszeldine, R. S., Giles, M. R., & Brown, S. (Eds), *Geology of the Brent Group*. Geological Society of London, Bath U.K. p. 329-350.

Glasmann, J. R., Lundegard, P. D., Clark, R. A., Penny, B. K., Collins, I. D., 1989, Geochemical evidence for the history of diagenesis and fluid migration: Brent sandstone, Heather field, North Sea *Clay Minerals*, **24**, p. 255-284.

Glennie, K. W.,1990, *Introduction to the Petroleum Geology of the North Sea* (third edition) Oxford, Blackwell Scientific Publications.

Habermehl, M.A., 1980, The Great Artesian Basin, Australia, BMR. J. Australian Geol. Geophys., **5**, p. 9-38.

Hamilton, P.J., Fallick, A.E., Macintyre, R.M., & Elliott, S.,1987, Isotopic tracing of provenance and diagenesis of lower Brent Group sands, North Sea. In Brooks, J., & Glennie, K.W., (eds.), *Petroleum Geology of NW Europe*, Graham & Trotman, London, p.939-949.

Harris, N. B., 1992, Burial diagenesis of Brent sandstones: a study of Statfjord, Hutton and Lyell fields. In Morton, A. C., Haszeldine, R. S., Giles, M. R., & Brown, S. (Eds), *Geology of the Brent Group*. Geological Society of London, Bath U.K. p. 351-375.

Haszeldine, R. S., Brint, J. F., Fallick, A.E., Hamilton, P. J., & Brown, S., 1992, Open and restricted hydrologies in Brent Group diagenesis: North Sea. In Morton, A. C., Haszeldine, R.S., Giles, M. R., & Brown, S.(Eds.), *Geology of the Brent Group*. Geological Society of London, Bath UK. p. 401-419.

Helgeson, H. C., & Murphy, W.M., 1983, Calculations of mass transfer among minerals and aqueous solutions as functions of time and surface are in geochemical processes. 1. computational approach. Math. Geol.,**15**, p.109-131.

Hogg A.J.C.,1989, Petrographic and isotopic constraints on the diagenesis and reservoir properties of the Brent Group sandstones, Alwyn South, Northern U.K. North Sea *D. Phil. Thesis* University of Aberdeen, Scotland, 414p.

Hurst, A., & Irwin, H., 1982, Geologic modelling of clay minerals in sandstones, Clay Min., **17**, p.5-22.

Kantorowicz, J.D., 1990, The influence of variations in illite morphology on the permeability of Brent Group sandstones, Cormorant field, U.K. North Sea. Marine & Petroleum Geology, **7**, p.66-74.

Lambert S.J., Epstein, S., 1980, Stable isotope investigations of an active geothermal system in Valles Caldera, Jemez Mountains, New Mexico. J. Volcan. Geotherm. Res., **8**, p.111-129.

Larter, S., & Horstad, I., 1992, Migration of petroleum into Brent Group reservoirs: some observations from the Gullfaks field, Tampen Spur area North Sea. In Morton, A. C., Haszeldine, R.S., Giles, M. R., & Brown, S.(Eds.), *Geology of the Brent Group*. Geological Society of London, Bath UK. p.441-452.

Longstaffe, F., & Ayalon, A., Hydrogen-isotope geochemistry of diagenetic clay minerals from Cretaceous sandstones, Alberta, Canada: evidence for exchange. Applied Geochemistry, **5**, p.657-668.

Manheim, F.T., 1967, Evidence for submarine discharge of water on the Atlantic continental slope of the southern United States. Trans. New York Acad. Sci., **11**, p.839-835.

Mullis, A.M., & Haszeldine, R.S., 1994, Numerical modelling of diagenetic hydrogeology at a graben edge: Brent Group oilfields, North Sea. Journ. Geol. Soc. Lond. (accepted).

Nadeau, P.H, & Hurst, A., 1992, Applications of back scattered electron microscopy to the quantification of clay mineral microporosity, Journal of Sedimentary Petrology, **61**, p.921-925.

O'Neil, J. R., & Kharaka, Y. K., 1976, Hydrogen and oxygen isotopic exchange reactions between clay minerals and water. Geochim. Cosmochim. Acta, **40**, p.241-246.

Richards, P.C., An introduction to the Brent Group, a literature review. In Morton, A. C., Haszeldine, R.S., Giles, M. R., & Brown, S.(Eds.), *Geology of the Brent Group*. Geological Society of London, Bath UK. p. 15-26.

Savin, S.M., & Lee, M., 1988, *Isotopic studies of phyllosilicates*. In Miner. Soc. Am. Reviews in Mineralogy, 16, p.188-223.

Shanmugan, G., 1990, Porosity prediction using erosional unconformities. In Prediction of reservoir quality using chemical modelling, Eds. I.D. Meshri & PJ Ortoleva, AAPG memoir **49**, p.1-23.

Sheppard, S.M.F., 1986, *Characterization and isotopic variations in natural waters.* In Miner. Soc. Am. Reviews in Mineralogy, 16, p.165-183.

Surdam, R.C., Boese, S.W., Crossey, L.J., 1984, The chemistry of secondary porosity, In *Clastic Diagenesis,* McDonald, D, Surdam, R., (Eds.), American Association of Petroleum Geologists Memoir, **37**, p.127-151.

Small, J.S., Hamilton, D.L., Habesch, S., 1992, Experimental simulation of clay precipitation within reservoir sandstones. *Journ. Sed. Pet.*, **62**, p. 508-529.

Small, J.S., 1993, Experimental determination of rates of precipitation of authigenic kaolinite and illite. *Clays & Clay Minerals,* **41**, p.191-208.

Wheatley, T.J., Biggins, J., Buckingham, & Holloway, N.H.,1987, The geology and exploration of the transitional shelf, an area to the west of the Viking Graben. In Brooks, J., & Glennie, K.W., (eds.), *Petroleum Geology of NW Europe,* Graham & Trotman, London, p. 979-989.

Yielding, G., Badley, M.E., & Roberts, A.M., 1992, The structural evolution of the Brent Province. In Morton, A. C., Haszeldine, R.S., Giles, M. R., & Brown, S.(Eds.), *Geology of the Brent Group.* Geological Society of London, Bath UK. p. 27-43.

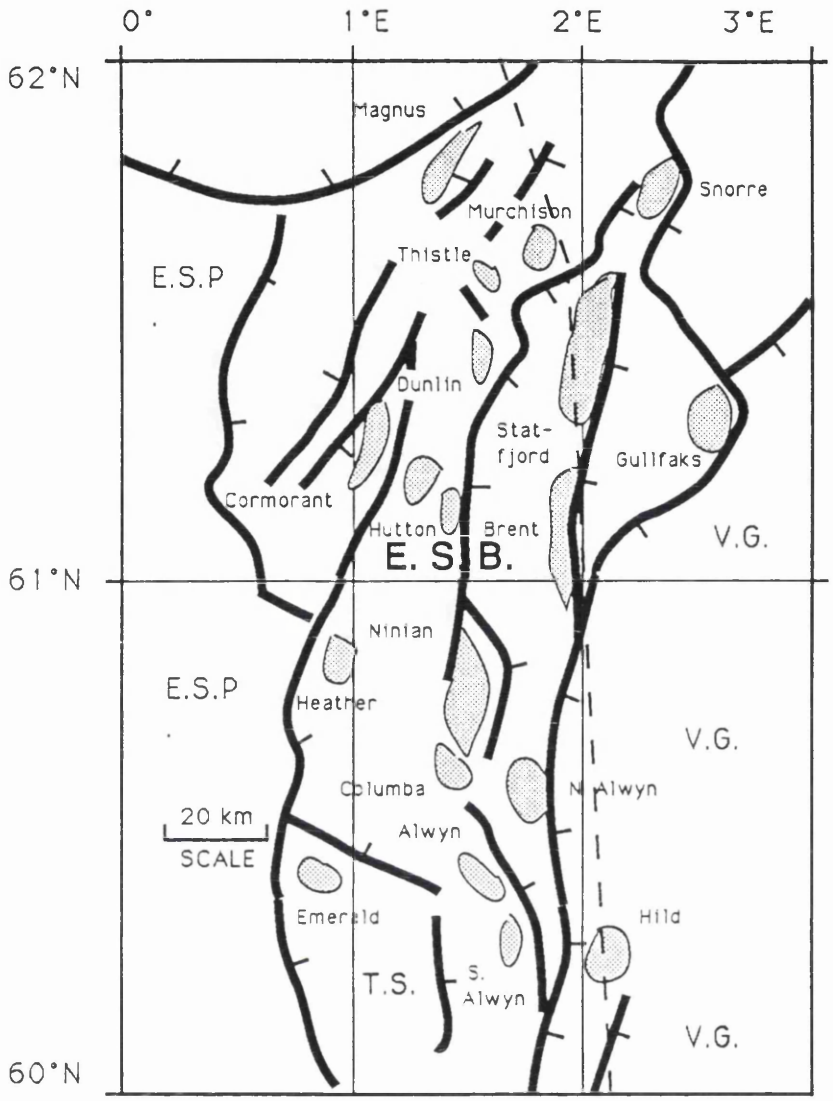

Figure 1. Map of the East Shetland Basin showing the location of the oilfields discussed in the text.

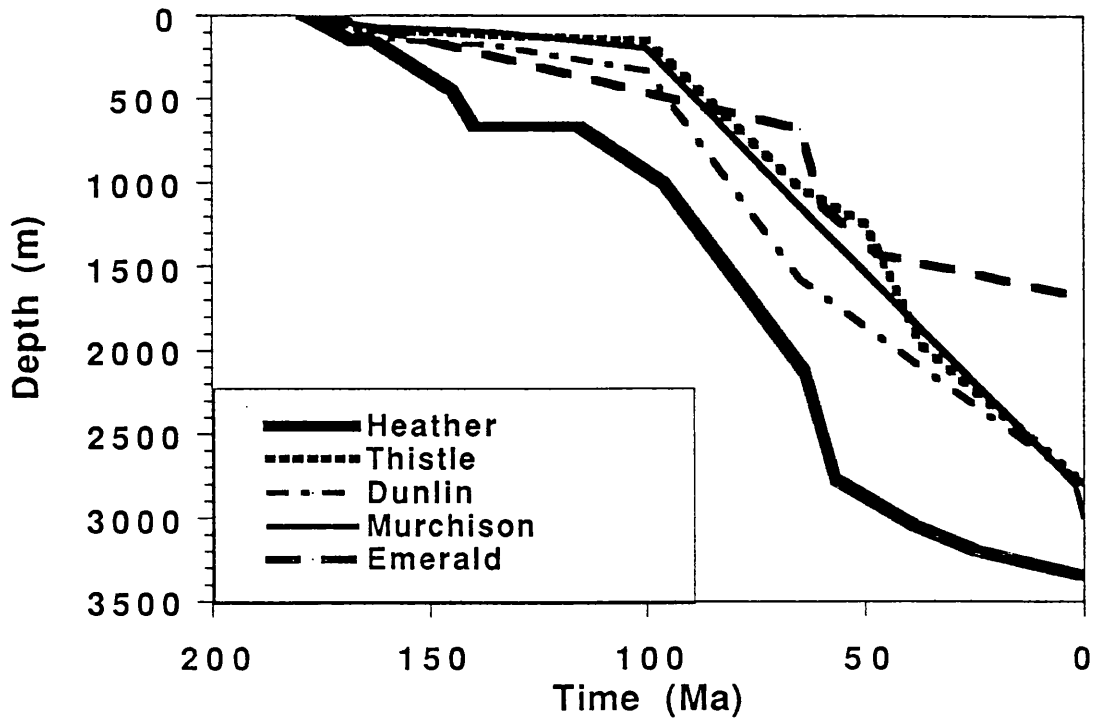

Figure 2. Schematic burial curves for the oilfields studied. Redrawn in part from Brint (1989) and Glasmann *et al.* (1989).

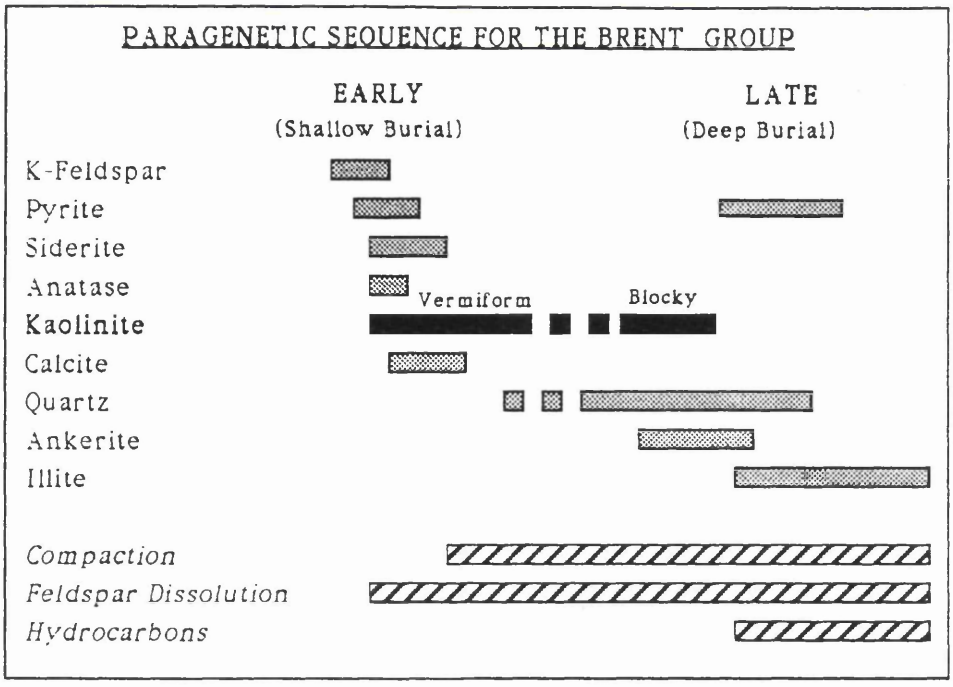

Figure 3. Generalised paragenetic sequence of mineral growth for the Brent Group.

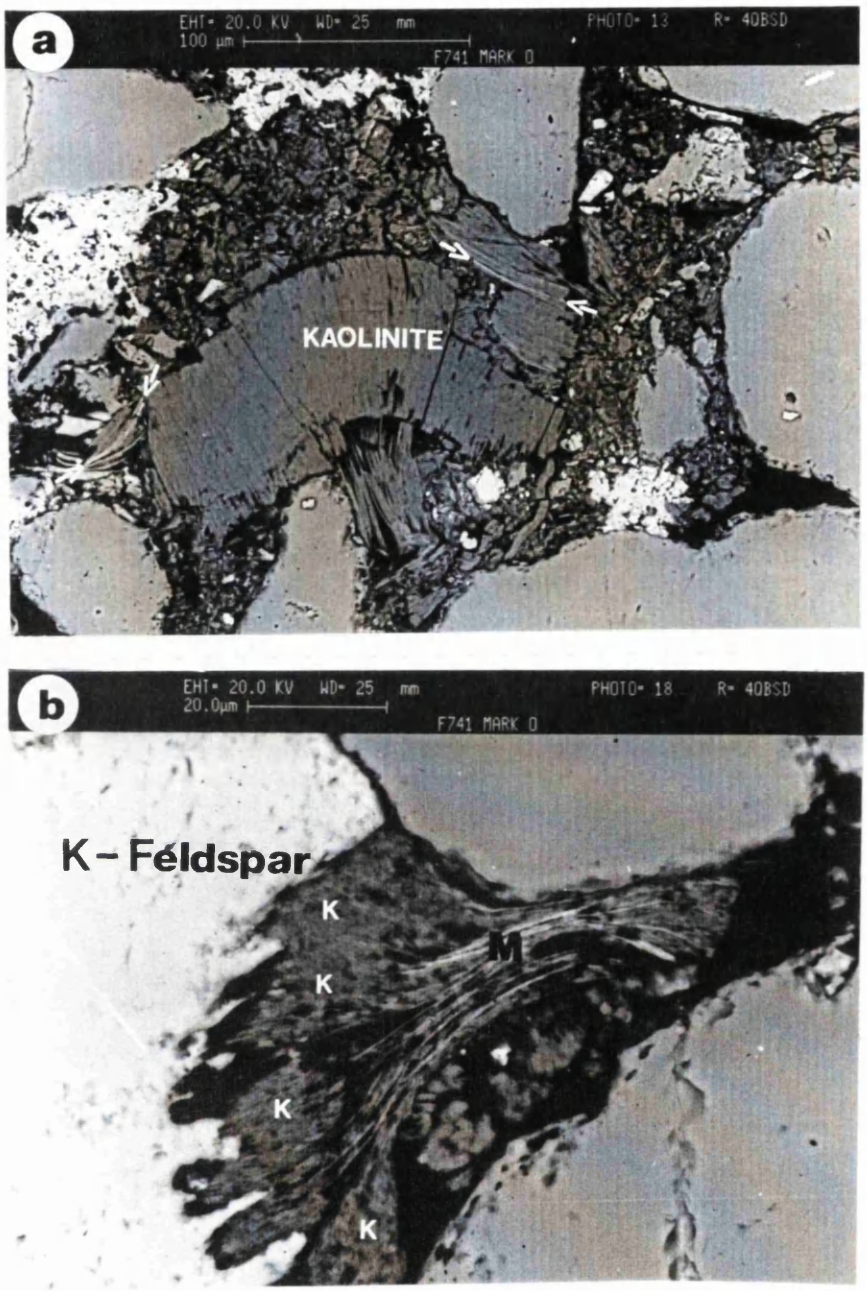

Figure 4. a) Large vermiform kaolinite crystal. Note that very thin sheets of muscovite (light in colour, arrowed) occur within the kaolinite crystal. This suggests that the kaolinite nucleated upon mica originally. Emerald oilfield, 2/10a-7, 1649.4m TVD
b) Vermiform kaolinite (K) nucleated between the sheets of an expanded muscovite (M). Immediately adjacent to the mica is a K-feldspar clearly dissolved. Kaolinite precipitated in the secondary porosity created by feldspar corrosion. This suggests the Al and Si were supplied by breakdown of detrital feldspar. Same sample as in 4 a).

Figure 5. Typical appearance of blocky kaolinite. This type of kaolinite consists of very euhedral, sub-hexagonal plates. Murchison oilfield, Well 211/19-3, 3148mTVD.

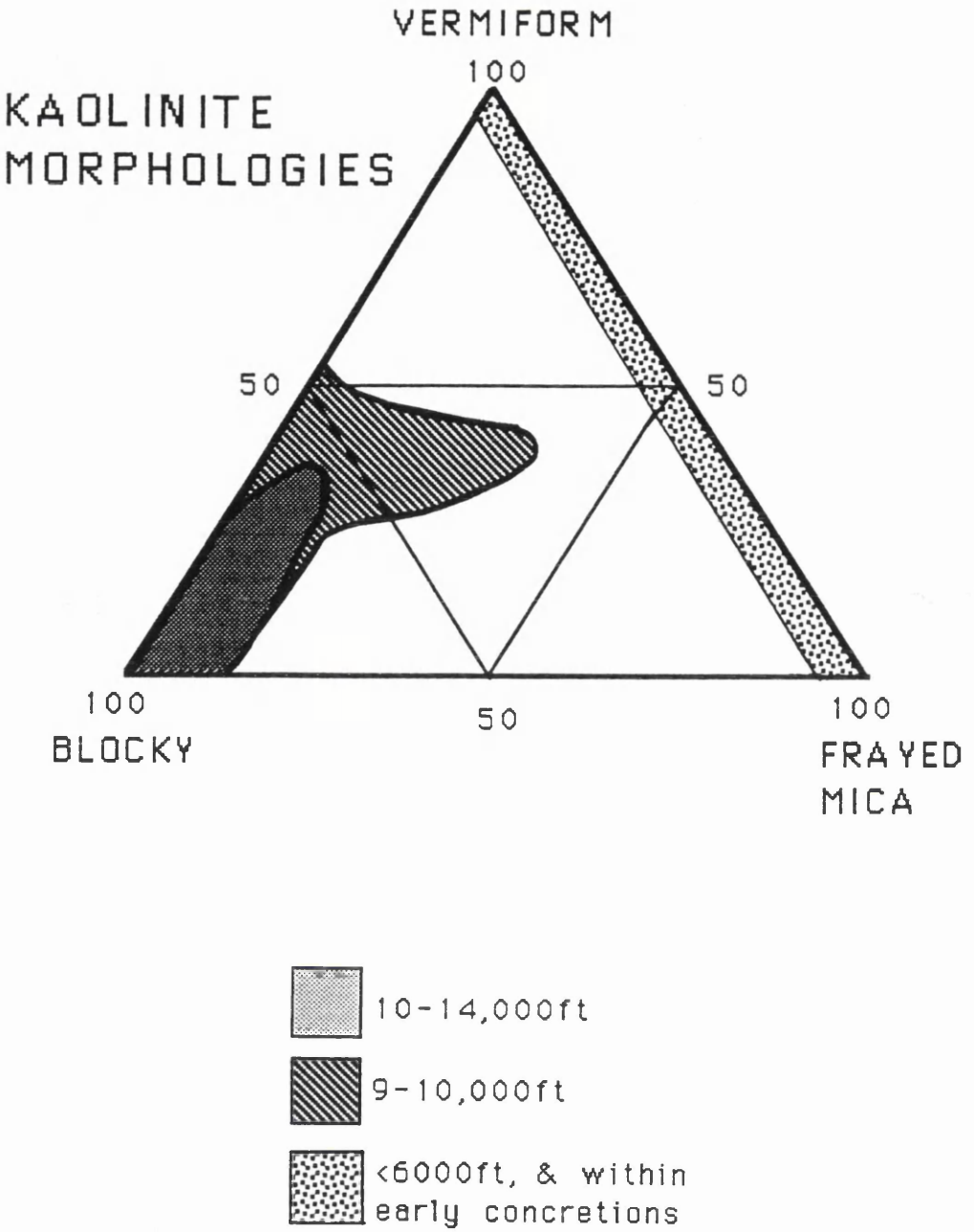

Figure 6. Point count data on the distribution of various kaolinite morphologies with present day depth of burial. Vermiform kaolinite and kaolinite seen in association with detrital micas predominate within shallow buried sandstones and within early diagenetic calcite concretions. With increasing depth of burial the relative amount of blocky kaolinite in samples becomes increasingly volumetrically important. Data from Table 1.

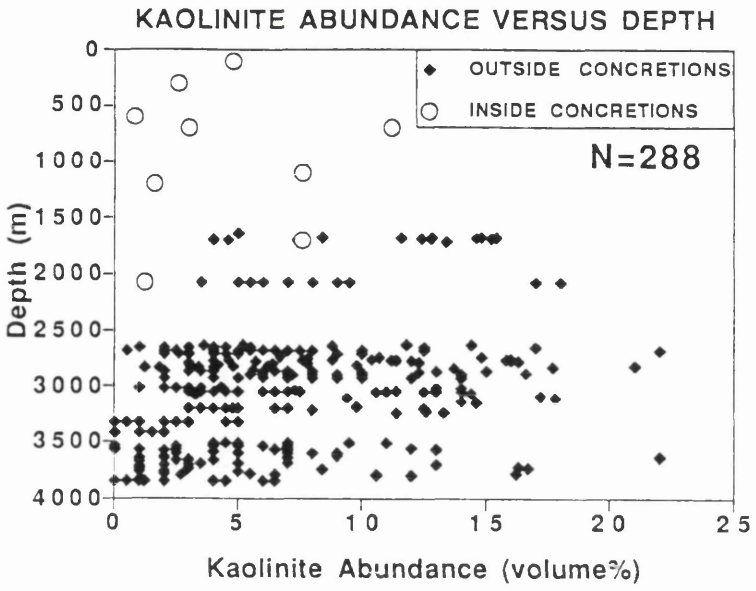

Figure 7. Compilation of point count data showing the variation in kaolinite abundance with present day depth of burial. Kaolinite occurring within early diagenetic calcite concretions has also been plotted, the depth of cementation being calculated from the minus cement porosities of the concretions in conjunction with the compaction curves of Baldwin & Butler (1985). Note that kaolinite content within concretions is lower than that outside concretions, suggesting extra kaolinite has precipitated through time. Kaolinite abundance is highly variable at any one depth. Data from Brint (1989); Giles et al. 1992, and Harris (1992) plus data of the authors from the Emerald oilfield .

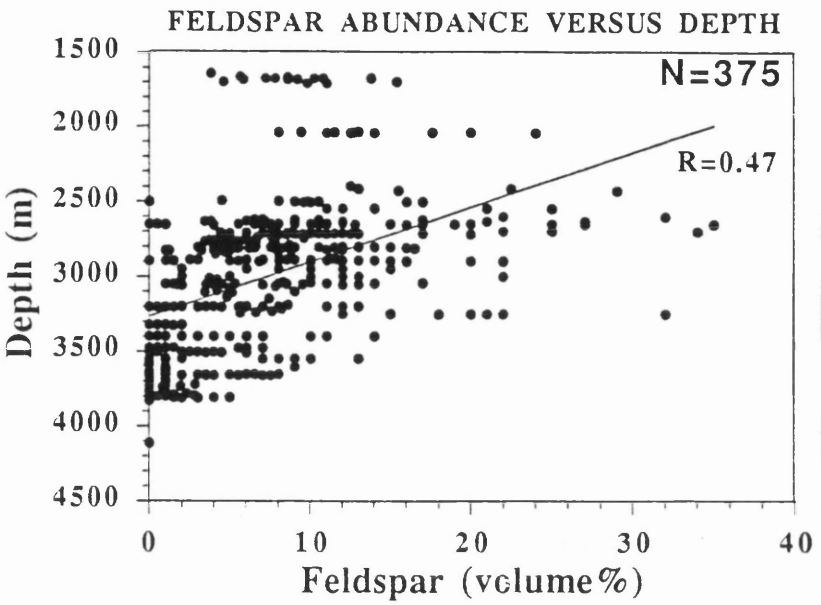

Figure 8. Variation in feldspar abundance with present day depth in the Brent Group. There is a general decline in feldspar content with increasing depth. Compilation of point count data from Brint (1989); Giles *et al.* (1992); Harris (1992), plus data of the authors from the Emerald oilfield.

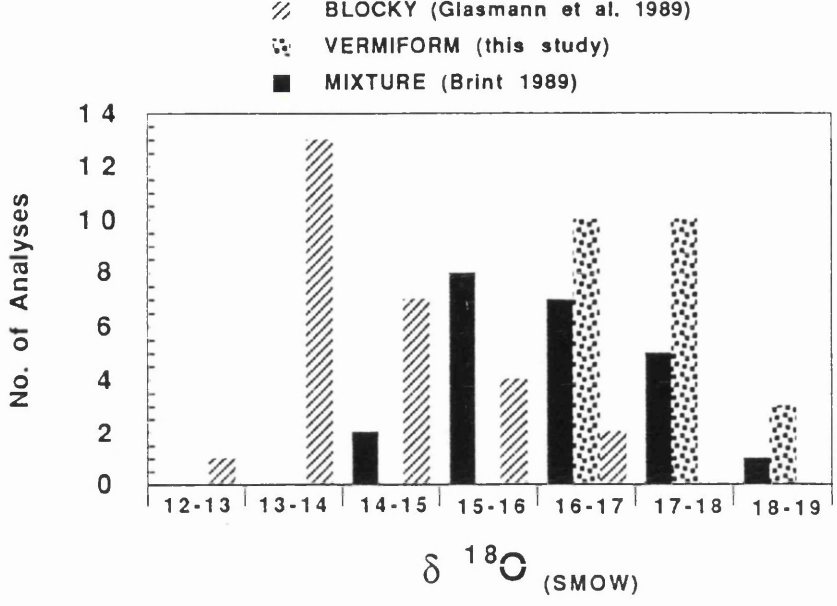

Figure 9. Histogram showing the variation in $\delta^{18}O$ of kaolinite separates with clay morphology. Blocky kaolinite has the lowest $\delta^{18}O$, while vermiform kaolinite has the highest. Mixtures of vermiform and blocky kaolinite have intermediate $\delta^{18}O$. Data from Brint (1989); Glasmann *et al.* (1989), plus unpublished data of the authors from the Emerald oilfield. Data presented in Table 2.

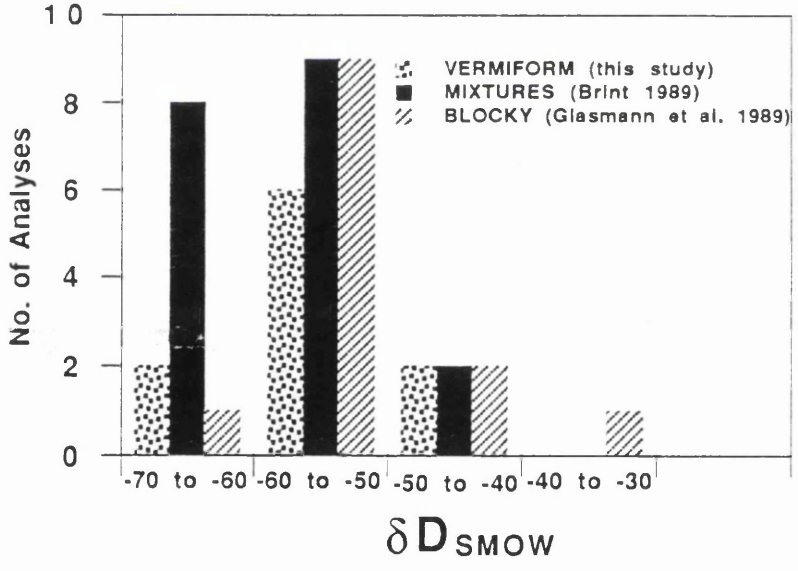

Figure 10. Histogram showing the variation in δD of kaolinite separates with clay morphology. There is no systematic variation in δD with kaolinite morphology. Data from same references as in Figure 9, and Table 2.

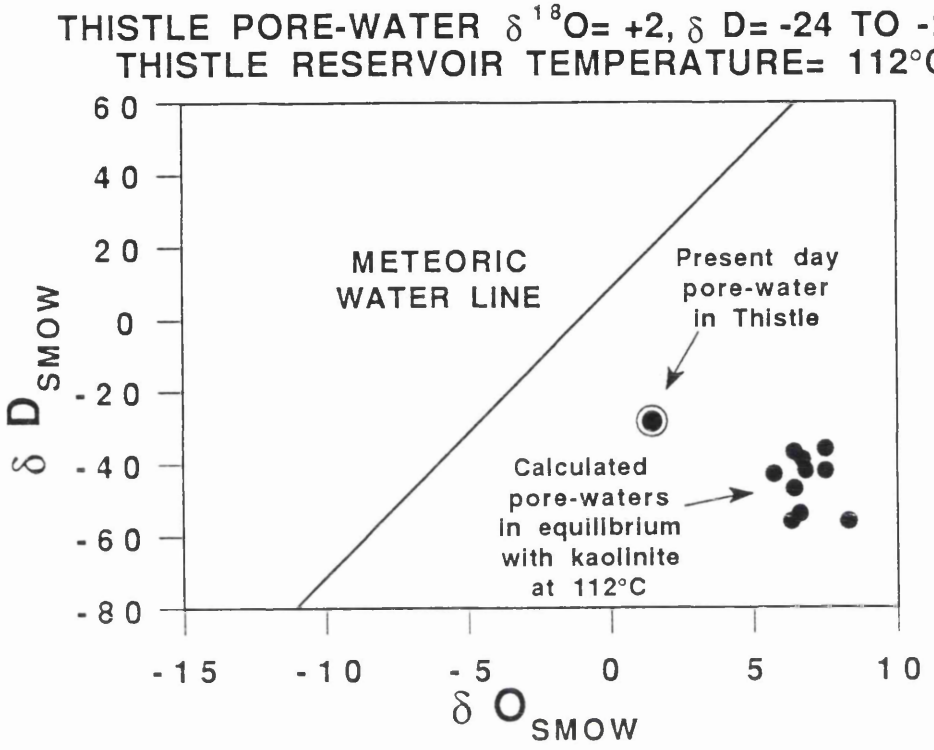

Figure 11. $\delta^{18}O$ versus δD plot showing the isotopic composition of waters that would be in isotopic equilibrium with diagenetic kaolinite in the Thistle oilfield at present day reservoir temperatures (112°C). The calculated water isotopic compositions are not the same as present day formation waters. This indicates that it is unlikely that isotopic exchange between kaolinite and formation water has occured. Kaolinite mineral values from Brint (1989), present day Thistle pore-water composition from Haszeldine *et al.* (1992). Fractionation equations used were those of Savin & Lee (1988) for oxygen and Lambert & Epstein (1980) for hydrogen.

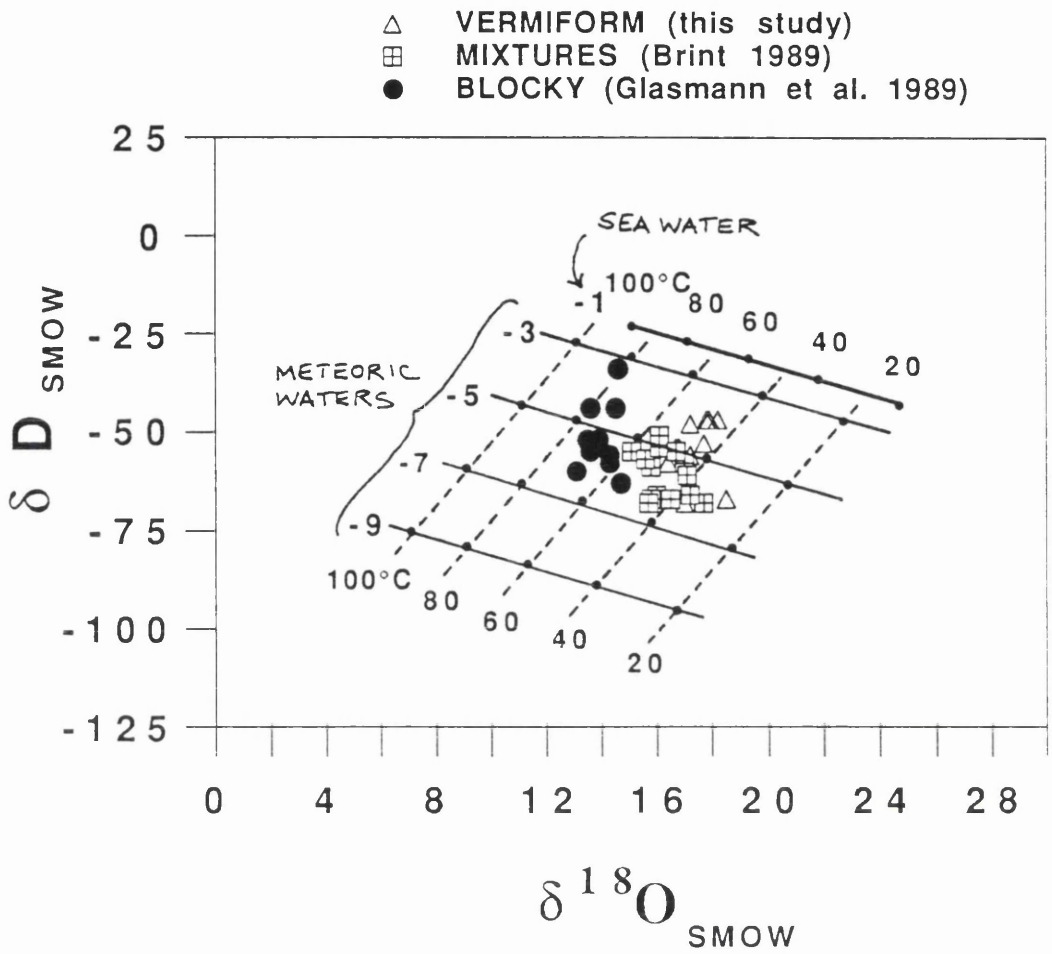

Figure 12. $\delta^{18}O$ versus δD plot showing the stable isotopic compositions of vermiform kaolinite, blocky kaolinite, and mixtures of the two types. Solid black lines represent the stable isotopic composition of kaolinite that would have precipitated from a meteoric water with a specific $\delta^{18}O$ composition ($\delta^{18}O$= -3, -5, -7, or -9‰). Broken black lines represent constant temperature. The isotopic composition of kaolinite which precipitated from ancient sea water with $\delta^{18}O$= -1‰ ; δD= -10‰ is also shown (Sheppard 1986). Both vermiform and blocky kaolinite precipitated from waters of similar isotopic composition ($\delta^{18}O$= -6.5 to -3.5‰). However vermiform kaolinite precipitated at 25-50°C and blocky kaolinite at 50-80°C. Fractionation equations used were those of Savin & Lee (1988) for oxygen, and Lambert & Epstein (1980) for hydrogen. $\delta^{18}O$ and δD compositions for meteoric waters were taken from the meteoric water line of Craig (1961).

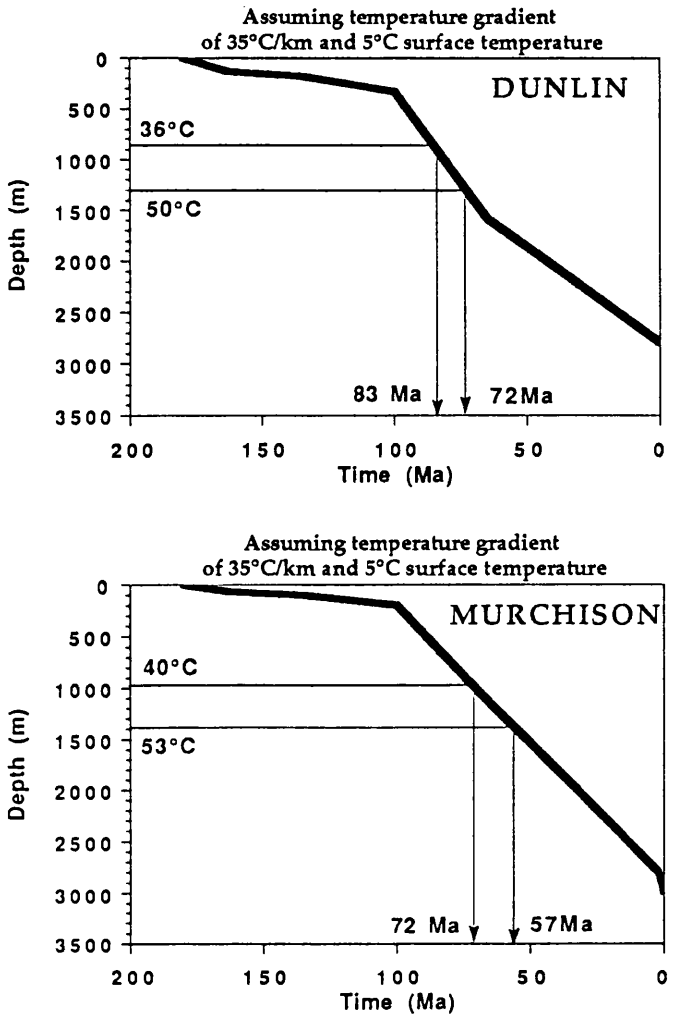

Figure 13. By combining kaolinite growth temperatures with the subsidence histories of the individual oilfields, it is possible to estimate the time at which kaolinite precipitated. Data from Table 3. Plots were constructed assuming a temperature gradient of 35°C/km and surface temperature of 5°C existed at the time of cementation. Burial curves redrawn in part from Brint (1989) and Glasmann *et al.* (1989). For further discussion see text.

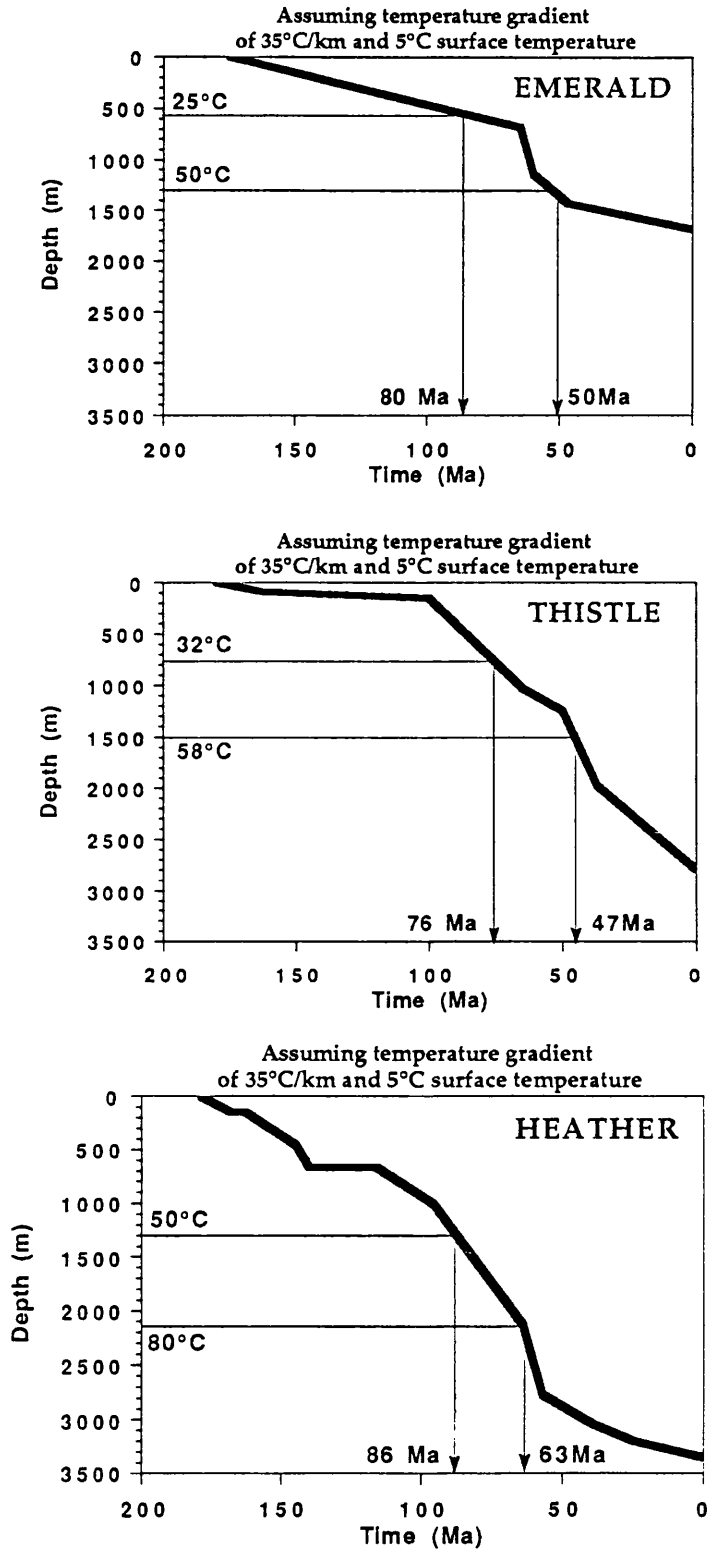

Figure 13. (continued)

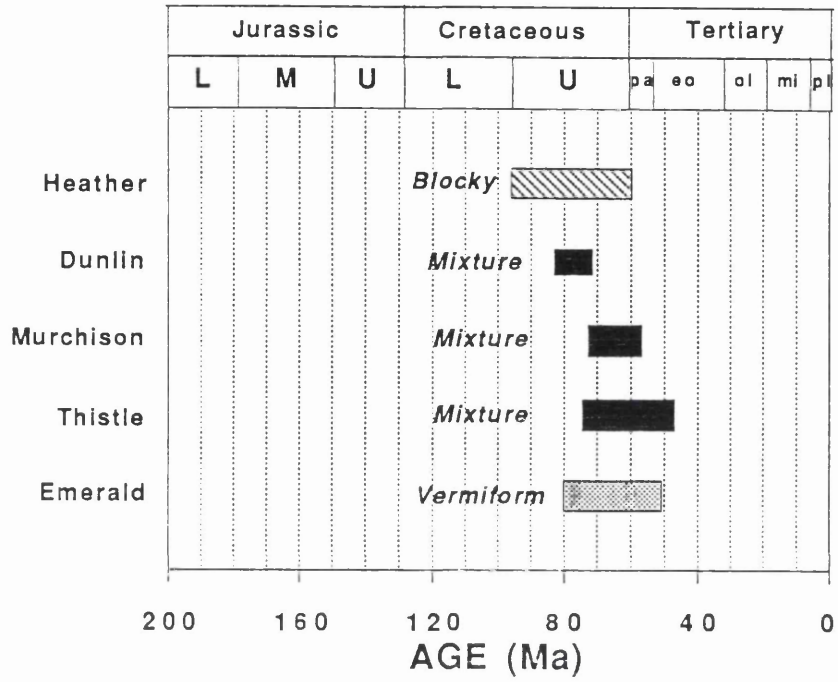

Figure 14. Plot showing the timing of kaolinite cementation in different Brent Group oilfields. Most kaolinite precipitated during the late Cretaceous to early Eocene. Data from Table 3. See text for further information.

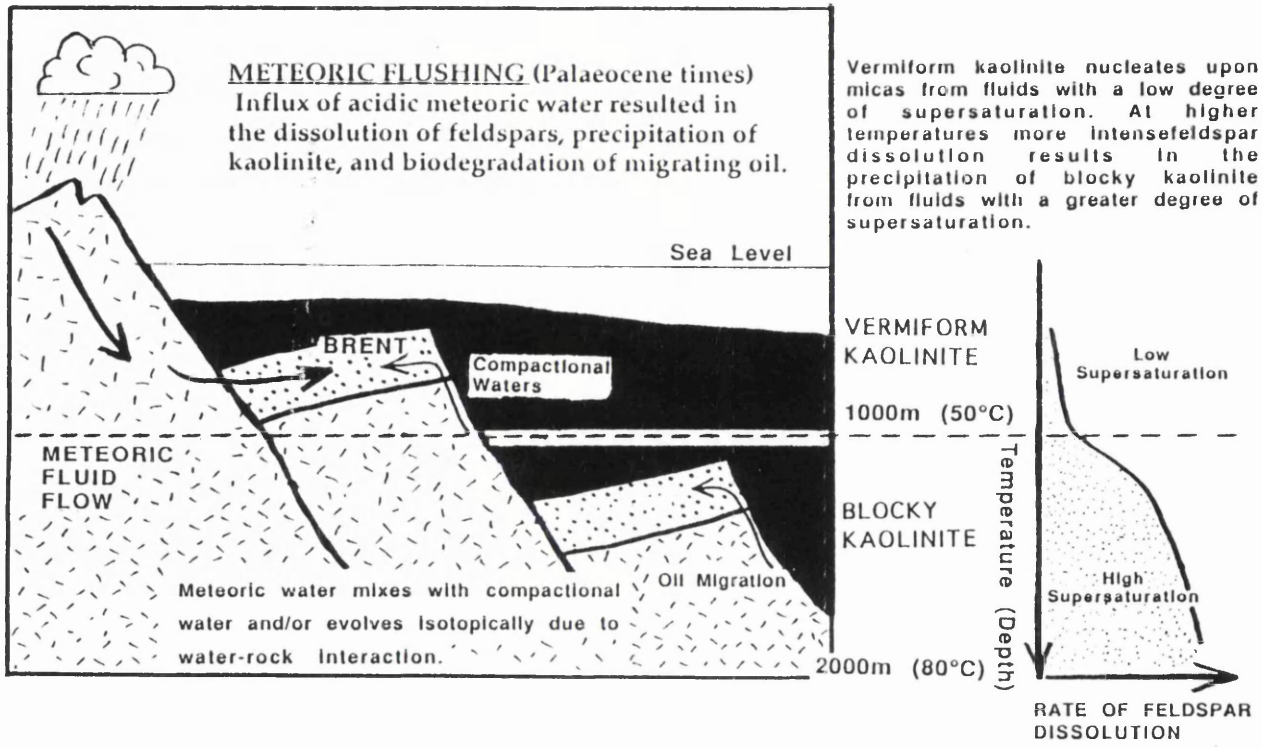

Figure 15. Schematic model for the growth of different kaolinite morphologies in the Brent Group.

Table 1. Percentage of different kaolinite morphologies present in Brent Group sandstones. Point count data, 200 points per thin section.

Depth(m)	Well	Field	%Vermiform	%Blocky	%Frayed	Mica
3130.5	211/19-3	Murchison	34	56	10	
3159.8	211/19-3	Murchison	4	92	4	
3151.2	211/19-3	Murchison	12	84	4	
3167.7	211/19-3	Murchison	18	78	4	
3100.9	211/19-4	Murchison	12	88	0	
3062.2	211/19-4	Murchison	12	86	2	
3091.8	211/19-4	Murchison	18	78	4	
3072.8	211/19-4	Murchison	12	88	0	
3055.5	211/19-4	Murchison	6	94	0	
3095.1	211/19-4	Murchison	16	54	30	
2852.1	211/19-1	Thistle	50	50	0	
2894.3	211/19-1	Thistle	32	40	28	
2853.7	211/19-1	Thistle	38	16	46	
2933.2	211/19-1	Thistle	20	64	10	
2929.3	211/19-1	Thistle	20	78	2	
2907.3	211/18-A30	Thistle	26	66	8	
2970.7	211/18-A30	Thistle	12	76	12	
2894.5	211/18-A30	Thistle	34	64	2	
2934.8	211/18-A30	Thistle	12	74	14	
2925.9	211/18-A30	Thistle	22	72	6	
3035.7	211/18-A31	Thistle	22	78	0	
3174.1	211/18-A45	Thistle	14	74	12	
4303.96	211/18-A45	Thistle	20	74	6	
4288.7	211/18-A45	Thistle	6	82	12	
3583.8	211/18-A10	Thistle	50	42	8	
3602	211/18-A10	Thistle	22	56	22	
2874.1	211/18-A07	Thistle	20	70	10	
2849.7	211/18-A07	Thistle	42	38	20	
2857.3	211/18-A07	Thistle	40	56	4	
3769.8	3/13a-1	Alwyn area	0	100	0	
3764.9	3/13a-1	Alwyn area	0	100	0	
3811.3	3/13a-1	Alwyn area	0	90	10	
1683.9	3/11b-3	Emerald	90	0	10	
1682.7	3/11b-3	Emerald	90	0	10	
1680.9	3/11b-3	Emerald	94	0	6	
1667.5	2/10-a6	Emerald	98	0	2	
1674.4	2/10-a6	Emerald	93	0	7	
1708.5	3/11b-5	Emerald	95	0	3	
1664.2	2/10-a7Z	Emerald	95	0	3	
1671	2/10-a6	Emerald	97	0	3	
1675.6	2/10-a6	Emerald	98	0	2	
1675.9	2/10-a6	Emerald	99	0	1	
1676.5	3/11b-3	Emerald	99	0	1	
1675.3	3/11b-3	Emerald	100	0	0	
1696.9	3/11b-3	Emerald	95	0	5	
1700	3/11b-5	Emerald	98	0	2	
1696.3	3/11b-5	Emerald	97	0	3	
1799.6	2/10-A7Z	Emerald	99	0	1	
2793.6	211/18-A31	Thistle	20	0	80	Concretion
2974.3	211/18-A31	Thistle	64	0	36	Concretion
2850.6	211/23-4	Dunlin	5	0	90	Concretion
2851.8	211/23-4	Dunlin	6	0	89	Concretion
2850.3	211/23-4	Dunlin	0	0	100	Concretion
1667.4	2/10-a6	Emerald	21	0	79	Concretion
1674.4	2/10-a6	Emerald	35	0	65	Concretion
1664.2	2/10-a6	Emerald	30	0	70	Concretion

Table 2. Stable isotopic data for Brent Group kaolinite

DEPTH (m)	WELL	FIELD	SIZE (μm)	$\delta^{18}O$	δD	SOURCE
1672.8	2/10-a6	Emerald	<0.5	18.2		This study
1672.8	2/10-a6	Emerald	0.5-2	16.7	-55	This study
1672.8	2/10-a6	Emerald	2-10	17.7	-53	This study
1672.8	2/10-a6	Emerald	53-64	17.8		This study
1672.8	2/10-a6	Emerald	53-64	18.3	-47	This study
1672.8	2/10-a6	Emerald	53-64	17.9		This study
1672.8	2/10-a6	Emerald	2-10	18.1		This study
1648.7	2/10-a7	Emerald	2-10	17.0	-68	This study
1638.6	2/10-a7	Emerald	<53	16.5		This study
1638.6	2/10-a7	Emerald	0.5-2	17.0		This study
1679.5	2/10-a7	Emerald	0.5-2	16.5		This study
1638.6	2/10-a7	Emerald	<0.5	17.0		This study
1638.6	2/10-a7	Emerald	2-10	17.2		This study
1679.5	2/10-a7	Emerald	<0.5	16.1	-54	This study
1638.6	2/10-a7	Emerald	2-10	16.9	-54	This study
1638.6	2/10-a7	Emerald	0.5-2	17.7		This study
1679.5	2/10-a7	Emerald	<0.5	16.3	-54	This study
1681.6	3/11-b3	Emerald	0.5-2	16.4	-58	This study
1681.6	3/11-b3	Emerald	2-10	17.2	-56	This study
1679.5	3/11-b3	Emerald	2-10	16.8		This study
1682.8	3/11-b3	Emerald	2-10	17.2	-49	This study
1681.6	3/11-b3	Emerald	64-85	18.5	-67	This study
2628	211/18-A45	Thistle	2-5	16.9	-48	Brint 1989
2630	211/18-A45	Thistle	2-5	16.0	-66	Brint 1989
2631	211/18-A45	Thistle	2-5	16.0	-66	Brint 1989
2634	211/18-A45	Thistle	2-5	16.9	-54	Brint 1989
2637	211/18-A45	Thistle	2-5	17.7	-68	Brint 1989
2793	211/18-A30	Thistle	2-5	16.2		Brint 1989
2800	211/18-A30	Thistle	2-5	16.1	-54	Brint 1989
2812	211/18-A30	Thistle	2-5	15.7		Brint 1989
2741	211/18-A31	Thistle	2-5	15.8	-59	Brint 1989
2756	211/18-A31	Thistle	2-5	15.8	-49	Brint 1989
2765	211/18-A31	Thistle	2-5	16.9		Brint 1989
2768	211/18-A31	Thistle	2-5	15.1	-55	Brint 1989
3012	211/19-4	Murchison	2-5	17.1	-61	Brint 1989
3038	211/19-4	Murchison	2-5	18.3		Brint 1989
3048	211/19-4	Murchison	2-5	17.0	-58	Brint 1989
3056	211/19-4	Murchison	2-5	16.7	-55	Brint 1989
3187	211/19-6	Murchison	2-5	14.7	-63	Brint 1989
3228	211/19-6	Murchison	2-5	14.9		Brint 1989
2875	211/23-2	Dunlin	2-5	15.6	-57	Brint 1989
2880	211/23-2	Dunlin	2-5	16.1	-54	Brint 1989
2884	211/23-2	Dunlin	2-5	16.7		Brint 1989
2711	211/12-3	Dunlin	2-5	15.8	-67	Brint 1989
2757	211/12-3	Dunlin	2-5	16.5		Brint 1989
2761	211/12-3	Dunlin	2-5	17.2		Brint 1989
2765	211/23-4	Dunlin	2-5	16.7	-67	Brint 1989
2831	211/23-4	Dunlin	2-5	18.3	-58	Brint 1989
2838	211/23-4	Dunlin	2-5	17.2	-66	Brint 1989
3720	3/13a-1		2-5	15.7		Brint 1989
3353.1	2/5-3	Heather	2-10	13.5	-52	Glasmann et al. 1989
3363.5	2/5-3	Heather	2-10	13.5		Glasmann et al. 1989
3373.6	2/5-3	Heather	2-15	14.1		Glasmann et al. 1989
3388.3	2/5-3	Heather	0.5-2	14.2		Glasmann et al. 1989
3388.7	2/5-3	Heather	2-15	13.5		Glasmann et al. 1989
3417.3	2/5-3	Heather	2-15	12.3		Glasmann et al. 1989
3421.4	2/5-3	Heather	2-15	13.2		Glasmann et al. 1989
2962.7	2/5-4	Heather	2-15	13.9	-52	Glasmann et al. 1989
3325.9	2/5-9	Heather	2-15	14.6	-34	Glasmann et al. 1989
3325.9	2/5-9	Heather	10-20	14.5	-44	Glasmann et al. 1989
2891.5	2/5-8B	Heather	2-15	16.4		Glasmann et al. 1989
2891.5	2/5-8B	Heather	0.2-0.5	15.0		Glasmann et al. 1989
2891.5	2/5-8B	Heather	0.1-0.2	15.5		Glasmann et al. 1989
2894.2	2/5-8B	Heather	2-15	15.6		Glasmann et al. 1989
2910.9	2/5-8B	Heather	2-15	15.5		Glasmann et al. 1989
2910.9	2/5-8B	Heather	0.2-0.5	16.5		Glasmann et al. 1989
3569.6	2/5-12A	Heather	2-15	13.6	-44	Glasmann et al. 1989
3581.9	2/5-12A	Heather	2-15	13.1	-60	Glasmann et al. 1989
3590	2/5-12A	Heather	2-15	13.6	-54	Glasmann et al. 1989
3619.8	2/5-H4	Heather	2-15	13.7	-54	Glasmann et al. 1989
3621.3	2/5-H4	Heather	2-15	13.5		Glasmann et al. 1989
3625.4	2/5-H4	Heather	2-15	13.6	-53	Glasmann et al. 1989
3646.2	2/5-H4	Heather	2-15	13.6	-55	Glasmann et al. 1989
3648	2/5-H4	Heather	2-15	14.1		Glasmann et al. 1989
3654.6	2/5-H4	Heather	2-15	14.3	-56	Glasmann et al. 1989
4323.9	2/5-H34	Heather	2-15	14.3	-58	Glasmann et al. 1989

Table 3. Temperature and timing of kaolinite precipitation in Brent Group oilfields.

Field	Growth Temp. (°C)	Timing (Ma)	Depth of Cementation (m)	Kaolinite Type
Emerald	25-50	50-80	571-1286	Vermiform
Thistle	32-58	47-76	771-1514	Mixture
Murchison	40-53	57-72	1000-1371	Mixture
Dunlin	36-50	72-83	886-1286	Mixture
Heather	50-80	63-86	1286-2143	Blocky

CHAPTER 5

EVIDENCE FOR RESETTING OF FLUID INCLUSION TEMPERATURES FROM QUARTZ CEMENTS IN OILFIELDS

Mark Osborne, and R. Stuart Haszeldine
Department of Geology & Applied Geology, Glasgow University, Glasgow, G12 8QQ, Scotland.

5.1 ABSTRACT

Quartz is a major pore-occluding cement in North Sea oilfield reservoir sandstones. Fluid inclusions yield homogenisation temperatures (Th) which have been thought to represent growth temperatures for the host quartz. However, early diagenetic inclusions from the detrital grain-overgrowth boundary yield excessively high palaeotemperatures which do not match the growth temperatures calculated from the depth of cementation. The temperatures of these inclusions increase with present day depth of burial, and approach present day reservoir temperatures. This suggests that the inclusions have begun to reset towards present day P-T conditions. The Th of the inclusions hence represent burial temperatures rather than growth temperatures for the quartz. Experimental studies indicate that the amount of resetting undergone by an inclusion varies depending upon its size, shape, and fluid composition. A relationship between inclusion Th and the above variables has been observed in inclusions from deeply buried quartz cements in the North Sea.

5.2 INTRODUCTION

Fluid inclusion studies of authigenic minerals have been widely used in attempts to understand the diagenetic history of sedimentary rocks (Roedder 1979; Burruss 1981; Haszeldine *et al.* 1984, 1992; Burley *et al.* 1989; Barker & Goldstein 1991). Primary inclusions, when subjected to microthermometry and UV-light microscopy, are thought to yield information on the growth temperature of a diagenetic mineral, together with the salinity, composition, and presence of hydrocarbons within diagenetic palaeofluids.

A major problem in such studies has been that resetting (re-equilibration), of fluid inclusion homogenisation temperatures (Th) can

occur when the host mineral is subjected to temperatures and pressures higher than those at which it initially formed. This has been shown to be particularly important in carbonates and other cleaved minerals (Burruss 1987; Goldstein 1986; Bodnar & Bethke 1984; Barker& Goldstein 1991). Hence upon deeper burial inclusions may be reset so that T_h measured becomes representative of burial temperatures rather than growth temperatures. Our paper attempts to assess whether or not fluid inclusions from quartz cements in the Brent Group of the North Sea show evidence of resetting.

5.3 TECHNIQUES USED

For fluid inclusion studies measurements were made on a Linkam TH 600 heating/freezing stage used in conjunction with a Leitz-Dialux 20-EB binocular microscope. Doubly polished wafers of sandstones 40-100μm thick were prepared using the method of Crosbie (1981). Fluid inclusions within quartz overgrowths were subjected to heating and freezing experiments. The stage was calibrated using standard compounds of a known melting point. Fluid inclusion volumes were calculated using the method of Bodnar (1983), and shape factors assigned to the inclusions using the methodology of Bodnar *et al.* (1989).

5.4 FIELD DATA

The data used in this study comes from 14 different North Sea oilfields, the majority of which lie in the East Shetland Basin and the Viking Graben (see Glennie 1990, for a summary of the geology). Sample points span a depth range of 1676-4450m. Most data come from quartz cemented sandstones in the deltaic and shallow marine Middle Jurassic Brent Group, or laterally equivalent facies in the Norwegian North Sea. The remaining data is from Upper Jurassic North Sea submarine fan sandstones. The present day depth of the samples in all cases is thought to represent the maximum depth of burial. A "pressure correction" has not been applied to any of the inclusion data because Raman probe analyses of oilfield fluid inclusions show appreciable methane to be present (Malley *et al.* 1986). Thus a temperature correction to obtain a trapping temperature hotter than the T_h is not advisable (Hanor 1980).

5.5 QUARTZ CEMENTS & THEIR FLUID INCLUSIONS

Quartz overgrowths are a major pore-occluding cement in Brent Group reservoir sandstones. From Figure 1 it can be seen that the volume of quartz cement present in the Formations of the Brent Group increases with present day depth of burial. Only minor amounts of quartz cement occur at less than 9000ft (2700m) burial, while deeper than 9000ft there is a clear trend of increasing volumes of quartz cement with depth. There are no systematic variations in the volume of quartz cement between facies, therefore quartz overgrowth development seems to be depth (i.e. temperature) related.

At depths of <2.0km, quartz overgrowths are generally thin (50μm thick) and irregular and appearance (Figure 2a). Numerous tiny subhedral-euhedral crystals of quartz are observed adhering to the surface of the detrital grain (Figure 2b). Fluid is trapped in the numerous cavities which exist between these crystals, and so fluid inclusions are formed. With deeper burial, these early microcrystalline aggregates would become enveloped by later, more extensive, euhedral overgrowths, with a low microporosity. This observation explains why most fluid inclusions in the Brent Group are trapped close to the surface of the detrital grain, while relatively few occur further out in the overgrowth itself. This means that the majority of fluid inclusions in the Brent Group are early diagenetic in origin, as they are trapped within the first stages of quartz overgrowth.

At depths >3.0km quartz overgrowths are generally thick and euhedral, and single, optically continuous prisms are sometimes observed to envelop detrital grains (Figure 3a&b). Fluid inclusions are largely confined to the grain-overgrowth boundary, or to fractures within the detrital grain (Figure 3c). However a few inclusions, some hydrocarbon bearing, are found within the overgrowth itself.

Euhedral, tiny crystals of microquartz are occasionally observed to infill the secondary porosity created by feldspar dissolution (Figure 4a) Quartz overgrowths are observed to envelop blocky kaolinite and illite. This suggests that the later stages of quartz cementation post-dated or coincided with kaolinite and illite precipitation (Figure 4b). As the outer zones of some quartz overgrowths contain hydrocarbon inclusions, we can deduce that the later stages of quartz cementation were occurring at the same time as oil was migrating.

5.6 EVIDENCE FOR RESETTING FROM FIELD DATA

1. In many instances the onset of quartz cementation in the sandstones is thought to have been relatively early diagenetic event, commencing at 1800-2000m at temperatures of about 70°C (Giles *et al.* 1992, Hogg *et al.* 1992). However quartz cements are found within early diagenetic calcite doggers (Harris 1992), and 1-2% quartz cement is present in the shallow buried Emerald oilfield (1600m), suggesting that cementation may have began even earlier. The majority of fluid inclusions in oilfield sandstones are preserved at the overgrowth-detrital grain boundary, therefore they were also trapped diagenetically early and should thus yield relatively low homogenisation temperatures (from 60-80°C upwards). However the homogenisation temperatures obtained from inclusions in North Sea authigenic quartz are much higher (from 80-140°C, e.g. Figure 5).

2. Inclusions from diagenetic quartz inside calcite concretions (i.e. quartz which predated a texturally early calcite cement), yield similar homogenisation temperatures to diagenetic quartz cements outside concretions (Walderhaug 1990). If no resetting had occurred then the quartz cement outside the concretions would have yielded hotter growth temperatures.

3. In histograms of fluid inclusion populations there is usually an asymmetry present in the inclusion distribution pattern, the histogram often possessing a high temperature "tail". Furthermore a very wide spread in T_h values is seen if a large number of measurements (>100) are taken from one sample at a single depth (Figure 5; Table 1). We suggest that both features could be caused by resetting of inclusions to higher temperatures. Similar wide variations in T_h values are observed in reset fluid inclusion populations from carbonates (Goldstein 1986).

4. Scatter plots of maximum, modal, and minimum T_h show a correlation of increasing T_h with present day depth, using all available North Sea data (Figure 6; Table 2). A similar trend of increasing T_h with maximum palaeotemperature has been seen in fluid inclusions from carbonates by Barker & Goldstein (1991), which they likewise attribute to resetting. As well as occuring on a basin wide scale, an increase of T_h with depth has also been observed within individual oilfields such as Tartan

(Burley *et al.* 1989). This is what would be expected if resetting is indeed a pervasive phenomenon.

5. The amount of resetting undergone by a fluid inclusion has been shown experimentally to be partly dependent upon its size (Roedder & Skinner 1968; Leroy 1979; Bodnar & Bethke 1984; Bodnar *et al.* 1989). Inclusions which are small are more resistant to resetting than those which are large. Thus in a reset fluid inclusion population large inclusions should yield higher T_h than small inclusions. This has been observed in a deeply buried sample from the South Brae oilfield (Figure 7; Table 3). The location and general appearance of these inclusions is shown in Figure 8.

6. Resetting has been found experimentally to be partly dependent upon inclusion shape (Leroy 1979; Bodnar & Bethke 1984; Bodnar *et al.* 1989). Irregularly shaped inclusions could thus be reset to greater extent, and hence yield higher T_h, than regular inclusions. This has likewise been observed in a fluid inclusion population from the South Brae oilfield (Figure 9; Table 3).

5.7 DISCUSSION

In the Brent Group most inclusions are trapped close to the boundary between the detrital grain and the overgrowth, or within healed fissures in the grain (Figure 10). A few late diagenetic inclusions occur further out into the overgrowth itself. This means that most inclusions are early diagenetic in origin and should therefore be preserving relatively low temperatures. However from Figure 6 we can see that minimum T_h records increases with depth of burial. The fact that early diagenetic inclusions from deeply buried samples do not yield low temperatures is highly suspicious, suggesting at least some resetting has occurred. Because some inclusions were trapped during late diagenesis we would certainly expect some of the inclusions to yield higher temperatures indicating entrapment during deep burial conditions, but because these are relatively scarce they should not predominate in any sample studied. It is thus likely that the temperatures obtained from deeply buried fluid inclusions will be derived mainly from reset early diagenetic inclusions. However it appears

that the Th yielded by such inclusions represents burial temperatures rather than genuine growth temperatures for the host quartz.

In Figure 11 we have plotted Th versus present day Formation temperatures for the small number of samples where we have both types of information. At low temperatures modal Th is similar to Formation temperatures. At higher temperatures the fit between modal temperatures and Formation temperatures is less good, though most modes come within 20°C of the maximum burial temperature. When fluid inclusions in carbonates are reset the modal Th of the population closely approaches the maximum burial temperature obtained (Barker & Goldstein 1991). However, as can be seen from Figure 11, modal Th of fluid inclusions in quartz approach, and do not exactly coincide with, Formation temperatures. This is to be expected for although experimental studies of carbonates have shown that overheating causes the mean or modal Th of an inclusion to approach maximum temperature attained (Prezbindowski & Larese 1987), other studies indicate that not every fluid inclusion in a sample resets to the peak burial temperature (Goldstein 1986;1988;1990). Thus although the Th of many fluid inclusions may increase, they may not increase sufficiently to coincide with Formation temperatures. The confining strength of the mineral has an important effect, for although fluid inclusions will be reset when the internal pressure exceeds the external pressure during burial, resetting will cease when the internal pressure equals the external pressure *plus the strength of the mineral.* (Bodnar & Burruss 1991). Quartz has a greater confining strength than cleaved and less competent carbonate minerals, so we would not necessarily expect modal Th of reset fluid inclusions in quartz to exactly match Formation temperatures.

Furthermore experimental studies have shown that fluid inclusions in quartz take a finite time to reset when P-T conditions are changed (Gratier & Jennaton 1984; Sterner & Bodnar 1989), whereas fluid inclusions in calcite are thought to reset more or less instantaneously. Thus the discrepancy between modal Th and formation temperature can be explained if the inclusions have not yet had sufficient time to re-equilibrate with todays P-T conditions, due to rapid subsidence. This time lag effect is discussed in detail in Haszeldine & Osborne (1993).

5.7.1 Resetting mechanism

The data we have compiled does not permit us to rigorously demonstrate the exact process whereby inclusions in authigenic quartz are reset. However, the number of possible mechanisms is very small, and from these we can deduce what must be the most likely cause of resetting during burial diagenesis.

The basic situation producing resetting is outlined in Figure 12. Deep burial of the rock increases the P and T of pore fluids along a pressure gradient (100bars/km, 35°C/km). At the same time the internal P and T of an inclusion increases along an isochore, a line of constant volume. The position and slope of this isochore varies depending upon the salinity and Th of the inclusion. In the example given an inclusion with Th of 75°C and salinity of 1Wt% is trapped at 112°C and 3.2 km depth. If the rock has increased in temperature by 48°C due to an additional 1.4 km of subsidence, then for the PVT isochore relationship, this inclusion will have an increase of internal pressure of 500 bars (50 MPa) relative to external pore fluid pressures. This increase in internal pressure can cause an inclusion to be reset in two different ways.

1. Plastic deformation or stretching (Bodnar & Bethke 1984).

2. Brittle deformation or decrepitation (Roedder 1984).

An important difference between the two processes is that decrepitation can produce microfractures which reach the grain boundary of the overgrowth. Thus decrepitated inclusions can exchange fluids with their external environment, resetting temperature, pressure and chemical composition of the aqueous contents.

Many workers (e.g. Leroy 1979) have measured the overpressure required to produce total decrepitation of fluid inclusions in quartz. The values differ depending on the size and shape of the inclusion as large, irregularly shaped inclusions are more susceptible to decrepitation than small spherical inclusions. The general overpressure value is between 850 and 1000 bars, but for small inclusions is greater than 2500 bars. Such internal pressures will not be generated within the realm of burial diagenesis, and so decrepitation is an unlikely mechanism for resetting of fluid inclusions in quartz cements.

In another experimental study of quartz Bodnar *et al.* (1989) discovered that substantial numbers of inclusions deformed by stretching rather than decrepitation. Stretching behaviour was confined to small inclusions (<6mm), similar in size to those r in authigenic quartz. In this experiment inclusions were incrementally overheated in order to raise their internal pressures gradually. Increase in the Th of inclusions was observed to occur before total decrepitation was produced. This increase in Th must have been produced by stretching or partial decrepitation. Thus resetting can occur for lower values of overpressure than those required to fully decrepitate the inclusion. They also managed to reset the Th of 20% of the inclusions by as much as 30°C for overpressure values of only 400 bars. Overpressures of this magnitude could easily be produced during deep burial of inclusion bearing cements, making stretching the most likely method of resetting in authigenic quartz.

Although only about 20% of inclusions were succesfully reset in the above experiment, this does not prove that the remaining inclusions would always be resistant to the resetting process. This is because resetting of fluid inclusions in quartz has also been found to be time dependent. Sterner and Bodnar (1989) discovered that once the resetting process begins, fluid inclusions come closer to re-equilibration with the new P-T conditions with increasing time. Furthermore stretching and change in the shape of an inclusion is likely to be a kinetically governed process (Gratier & Jennaton 1984), and will therefore proceed only very slowly at low temperatures and pressures. All the experimental studies have a duration of a few years at most, but in a geological situation there are often tens of millions of years available for resetting to proceed. Thus the experimental data does not rule out the possibility that fluid inclusions in quartz could reset slowly, over long periods of time, for relatively low values of overpressure.

A further objection to the usefulness of overpressure data derived by experiment is the fact that experimental conditions rarely conform to those existing in nature. Hydrothermally grown single crystals of synthetic quartz are used in such experiments because they have few structural defects and are free of microcracks, which can facilitate brittle failure. However in nature most fluid inclusions in quartz form at the junction between detrital grain and overgrowth, where two overgrowths conjoin, or within healed microfissures (Burley *et al.* 1989). Overgrowths themselves are not structurally homogenous but are formed from a

number of crystal subunits (Pittman 1972). Thus in quartz overgrowths, fluid inclusions are often trapped along boundaries which are planes of weakness, rich in structural discontinuities. Because of the existence of such structural weaknesses fluid inclusions in quartz overgrowths may be *even more* susceptible to stretching and even to decrepitation than the experimental data would indicate. Resetting could thus occur for lower values of overpressure than those published in the literature.

5.7.2 Fluid inclusion salinities

The Brent Group data (Figure 13; Table 4) shows that most inclusions are only slightly saline, as 93% of the inclusions have salinities of <5Wt% NaCl equivalent, while some salinities are as low as 0.5Wt%, indicating fresh water. The preponderance of brackish water inclusions suggests that evaporitic brines, ascending from deep in the basin, were not of major importance in quartz precipitation. Some of the more saline inclusions could represent partial mixing of palaeo-meteoric water with compactional brines, or they could indicate that the fluid compartment was connected to Triassic evaporites. In any case these high salinity inclusions form only a very small part of the total population.

There is a tendency for higher salinity inclusions to have lower T_h than inclusions which are only slightly saline (Figure 13). This is the opposite of what might be expected, for as depth of burial increases we would expect the T_h of inclusions in succesive generations of quartz overgrowth become gradually hotter. Inclusion salinities should also increase with depth in sedimentary basins, as depositional meteoric pore fluids are replaced by hot brines expelled from compacting sediments.

The fact that the high salinity inclusions have lower T_h than low salinity inclusions can be explained if the former have been less susceptible to resetting. Potter & Brown (1977) have remarked that aqueous inclusions with salinities up to halite saturation are more compressible than pure water in the temperature range of diagenesis. This implies that the higher the salinity of the inclusion the more compressible are its contents. Upon deep burial, high salinity inclusions will develop smaller internal overpressures than than low salinity inclusions (Burruss 1987), and thus be less susceptible to resetting. Resetting of aqueous inclusions is thus dependent upon the salinity of the contents; the lower the salinity the greater the amount of resetting.

If resetting of inclusions in quartz was accomplished by decrepitation as well as by stretching, then the inclusion contents would be able to exchange fluid with their external environment. As pore water salinity generally increases with depth of burial, decrepitated inclusions would potentially show an increase in salinity with rising homogenisation temperature (redrawn from Reynolds *et al.* 1990) (Figure 14). We certainly do not see this trend from inclusions in authigenic quartz, which supports the hypothesis that resetting occurs predominantly by stretching. Indeed many of the highest temperature inclusions in the Brent Group have relatively low salinities. If the inclusions have only been stretched they will have retained their original salinities. This means they will still provide useful information on the composition of ancient pore fluids.

5.7.3 Petroleum inclusions

Late diagenetic inclusions in the Brent Group sometimes contain hydrocarbons, indicating that oil migration was occurring at the same time as the later stages of quartz cementation. It has been pointed out by Burruss (1987) that resetting should be less common in petroleum inclusions compared to aqueous inclusions because hydrocarbon bearing fluids are generally far more compressible than water. It is interesting to note in this respect that hydrocarbon bearing inclusions often yield lower homogenisation temperatures than aqueous inclusions which were trapped simultaneously (Burruss 1981). Admittedly hydrocarbon and aqueous inclusions which were originally trapped at the same P and T may yield slightly different Th because the PVT properties of the two fluids are different. However, if resetting of aqueous inclusions has indeed occured, then it is very likely that part of the discrepancy in Th between aqueous and petroleum inclusions is also a product of resetting.

The fact that petroleum inclusions from quartz in the Brent Group yield lower temperatures (Th 55-95°C) than aqueous inclusions (Th 95-135°C) (Malley *et al.* 1986) can thus potentially be explained if the petroleum inclusions have undergone little or no resetting. Thus in overgrowths which contain both petroleum and aqueous inclusions the former may yield approximate temperatures for cementation, while the latter, due to greater amounts of resetting, record only burial temperatures.

It is often difficult to ascertain the true trapping temperatures of such petroleum inclusions due to a lack of knowledge about the exact

composition and PVT properties of the fluid involved. However if these can be calculated using data from fluid inclusion extracts or reservoired oils then meaningful minimum temperatures for quartz formation could possibly be obtained. Temperature data from petroleum fluid inclusions should be used with caution because during burial heating hydrocarbon cracking or bitumen precipitation could occur within the inclusions, limiting their usefulness. However research using petroleum inclusions is still in its infancy, so it is premature to condemn them.

5.7.4 Recognition of resetting

The main implication of resetting is that homogenisation temperatures for fluid inclusions are not necessarily an accurate record of the growth temperature for the host quartz if the cement has been deeply buried. Uncritical acceptance of reset fluid inclusion data is only likely to lead to erroneous interpretation.

Of the minerals barite, calcite, fluorite, sphalerite and quartz commonly used in fluid inclusion studies, quartz is thought to be the most reliable (Ulrich & Bodnar 1988). We surmise however, from the fluid inclusion data we have examined, that fluid inclusions in authigenic quartz are continually resetting as the mineral subsides. This means that maximum, modal and minimum T_h gradually increase with depth of burial. Conversely, many other researchers have regarded T_h as a valid estimate of growth temperature for the host quartz. This has led to the suggestion that quartz precipitated from fluids which were hotter than the calculated geothermal gradient, and that ascending, hot, basinal, brines must have been responsible for the mineralising event (Haszeldine *et al.* 1984a,b; Jourdan *et al.* 1987; Burley *et al.* 1989).

However in the most detailed of these studies, that of the Tartan reservoir (Burley *et al.* 1989), inclusion T_h is observed to increase systematically with depth of burial. Inclusion temperatures define an apparent geothermal gradient of 34°C/km, similar to that of the present day, and the hottest fluid inclusions come within 10°C of Formation temperatures. Furthermore, at any one depth, higher salinity inclusions yield lower T_h than inclusions which are less saline. As has been discussed earlier, these observations can all be explained by the resetting hypothesis. If inclusion T_h has been reset to higher temperatures, then influx of hot

fluids from depth is not required in order to explain the fluid inclusion data.

Our examination of data from the North Sea suggests that there are a number of observations which can be consistently explained by the resetting hypothesis. If a large number of these features is present within a fluid inclusion population, then it is wise to consider the possibility that the inclusions have been reset.

The most striking piece of evidence is the trend showing increase in Th min., Th mode , and Th max. with maximum depth of burial (Figure 6). Modal Th is seen to approach present day burial temperatures (Figure 11). When resetting has occurred hydrocarbon inclusions may have lower Th than saline inclusions, and there may also be a decrease in the Th of aqueous inclusions with increasing salinity (Figure 13). Large inclusions may yield higher Th than small inclusions. A distinct asymmetry in the fluid inclusion histogram may be present. A wide spread in Th within a population from a single depth will also be observed (Figure 5). In addition, there is unlikely to be any temperature zonation of inclusions across the overgrowth, *unless* the inclusions have widely differing salinities.

Because experimental studies have shown that resetting of an inclusion is dependent upon its size, shape, composition, and location (Leroy 1979; Bodnar & Bethke 1984), great discrimination must be exercised in selecting inclusions for microthermometry. We recommend that where the object of the study is to obtain growth temperatures, measurements should be restricted to highly saline aqueous inclusions which occur within the overgrowth itself, and do not lie along structural boundaries. Small, primary, spherical inclusions should be measured in preference to those which are large and irregularly shaped. Hydrocarbon inclusions are potentially the most useful in diagenetic studies, if the size of the "pressure correction" can be accurately assessed. By examining *all* the fluid inclusion types occuring in a sample it is possible to obtain information on both growth *and* burial temperatures, along with compositional data on the evolution of diagenetic pore fluids through time.

5.8 CONCLUSIONS

1. Fluid inclusions in authigenic quartz are continually being reset as the mineral subsides, perhaps due to stretching of the inclusion. This means that maximum, modal and minimum T_h gradually increase with depth of burial.

2. Hydrocarbon inclusions have undergone smaller amounts of resetting, and may yield accurate growth temperatures, if the PVT properties of the fluid can be ascertained.

3. Aqueous inclusions have usually been reset and record only burial temperatures. The higher the original salinity of an inclusion, the less susceptible it is to resetting. It should still be possible to determine original salinity variations between inclusion populations.

4. Inclusions may have been reset by varying amounts depending upon their size and shape. Large and irregularly shaped inclusions are the most susceptible to resetting.

5.9 ACKNOWLEDGEMENTS

Ian Samson is thanked for pointing out the relevance of Bodnar's work to our own, while Melvyn Giles (Shell Research) gave helpful and constructive reviews of an earlier draft of this paper. Mark Osborne gratefully acknowledges the receipt of NERC grant GT4\89\GS\044.

5.10 REFERENCES

Barker, C.E., and Goldstein, R. H.,1991, A fluid inclusion technique for determining maximum temperature in calcite and its comparison to the vitrinite reflectance geothermometer: *Geology*, 18, p.1003-1006.

Bodnar, R. J., 1983, A method of calculating fluid inclusion volumes based on vapour bubble diameters and PVTX properties of inclusion fluids *Econ. Geol.*, 78, p. 535-542.

Bodnar, R. J., and Bethke, P. M.,1984, Systematics of stretching in fluid inclusions I: fluorite and sphalerite at 1 atmosphere confining pressure: *Econ. Geol.*, 79, p. 141-161.

Bodnar, R. J., Binns, P. R., and Hall, D. L., 1989, Synthetic fluid inclusions-VI Quantitative evaluation of the decrepitation behaviour of fluid inclusions in quartz at one atmosphere confining pressure *J. Metamorphic Geol.*, 7, p. 229-242.

Bodnar, R. J., and Burruss, R. C., 1991, Comment and Reply on Fluid-inclusion technique for determining maximum temperature in calcite and its comparison to the vitrinite reflectance geothermometer *Geology* 19 p. 1241-1242

Brint, J. F.,1989,Isotope diagenesis and palaeofluid movement: Middle Jurassic Brent sandstones, North Sea *D. Phil. Thesis* University of Strathclyde, Scotland, 288 p.

Burley, S. D., Mullis, J., and Matter, A.,1989, Timing diagenesis in the Tartan reservoir (UK North Sea) constraints from combined cathodoluminescence microscopy and fluid inclusion studies: *Mar.and Petrol. Geol* 6, p. 98-120.

Burruss, R. C.,1981, Hydrocarbon fluid inclusions in studies of sedimentary diagenesis *in Mineralogical Association of Canada, short course in fluid inclusions; applications to petrology*, Hollister, L. S. , and Crawford, M. L., eds. , p. 138-156.

Burruss, R. C.,1987, Diagenetic paleotemperatures from aqueous fluid inclusions reequilibration of inclusions in carbonate cements by burial heating: *Mineral. Mag.*, 51, p. 477-481.

Crosbie, T., 1981, Polished wafer preparation for fluid inclusion and other studies: *Trans. Inst. Min. & Metal.*, 90, p.82-83.

Ehrenberg, S. N., 1990, Relationship between diagenesis and reservoir quality in sandstones of the Garn Formation, Haltenbanken, Mid Norwegian Continental Shelf *Am. Assoc. Petrol. Geol. Bull*, 74, p. 1538-1558.

Giles, M.R., Stevenson, S., Martin, S. V., Cannon, S. J. C., Hamilton, P. J., Marshall, J. D., & Samways, G. M., 1992, The reservoir properties and diagenesis of the Brent Group; a regional perspective. In Morton, A. C., Haszeldine, R. S., Giles, M. R., & Brown, S., (Eds), *Geology of the Brent Group*. Geological Society of London, Bath UK. p. 289-327.

Glasmann, J. R., Lundegard, P. D., Clark, R. A., Penny, B. K., Collins, I. D., 1989 a, Geochemical evidence for the history of diagenesis and fluid

migration: Brent sandstone, Heather field, North Sea *Clay Minerals*, 24, p. 255-284.

Glasmann, J. R., Clark, R. A., Larter, S., Briedis, N. A., and Lundegard, P. D.,1989 b, Diagenesis and hydrocarbon accumulation, Brent sandstone (Jurassic), Bergen High area, North Sea *Am. Assoc. Petrol. Geol. Bull.*, 73, no. 11, p. 1341-1360.

Glennie, K. W.,1990, *Introduction to the Petroleum Geology of the North Sea* (third edition) Oxford, Blackwell Scientific Publications.

Goldstein, R. H., 1986, Re-equilibration of fluid inclusions in low temperature calcium carbonate cement *Geology*, **14**, p. 792-795.

Goldstein, R. H., 1988, Cement stratigraphy of Pennsylvanian Holder Formation, Sacramento Mountains, New Mexico *Am. Assoc. of Petrol. Geol. Bull*, **72**, p. 425-438.

Goldstein, R. H., 1990, Petrographic and geochemical evidence for the origin of paleospeleothems, New Mexico: Implications for the application of fluid inclusions to studies of diagenesis *J. Sed. Pet.*, 60, p. 282-292.

Gratier, J.P. and Jenatton, L., 1984, Deformation by solution-deposition, and re-equilibration of fluid inclusions in crystals depending on temperature, internal pressure and stress *J. Struct. Geol.* 6, p. 189-200.

Hanor, J. S. ,1980, Dissolved methane in sedimentary brines; potential effect on the PVT properties of fluid inclusions *Econ. Geol.*, 75, p. 603-617.

Harris, N. B., 1992, Burial diagenesis of Brent sandstones: a study of Statfjord, Hutton and Lyell fields. In Morton, A. C., Haszeldine, R. S., Giles, M. R., & Brown, S. (Eds), *Geology of the Brent Group*. Geological Society of London, Bath U.K. p. 351-375.

Haszeldine, R. S., Samson, I. M., and Cornford, C.,1984a, Dating diagenesis in a petroleum basin, a new fluid inclusion method: *Nature*, 307, p. 354-357.

Haszeldine, R.S., Samson, I.M. and Cornford, C. 1984b, Quartz diagenesis and convective fluid movement: Beatrice oilfield, North Sea *Clay Minerals*, **19**, p. 391-402.

Haszeldine, R. S., Brint, J. F., Fallick, A.E., Hamilton, P. J., & Brown, S., 1992, Open and restricted hydrologies in Brent Group diagenesis: North Sea. In Morton, A. C., Haszeldine, R.S., Giles, M. R., & Brown, S.(Eds.), *Geology of the Brent Group*. Geological Society of London, Bath UK. p. 401-419.

Haszeldine, R. S., and Osborne, M. 1993, Fluid inclusion temperatures in diagenetic quartz reset by burial: implications for oilfield cementation. In Horbury, A., and Robinson, A. (Eds), Diagenesis and basin development, *Am. Assoc. Petrol. Geol. Memoir* (accepted).

Hogg A.J.C.,1989, Petrographic and isotopic constraints on the diagenesis and reservoir properties of the Brent Group sandstones, Alwyn South, Northern U.K. North Sea *D. Phil. Thesis* University of Aberdeen, Scotland, 414p.

Hogg, A.J.C., Sellier, E. & Jourdan, A. J., 1992, Cathodoluminescence of quartz cements in Brent Group sandstones, Alwyn South. In Morton, A. C., Haszeldine, R.S., Giles, M.R., & Brown, S., (Eds) *Geology of the Brent Group.* Geological Society of London, Bath UK. p. 421-440.

Jourdan, A., Thomas, M., Brevart, O., Robson, P., Sommer, F., and Sullivan, M.,1987, Diagenesis as the control of Brent sandstone reservoir properties in the Greater Alwyn area (East Shetland Basin) *in* Petroleum Geology of North West Europe, Brooks, J., and Glennie, K., eds., Graham and Trotman, p. 951-961.

Konnerup-Madsen, J., and Dypvik, H., 1988, Fluid inclusions and quartz cementation in Jurassic sandstones from Haltenbanken, offshore Mid-Norway *Bull. Mineral,* **111**, p. 401-411.

Leroy, J., 1979, Contribution a l'etalonnage de la pression interne des inclusions fluides lors de leur decrepitation *Bull. Mineral.,* **102**, p. 584-593.

Malley, P., 1984a, Les inclusions fluides associeesaux nourrisages siliceux observes dans neuf puits du Jurassique du Brent (Mer du Nord). *Unpublished contract report,* Compagnie Francaise des Petroles, Centre de Sedimentologie et Geochemie de la surface, Strasbourg. 27p.

Malley, P., 1984b, Les inclusions fluides associees aux differentes phases diagenetiques du Jurassique du Brent, Mer du Nord. Rapport Final. Les inclusions fluides dans les mineraux du gres du Springhill, Argentine. *Unpublished contract report.* Compagnie Francaise des Petroles, Centre de Sedimentologie et Geochemie de la Surface, Strasbourg. 25p.

Malley, P., Jourdan, A., Weber, F. ,1986, Etude des inclusions fluides dans les nourrissages siliceux des gres reservoirs de Mer du Nord: une nouvelle lecture possible de l'histoire diagenetique du Brent de la region D' Alwyn *Acad..Sci.Paris* 302, p. 653-658.

Moge, M., 1985, Evolutions diagenetiques et characteristiques petrophysiques de formations greseuses a porosite secondaire *D. Phil. Thesis*, University of Nancy 125p.

Pittman, E. D.,1972, Diagenesis of quartz in sandstones as revealed by scanning electron microscopy *Earth Sci. Rev.* 26, p. 69-112.

Potter, II, R. W., and Brown, D. L., 1977, The volumetric properties of aqueous sodium chloride solutions from 0° to 500°C at pressures up to 2000 bars based on a regression of available data in the literature *US Geol. Surv. Bull.*, 1421-C, p. 1-6.

Prezbindowski, D. R., and Larese, R. E., 1987, Experimental stretching of fluid incusions in calcite- implications for diagenetic studies *Geology*, 15, p. 333-336.

Reynolds, J., Goldstein, R., Burley, S., and Turner, G.,1990, *Systematics of fluid inclusions in authigenic minerals and applications in sedimentary basin analysis*: Short course at the University of Manchester, England.

Roedder, E. 1979, Fluid inclusion evidence on the environments of sedimentary diagenesis, a review: *SEPM Spec. Publ.* 26, p. 89-107.

Roedder, E., 1984, *Fluid inclusions,in* Ribbe, P.H., ed., Reviews in Mineralogy 12, Mineralogical Society of America, p. 644.

Roedder, E., and Skinner, B. J., 1968, Experimental evidence that fluid inclusions do not leak *Econ. Geol.*, v. 63, p. 715-730.

Sterner, S. M., and Bodnar, R. J., 1989, Synthetic fluid inclusions-VII. Re-equilibration of fluid inclusions in quartz during laboratory simulated metamorphic burial and uplift *J. Metamorphic Geol.*, 7, p. 243-260.

Ulrich, M. R., and Bodnar, R. J., 1988, Systematics of stretching of fluid inclusions II: Barite at 1 atm confining pressure *Econ. Geol.*, 83, p. 1037-1046.

Walderhaug, O., 1990, A fluid inclusion study of quartz cemented sandstones from offshore Mid- Norway ; possible evidence for continued quartz cementation during oil emplacement *J. Sed. Pet.*, 60, p. 203-210.

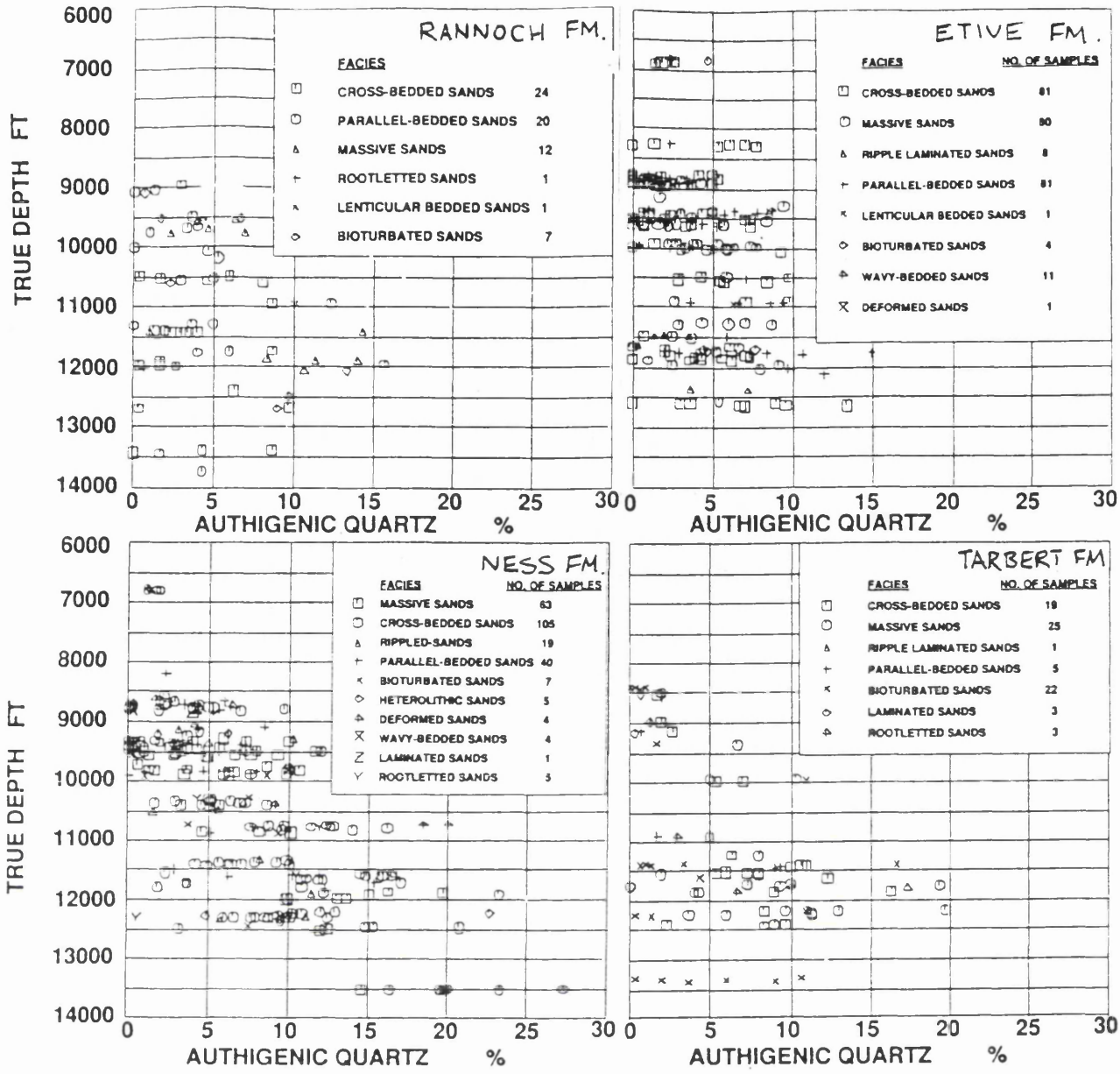

Figure 1. Point count data for Brent Group sandstones showing an increase in the abundance of quartz cement with depth. Data from Giles *et al.* 1992.

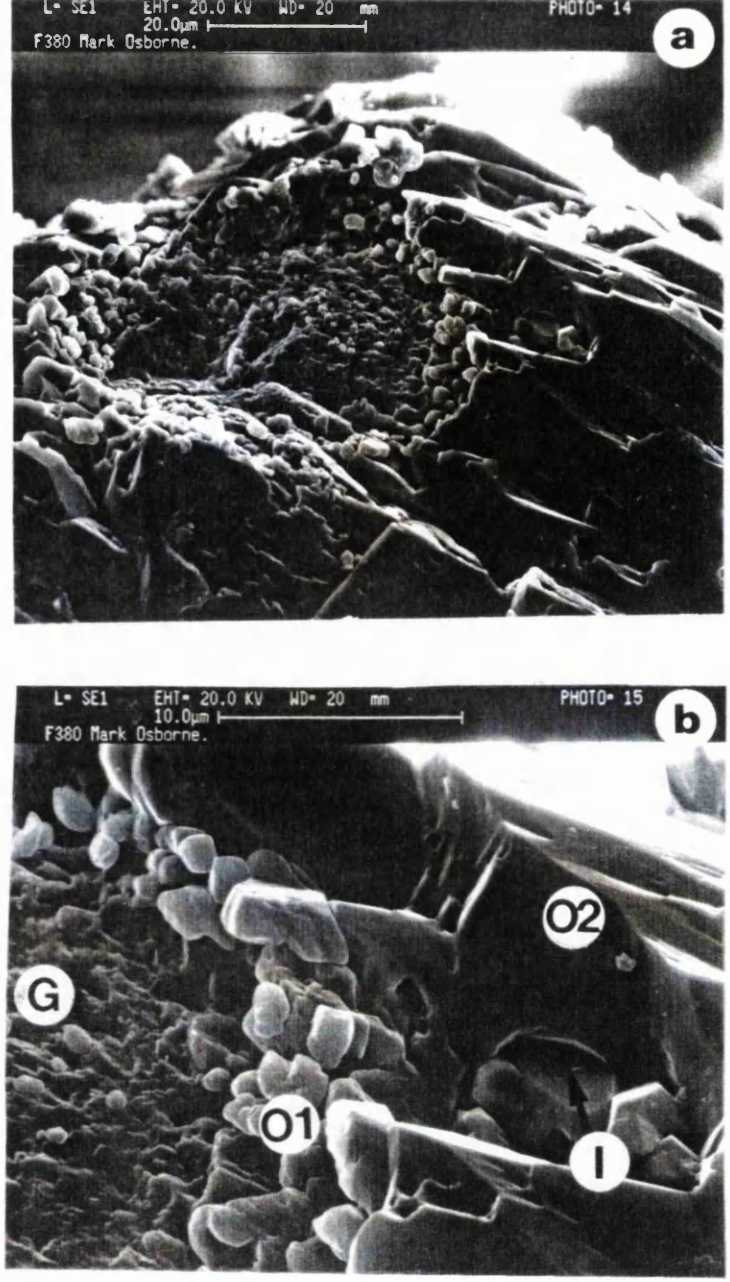

Figure 2.a) SEM photomicrograph of a typical quartz overgrowth from a shallow buried Brent Group sandstone. Overgrowths are irregular in appearance and consist of numerous crystal subunits. Emerald oilfield, Well 2/10-a7, 1674.4m TVD.

b) Higher magnification view of 2a. Tiny crystals of quartz (O1) have nucleated upon the surface of the detrital grain (G). Fluid is trapped in the cavities between these crystals forming fluid inclusions (I). Later, more euhedral overgrowths (O2) envelop this early generation of quartz cement.

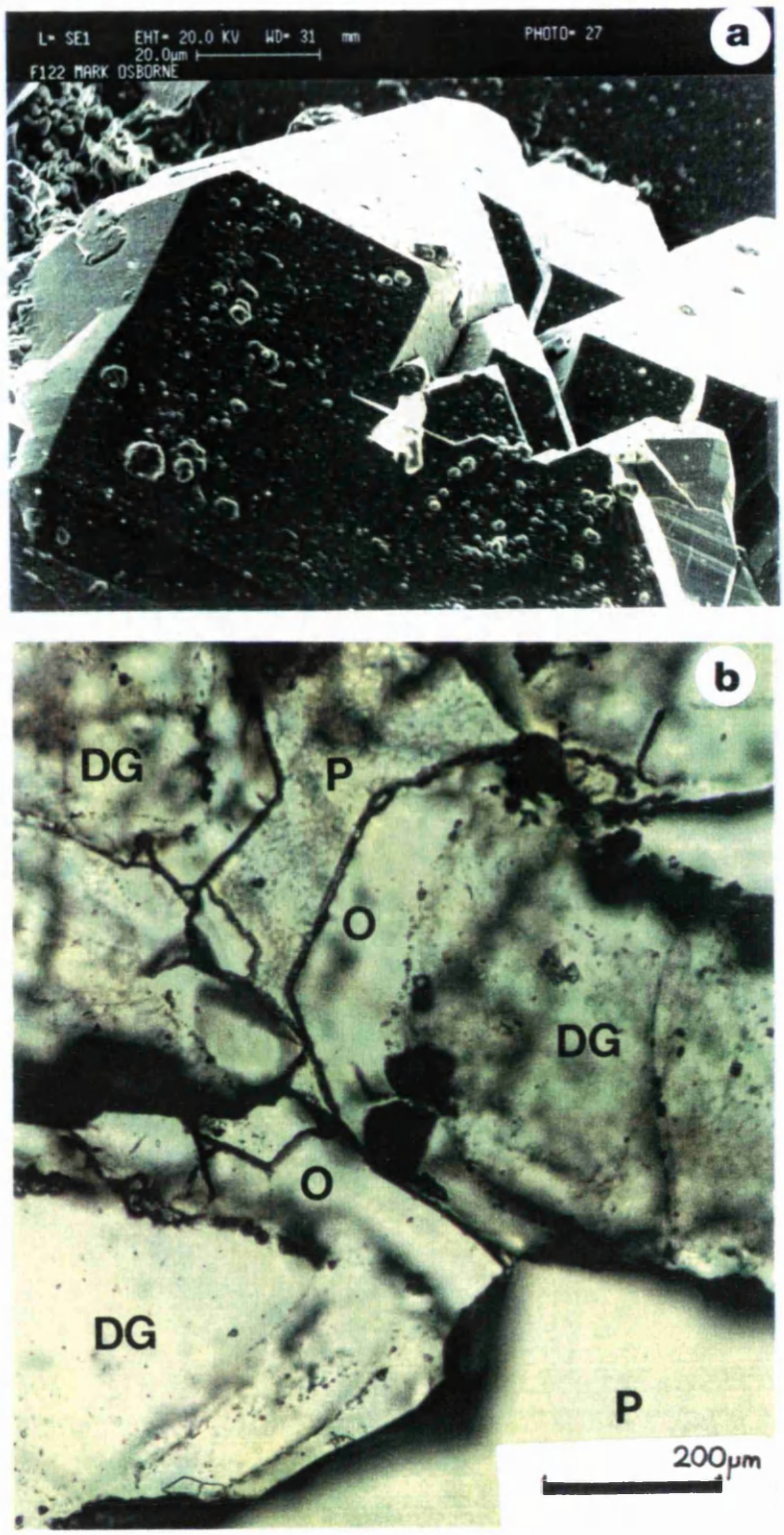

Figure 3a) In deeply buried Brent Group sandsones overgrowths are thicker and more euhedral. SEM photomicrograph of a large, euhedral quartz overgrowth. NW Hutton oilfield, Well 211/27-a2, 3751.8m TVD.

b) Photomicrograph of a fluid incusion wafer showing cloudy, inclusion rich detrital grains (DG), enveloped by clear quartz overgrowths (O). P=porosity. Same sample as in 3a.

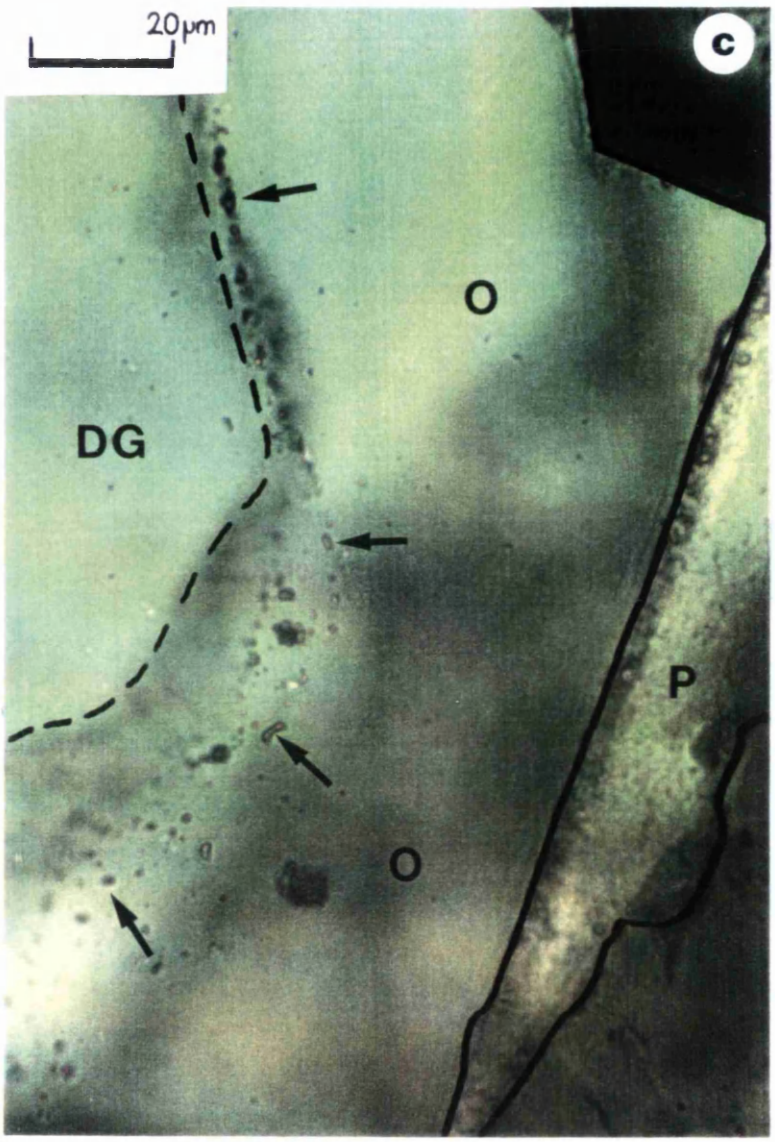

Fig3. c) Photomicrograph of a fluid inclusion wafer. Most fluid incusions (arrowed) occur close to the boundary between the overgrowth (O) and the detrital grain (DG). P=porosity. Same sample as in 3b.

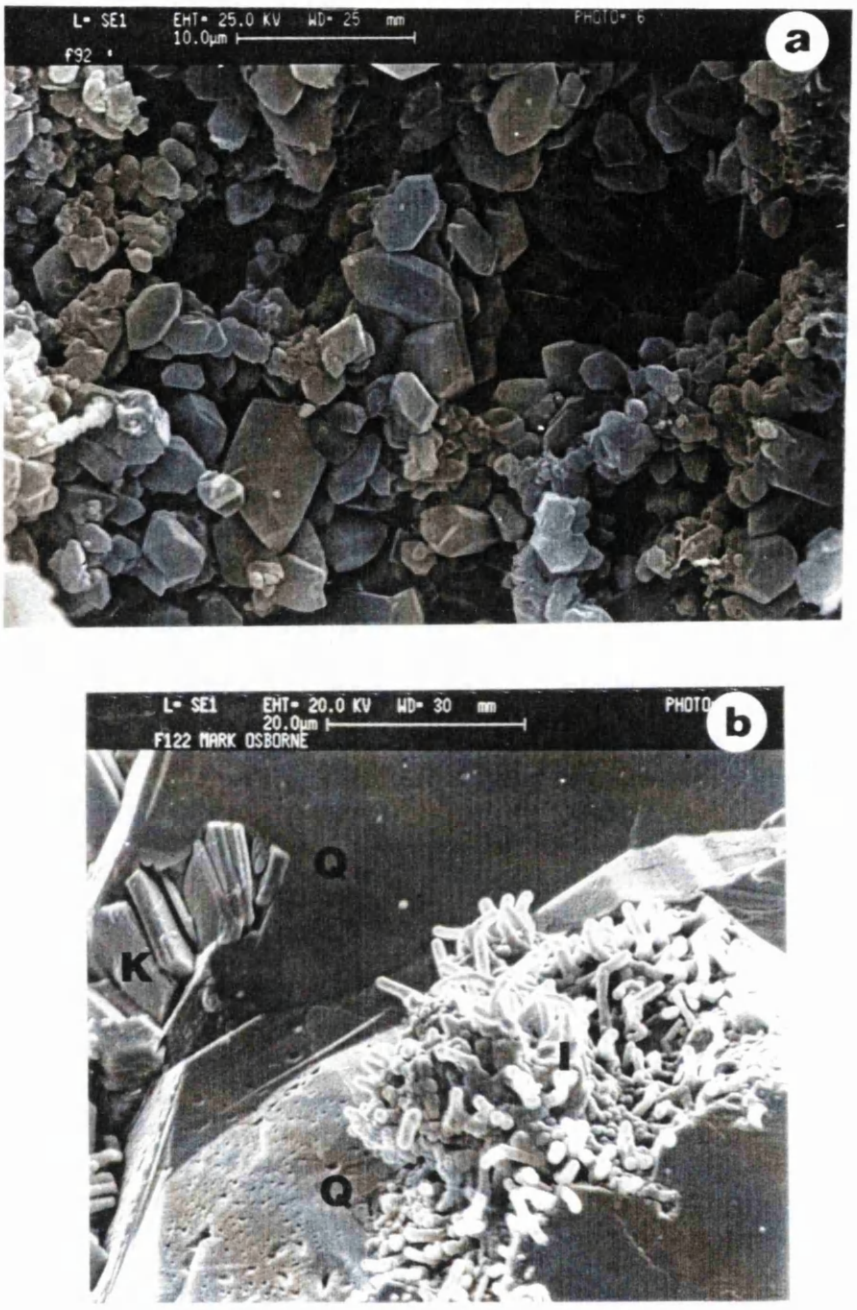

Figure 4. a) Euhedral, tiny crystals of microquartz. These are observed to infill the secondary pore-space created by feldspar dissolution. NW Hutton oilfield, Well 211/27-a2, 3781.1m TVD.

b) Blocky kaolinite (K) and fibrous illite cement (I) are enveloped by quartz cement (Q). This indicates that some quartz cement either post-dated or was co-genetic with kaolinite and illite precipitation. NW Hutton oilfield, Well 211/27-a2, 3781.1m TVD.

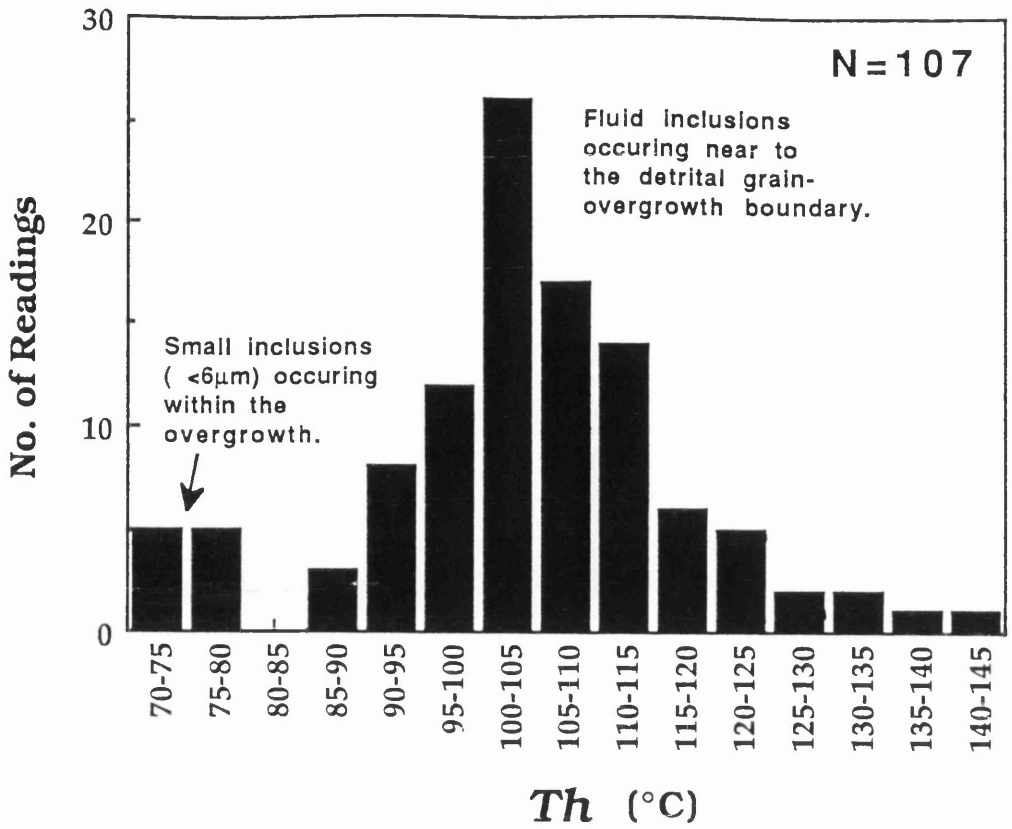

Figure 5. Fluid inclusion histogram for quartz cement from the N.W. Hutton oilfield (Well 211/27-a2, 3751m TVD). Note the wide spread in T_h and the asymmetry in the histogram.

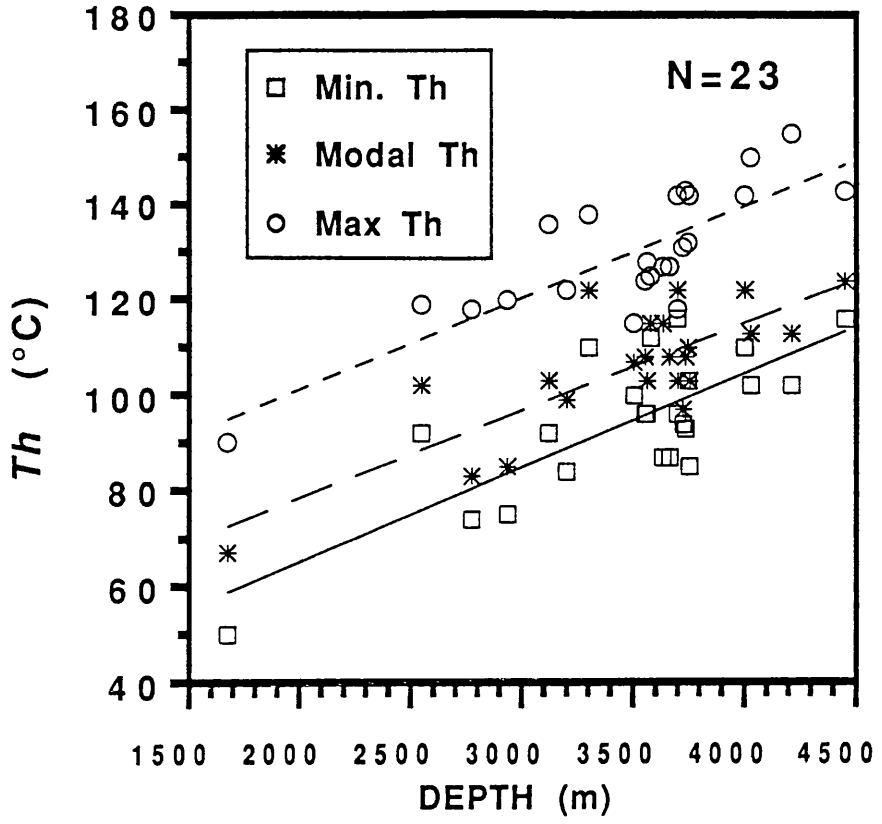

Figure 6. Fluid inclusion populations from North Sea quartz cements have minimum, modal and maximum T_h which increases with present day depth of burial. Correlation coefficient (R) between depth and Max. T_h=0.8088, Modal T_h=0.798 and Min. T_h=0.768. Data from Malley (1984a,b); Moge (1985); Malley *et al.* (1986); Jourdan *et al.* (1987); Crocket *et al.* (1988) quoted in Hogg (1989); Konnerup-Madsen & Dypvik (1988); Brint (1989); Glasmann *et al.* (1989 a&b); Hogg (1989); Ehrenberg (1990); Walderhaug (1990). Unpublished data of C. Macauley, O. McLaughlin and M. Osborne is also included.

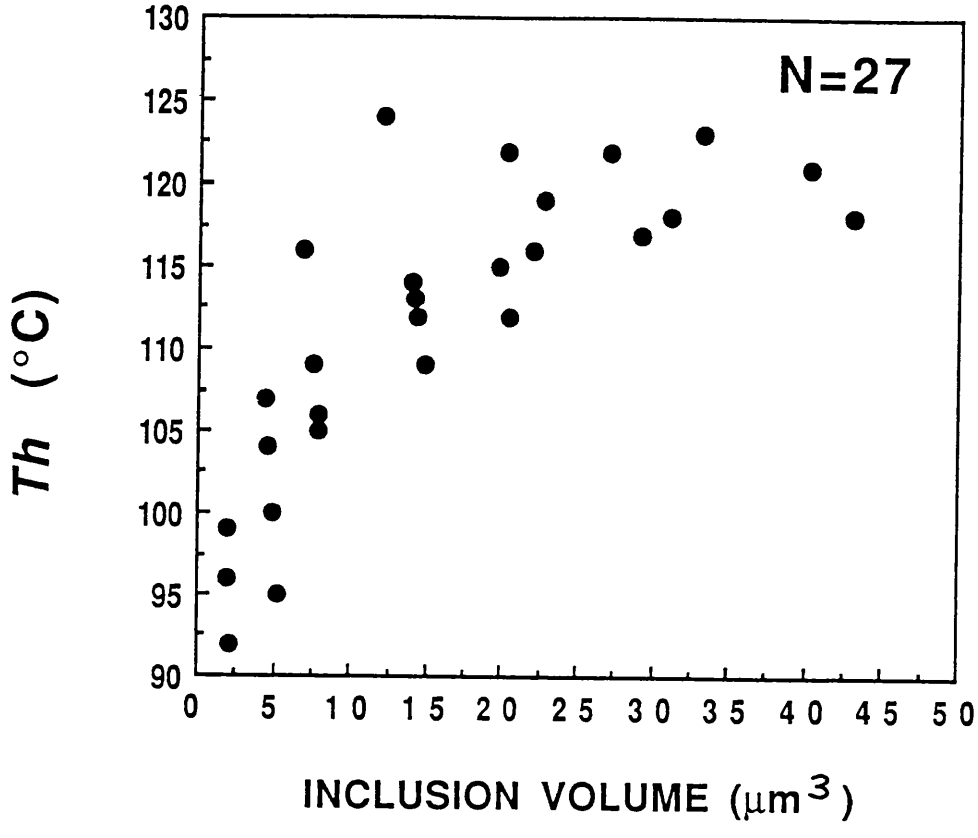

Figure 7. Relationship between inclusion volume and Th in the S. Brae fluid inclusions (Well 16/7a-A11, 4265.5m). All the inclusions came from a single grain, and occured close to the grain-overgrowth contact. The larger inclusions have the highest homogenisation temperatures. Inclusion volume is calculated using the method of Bodnar (1983). For further discussion see text.

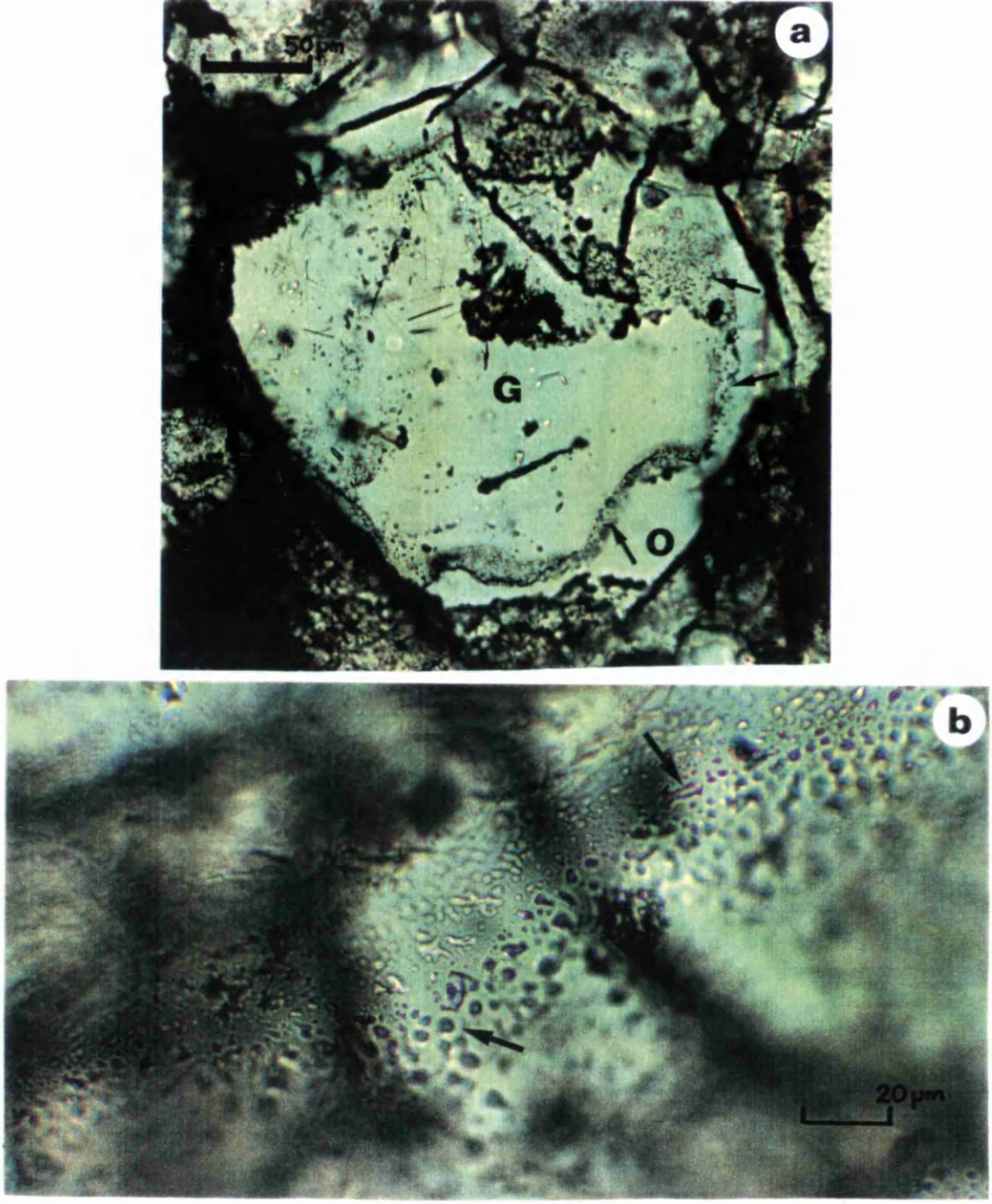

Figure 8. Typical appearance of fluid incusions in quartz cement from the S. Brae oilfield.

a) Photomicrograph of a fluid inclusion wafer showing a cloudy inclusion rich detrital grain (G) enveloped by clear quartz overgrowths (O). Inclusions are trapped adjacent to the detrital grain (arrowed). Well 16/7a-A11, 4265.5m TVD).

b) High magnification view of fluid inclusions occuring at the overgrowth detrital grain boundary. Some inclusions are spherical in shape, but others are more irregular. Inclusions are arrowed. Same sample as in Figure 8a.

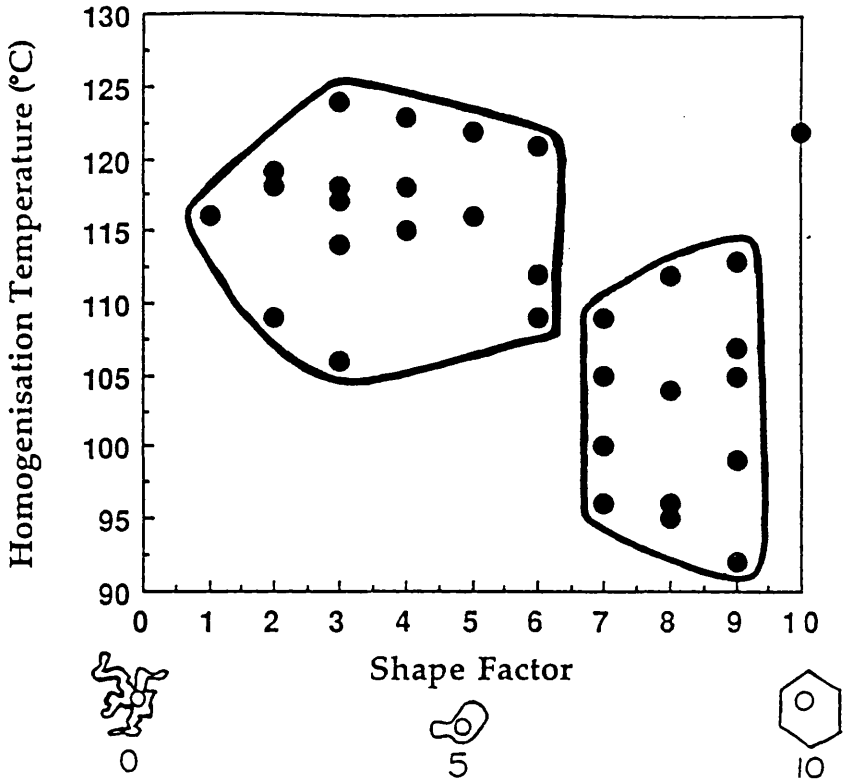

Figure 9. Relationship between shape factor and T_h of the S. Brae inclusions. Irregular, non-symmetrical inclusions seem to yield the highest temperatures. For further discussion see text.

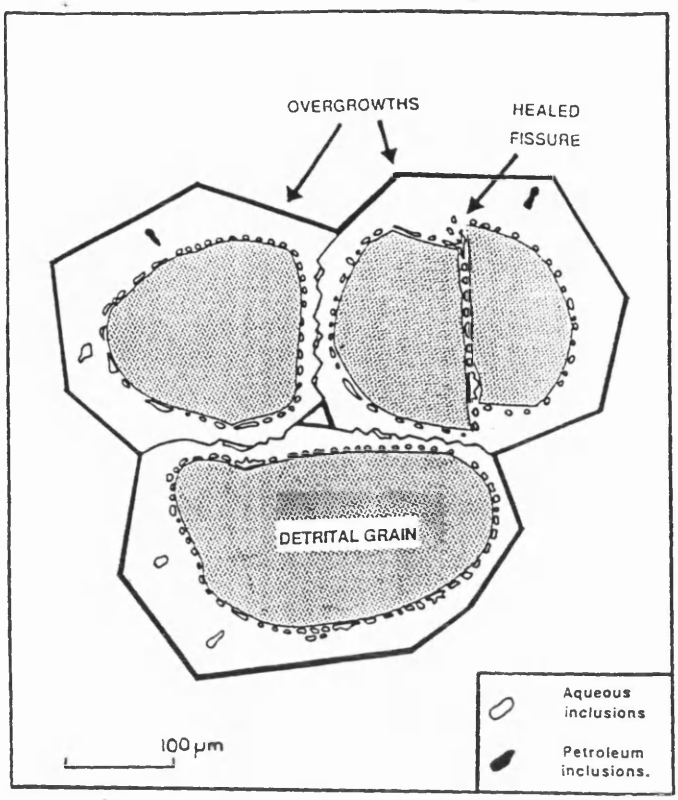

Figure 10. Schematic petrographic model showing the various fluid inclusion types occuring in Brent Group authigenic quartz. Most inclusions occur close to the grain-overgrowth boundary, or within healed fractures in the detrital grain. These were trapped during early diagenesis. Sparse late diagenetic inclusions, some hydrocarbon bearing, can be found in the overgrowth itself.

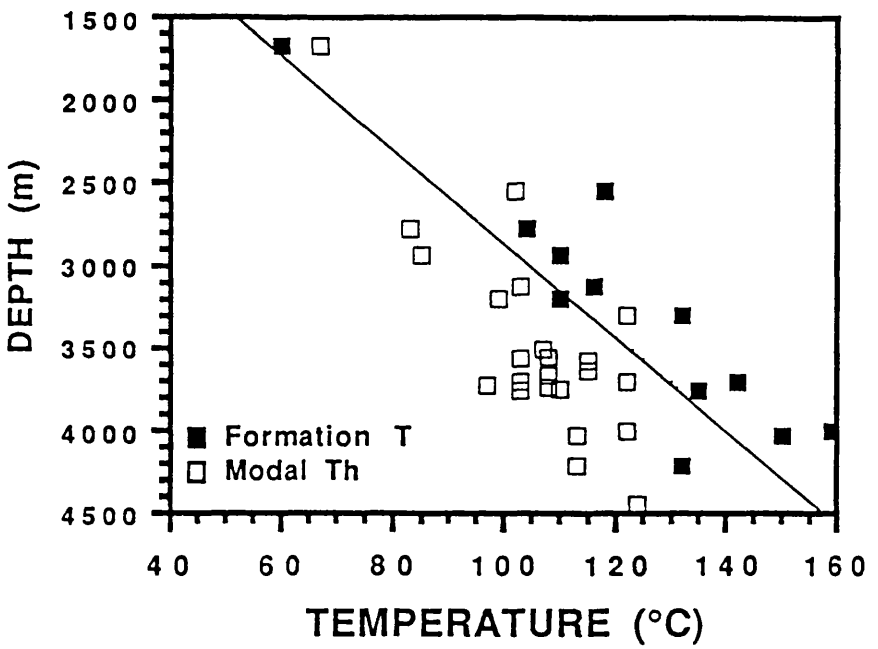

Figure 11. Scatter plot showing the relationship between T_h and formation temperatures. Inclusion T_h approaches but does not exactly coincide with maximum burial temperatures.

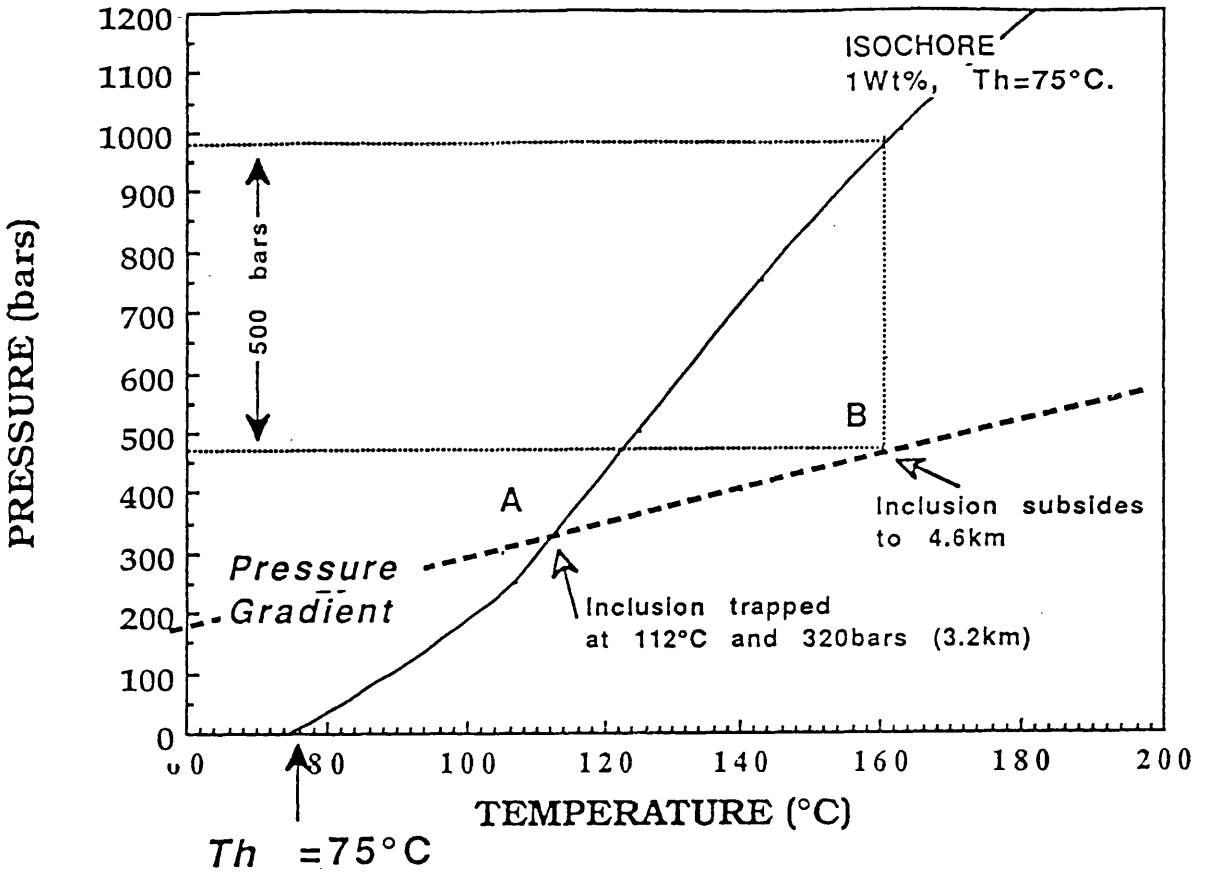

Figure 12. Pressure-temperature diagram for an inclusion trapped at point A (112°C and 320 bars) and subsiding 1.4km to point B. The inclusion will experience a rise in internal pressure 500 bars greater than external pore pressures. See text for additional explanation.

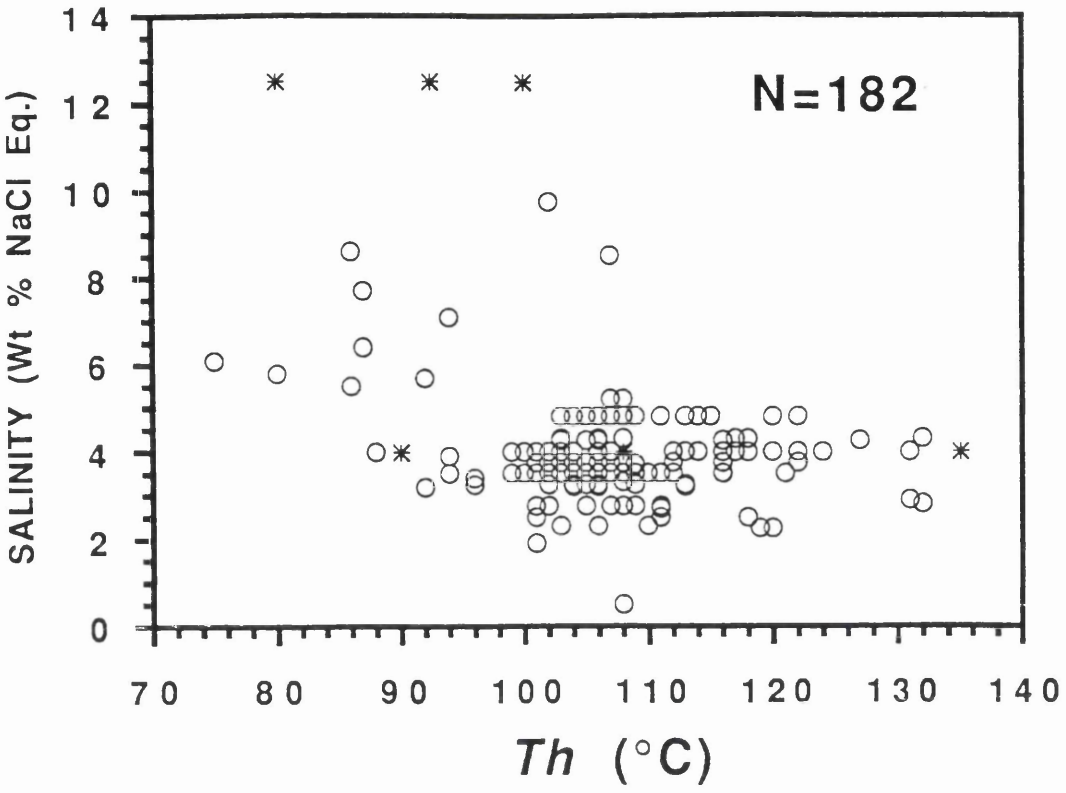

Figure 13. Relationship between salinity and T_h in fluid inclusions from the Brent Group. Low salinity inclusions yield the highest temperatures. For further discussion see text. Data from Brint (1989); Crocket et al. (1988) qouted in Hogg (1989); Hogg (1989); Malley (1984a,b,); Malley et al.(1986); plus unpublished data of the authors.

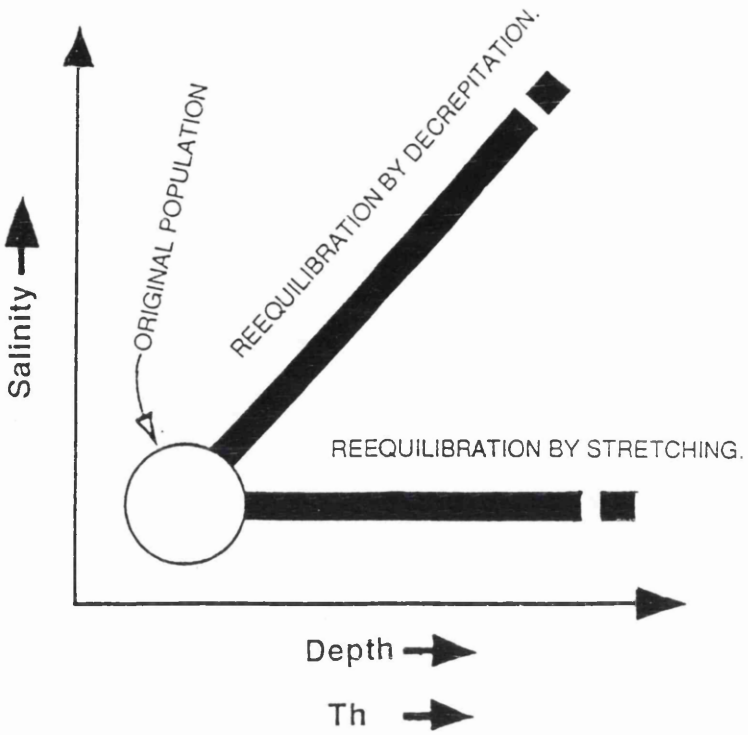

Figure 14. Hypothetical plot of temperature against salinity (from Reynolds et al. 1990). The two trends intersect at a single point representing the characteristics of the original fluid inclusion population before resetting. The horizontal trend is due to resetting by inclusion stretching. The inclined trend is due to resetting by decrepitation during increasing temperature and salinity.

Table 1 Fluid inclusion data for the NW Hutton oilfield (Well 211/27-a2)

3751m TVD				3780m TVD		3725m TVD	
Inclusion	Th (°C)	Inclusion	Th (°C)	Inclusion	Th (°C)	Inclusion	Th (°C)
1	72.6	55	135	1	115	1	99
2	73.5	56	108	2	116	2	119
3	74.4	57	118	3	110	3	110
4	73.6	58	99	4	110	4	106
5	75.3	59	101	5	116		
6	76.1	60	90	6	104		
7	123	61	99	7	107		
8	92	62	100	8	113		
9	113	63	103	9	97		
10	88	64	90	10	99		
11	114	65	97	11	137		
12	112	66	116	12	93		
13	123	67	104	13	127		
14	123	68	100	14	119		
15	97	69	102	15	106		
16	142	70	110	16	116		
17	94	71	119	17	108		
18	119	72	105	18	116		
19	102	73	106	19	97		
20	98	74	75	20	110		
21	104	75	71				
22	113	76	77				
23	107	77	77				
24	105	78	106				
25	100	79	106				
26	100	80	106				
27	103	81	110				
28	95	82	100				
29	107	83	102				
30	103	84	108				
31	101	85	114				
32	103	86	103				
33	102	87	106				
34	90	88	106				
35	114	89	108				
36	115	90	110				
37	102	91	101				
38	102	92	99				
39	92	93	105				
40	94	94	97				
41	98	95	106				
42	99	96	106				
43	95	97	115				
44	110	98	116				
45	102	99	110				
46	85	100	109				
47	113	101	127				
48	87	102	132				
49	111	103	104				
50	125	104	104				
51	123	105	132				
52	120	106	106				
53	101	107	101				
54	100						

Table 2. Homogenisation temperatures and present day depth of burial -a compilation of the available published and unpublished data.

Depth (m)	Min. Th(°C)	Modal Th(°C)	Max. Th(°C)	Oilfield	Source
4215	102	113	155	S. Brae	McLaughlin 1992 (unpublished)
4029	115	131	150	Huldra	Glasmann et al. 1989
3755	85	123	142	NW Hutton	Osborne (this study)
3736	93	108	143	Alwyn S.	Hogg 1989
3724	94	97	131	3/13a-1	Brint 1989
3700	96	103	120	Alwyn S.	Hogg 1989
3665	87	108	127	Alwyn S.	Hogg 1989
3561	96	103	128	Alwyn S.	Hogg 1989
3450	80	107	133	Haltenbanken	Ehrenberg 1990
3200	84	99	122	Murchison	Brint 1989
3122	92	103	136	Magnus	Macaulay 1990 (unpublished)
2934	75	85	120	Heather	Glasmann et al. (1989)
2775	74	83	122	Thistle	Brint 1989
2547	92	99	119	Haltenbanken	Walderhaug 1990
4450	116	124	143	Haltenbanken	Ehrenberg 1990
3450	89	95	104	Haltenbanken	Konnerup-Madsen & Dypvik 1988
3430	105	107	110	"Viking Graben"	Moge 1986
1676	50	67	90	Emerald	Osborne (this study)
3450	80	100	135	Alwyn area	Malley et al. 1986
3657	107	108	127	Alwyn area	Malley et al. 1984 a&b
3748	105	110	132	Alwyn area	Malley et al. 1984 a&b
3564	96	111	124	Alwyn area	Malley et al. 1984 a&b

Table 3. Fluid inclusion data for the S. Brae oilfield, Well 16/7a-A11, 4265.5m TVD. Observations by M. Osborne.

Volume (μm^3)	Th (°C)	Bubble Size (μm)	Shape Factor
7.930	105.000	0.860	7.000
14.330	112.000	1.080	8.000
4.340	107.000	0.720	9.000
1.950	96.000	0.500	7.000
40.190	121.000	1.580	6.000
14.130	113.000	1.080	9.000
11.990	124.000	1.080	3.000
6.760	116.000	0.860	1.000
22.650	119.000	1.300	2.000
31.090	118.000	1.440	3.000
1.950	96.000	0.500	8.000
7.800	106.000	0.860	3.000
1.850	99.000	0.500	9.000
4.340	107.000	0.720	9.000
5.300	95.000	0.720	8.000
7.450	109.000	0.860	6.000
2.100	92.000	0.500	9.000
4.520	104.000	0.720	8.000
4.850	100.000	0.720	7.000
13.910	114.000	1.080	3.000
7.450	109.000	0.860	2.000
31.090	118.000	1.440	2.000
19.710	115.000	1.220	4.000
14.900	109.000	1.080	7.000
33.180	123.000	1.500	4.000
43.020	118.000	1.700	4.000
27.080	122.000	1.440	5.000
29.110	117.000	1.440	3.000
20.260	122.000	1.080	10.000
20.420	112.000	0.860	6.000
22.080	116.000	1.080	5.000

Table 4. Compilation of fluid inclusion salinity data for the Brent Group

Malley et al. 1984 a,b

Th (°C)	(Wt. % NaCl eq.)	*Th* (°C)	(Wt. % NaCl eq.)
114	4.00	99.	3.50
112	3.75	99.	4.00
112	3.75	104	3.50
107	3.75	104	3.75
108	3.75	108	3.50
112	3.75	108	3.50
122	3.75	104	4.00
108	3.75	104	3.75
116	3.75	102	3.75
116	4.25	102	4.00
127	4.25	102	3.50
120	4.80	103	3.50
122	4.00	103	3.75
108	2.75	103	3.75
111	2.75	107	4.00
109	2.75	104	3.75
109	2.75	107	3.75
107	2.75	99.	3.50
114	4.00	99.	3.50
112	3.75	100	4.00
112	3.75	106	4.80
107	3.75	106	4.30
108	3.75	106	4.25
112	3.75	108	4.80
122	3.75	101	3.75
108	3.75	101	4.00
116	3.75	101	3.75
116	4.25	101	3.75
127	4.25	101	3.75
120	4.80	104	3.25
122	4.00	104	3.50
108	2.75	104	3.50
111	2.75	96.	3.25
109	2.75	101	2.50
109	2.75	113	3.25
107	2.75	112	3.50
108	5.20	122	4.80
114	4.00	111	4.80
111	3.50	104	4.00
111	3.50	120	2.25
111	4.80	111	2.50
115	4.80	119	2.25
105	4.80	118	2.50
105	4.80	106	3.25
105	4.25	107	3.50
121	3.50	107	4.00
105	4.80	107	4.00
105	2.75	106	3.75
105	3.25	106	3.25
109	3.50	116	4.00
109	3.25	112	3.75
106	3.50	116	3.50
106	3.50	112	3.50
103	4.80	118	4.00
103	3.50	124	4.00
107	8.50	120	4.00
		112	4.00
		113	4.00

Brint 1989

Th (°C)	(Wt. % NaCl eq.)
86.	5.5
88.	4.0
96.	3.4
104	3.2
131	2.9
111	2.7
101	1.9
87.	6.4
80.	5.8
87.	7.7
94.	7.1
75.	6.1
92.	5.7
94.	3.5
109	3.7
94.	3.9
86.	8.6
92.	3.2

Hogg 1989

Th (°C)	(Wt. % NaCl eq.)
102	9.75
107	5.20
107	3.50
101	3.50
101	2.75
102	2.75
106	3.50
101	1.90
106	3.20
102	3.25
104	3.20
112	3.50
106	3.20
117	4.00
103	2.30
113	3.20
110	2.30
108	3.30

Malley et al. 1984 a,b

Th (°C)	(Wt. % NaCl eq.)
90.0	4.00
108.	4.00
135.	4.00
80.0	12.5
92.5	12.5
100.	12.5

Osborne (NW Hutton, this study)

Th (°C)	(Wt. % NaCl eq.)
106	2.3
132	2.8

Crocket et al. 1988

Th (°C)	(Wt. % NaCl eq.)
108	0.5

APPENDIX 1

FLUID INCLUSION TEMPERATURES IN DIAGENETIC QUARTZ RESET BY BURIAL: IMPLICATIONS FOR OILFIELD CEMENTATION.

R.Stuart Haszeldine, Mark Osborne,

Department of Geology & Applied Geology,

University of Glasgow, Glasgow, G12 8QQ, Scotland, U.K.

Submitted to AAPG Memoir "Diagenesis and basin development".

Eds A Horbury, A Robinson

Version 2 July 92

ABSTRACT

Fluid Inclusion (FI) temperatures in diagenetic quartz are often used as crucial evidence to infer abnormally hot paleo-temperatures, and precipitation of pore-filling quartz cements following advection of large volumes of hot waters from depth. However, we consider that FI temperatures do not record their original paleo-temperatures.

North Sea and Norwegian Jurassic oilfield sandstones show volumes of diagenetic quartz cement which today increase monotonically with depth from 1.8km to at least 4.2km. Minimum, modal and maximum FI temperatures within this diagenetic quartz all show a progressive temperature increase with depth. If subsidence of an oilfield was slow during the past 5 Ma, then those FI modal temperatures coincide exactly with rock temperature. But if subsidence was rapid ($>10 m.Ma^{-1}$), then FI modal temperatures systematically lag beneath rock temperatures. Additional geological evidence favoring resetting includes:- high temperature quartz FI in texturally and isotopically shallow veins; and high temperature quartz FI inside and outside shallow-formed carbonate cement. Laboratory experiments also show some resetting of quartz FI within one year of overheating. The resetting mechanism is unlikely to be by fracturing and leakage, but more likely to be via stretching and local shape change. Inclusion compositions are probably unaltered.

A FI temperature distribution from any single depth records the pauses in subsidence and maximum burial temperature, but *does not simply record the temperature of quartz growth.* Resetting of FI negates temperature evidence for massive circulation of hot basinal fluids transporting quartz. We conclude that diagenetic quartz in these rift basin sandstones may be supplied by local diffusion, so that cement volumes are inherently predictable.

INTRODUCTION

Quartz cement is an important cause of porosity reduction during deep burial diagenesis of oilfield sandstones. Such cements can form 5-15% of the whole rock volume and so can reduce porosity by 50% (eg Giles *et al* 1992). The processes by which such quartz cements originate are thus crucially important both industrially - to understand why sandstone reservoirs contain only half the hydrocarbons they might- and intellectually, to understand how ions forming 15% of a rock can be moved in the sub-surface. Two rival hypotheses are current to explain quartz cements. Neither diagenetic cement textures nor isotopic evidence are conclusive in testing between these two hypotheses (Haszeldine *et al.* 1992), so that FI evidence has a pivotal role, and its reliability must be examined closely. The two hypotheses are:-

1) Quartz grew as a mineralising event transported by hot fluids which circulated in the deep basin (Haszeldine *et al.* 1984a,b, Jourdan *et al* 1987, Burley *et al.* 1989, Glasmann *et al* 1989b).

2) Quartz grew during a geologically long time span at equilibrium temperature; ions were locally supplied (Blanche and Whitaker 1979, Walderhaug 1990, Bjorlykke *et al* 1992).

Evidence of "elevated temperatures" from fluid inclusions (FI) (Haszeldine *et al.* 1984, Burley *et al.* 1989) is frequently used as critical data to support the first hypothesis. Here we have compiled a large FI data set from published and unpublished North Sea and Norwegian information to test the accuracy of the FI paleo-temperature record. We find that FI homogenisation temperatures in diagenetic quartz show a correlation with present day burial depth and an excellent correlation with burial temperature, when corrected for subsidence rate. We conclude that FI in diagenetic quartz are reset during burial, and do not record the simple paleo-temperatures of quartz growth. Thus the key evidence

evidence supporting hypothesis 1 is probably wrong. It is very probable that diagenetic quartz grew over a long time span, supplied by local diffusive processes rather than by large scale fluid advection. Consequently, porosity reduction by quartz cementation can potentially be modelled as a closed system.

FLUID INCLUSIONS IN DIAGENETIC QUARTZ.

Of critical importance in the following discussion is the simple observation that quartz cement increases monotonically with depth, especially as this can be documented within a single field (Scotchman *et al.* 1989) moving 1km vertically over an 8km lateral distance. Regional compilations of middle-Jurassic data show the same effect (Glasmann *et al* 1989a, Ehrenberg 1990, Giles *et al.* 1992, Bjorlykke *et al* 1992). These data imply that quartz cement has formed, and is still forming, gradually with depth (Fig. 1), commencing around 70°C, 2km. If quartz had formed from a single short-term mineralising event in ancient times, then sandstones would have been cemented in relation to their paleo-depth, and would not show a relationship of quartz cement to their present depth.

During burial of sandstones, diagenetic quartz nucleates on detrital grains to form overgrowths which may reach 100 μm thick and gradually fill primary porosity. The great majority of FI (Fig. 2) form at the boundary between the detrital sand grain and the overgrowth or at boundaries of cathodoluminescence growth zones, suggesting diastems in the growth history. Burley *et al* (1989) and Hogg *et al* (1992) show that growth zones within these overgrowths are, in general, concentric, so that FI at a grain/overgrowth boundary would have been trapped at about the same temperature. Inclusion workers attempt to select primary unaltered FI from these populations to obtain accurate temperature and

salinity measurements. Inevitably these are biased towards the start of quartz growth. Raman probe analyses of oilfield basin FI show appreciable methane contents, meaning that a "pressure correction" is not necessary to obtain a hotter trapping temperature than the measured homogenisation temperature (T_h) (Hanor 1980).

WHY RESETTING MIGHT OCCUR- FLUID INCLUSION SYSTEMATICS

When a fluid inclusion is trapped during mineral growth in the subsurface it is assumed that one aqueous fluid phase is present, without any free vapour. Surface pressures and especially temperatures are lower than the subsurface reservoir, and this volume decrease of the liquid forces a small vapour bubble to nucleate within the aqueous fluid inclusion. Heating the inclusion in a laboratory mimics the burial temperature of original growth, and the vapour bubble merges again into one fluid. This is the "homogenisation temperature" and $T_{h\ original}$ on Fig. 3 shows that this represents the minimum trapping temperature of that particular inclusion, ie the minimum growth temperature of that mineral. This relies on several crucial assumptions:- 1) That the isochore B-C is steep, so that the temperature of entrapment approximates to that measured by $T_{h\ original}$. In sedimentary basins, the aqueous fluid inside inclusions is analysed to be methane-rich, so that this condition is true and any "pressure correction" can be neglected (Hanor 1980, Burley *et al* 1989). 2) The inclusion has remained a closed system, neither losing nor gaining fluid or vapour. 3) The inclusion has maintained a constant volume. 4) The fluid was trapped as a single aqueous phase. Conditions 2 and 3 can both potentially be violated for FI in minerals grown in a subsiding sedimentary

basin, where pressures and especially temperatures outside the inclusions increase due to additional burial after their growth.

As an inclusion is buried and becomes heated, the aqueous fluid trapped within it attempts to expand, within the fixed volume of the inclusion. The pressure within the inclusion consequently increases until at some point the strength of the host mineral is exceeded, and the inclusion succeeds either in expanding in volume, or in losing some of its contents. Experimental studies show that this can occur in two ways:- Plastic deformation and stretching (Bodnar & Bethke 1984); or Brittle deformation and fracture decrepitation (Roedder 1984).

For decrepitation to occur, microfractures must have developed from the inclusion towards lower pressure space at the edge of the grain, or within another inclusion; fractures of the correct diameter may even selectively "pump" water out of inclusions (Bakker & Jansen 1990). These fractures permit the inclusion to lose fluids to its external environment. Once the fractures heal, the growth temperature, pressure and chemical composition of that inclusion's contents will have changed. Loss of fluid from the inclusion has lowered the internal density of the inclusion, and must result in a new, higher, homogenisation temperature. Decrepitated inclusions can potentially be recognised during petrographic observation, as they are often surrounded by a halo of small secondary inclusions (Sterner & Bodnar 1989).

As an alternative response to the increased internal pressure, the inclusion may deform plastically and non-elastically, and "stretch", so that the volume of the inclusion increases. This again results in a decrease in the density of the fluid and an increase in the new homogenisation temperature (Fig. 3, $T_{h\,new}$). As there has been no loss of fluid, the inclusion contents retain their original chemical composition. This size change is impossible to detect petrographically, for an inclusion of 5 wt%NaCl fluid composition, a density

change of only 3% is needed to produce a temperature increase from 100 to 150°C, equating to a spherical diameter change in an inclusion from 5 to 5.05µm.

EXPERIMENTAL DATA

The problem for fluid inclusion studies in situations of increasing temperature, such as subsiding hydrocarbon basins, is to decide the limits to strength and ability of each mineral to resist decrepitation or stretching with increased temperature. It is well established that minerals such as fluorite and sphalerite are "weak" (Bodnar and Bethke 1984). Laboratory experiments have been undertaken to measure the internal overpressure required to decrepitate fluid inclusions in quartz. These experiments are usually undertaken by short term heating (days or months) of artificially grown inclusions in laboratory quartz. Robinson *et al* (1992) have reviewed experimental results and have confidence in FI data partly because they have been impressed by reports from Bodnar *et al* (1989) and from Sterner and Bodnar (1989) which emphasise large decrepitation pressures rather than stretching as FI resetting mechanisms for quartz. We have examined these and other workers publications, and come to differing conclusions on processes. The experimental values obtained depend upon the size of the inclusion (Bodnar *et al* 1989). Small inclusions (5µm) require internal overpressures of >2,500bars, whereas large inclusions (30µm) require overpressures of only 850-1,000 bars. Neither of these values is likely to be achieved in a hydrocarbon burial setting, where Burrus (1987) has shown that internal overpressures resulting from 70°C (2km) of subsidence will only reach 400 bars. Thus, subsidence-related decrepitation of inclusions in authigenic quartz can be rejected.

By contrast, Gratier (1982), Gratier and Jenatton (1984) have experimentally observed plastic and diffusive deformation and stretching of fluid inclusions in quartz. These experiments on inclusions in synthetic quartz, at internal overpressures as low as 5MPa (50 bars) and temperatures sometimes increased from only 212 to 217°C, produced shape changes from irregular towards spherical or negative crystal inclusion shapes within 120 days. Inclusions which changed shape and did not fracture were observed to increase in T_h, inferred by Gratier and Jenatton (1984) to be due to the density decrease of the fluid inside the inclusion. These changes in FI shape were deduced to have a kinetic barrier, so that FI in synthetic quartz produced measurable changes within days, whereas natural FI in quartz would have needed 4 years to achieve similar changes. This slow time dependency is important for our arguements (below) of slow geological resetting rates in natural systems.

Likewise, Bodnar *et al* (1989) found to their surprise that many inclusions underwent non-elastic stretching before undergoing brittle fracture. Stretching occurred at low overpressures and was often followed by decrepitation upon increased heating. This behaviour was confined to the smaller inclusions (<6μm) in their experiment- similar in size to those occurring naturally in diagenetic quartz. Internal overpressures in these inclusions were thought by Bodnar *et al* (1989) to be only 400 bars, and so are achievable during burial. About 20% of the inclusions increased in temperature by up to 30°C during this 12 month experiment. Although the majority of the inclusions did not increase in temperature, these experiments still demonstrate that the process of resetting by stretching of inclusions in quartz is feasible. Sterner and Bodnar (1989) found experimentally that this resetting process is time dependant- once it has begun, then individual inclusions come closer to re-equilibration with new P-T conditions with increasing time. In laboratory experiments, very long times are a difficult variable to alter; by looking back in time to the geological record, we

can see the end effect of any resetting processes. This is what we attempt to do in the bulk of this paper.

PATTERNS IN FLUID INCLUSION TEMPERATURE DISTRIBUTIONS.

Roedder (1984) explains the different types of information available from FI. Here we are only concerned with homogenisation temperatures which are commonly interpreted to yield the growth temperature of diagenetic quartz (Haszeldine *et al.* 1984a, Ehrenberg 1989, Glasmann 1989a, b, Burley *et al.* 1989). A cartoon histogram of FI homogenisation data (cf Glasmann *et al* 1989a, Haszeldine *et al* 1992) is shown in Fig. 4. This shows one or more modes, with isolated reading at lower temperatures and a skewed tail towards hotter temperatures. Empirically, we find that this pattern requires a large number of readings (greater than 40, preferably >100) to be measured at each individual depth. This pattern is blurred if data from different depths are merged, and the full pattern does not appear in smaller data sets. We propose that $T_{h\ min,\ mode\ and\ max}$ in these spectra are important.

EMPIRICAL GEOLOGICAL DATA

We have compiled all published FI data from North Sea quartz cements and combined these with our own measurements. When homogenisation temperature is plotted against present day burial depth of sandstones (Fig. 5) a pattern of increasing temperature with present depth is seen. Notice that the minimum temperature of each distribution also increases with depth. When a $35^{o}C.km^{-1}$ temperature gradient, typical of today's North Sea is projected for comparison

with present-day rock temperatures (Fig. 5), we observe that some modes coincide very closely with the rock temperature today, whereas others are too cool. Also apparent is that temperature maxima in FI histograms rarely exceed today's rock temperature.

This simple co-relation of depth and FI temperature (which contains minimal interpretation), made us suspect that FI temperatures are partly a record of todays temperature not a record of ancient temperatures. However, there is no simple graphical fit to the data (Fig. 5); fits can be made ranging from a 35°C km^{-1} temperature gradient to a 18°C km^{-1} temperature gradient. The full interpretation is necessarily more complex (see below).

EVIDENCE THAT HOMOGENISATION TEMPERATURES ARE RESET.

It has been established experimentally (Bodnar and Bethke 1984) and geologically (Goldstein 1986, Barker and Goldstein 1990) that FI in soft cleaved minerals such as carbonates are reset and show a good correlation with maximum paleo-temperatures of a sediment. Metamorphic quartz FI are also reset during experimental or natural overheating (Sterner and Bodnar 1989). It is therefore logical to ask if FI in diagenetic quartz can also be reset during burial and heating after their growth. Several lines of geological evidence suggests that this has indeed taken place.

1. Temperature profiles.

Quartz cement volume increases with present day depth in Mid- and Upper Jurassic sandstones from the North Sea (Fig. 1), and so is here inferred to grow gradually through a depth range. Thus inclusions within the overgrowth would be expected to increase in homogenisation temperature from the detrital grain

rim towards the last formed edge of the diagenetic overgrowth. We have looked for this effect in inclusions from Emerald, NW Hutton, and South Brae, and re-examined data from Alwyn South (Hogg 1989). In none of these is any systematic temperature profile observed within overgrowths. Only in the Tartan Field study (Burley *et al.* 1989) has any systematic increase in FI temperatures been shown throughout an overgrowth. Even here, no oscillations of temperature (from hot and cool fluids) are recorded. The Tartan case, however, may be complicated because the cooler FI are very saline whereas the hotter are not. Osborne and Haszeldine (1992) point out that saline FI are reset less than pure water, so that this alternative to hot fluid pulses is feasible in Tartan. We note also that the Tartan FI temperature "palaeogradient" is 34°C km^{-1}, just as it is today, and the hottest FI are within 10°C of present reservoir temperatures (Burley *et al.* 1989, figs. 13, 15). These features suggest that Tartan FI are reset.

2. Lowest FI temperatures.

These provide minimum temperatures for the commencement of overgrowths. Fig. 5 shows that minimum temperatures today increase with present day sandstone depths. One interpretation of this is that quartz growth in the same sandstone facies in different oil fields, and even within the same oil field, was initiated at different temperatures. If an equilibrium temperature gradient is assumed, this implies that some sandstones grew quartz cement at 2km, whereas others had no quartz cement until 4km. When we remember that the percentage of quartz cement today clearly increases with depth (Fig. 1), and if this quartz cement commences at around 70°C, we consider the variable temperature and depth interpretation of FI evidence to be too simple and incorrect.

By contrast a more satisfactory explanation is that quartz cement in these sandstones has been and still is commencing growth at around 70°C (65-90°C).

This is shown by the intercepts on Fig 1. If the original (coolest temperature) FI are continually resetting with depth to increase their apparent temperature, then there can be no certain FI record of these lowest temperatures. Indeed, we see from Fig. 5 that $T_{h\ min}$ does increse progressively with today's depth (not paleo-depth). If FI at grain-overgrowth boundaries did indeed grow at different temperatures in the past from a rising hot fluid it is difficult to see how the present day quartz volume : depth profile and $T_{h\ min}$ profile could result. Neither can these FI be responding to a present-day hot rising fluid, for the deeper FI temperatures are cooler than rock temperature. This is discussed further below.

3. Hot paleo temperatures.

Quartz FI temperature <u>modes</u> in these sandstones are always at, or below, present day reservoir temperature and generally increase with present day depth (Fig. 5). Some FI <u>maxima</u> exceed present day rock temperature; these are not uplifted, but are thought to result from FI stretching (see 6 below). If quartz is hypothesized to have started growth in the geological past, when a sandstone was at a shallower burial depth than today, so the FI temperatures recorded today are too hot when related to an equilibrium $35^{o}Ckm^{-1}$ temperature gradient in the geological past. One interpretation of this is to invoke a period of hot fluid circulation, which heated the sandstone and also transported the quartz cement (Haszeldine *et al.* 1984a,b, Jourdan *et al.* 1987, Burley *et al.* 1989). This leads to very great problems.

Firstly, the key problem is that a huge volume of fluid (at least 10^{6} pore volumes) is needed to transport the volumes of quartz cement, due to the very low solubility of quartz in oilfield brines. However, such large volumes of fluid are not available during burial diagenesis (Haszeldine *et al* 1984b). Transporting heat into the rock with this volume of fluid is easy, and simple calculations show

that only one pore volume of water flow every 10^3 yr would suffice to keep a 2km deep sandstone at 130 °C.

Secondly, if quartz cement was transported by hot fluid, then the fluid should be cooling to precipitate quartz (Fig. 6). A cooling fluid would fossilise a high apparent temperature gradient. By contrast if a rising fluid was keeping its heat and not cooling, its temperature would not change much vertically and a low apparent temperature gradient would be fossilised. The North Sea FI data apparently record an equilibrium to low 35-18°C.km^{-1} gradient (Fig 5), implying a fluid rising but not cooling to precipitate quartz. If a rising fluid had cooled beneath the surface, then a high gradient and high temperatures would exist in the shallow basin (Fig. 6). Notice that these temperatures lie right of the equilibrium line in Fig. 6, whereas the real-life data (Fig. 5) lie left of it. We have attempted to backstrip our samples to infer convincing episodes of hot fluids in the geological past, which are preserved unaltered in the FI today, but without success, as the subsidence histories of the North Sea and the Norwegian margin are so different.

4. Shallow veins.

In the Fulmar field (Johnson *et al.* 1986), subvertical veins 0.5-5cm wide occur, filled with carbonate and silica. In core these are observed to be ptygmatically compacted in silty sediment. This texture clearly demonstrates that such vein-fills were crystallised at shallow burial depths (0.1-1km), whilst compaction of surrounding sediment was dominant. Macaulay *et al* (1993) have measured FI temperatures and quartz $\delta^{18}O$ from these veins. The compaction of ptygmatic folds and $\delta^{18}O$ data are interpreted to indicate a growth temperature of 40°C from seawater. By contrast, the FI in these quartz veins record a temperature mode of 119°C which compares well with present day reservoir temperature

(129°C). We infer that these FI were formed around 40°C and have been reset during burial.

5. Shallow overgrowths.

Walderhaug (1990) studied quartz FI from a mid-Jurassic sandstone in the Norwegian Haltenbanken area (geological setting in Ehrenberg 1990). He observed minor quartz overgrowths which pre-dated calcite cement, and major quartz overgrowths which post-dated calcite cement. Quartz overgrowths both inside and outside the calcitic sandstone show FI temperatures with coincident identical modes of 94, 100°C, and a maximum T_h of 118°C. The present reservoir temperature is also 118°C. Walderhaug (1990) suggests that quartz started growth above 90°C and the calcite cement post-dated this.

Alternatively, we interpret that the FI in these minor quartz overgrowths formed around 70°C throughout the sandstone (see Ehrenberg's compilation from this same area on Fig 1). One sandstone was occluded by calcite at relatively shallow depths. The other sandstone continued to cement with quartz until hydrocarbon charging. All inclusions subsided with the sandstone and have been reset from their minimum growth temperatures towards present day reservoir temperatures.

An analogous effect is recorded in diagenetic calcites from the Middle and Upper Jurassic, Upper Viking Graben by Moge and Pagel (1990), where pre-quartz and post-quartz calcite cements are isotopically distinct but show identical ranges of homogenisation temperatures. These have modes 5°C above, and identical with, the intervening quartz (105°C) respectively.

6. Experimental data

Bodnar, Binns and Hall (1989) undertook experiments where artificially grown FI in quartz were heated from 330-370°C for one year to induce excess

pressures of 400 bars inside the inclusions. The temperature distribution of homogenisation temperatures was recorded before and after these runs. A distinct increase occurred in the FI mode (Fig. 7). In a different experiment, Sterner and Bodnar (1989) heated and then cooled FI in quartz from metamorphic temperatures to induce internal pressure difference of 1000 bars. In both cases FI temperature modes were changed. We suggest that these experiments indicate that quartz FI are less susceptible to resetting by overheating than other minerals, but will inevitably slowly increase or decrease in homogenisation temperature, and even reform to trap cooler temperature samples of a second, saline pore fluid.

7. Correlation with subsidence

We have noted that the simple plot of FI temperature against present-day depth (hence temperature) shows an overall trend of increasing FI temperature with depth (Fig. 5), with a wide scatter. This should not be interpreted as a simple control of FI temperature by present day temperature. We noted from experimental evidence that FI temperatures show a small increase after an overheating time of only one year. Therefore, we have investigated the effect of geological time on particular FI populations. We have used subsidence (geohistory) curves for the few oilfields where we also know the present day temperature and have fluid inclusion data. These curves enable us to estimate total subsidence in metres during the past 5 Ma, *this is a crude measure of subsidence rate.* We have plotted this value against the *difference* between modal FI temperatures in quartz cement and present day sandstone temperatures. We find a strong linear correlation (Fig. 8), significant at the 99% confidence level. Oilfields which have remained within 50m of their present depth during the past 5 Ma show T_h which are within a few degrees Centigrade of todays sandstone temperature. By contrast, oilfields which have subsided more rapidly (greater

than 100m) within the last 5 million years show T_h populations which are too cool, and lag the present day sandstone temperature. The most extreme value, from the North Sea Central Graben was predicted to within 5°C by extrapolation from our slower subsiding dataset.

An identical pattern of FI values to that in Fig. 5 is recorded from Haltenbanken by Ehrenberg (1990) and Grant and Oxtoby (1992). Where they provide enough supporting data we have replotted temperature, subsidence and fluid inclusion spectra in the same format as Fig. 8; and obtain a good fit. Thus, similar effects are observed in the Viking Graben and Central Graben failed rifts; and the Haltenbanken continental margin.

DISCUSSION.

We have seen firstly, that the monotonic increase in quartz cement volume with present-day depth is difficult to explain by an ancient mineralising event. Secondly that the temperature gradient of FI today of less than 35°C/km is evidence against the ascent of an ancient hot fluid cooling and precipitating transported quartz. Thirdly, by contrast, the increase of quartz cement with depth makes it much more probable that quartz grew, and is still growing, throughout a long time span over a range of temperatures. Independent evidence for this process comes from a detailed isotopic study of the Magnus oil field (Macaulay *et al.* 1992) where stratified and distinct pore waters existed adjacent to each other for at least 35 Ma. This field shows the same diagenetic minerals as the other sands in our compilation, including 5-10% diagenetic quartz, which must have been supplied through a stationary pore fluid. If moving fluids did not transport diagenetic quartz, then some type of <u>diffusive</u> supply of silica cement must be inferred. Mullis (1992) has shown numerically that diffusion is a

geologically rapid process, and that the theoretical distance of silica transport is limited only by laboratory-derived solution residence times (rather than by geological information). Fourthly, we have demonstrated several independent geologically-based lines of reasoning which suggest that T_h values recorded today have been reset towards present day temperatures Fifthly, geological data sets show that a FI population needs increased temperature over a time span of at least 5 Ma (Fig. 8) to complete re-equilibration. Osborne and Haszeldine (1992) discuss the resetting mechanism in detail, concluding that stretching and FI shape change to produce a volume change of only 1-3% are quite sufficient to accommodate the temperature changes needed.

Diagenetic quartz overgrowths commence forming at or before a 70°C threshold temperature, perhaps depending upon the sediment's lithology and inter-grain stress (overpressure). At such shallow depths, FI temperature distributions are not strongly controlled by slow or by rapid subsidence (Fig. 9a,b). If subsequent subsidence is slow, inclusions in a sandstone re-equilibriate and record maximum burial temperatures (Fig. 9c). Alternatively the sandstone may have subsided rapidly; in this case FI population lags reservoir temperature below the equilibrium temperature line (Fig. 9d). The resetting process is always active, but needs time to complete. Consequently these populations preserve temperature modes from depths where they were in equilibrium. If such a sandstone then subsided slowly at its maximum depth (Fig. 9e), a high temperature skewed tail will gradually form by depleting the lower temperature FI. This is the case in the Tartan field (Burley *et al.* 1989).

The shape of an FI temperature distribution can, therefore, give information on pauses in subsidence, on the maximum temperature experienced, but only an approximate guide to its original growth temperature. The bulk fluid composition within FI remains intact, although interpreted salinity values will need correction for density changes resulting from slight increases in FI volume.

Relative salinities will be unaffected. We have not attempted extensive compilations of FI data in uplifted sandstones.

CONCLUSIONS.

1. The full temperature distribution of T_h measurements must be used when interpreting FI data. This entails at least 40 measurements for each sample depth, and no hot temperature "cutoff".
2. FI temperatures are slowly reset upwards to values in equilibrium with prevailing rock temperatures. This process takes at least 5 Ma, and may occur via stretching and shape changes.
3. If subsidence is rapid, T_h values lag below rock temperature, and preserve modal temperatures which record equilibrium at cooler temperatures.
4. Re-equilibriation at hotter temperatures gradually depletes the coolest first-formed FI, which progressively stretch to produce an equilibrium temperature skewed tail to the population at each depth. Eventually the equilibrium FI mode is re-established within a few degrees Centigrade of rock temperature. This could find an application in estimating maximum burial temperatures of uplifted rocks, and in recording temperatures (hence times) of slow subsidence.
5. There is an excellent correlation of the lag in T_h mode relative to present rock temperature, and metres of subsidence during the past 5 Ma. This may have predictive value in reconstructing the most recent subsidence history, often the most important in terms of hydrocarbon generation.
6. FI contents are intact, so that their relative salinity ranking is still feasible. However, corrections should be made if <u>absolute</u> salinity values are needed.

7. There is no evidence of high paleo-temperature gradients in FI populations from the North Sea Jurassic. This quartz did not grow by circulation of hot waters. We propose that quartz grew slowly in relation to burial depth, probably by some type of local diffusive supply.

ACKNOWLEDGEMENTS

MO was funded by NERC, the SURRC is supported by NERC and the Scottish Universities. Sovereign Oil provided Emerald core. Iain Samson (Windsor Univ, Canada) pointed us to the significance of Bodner's work. Stuart Burley (Manchester Univ) and Mark Wilkinson (Glasgow) commented on an early draft of this paper. Referees comments by Jim Boles (Santa Barbara), Andrew Robinson, Norman Oxtoby, Andrew Hogg, Tim Primmer, and Craig Smalley (BP) improved our speculations.

REFERENCES CITED

ABBOTS, I.L. 1991, United Kingdom oil and gas fields, 25 years commemorative volume. Geological Society, London 573p.

BAKKER, R.J. and J.B.H. JANSEN, 1990, Preferential water leakage from fluid inclusions by means of mobile dislocations. Nature, v.345, p.58-60.

BARKER, C.E. and R.H. GOLDSTEIN, 1990, Fluid inclusion technique for determining the maximum temperature in calcite and its comparison to the vitrinite reflection geothermometer. Geology, v.18, p.1003-1006.

BJORLYKKE, K., T. NEDKVITNE, M. RAMM, and G.C. SAIGAL, 1992, Diagenetic processes in the Brent Group (Middle Jurassic) reservoirs of the North Sea-an overview. In A.C. MORTON, R.S. HASZELDINE, M.R. GILES, and S. BROWN, (Eds) Geology of the Brent Group. Geological Society London, Bath UK. p.263-288.

BLANCHE, J.B. and J.H.McD. WHITAKER, 1978, Diagenesis of parts of the Brent Sand Formation. Journal Geological Society, London. v.135, p.73-82.

BODNAR, R.J. and P.M. BETHKE, 1984, Systematics of stretching of fluid inclusions. i). fluorite and sphalerite at one atmosphere confining pressure. Economic Geology v.79, p.141-161.

BODNAR, R.J., P.R. BINNS, and D.L. HALL, 1989, Synthetic fluid inclusions vi). Quantitative evaluation of the decrepitation behaviour of fluid inclusions in quartz at one atmosphere confining pressure. Journal Metamorphic Geology v.7, p.229-242.

BURLEY, S.D., J. MULLIS, and A. MATTER, 1989, Timing diagenesis in the Tartan Reservoir (UK North Sea); constraints from combined cathodoluminescence microscopy and fluid inclusion studies. Marine and Petroleum Geology., v.6, p.98-120.

EHRENBERG, S.N. 1990, Relationship between diagenesis and reservoir quality in sandstones of the Garn Formation, Haltenbanken, Mid-Norwegian

Continental Shelf. American Association Petroleum Geologists Bull. v.74, p.1538-1558.

GILES, M.R., S. STEVENSON, S.V. MARTIN, S.J.C. CANNON, P.J. HAMILTON, J.D. MARSHALL, and G.M. SAMWAYS, 1992, The reservoir properties and diagenesis of the Brent Group; a regional perspective. In A.C. MORTON, R.S. HASZELDINE, M.R. GILES, and S. BROWN, (Eds) Geology of the Brent Group. Geological Society London, Bath UK. p.289-328

GLASMANN, J.R., R.A. CLARK, S. LARTER, N.A. BRIEDIS, and P.D. LUNDEGARD, 1989a, Diagenesis and hydrocarbon accumulation, Brent Sandstone (Jurassic) Bergen high area, North Sea. American Association Petroleum Geologists Bull. v.73, p.1341-1360.

GLASMANN, J.R., P.D. LUNGERDARD, R.A. CLARK, B.K. PENNY, D. COLLINS, 1989b, Geochemical evidence for the history of diagenesis and fluid migration: Brent Sandstone, Heather Field, North Sea. Clay Minerals., v.24, p.255-284.

GOLDSTEIN, R.H. 1986, Re-equilibration of fluid inclusions in low temperature calcium carbonate cement. Geology. v.14, p.792-795.

GRANT, S.M. and N.H. OXTOBY, 1992 Fluid inclusion data from quartz cements in Mesozoic sandstones from Haltenbanken, Mid-Norway. Journal Geological Society London, in press.

GRATIER, J.P. 1982, Approche experimentale et naturelle de la deformation des roches par dissolution-cristallisation avec transfert de matiere. Bulletin de Mineralogie v.105, p.291-300.

GRATIER, J.P. and L. JENATTON, 1984, Deformation by solution-deposition, and re-equilibration of fluid inclusions in crystals depending on temperature, internal pressure and stress. Journal of Structural Geology v.6, p.189-200.

HANOR, J.S. 1980 Dissolved methane in sedimentary brines: Potential effect on the PVT properties of fluid inclusions. Econ. Geol. v.75, p.603-617.

HASZELDINE, R.S., I.M. SAMSON, and C. CORNFORD, 1984a, Dating diagenesis in a petroleum basin, a new fluid inclusion method. Nature, v.307, p.354-357.

HASZELDINE, R.S., I.M. SAMSON, and C. CORNFORD, 1984b, Quartz diagenesis and convective fluid movement: Beatrice oilfield, North Sea. Clay Minerals, v.19, p.391-402.

HASZELDINE, R.S., J.F. BRINT, A.E. FALLICK, P.J. HAMILTON, and BROWN, S. 1992, Open and restricted hydrologies in Brent Group diagenesis: North Sea. In A.C. MORTON, R.S. HASZELDINE, M.R. GILES, and S. BROWN, (Eds) Geology of the Brent Group. Geological Society London, Bath UK. p.401-420.

HOGG, A.J.C. (1989) Petrographic and isotopic constraints on the diagenesis and reservoir properties of the Brent Group sandstones, Alwyn South. Unpub PhD thesis Univ Aberdeen UK, 414p.

HOGG, A.J.C., E. SELLIER, and A.J. JOURDAN, 1992, Cathodoluminescence of quartz cements in Brent Group sandstones, Alwyn South. In A.C. MORTON, R.S. HASZELDINE, M.R. GILES, and S. BROWN, (Eds) Geology of the Brent Group. Geological Society London, Bath UK. p.421-440.

JOHNSON, H.D., T.A. MACKAY, and D.J. STEWART, 1986, The Fulmar oil field (Central North Sea): Geological aspects of its discovery, appraisal and development. Marine and Petroleum Geology. v.3, p.99-125.

JOURDAN, A., M. THOMAS, O. BREVART, P. ROBSON, F. SOMMER, and M. SULLIVAN, 1987 Diagenesis as the control of Brent Sandstone Reservoir properties in the Greater Alwyn area. In: J. Brooks and K. Glennie, (eds.). Petroleum Geology of Europe. Graham and Trotman, London. p.951-961.

KONNERUP-MADSEN, J., and H. DYPVIK, 1988, Fluid inclusions and quartz cementation in Jurassic sandstones from Haltenbanken, offshore mid-Norway. Bulletin de Mineralogie, v.111, p.401-411.

MACAULAY, C.I., R.S. HASZELDINE, and A.E. FALLICK, 1992, Isotopic evidence for 35 Ma stratified pore waters; Magnus Field, North Sea. American Association Petroleum Geologists Bull., in press.

MACAULAY, C.I., 1993 Hot fluid inclusions from early silica veins in the Fumar field, evidence for resetting. Marine and Petroleum Geology, submitted.

MALLEY, P., A. JOURDAN, and F. WEBER, 1986, Etude des inclusions fluides dans les nourrisages siliceux des gres reservoirs de Mer du Noir: Une nouvelle lecture possible de l'historie diagenitique de la region d'Alwyn. Acadamie des Sciences Paris, v.302, p.653-658.

MOGE, M. and M. PAGEL, 1990, Petrography, fluid inclusion and stable isotopes of Jurassic carbonate-cemented sandstones (Viking Graben, North Sea). Geochem. of Earth's Surface. 2nd Internat. Symp. Aix, France. p.243-245.

MULLIS, A. 1992, A numerical model for porosity modification at a sandstone-mudstone boundary by quartz pressure solution and diffusive mass transfer. Sedimentology v.39, p.233-239.

OSBORNE, M., and R.S. HASZELDINE, 1992, Fluid inclusions in diagenetic quartz record oilfield burial temperatures, not precipitation temperatures. Marine and Petroleum Geology, in press.

ROBINSON, A., S. GRANT, and N. OXTOBY, 1992 Evidence against natural deformation of fluid inclusions in diagenetic quartz. Marine and Petroleum Geology v.9, in press.

ROEDDER, E. 1984, Fluid inclusions: In: P.H. Ribbe, (ed.). Reviews in Mineralogy., v.12, Mineralogical Society, America, 644p.

SCOTCHMAN, I.C., L.H. JOHNES, and R.S. MILLER, 1989 Clay diagenesis and oil migration in Brent Group sandstones of NW Hutton Field, UK North Sea. Clay Minerals, v.24, p.339-374.

STERNER, S.M. and R.J. BODNAR, 1989, Synthetic fluid inclusions vii. Re-equilibriation of fluid inclusions in quartz during laboratory-simulated

metamorphic burial and uplift. Journal Metamorphic Geology v.7, p.243-260.

WALDERHAUG, O. 1990, A fluid-inclusion study of quartz-cemented sandstones from off-shore Mid-Norway, possible evidence for continued quartz cementation during oil emplacement. Journal Sedimentary Petrology v.60, p.203-210.

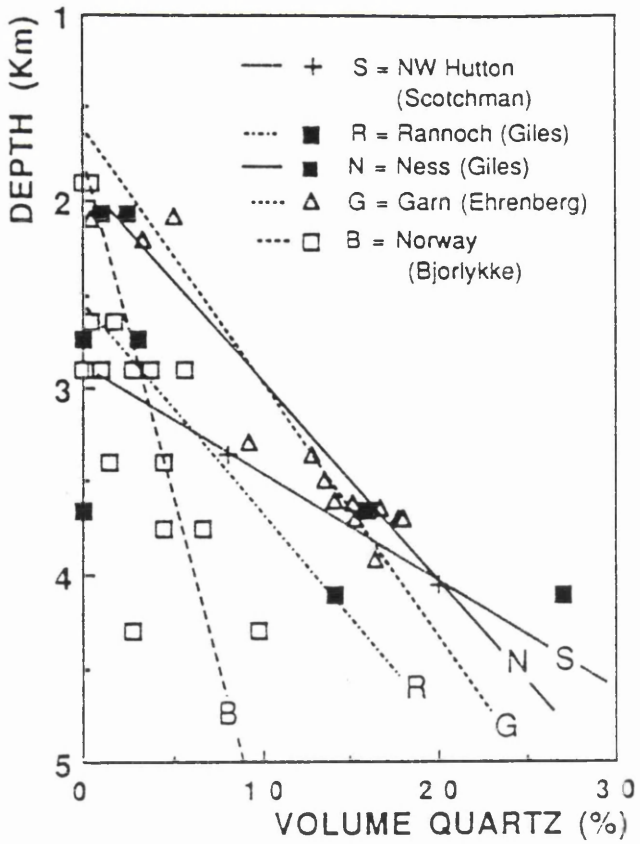

Fig. 1 Quartz overgrowth volume increases with present day burial depth in the Middle Jurassic Brent Group and Garn Formation. Data replotted from Scotchman *et al.* 1989, Ehrenberg 1990, Giles *et al.* 1992, Bjorlykke *et al.* 1992).

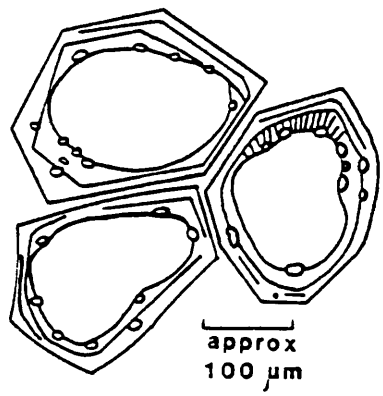

Fig. 2 Schematic Cathode Luminescence (CL) thin section view of quartz overgrowth showing location of diagenetic FI preferentially at grain-overgrowth boundaries (Burley *et al* 1989, Hogg *et al* 1992). Fewer FI occur at CL boundaries within the overgrowth, and still fewer as isolated FI within one CL zone.

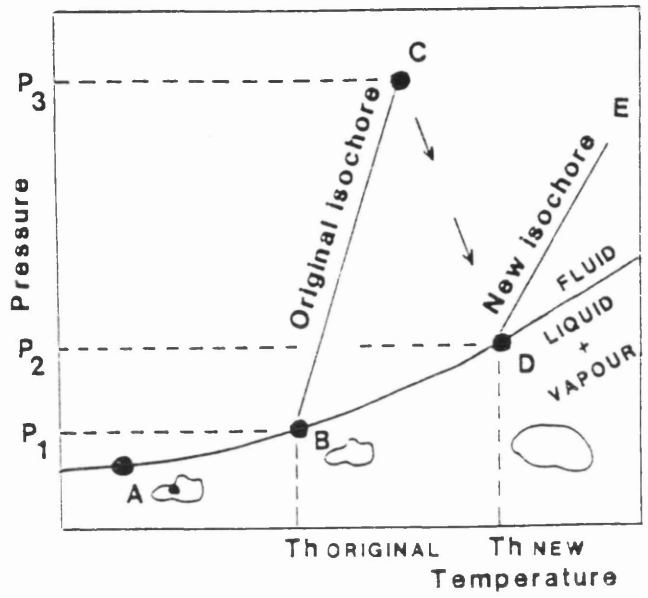

Fig.3 Pressure-Temperature phase relations of an aqueous fluid inclusion. When heated from the surface (A), the liquid-vapour curve is followed until the homogenisation temperature $T_{h\ original}$, where the vapour bubble disappears (B). Upon further heating (burial through time), the isochore relating to the fluid density is followed, and the internal pressure increases P_1-P_3. At C the inclusion "stretches" or fractures in order to release the internal overpressure down to P_2. If stretched by shape change, its volume increases, so the homogenisation temperature rises to $T_{h\ new}$ (D). Continued burial and heating will follow a new isochore D-E corresponding to the new fluid density.

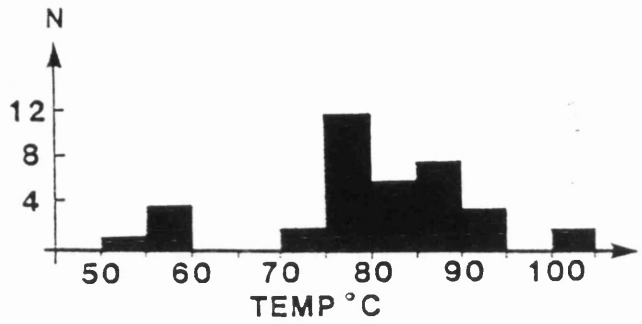

Fig. 4 Idealised FI temperature distribution, showing isolated low temperature readings, and one or more modes within the body of data, and skewed high temperature tail. Such patterns need more that 40 readings at each depth to be visualised.

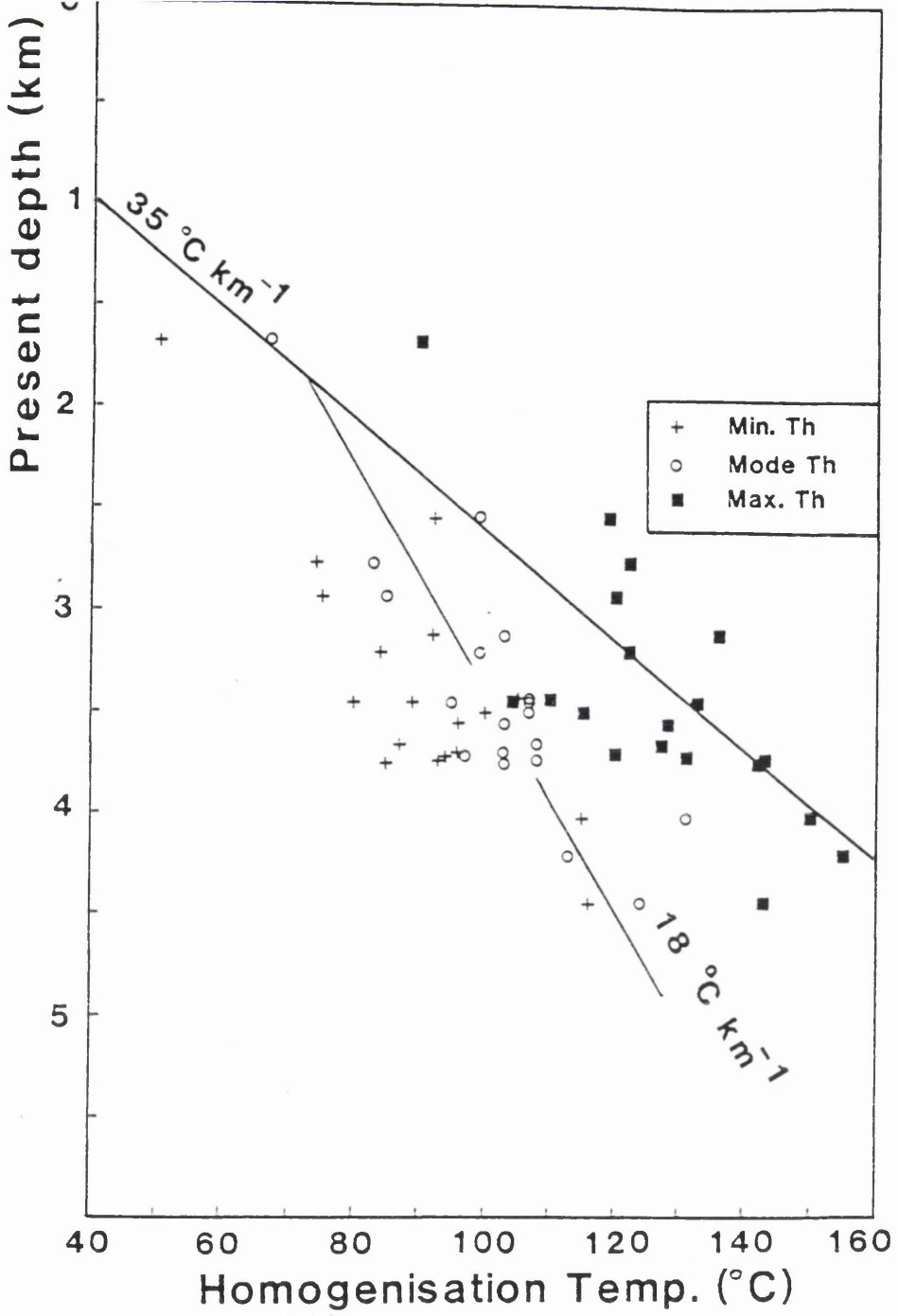

Fig. 5 Compilation of published and unpublished FI homogenisation data from North Sea plus Haltenbanken, showing minimum mode, maximum temperatures against present day burial depth. All areas today have a temperature gradient of about 35 (superimposed for comparison) and are at their maximum burial depth. A range of line fits can be proposed, with gradients ranging 18-35°Ckm^{-1}. Gradients of more than 35°Ckm^{-1} or less than 18°Ckm^{-1} can be excluded. Data from Haszeldine *et al* (1992), Glasmann *et al* (1989a,b), Hogg (1989), Jourdan *et al* (1987), Konnerup-Madsen and Dypvik (1988), Malley *et al* (1986), Walderhaug (1990); unpublished Glasgow University data from Macaulay (Fulmar), McLaughlin (South Brae), and Osborne (Emerald) see Table 1.

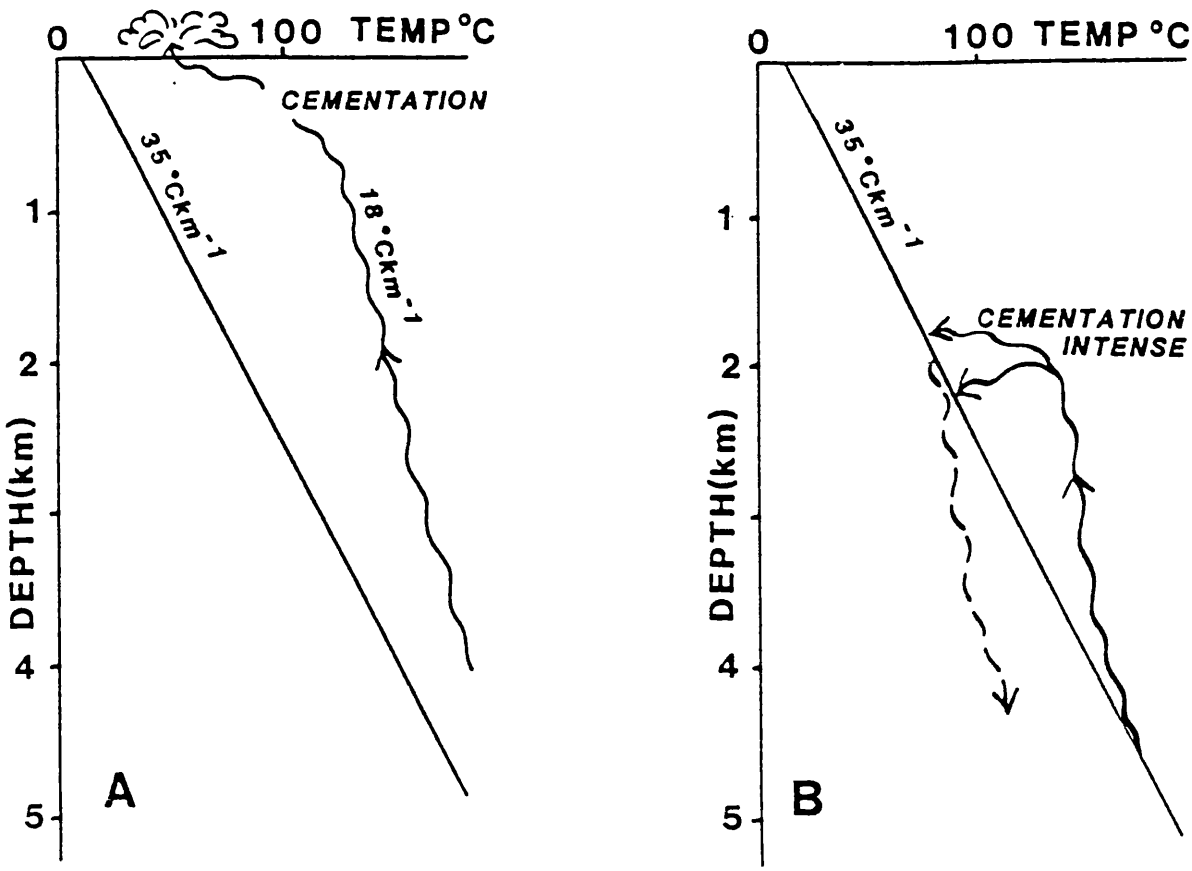

Fig.6 Cartoons illustrating the equilibrium temperature gradient of $35^{o}Ckm^{-1}$, and temperature gradient possibilities for:- A) Rising hot fluids cementing near the surface, and discharging as warm springs. B) Rising hot fluids cooling and cementing in the subsurface. The rising fluid is shown with an approximate $18^{o}Ckm^{-1}$ gradient, to enable comparison with Fig.5. Both A and B rising fluid temperature gradients lie right of the $35^{o}Ckm^{-1}$ line, indicating hydrothermal conditions, rather than to the left as in Fig. 5. In alternative B most silica cementation must have occurred during the rapid cooling high gradient at around 2km. We find no FI evidence of such a high palaeo-gradient wihin individual oilfields (eg $34^{o}Ckm^{-1}$ paleo-gradient between up and down fault blocks in Burley *et al* 1989). A very fortuitous combination of post-cementation subsidence must also be proposed for both Haltenbanken and the North Sea to produce the present-day trends of gradually increasing silica cement with depth (Fig 1).

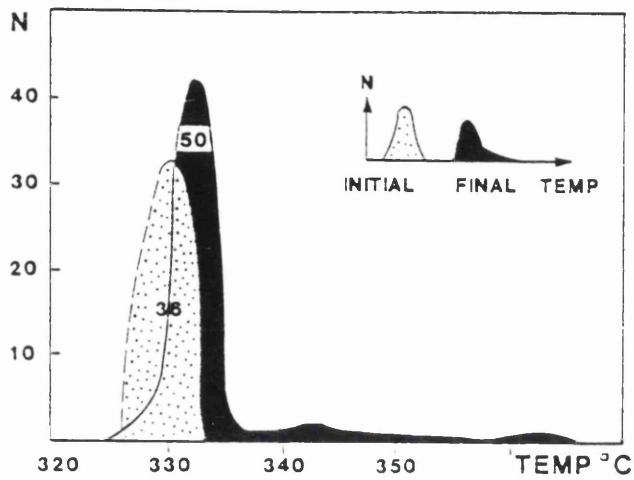

Fig. 7 Experimental data from Bodnar *et al.* 1989 showing that FI temperatures from 36 FI before heating are cooler than 50 different FI in the same sample after heating for one year at 400 bar internal pressure. This shows that quartz FI can reset slowly when heated above growth temperatures (cf Gratier and Jenatton 1984).

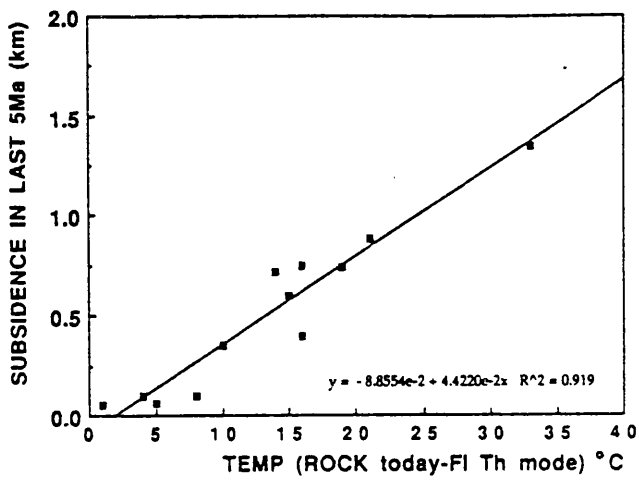

Fig. 8 Plot of subsidence in last 5 Ma against temperature difference (todays rock temperature minus FI mode). This shows "lag" of FI resetting is directly proportional to rate of subsidence. Data from Table 1

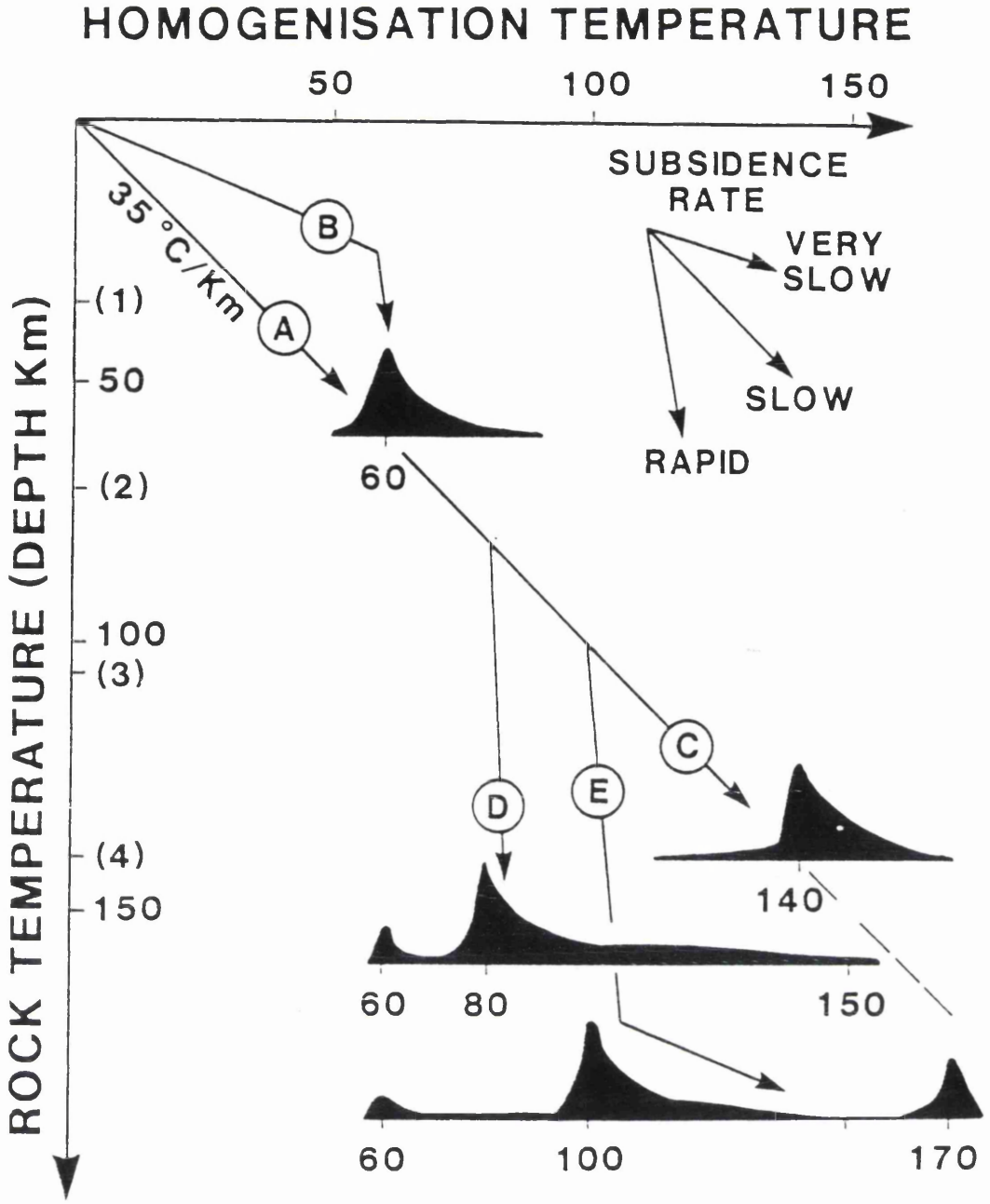

Fig. 9 Cartoon explanation of subsidence pathways to result in different present day FI temperature distributions. This assumes that quartz grows continually from 70°C, most FI are trapped at at the grain-overgrowth boundary, and few FI are trapped during burial; all FI are reset. Compare real life data of Fig. 5:-

A + B slow and rapid arrival below 70°C threshold.

C shows subsidence and resetting.

D, E subsidence too fast for resetting.

FIELD	ROCK TEMP	FI MODAL	(ROCK-FI)	FI DEPTH (km)	5 Ma SUBS km
HEATHER	110	95	1	3.294	0.050
EMERALD	60	67	5	1.650	0.060
WALDERHAUG	118	102	16	2.547	0.400
THISTLE	104	83	21	3.400	0.881
ALWYN SOUTH	127	123	4	3.505	0.100
HULDRA	150	131	15	4.000	0.600
SOUTH BRAE	132	113	19	4.270	0.740
FULMAR	129	119	10	4.047	0.350
TARTAN	109	101	8	3.653	0.100
GARN WELL I	143	127	16	3.702	0.750
MAGNUS	116	102	14	3.075	0.720
QUAD 29 NE	183	150	33	5.480	1.350

Table 1 Data of measured fluid inclusion temperature in relation to present day rock temperature at sample depth and to subsidence in last 5Myr. This selection is only for fields where we have access through publications or released data to good quality well locations, burial curves, temperatures, and accurately located single depth fluid inclusion temperature distributions. Thus much published data has been excluded. Temperatures and stratigraphy from Abbots (1991), Heather (Glasmann *et al* 1989b), Emerald (Osborne unpub), Walderhaug (1990), Thistle (Haszeldine *et al* 1992), Alwyn South (Hogg 1989), Huldra (Glasmann *et al* 1989a), South Brae (McLaughlin unpub), Fulmar (Macaulay unpub), Tartan (Burley *et al* 1989), Well I (Garn) (Ehrenberg 1990), Magnus (Macaulay unpub), UK Central North Sea Quadrant 29 NE (Osborne unpub).